# Polymer Model System for Mechanosensitivity Studies: Decoupling Mechanics from Biological and Topographical Cues

zur Erlangung des akademischen Grades eines

**Doktors der Ingenieurwissenschaften (Dr.-Ing.)**

der Fakultät für Chemieingenieurwesen und Verfahrenstechnik des
Karlsruher Institut für Technologie (KIT)

genehmigte
DISSERTATION

von

## Dipl.-Ing. Robert Gralla-Koser
aus Sindelfingen

Ich versichere, dass die hier vorliegende Dissertation mit dem eingereichten und genehmigten Prüfungsexemplar der Doktorarbeit übereinstimmt.

**Schwetzingen, den 11. Dezember 2018**

. . . . . . . . . . . . . . . . . . . . . . . . . . . . . . . . . . . . . .
**(Robert Gralla-Koser)**

# Abstract

Sensing of mechanical stimuli is a basic biological process that influences a variety of cell functions such as cell division, motility, morphology, proliferation and differentiation. Especially in the case of stem cells it is of great interest to control their fate with means beside biological and chemical factors. Though, the mechanisms of mechanosensation are not completely understood. Substrate stiffness is a heavily investigated parameter, but available system pose different problems that hamper clear statement on its role in cellular functionality: Variation in substrate stiffness is linked to changes in biochemical and topographical cues. Some studies characterize stiffness at length and time scales not relevant for cellular receptors.

This thesis aimed at the development of a polymer model system with tunable stiffness in terms of substrate extensibility decoupled from substrate topography and density of cell adhesive motifs. This was achieved with biofunctionalized polymer brushes displaying controlled chain lengths. Unfolding of the polymer chains led to different substrate extensibilities that gave mechanical feed-back equivalent to varying stiffness. Thereby, surfaces were constantly flat and availability of the adhesion motif was controlled via grafting density. Length and functional group of the applied polymer chains were derived from the natural archetype tropoelastin - the most elastic biomolecule known.

Dense polymer brushes were fabricated via surface-initiated reversible addition–fragmentation chain transfer (RAFT) polymerization and mechanically characterized with atomic force microscopy (AFM) based single molecule force spectroscopy (SMFS). Contour length could be tuned via polymerization time as mapping of the polymer growth revealed a linear dependence in the investigated time range. Moreover, unfolding behavior similar to tropoelastin was observed. Roughness measurement and determination of grafting density verified substrate extensibility as the only variable parameter. For cell experiments, biofunctionalization was achieved via click reaction with bioactive peptide sequences derived from the C-terminus of tropoelastin. While functionality of the model system was validated with spreading behavior of REF52 cells dependent on substrate extensibility, hematopoietic stem/progenitor cells (HSPCs) displayed no changes in proliferation or differentiation.

In summary, a new model system for mechanosensitivity studies was established with tunable contour length that could be easily correlated to lengths of other proteins or cell compartments, which opens up new possibilities for interesting future studies.

# Zusammenfassung

Die Wahrnehmung mechanischer Reize ist ein grundlegender biologischer Prozess, der eine Vielzahl an Zellfunktionen beeinflusst wie z.B. Zellteilung, Beweglichkeit, Morphologie, Proliferation und Differenzierung. Insbesondere im Falle von Stammzellen ist es von großem Interesse ihr Schicksal mit Mitteln jenseits von biologischen und chemischen Faktoren zu beeinflussen. Die Mechanismen der Mechanosensitivität sind jedoch nicht vollständig verstanden. Substratsteifigkeit ist ein stark untersuchter Parameter, aber vorhandene Systeme werfen verschiedene Probleme auf, die eine klare Aussage über ihre Rolle in Zellfunktionen erschweren: Variation der Steifigkeit ist verbunden mit Veränderungen in biochemischen und topographischen Signalen. Andere Studien charakterisieren Steifigkeit in Längen- und Zeitskalen, die nicht für Zellrezeptoren relevant sind.

Diese Dissertation zielte darauf ab ein polymeres Modellsystem zu entwickeln, dessen einstellbare Steifigkeit von der Substrattopographie und Dichte an zelladhäsiven Motiven entkoppelt ist. Dies konnte mit biofunktionalisierten Polymerbürsten erreicht werden, die eine kontrollierte Kettenlänge aufwiesen. Entfaltung der Polymerketten führte zu unterschiedlichen Substratdehnbarkeiten, die mechanische Rückkopplung gaben, welche verschiedenen Steifigkeiten entsprechen. Dabei blieb die Oberfäche konstant eben und die Verfügbarkeit adhsäsiver Motive wurde mittels Propfdichte kontrolliert. Länge und funktionelle Gruppe der Polymerketten wurde vom natürlichen Vorbild Tropoelasstin - dem Biomolekül mit der höchsten bekannten Elastizität - abgeleitet.

Dichte Polymerbürsten wurden mit Hilfe von oberflächeninitiierter RAFT-Polymerisation (Reversible Additions-Fragmentierungs-Kettenübertragungs-Polymerisation) erstellt und mittels Einzelmolekülkraftspektroskopie mechanisch charakterisiert. Die Konturlänge konnte durch die Polymerisierungsdauer eingestellt werden, da das Polymerwachstum eine lineare Abhängigkeit zur Polymerisationsdauer im untersuchten Zeitbereich zeigte. Zudem wurde ein Entfaltungsverhalten ähnlich dem von Tropoelastin beobachtet. Rauhigkeitsmessungen und Bestimmung der Pfropfdichte bestätigten die Substratdehnbarkeit als einzigen variablen Parameter. Für Zellexperimente wurde die Biofunktionalisierung mittels Klickreaktion mit Peptidsequenzen erreicht, die vom C-Terminus von Tropoelastin abgeleitet sind. Während die Funktionalität des Modellsystems durch das Ausbreitungsverhalten von REF52 Zellen in Abhängigkeit zur Substratdehnbarkeit belegt wurde, zeigten blutbildende Stamm- und Vorläuferzellen keine Veränderung der Proliferation oder Differenzierung.

Zusammenfassend wurde ein neues Modellsystem für Mechanosensitivitätsstudien mit einstellbarer Konturlänge etabliert, die leicht mit der Länge anderer Proteine oder Zellbestandteile korreliert werden kann, was neue Möglichkeiten für interessante zukünftige Studien bietet.

# Contents

# Abbreviations

# 1. Introduction

## 1.1. Mechanosensation

Mechanosensation is the specific response to mechanical stimuli[1]. Mechanical stress can trigger physiological processes at different levels: You can feel pressure on a macroscopic level with your skin, specific cells in the ear act as mechanical sensors enabling us to hear[2], intracellular signals can be activated by stimulation of cell receptors[3] and even single proteins can alter their function by conformational change or partial unfolding driven by mechanical forces[4].

Furthermore, different organs can react to mechanical stress: Besides the before mentioned functions in the ear and skin[5], the heart and vascular systems change their morphology due to hemodynamic conditions[6, 7, 8], the permeability in the lung is increased by high airway pressures[9], bone adapts its structure to changes in mechanical load[10, 11], mechanosensitivity plays a role in the neuronal system for the perception of pain[12] and the muscle spindle helps locating body parts and resisting excessive muscle stretch[13], among other examples.

All these described processes, they rely on the conversion of sensed mechanical stimuli into electro- and biochemical activity within a cell, what is called mechanotransduction[3]. There are many structures in cells that are responsible for mechanotransduction as shown in Figure 1.1. It can occur at cell-cell junctions (A)[14], in primary cilia[15] or mechanically activated ion channels[16] at the cell membrane in contact with a fluid (B), at the cell nucleus (C)[17] as well as at the focal adhesion in contact with the extracellular matrix (D)[18]. This last point will be illuminated in detail as it enables material scientists to steer cell fate in vitro by replacing the extracellular matrix with biomaterials of different stiffness, shape or ligand density[19].

As early as 1980, Harris demonstrated that cells can generate external forces as they wrinkled the substrate surface when cultured on soft polymer substrates[21]. The basis for this force transmission is the highly interconnected cytoskeleton[22]. It is composed of filamentous actin, intermediate filaments and microtubules, each of them consisting of many monomers that can span through the entire cell[20]. The filamentous actin together with myosin filaments builds the contractile apparatus in the cell. It is connected to the nucleus as well as to the cell membrane[23], where it is linked via focal adhesions through transmembrane integrin receptors to the extracellular matrix. The extracellular matrix
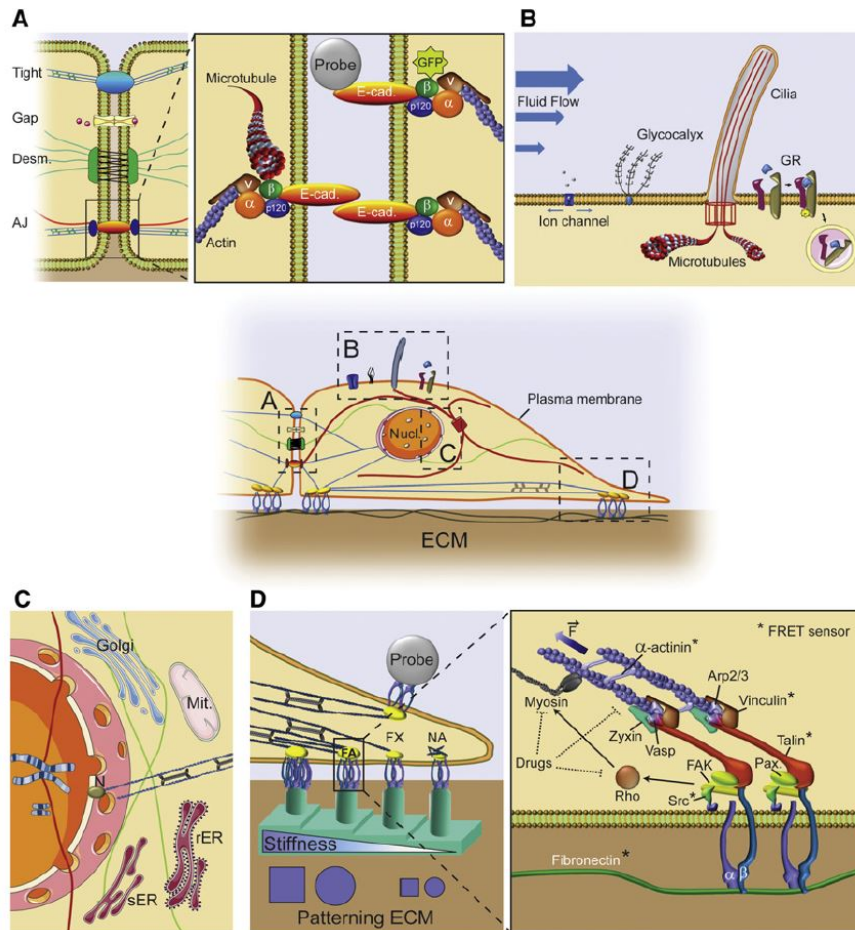
Figure 1.1.: Mechanotransduction can occur at different locations in the cell: At cell-cell junctions (A), at the cell membrane in contact with a fluid (B), at the cell nucleus (C), at the focal adhesion in contact with the extracellular matrix (D). With permission from [20].

consists of proteins (e.g. collagen, fibronectin, elastin and laminin), carbohydrates (e.g. hyaluronic acid) and proteoglycans.

Focal adhesions allow the transmission of force into the cell and out of the cell[24]: While external force transmitted through the focal adhesions can rearrange the whole intracellular structure via the cytoskeleton[25], cells can also deform the extracellular matrix by contraction caused by myosin-II pulling at the actin filaments[26, 27]. Cells respond to stiff substrates with a regulation of the cellular force exerted through focal adhesion sites and strengthening of the integrin-cytoskeleton linkage[28]. The following maturing of focal adhesions[18] allows for an increased intracellular tension, which is required for the activation of certain contractility pathways[29]. Moreover, focal adhesions contain also many signaling transduction molecules[30] and thus can act as biochemical signaling centers, too. Those activated pathways in turn can regulate stem cell fate[31]. However, for the mechanisms of intracellular signaling, the reader is referred to other reviews[32, 33, 34].

The following sections shall introduce to the possible reactions of stem cells in general and of hematopoietic stem cells in particular to mechanical stimuli and how their cell function can be directed by different substrate materials.

### 1.1.1. Mechanosensitivity of Stem Cells

Stem cells are capable of renewing themselves through cell division and they can differentiate into cells of multiple lineages. The mesenchymal stromal cells (MSCs) are a class of adult stem cells which can differentiate into cells of different tissues such as bones, cartilage, muscles, adipose tissue and neurons, potentially offering use in clinical applications. As they can be cultured long-term in special media without any irregularities, they function as a model system for stem cell studies[35]. The literature of this section refers mostly, but not exclusively, to research on (human) MSCs.

**Substrate Stiffness Can Influence Cellular Processes** The first signs for mechanosensation were observed in the 1950s and 60s, when cells aligned along grooves in a substrate by so-called contact guidance[36, 37], and in the 80s, when wrinkling of substrates by cells was demonstrated[21]. However, for a long time the focus in cell studies remained on the interaction of cells with biochemical stimuli, e.g. how the differentiation of MSCs could be driven by the culture medium[38]. It was not until the 90s, that the investigation of mechanosensation gathered impetus when evidence grew that cells feel and respond to the stiffness and other mechanical cues of their substrate[39].

The adhesion and motility of cells changed based on the stiffness of the substrate: Soft gels led to diffuse adhesions and high motility, whereas stiff gels yielded low motility and stable focal adhesions as seen in Figure 1.2, left[41]. This was followed by the observation that stiffness gradients guided cells towards stiffer regions by durotaxis[42]. This mecha-
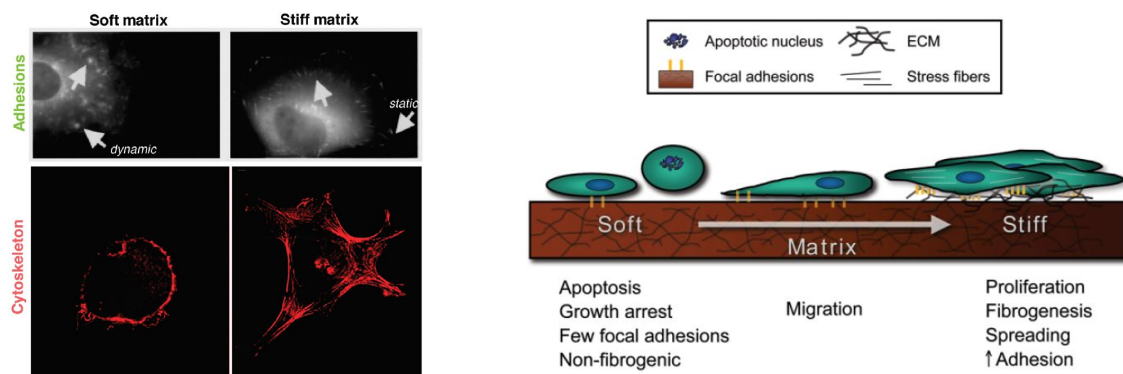


Figure 1.2.: Left: Substrates stiffness influences the focal adhesion, the cytoskeleton and thereby the shape of a cell. From [39]. Reprinted with permission from American Association for the Advancement of Science (AAAS). Right: Effects of matrix stiffness on cell behavior. With permission from [40].
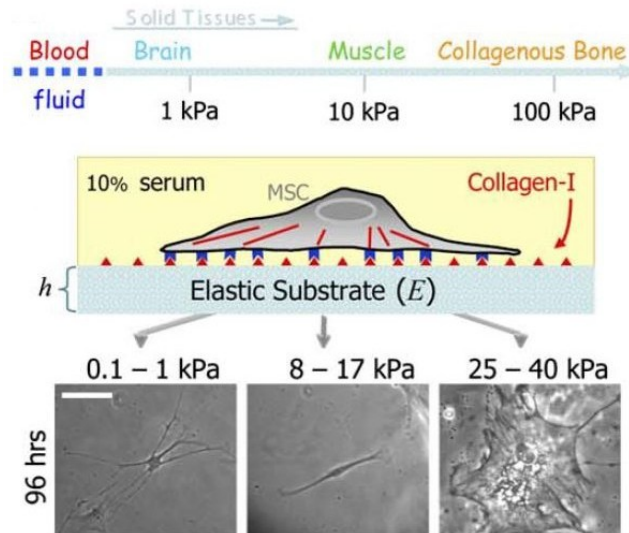
Figure 1.3.: Substrate stiffness directed the differentiation of MSCs. They differentiated into cells of that tissue whose mechanical properties corresponded to those of the substrate. Scale bar is 20 µm. With permission from [55].

nism could not only occur in single cells but also in cell collectives[43]. Substrate stiffness could regulate cell spreading[44] as well as cellular growth and apoptosis [45]. Further cellular responses to substrate stiffness are summarized in Figure 1.2.

The control of substrate stiffness could be utilized in medical applications. Matrix elasticity regulates the secretion of trophic and immunomodulatory molecules in MSCs[46, 47, 48] what could be useful for implants or wound healing[49]. Cardiomyocytes beat best on a matrix with heart-like elasticity while scar-like rigidity inhibited beating[50, 51]. However, malfunctioning mechanotransduction is the reason for many diseases[52] and substrate stiffness plays a role in cancer, too[53, 54].

**Substrate Stiffness as a Regulator for the Differentiation of MSCs** The publication that kicked off mechanosensitivity studies in stem cells was that of Engler et al. in 2006, which demonstrated that substrates stiffness directs the differentiation of MSCs[55]. MSCs were cultured on polyacrylamide (PAAm) gels whose elasticity was controlled through cross-linking and adhesion was provided by coating of the gels with collagen. In doing so, the stiffness of various tissues could be mimicked, from soft brain tissue, over muscles with intermediate stiffness to stiff collagenous bone as depicted in Figure 1.3. MSCs cultured on those substrates differentiated into cells of that tissue whose mechanical properties correspond to those of the substrate and showed tissue specific cell morphologies. When cultured on even softer substrates in the range of bone marrow (250 Pa), MSCs became quiescent but remained responsive for chemical stimuli as they differentiated into certain lineages when incubated with the respective induction medium[56].

The substrate stiffness has also an effect on cell morphology as cells cultured on soft

substrates showed less spreading, fewer stress fibers, and lower proliferation rates than human MSCs cultured on stiff substrates[57]. Furthermore, stiffness of the nucleus changed dependent on the substrate elasticity influencing gene expression and lineage determination[58]. MSCs even had a memory for their substrates previous mechanical state[59]. The use of a hydrogel with temporally controllable stiffness showed that the expression of a differentiation marker could be reversed when switching from high to low substrate stiffness, but only if the former cell culture was limited to short incubation times. This finding leads to potential implications for the isolation or storage of stem cells prior to the experiment.

Further research made clear, that the stiffness alone is not enough for directing stem cell fate, but the interplay between stiffness and presentation of adhesive ligands, which were different extracellular matrix proteins in the cited study[60]. Osteogenic differentiation of MSCs occurred only on stiff substrates coated with collagen type I, while the expression of myogenic differentiation markers were highest on substrates with intermediate stiffness coated with fibronectin, but also significant on stiff substrates with collagen type I or fibronectin. This suggested that the right combination of substrate stiffness and ligands is important for the regulation of MSC differentiation.

With the coating of flat substrates with a fibrous protein, the tethering of protein molecules to the substrate arose as an additional factor that has to be taken into account for a description of the mechanical system. That was tested with nonporous polydimethyl-siloxane (PDMS) and porous PAAm hydrogels with covalently attached collagen[61]. It was reported, that MSC differentiation was unaffected by the substrates' stiffness on the nonporous substrate while changing with substrate stiffness on the porous hydrogel. As the pore size increased with lower stiffness, it was concluded that anchoring points of the fibrous proteins were further apart on soft hydrogels, thus offering a more flexible attachment point for the cells that did not activate any intracellular signaling as shown in Figure 1.4.

However, this finding could not be confirmed by other studies[62]. A hydrogel with tunable pore size at constant stiffness was developed which showed no influence of neither pore size nor anchoring density on MSC differentiation. Furthermore, the viscoelastic properties of PDMS were highlighted and that stiffness measurements were dependent on the length and time scale as well as indenter geometry. At a cell relevant scale, the measured stiffness was higher than in the aforementioned study[61]. In addition, the stiffness of PDMS was always higher than that of PAAm hydrogels, thus it was possible that PDMS stiffness was outside the stiffness range cells can sense.

The image is further complicated as also the onset of stress stiffening played an important role in MSC differentiation[63]. This was demonstrated with the use of very soft hydrogels with a tunable stress-stiffening behavior by variation of polymer chain length between cross-linking points while keeping the stiffness constant. Shorter chain lengths showed an earlier onset of stress-stiffening than longer chains that could be correlated
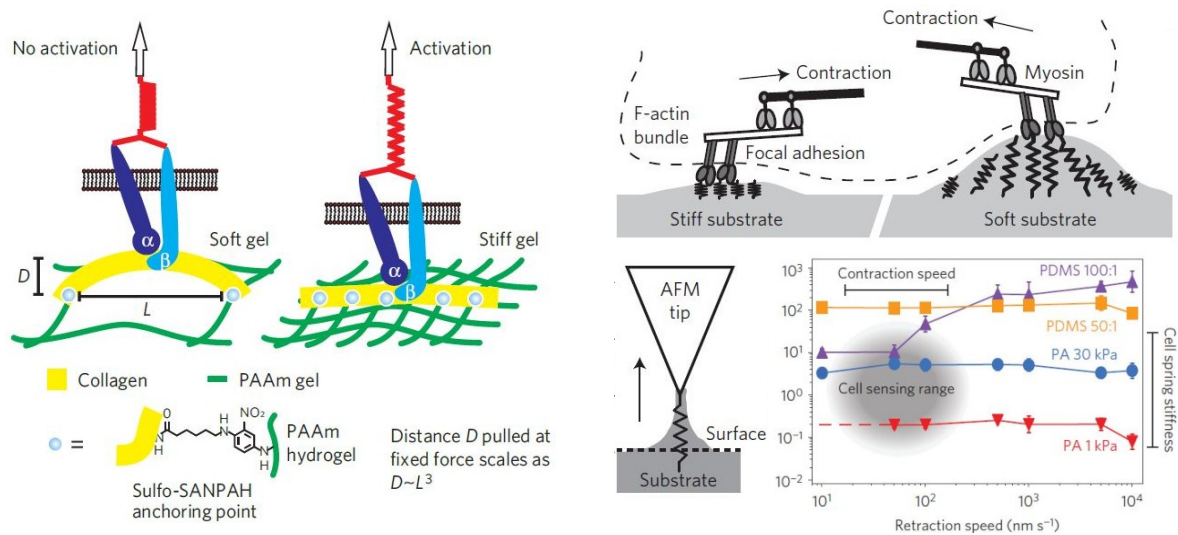
Figure 1.4.: Left: Tethering of adhesive proteins is proposed as an additional mechanical cue. With permission from [61]. Right: Scheme depicting the deformation of substrates from cells. Indentation via atomic force microscopy (AFM) is suggested as a cell relevant measurement method. With permission from [62].

with predominantly adipogenic commitment on short polymer bridges compared to longer ones. Additionally, MSCs could also be regulated by the mechanical energy dissipation of a substrate as tested with deformable polymer brushes[64].

One important difference of the aforementioned studies compared to the situation *in vivo* was the dimensionality: Most substrates offered a flat 2D surface while cells in a body are embedded into a 3D microenvironment. However, the commitment of MSCs still changed dependent on the stiffness of porous 3D hydrogels[65] but not the cell morphology[66]. Instead, integrin binding was regulated by substrate stiffness and adhesion ligands were reorganized on a nanoscale, that means, ligands clustered depending on the stiffness and thereby regulated differentiation[66]. In addition to that, a different study demonstrated that MSCs lineage commitment was dependent on the ability to generate traction on the environment[67]. While osteogenesis was favored by high traction, in case of low traction adipogenesis was enhanced.

It is concluded that the effect of Engler's landmark study of substrate matrix guiding stem cell differentiation of MSCs could be verified under the limited conditions of flat hydrogels coated with immobilized collagen type I[68], though generalizations have to be avoided. It is still under investigation which mechanical property of "soft" and "stiff" substrates is the key regulator for mechanotransduction.

**Substrate Stiffness as a Regulator for the Differentiation of Other Stem Cells**  Besides MSCs, the differentiation of embryonic stem cells could also be guided by substrate stiffness[69]. It was shown that cell spreading and growth were increased and osteogenic

differentiation was enhanced on stiff substrates compared to soft substrates. However, there were different findings on the maintenance of pluripotency in embryonic stem cells of human and murine cells: While soft substrates promoted homogeneous self-renewal in the murine cells[70], rigid substrates supported maintenance of pluripotency of human cells[71, 72].

Muscle stem cells showed robust regenerative capacity *in vivo* which was lost in culture on rigid plastic dishes. However, cultured on soft substrates with a stiffness similar to that of muscle tissue, they were capable of self-renewal *in vitro*[73] and could contribute to regeneration in injured and aged muscles after transplantation[74]. Even human embryonic stem cells retained their stemness in a soft matrix without exogenous factors, while stiffer matrices switched the cells to differentiation[75].

It can be concluded that in general, a tendency of maintenance of pluripotency could be observed on soft culture substrates[68]. A hint on the mechanism behind that could be gathered from a study that demonstrated an influence of mechanical cues on the orientation of the plane of cell division which in turn determined between symmetric and asymmetric cell division[76].

**Further Parameters Influencing Stem Cell Fate**  Substrate stiffness is a key factor in the mechanical regulation of stem cells though not the only one. Dimensionality is another one as mentioned before and the differences between 2D and 3D hydrogel culture were highlighted elsewhere[77]. Moreover, the interplay between ligands and stiffness did also play a role in 3D hydrogels[78].

However, differentiation can also be directed by cell shape. This could be controlled through patterning with islands of adhesive proteins. Cells could be confined to small island or spread on large ones[29], island shape could direct multicellular structures[79] or single cells[80] and shape of microwells directed differentiation[81]. All of these studies relied on the modeling of the cytoskeleton thereby provoking different cellular tensional states. Cells at convex edges of adhesive islands tended to exhibit osteogenesis while cells at concave edges underwent adipogenesis[79]. There was even a crosstalk possible between cell shape and substrate rigidity[82].

Another important factor is nanotopography: MSC adhesion, apoptosis and differentiation could be influenced by symmetric or disordered nanoholes[83, 84, 85] and glass substrates with controlled nanoroughness influenced adhesion, spreading and self-renewal of human embryonic cells[86]. Stem cell fate could be affected by micro-[87] and nanoposts[88]. Even epigenetics were modulated by microgrooved substrates[89, 90].

Surface chemistry is also a relevant factor as simple chemical functionalities such as *t*-butyl or phosphate could directly control MSC phenotype or, indirectly, guided the deposition or retention of proteins and thereby dictated MSC differentiation[91, 92]. Furthermore, surface chemistry also worked in tandem with substrate stiffness influencing MSC differentiation[93]. It was also possible that substrate materials degraded during cell cul-

ture with their by-products influencing stem cell fate[94]. In addition to that, the lineage commitment of MSCs was also tailored by the ligand density offered on a surface[95] and multivalent ligands controlled stem cell behavior via spatial control of receptors[96].

Expanding the focus from passive materials to active bioreactors, further mechanical stimuli come into play: Shear stress could induce osteogenic differentiation of MSCs[97] and small vibrations additionally prevented dietary-induced obesity in MSCs[98]. For more mechanical stimuli such as stretching forces or compression, the reader is referred to the following review[99].

Finally, with all discussed material properties it has to be considered whether these could also change the arrangement of cells and thus alter cell-cell contacts. For example, differentiation of MSCs could be influenced by soft or stiff surrounding cells[100].

A review summarized 15 different parameters of extracellular matrices and artificial scaffolds that guide stem cell fate[101]. This highlights the requirement of well defined systems for mechanosensitivity studies with the tunability of a single parameter while all other parameters remain constant.

## 1.1.2. Mechanosensitivity of hematopoietic stem/progenitor cells (HSPCs)

The whole blood system with all its different cell types originates from hematopoietic atem cells (HSCs). It has various functions such as oxygen transport, sealing of injuries through blood clotting or fighting pathogens with immune cells. Due to the limited life span of blood cells, HSCs give rise to billions of blood cells per day[102]. The life-long maintenance of the blood system without depletion of the stem cell pool is ensured by the balance between stem cell quiescence and proliferation[103]. This section shall discuss the factors regulating HSC function, especially which mechanical cues could guide it.

**Hematopoiesis**  The generation of blood cells is called hematopoiesis. HSCs differentiate via several maturation steps continuously loosing their self-renewal potential and becoming more and more specialized until mature blood cells arise[104]. The development from HSCs over multipotent and oligopotent progenitors to finally committed mature blood cells is depicted in Figure 1.5. Hematopoietic cells can be tracked and identified via their surface markers. CD34 is a marker characteristic for HSPCs as differentiated cells loose their ability for CD34 expression. CD38 arises during hematopoiesis[105].

**Clinical Use of HSCs**  The transplantation of HSCs is used for the treatment of many diseases, among which leukemia is the most prominent one[107], and has been carried out for over 60 years[108]. Following engraftment, HSCs can reconstitute the blood system of the patient by restoring the HSC pool.
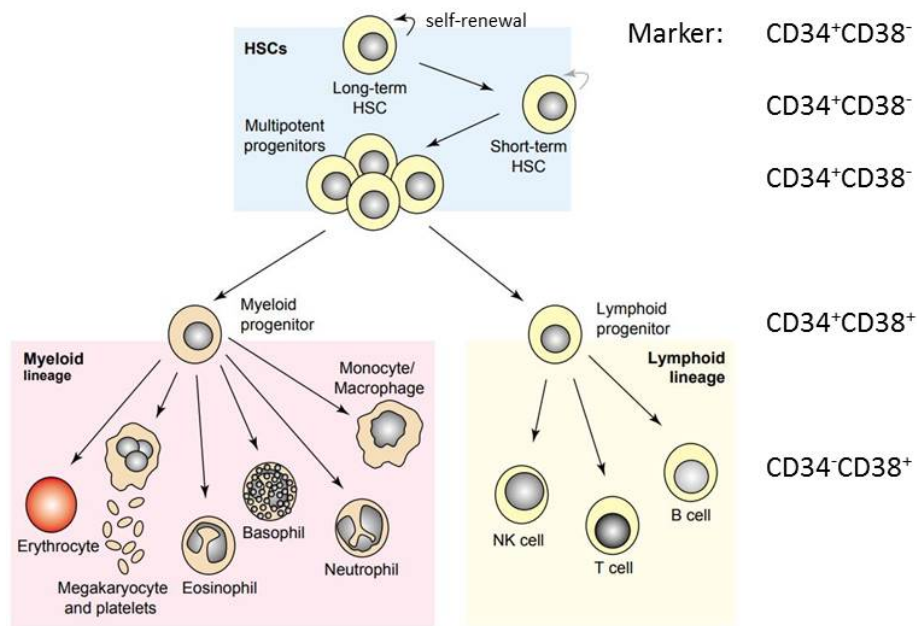
Figure 1.5.: Schematic and simplified drawing of the differentiation of HSCs during hematopoiesis and corresponding surface markers. Adapted with permission from [106].

The generation of HSCs from pluripotent stem cells is not possible yet[109], therefore HSCs have to be aquired from donations. For this purpose, HSCs can be obtained from bone marrow, peripheral blood or umbilical cord blood (UCB)[110]. While the donation of bone marrow and the collection from peripheral blood have risks and strong side effects, UCB can be collected without any harm to baby or mother. Furthermore, less stringent matching requirements for HSCs from UCB enable 95 % of the patients to find a matching unit in one of over 100 UCB banks worldwide[111].

A limiting factor for the use of UCB is the low dose of CD34$^+$ cells per UCB unit. This limits the utilization of one UCB unit to infants or adults with low body weight[112]. Therefore, an expansion of CD34$^+$ *in vitro* would be an desired solution. However, previous attempts have not achieved clinically relevant effects[113, 114] and new solutions have to be discussed.

**The HSC Niche** The HSC niche is a particular microenvironment in the bone marrow, where HSCs are located. It consists of two anatomically distinct cellular sites with intimate contact to each other. HSCs can move between these sites and simultaneously receive input from both[115]. Its existence was hypothesized as early as 1978[116], though its total functionality remains elusive yet[117, 118]. However, it is consent that the niche is the only place that enables HSCs to indefinite self-renewal[117]. There, a complex interplay of signals regulate the stem cell fate controlling self-renewal, proliferation and differentiation[118].

Up to now, most research on *in vitro* expansion of HSCs has been done on the investigation of biochemical factors. Soluble factors such as cytokines, developmental factors, chemical compounds and even oxygen play an important role in HSC regulation[119, 120]. The network of cell-segregated proteins surrounding the cells in tissues, called the extracellular matrix, provides signals by offering different adhesion sites and acting as a reservoir for other factors[115]. Furthermore, cell–cell contacts to nearby niche cells from multiple different cell populations steer HSC fate[121].

However, the influence of physical properties emerged recently and it became clear that only a combination of biochemical and physical cues could lead to a successful *in vitro* expansion of HSCs[122]. For example, HSC niches were embedded into a 3D porous, sponge-like network which seemed crucial for stem cell regulation[123, 118]. Moreover, HSPCs altered their signaling depending on the nanopatterning of extracellular matrix derived ligands[124]. In addition, shear stress induced from blood flow was a potent regulator of HSC formation[125, 126, 127].

**Influence of Mechanical Properties of the Environment on HSPCs**  Besides the mentioned physical factors, the focus shall be on the influence of elasticity on HSCs. The publication that influenced this dissertation the most demonstrated that the proliferation of undifferentiated HSCs could be enhanced on tropoelastin coated surfaces compared to uncoated standard tissue culture plates[128]. The extensibility of tropoelastin - the most elastic known biomaterial - was shown to be the critical factor for this effect as it failed to appear on truncations of tropoelastin or cross-linked proteins. A contour length of 125 nm was identified as the threshold for the beneficial effect of tropoelastin elasticity on the proliferation of HSPCs. Though it has to be kept in mind that the alteration of biomolecules - as carried out in this publication - did not only change their mechanical properties but also their biological activity.

A different publication investigated the migration behavior of HSCs in response to material stiffness[129]. It was shown before that one of the major cellular components of the HSC niche, osteoblasts, flattened during the egress of HSCs out of their niches[130]. A simplified *in vitro* model of a HSC niche demonstrated, that the flattening of osteoblasts was accompanied with a stiffening of these cells and that HSCs could react to that change of stiffness. With the aid of hydrogels of different Young's moduli it could be demonstrated that higher matrix substrate stiffness led to increased migration and adhesion of HSCs and could therefore facilitate their exit out of the niche. In contrast, soft substrates promoted stationary HSCs. Thus, this could be a potential signal for the retention of HSCs in their niche and to keep them in their quiescent state.

Further publications showed that HSPC spreading increased with substrate stiffness, but that effect was heavily dependent on the availability of ligands, as a low density of surface-bound collagen decreased cell spreading[131]. The important interplay of stiffness and surface ligands was confirmed by a study that showed that the proliferation

of HSCs increased with increasing substrate stiffness of substrates without cell adhesive molecules[132]. However, when fibronectin was chosen as a ligand, a proliferation peak could be observed on substrates with intermediate stiffnesses. The multipotency of these cells followed this effect, too.

In contrast, some publications stated contrary effects of matrix stiffness. A decreased proliferation as well as differentiation and more quiescent cells were demonstrated with an increase of matrix stiffness[133]. Reduced proliferation and higher frequency of quiescent cell in stiff matrices was confirmed elsewhere[134]. Both studies were conducted in 3D matrices in contrast to 2D substrates in the previous publications. That implied a different reaction of HSPCs to substrate stiffness dependent on the dimensionality. The latter publication assumed that the stiffness effect only occurred in combination with the spatial confinement of HSPCs within pores, which is not present in 2D substrates.

The mechanism behind the sensitivity of HSCs to substrate stiffness could rely on contractility of the motor protein myosin-II. The formation of cellular tension required a counterforce that is only provided by stiff substrates. Thus, myosin-II is more activated on stiff substrates than on soft ones[135]. Myosin-II was required for the polarization of HSCs which in turn promoted asymmetric division that was characteristic for stem cells. In contrast, soft matrices suppressed myosin-II and polarization, leading to symmetrical cell division and proliferation[136]. This was affirmed by the demonstration that stiff substrates coated with fibronectin could maintain the population of early hematopoietic progenitors[137].

### 1.1.3. Tropoelastin – model for mechanosensitivity studies

Tropoelastin is the soluble precursor monomer of elastin, the mature elastic fiber that gives the extracellular matrix and many tissues such as arteries, lung, heart valves, skin and tendon their strength and elasticity[138]. It is durable over a human lifespan and it shows repeated expansion and contractions without vanishing elasticity[139]. The importance of elastin for tissue function is emphasized by the diseases caused by abnormalities in the elastin gene such as arterial narrowing and sagging skin[140] or caused by destruction of elastin such as aortic rupture and fibrosis[141]. Its structural and cell signaling role make an elastin mimicry a desirable biomaterial and a potential candidate for tissue repair[142].

Tropoelastin is secreted by elastogenic cells such as fibroblasts, endothelial cells, smooth muscle cells, chondrocytes and keratinocytes[139]. However, it is difficult to isolate from *in vivo* tissues as it is quickly incorporated into growing elastic fibers[141]. Large quantities of tropoelastin have only become available when the production via recombinant expression in *Escheria coli* bacteria system was successful[143]. Soluble tropoelastin enabled techniques that were previously incompatible with the insoluble elastin. This promoted deeper understanding of its function and allowed the fabrication of new biomaterials[141, 144].
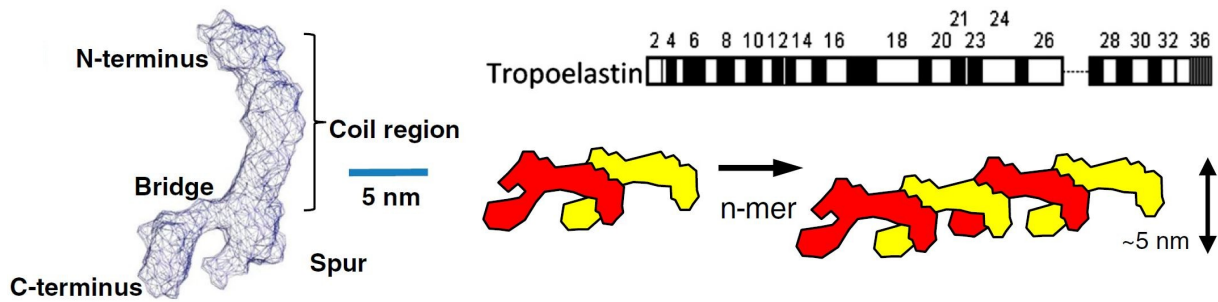
Figure 1.6.: Left: The tropoelastin molecules consists of specialized segments: The coil provides elasticity, while the bridge and the C-Terminus are responsible for mechanical coupling and cell interactions, respectively. Right, top: Diagram of the domain structure with hydrophobic regions depicted in black and hydrophilic ones in white. Right, bottom: Tandem assembly leading to the elastin fiber structure. With permission from [149].

**Structure and Mechanical Properties of Tropoelastin**  The shape of the 60 kDa protein is depicted in Figure 1.6. Adjacent to the N-terminus is a spring-like coil which primarily contributes to the elasticity of tropoelastin[145]. It is based on hydrophobic, extremely flexible domains[146], depicted in black in Figure 1.6 right, with VGVAPG being the most common repeating sequence[147]. The conformation in water is collapsed, thus elongation leads to exposure of hydrophobic regions to the surrounding water and arrangement of these water molecules. This results in a entropy based elasticity due to the decrease of structural conformations[148]. The tropoelastin molecule can be extended to approximately eight times its resting length of 20 nm without hysteresis[149], making it the most elastic biomaterial known[150]. The Young's modulus of single chains was determined as 3 kPa[149], while naturally cross-linked tropoelastin has a Young's modulus of 300 kPa to 600 kPa[151] and water-annealed tropoelastin films (60 °C ) one of 540 kPa[152].

Tropoelastin monomers have the intrinsic ability for self assembly which is called coacervation and it is the first step in the elastic fiber formation[153]. In this entropically-driven process, tropoelastin monomers are arranged from head to tail, facilitating cross-linking between monomers as seen in Figure 1.6 right, bottom. Coacervation can also be kicked off *in vitro* at physiological conditions[154]. The spur, sometimes also called hinge region, contains cross-linking sites important for the elastin fiber formation[155] and it contributes to the elasticity of tropoelastin, too[156]. The bridge region is less understood, but it may be involved in elastin fiber assembly as mutations in this region led to reduced elastin fiber formation[157]. Interactions between tropoelastin and cells could mainly, but not only, be ascribed to the C-terminal domain and are discussed below.

| Amino acid sequence | Receptor | Inhibitor |
|---|---|---|
| VGVAPG | EBP | lactose |
| GFPGGACLGKSCGRKRK (C-terminal domain) | GAG | heparin |
| GRKRK | integrin $\alpha_V\beta_3$ | EDTA |
| unknown (domains 17/18) | integrin $\alpha_V\beta_5$ | EDTA |
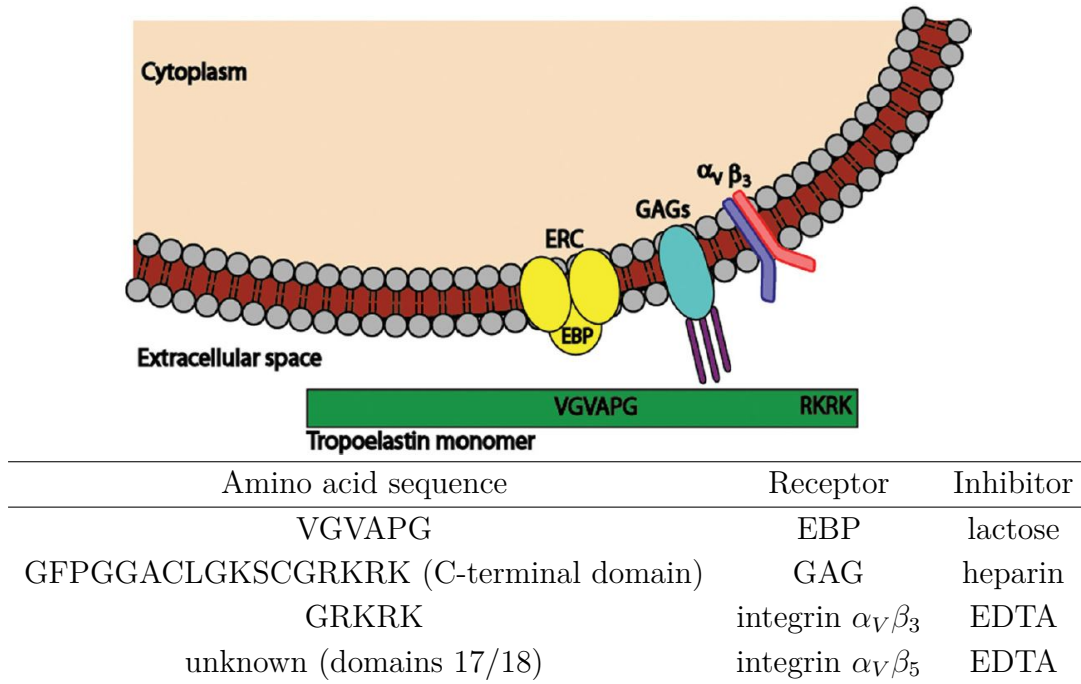
Figure 1.7.: Scheme of different binding sites of cells to amino acid sequences of tropoelastin. With permission from [165]

**Cellular Interaction of Tropoelastin**  In addition to the exceptional elastic properties, tropoelastin exhibited also cell signaling and adhesion properties. As described in Section 1.1.2, tropoelastin promoted the proliferation of undifferentiated HSCs[128].

Furthermore, fragments of tropoelastin and elastin could steer wound repair in skin, as they attracted the necessary cells to the injured sites and influence adhesion, proliferation and differentiation of these cells[158]: monocytes and fibroblasts migrated towards higher concentrations of the VGVAPG motif[159, 160]. Once attracted, the adhesion and proliferation of fibroblasts was promoted by tropoelastin and its derivates[159, 161], e.g. the attachment of fibroblasts to tropoelastin-coated surfaces was 10-fold higher than on tissue culture plate (TCP) at 1 h post-seeding[162]. The terminal differentiation of keratinocytes, which is required for the re-establishment of the epidermis, was induced by elastin peptides[163]. Finally, gene expression could be regulated to promote the angiogenic phenotype of endothelial cells[164]. Other cellular interactions with elastin peptides could induce protease release, calcium transport, production of extracellular matrix molecules or cell survival[165, 166].

Three different types of cell receptors were identified to mediate the described cellular interactions: The elastin binding protein (EBP), glycosaminoglycans (GAG) and integrins as summarized in Figure 1.7.

The transmembrane protein EBP was capable of binding to VGVAPG and other sequences in the form of XGXXPG in elastin[167, 168]. Fibroblasts, monocytes, endothelial

cells as well as vascular smooth muscle cells bound to tropoelastin via EBP[169, 170, 171]. Originally, EBP was regarded as an adhesion receptor as the adhesion of bovine fibroblasts and chondroblasts was inhibited by lactose when it released the EBP from the cells[172]. However, the adhesion of human fibroblasts and bovine chrondrocytes was unaffected by lactose[161, 173], therefore EBP was then associated with the detection of elastin fragments, resulting in various cellular responses such as promotion of proliferation or chemotaxis[170, 166].

Cell surface proteoglycans such as GAG[174] interacted with tropoelastin via its C-terminal domain[173, 175]. EBP-independent adhesion occured with bovine chondrocytes and human dermal fibroblasts on bovine tropoelastin and it could be inhibited by heparan sulfate, a class of GAG. It was thought, that GAG were involved in elastin fiber assembly[176].

The third group of protein receptors, integrins, bound in different ways to tropoelastin. The C-terminal motif GRKRK was identified as the amino sequence binding to the integrin $\alpha_V\beta_3$ of human dermal fibroblasts[161]. This was demonstrated with EDTA, which chelates cation required for integrin binding, and with integrin antibodies. Recently, an interaction of the fibroblast integrin $\alpha_V\beta_5$ with the domains 17 and 18 of tropoelastin was shown, but the specific motif responsible for this is unknown[177].

## 1.2. Development of Synthetic Matrices for Mechanosensitivity Studies

An ideal system for mechanosensitivity studies has to fulfill different criteria: It offers tunable stiffness in a cell relevant range which roughly correlates with the stiffness of tissues available in human bodies*. Furthermore, the variation of stiffness should be decoupled from other material parameters such as roughness, hydrophobicity, chemical reactivity or biological activity, i.e. stiffness can be varied as the only parameter. A fully synthetic material would also offer high reproducibility due to low adsorption of serum and proteins as well as a better availability than proteins.

This section gives an overview of frequently used systems for mechanosensitivity studies and introduces to the chemical synthesis of a new kind of model system based on polymer brushes.

### 1.2.1. Polymerization Techniques

The key for tunable material properties of polymers is a small polydispersity $Đ$, that means a narrow distribution of the polymer chain lengths. This can be achieved with the

---

*Substrates appearing stiff to cells (some $10\,\mathrm{kPa}$[68]) would still be perceived as soft for humans in everyday life (rubber $0.3\,\mathrm{MPa}$ to $30\,\mathrm{MPa}$[178]).
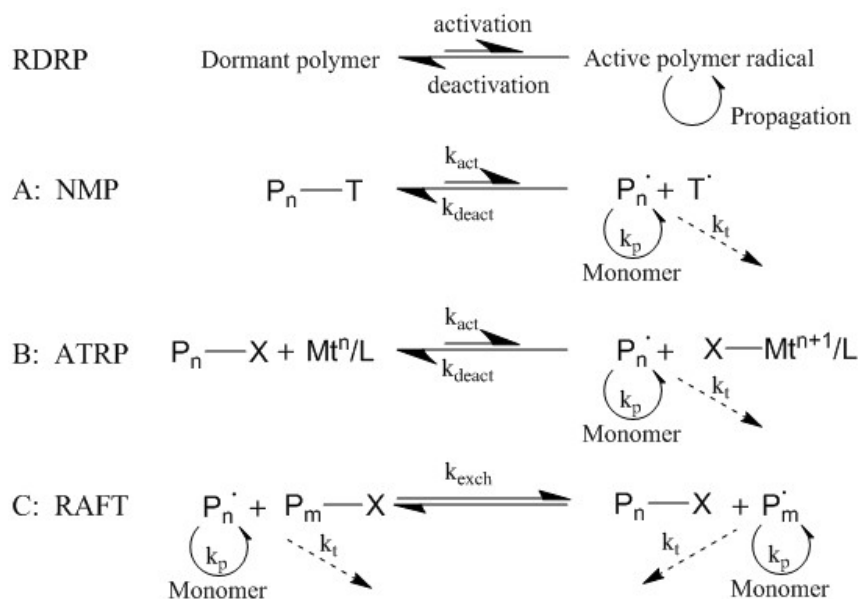
Figure 1.8.: Basic principle of RDRPs and its three main methods.
nitroxide-mediated polymerization (NMP): Thermal dissociation of dormant species ($k_{act}$) provides a low concentration of radicals.
atom transfer radical polymerization (ATRP): Activation of transition metal ($k_{act}$) from a dormant species with a radically transferable atom.
reversible addition–fragmentation chain transfer (RAFT): Majority of chains are dormant. They participate in transfer reactions ($k_{exch}$) with a low concentration of active radicals.
Rate of polymerization $k_p$ and termination $k_t$. Adapted with permission from [179] and [181].

class of reversible-deactivation radical polymerizations (RDRPs)[179], previously known as controlled/"living" radical polymerizations[180].

In those polymerizations, the propagating active polymer radical can reversibly react with a deactivating component, putting the polymer chain into a dormant state as seen in Figure 1.8, top. With a high concentration of the deactivating component, the equilibrium can be shifted to the dormant state. With the small number of remaining active polymer radicals, the probability of a termination reaction of two polymer radicals is minimized. Thereby, the lifetime of growing polymer chains can be prolonged to hours, thus offering the possibility to control the molecular weight with the duration of the experiment.

Compared to ionic living polymerizations, another technique that offers narrow molecular weight distributions, radical polymerization is more robust as it can be carried out in bulk, solution or emulsion, applied to a great number of monomers with tolerance to the presence of different functional groups and achieving complex polymer architectures and compositions[181].

**Examples of RDRPs** The first remarkable appearance of a RDRP technique was in 1993, when Georges et al.[182] demonstrated a simple method for the use of NMP for the controlled polymerization of styrene with low polydispersity and predictable molecular weights. The fundamental mechanics are depicted in Figure 1.8. It relies on radicals in alkoxyamine species that are stabilized due to bulky moieties around the radical center[183]. However, its drawback is low versatility.

Therefore, ATRP has become the most widely used RDRP technique quickly after its discovery in 1995[184, 185] due to its flexibility for end groups, catalytic species, architectures and compositions[186, 187]. This polymerizations relies on the removal of radical activity of the polymer chain upon reversible atom transfer catalyzed with transition-metal complexes, e.g. Cu(I). Due to these complexes, the polymerization is sensitive to moisture as well as air, causing a more complex reaction setup. Furthermore, due to the toxicity of copper, the use of ATRP in biological systems is problematic and high efforts are required to remove the catalysts for making this polymerization industrially acceptable[188].

**RAFT** The predestined technique for biomedical applications is the RAFT polymerization[189]. Without the need for a metal catalyst and with the capability of adopting this technique to a wide range of monomers, it has quickly become a widely used polymerization method. It was conducted for the first time in 1998[190, 191] and relies on the reaction of propagating polymer chains with dithioester as so-called chain transfer agents, thereby transferring the activity from one polymer chain to another. Due to the transfer instead of removal of polymer activity, the total number of propagating radicals is not reduced and therefore, the overall polymerization rate is higher than in other RDRP techniques[192].

The basic principle of the RAFT polymerization is shown in Figure 1.9[193, 194]. The reaction starts with an initiator (e.g. 2,2-bis-azobis-isobutyronitrile (AIBN)) leading to the growing polymer chain $P^{\bullet}_n$. Upon reaction of the propagating chain with the RAFT agent **1**, the RAFT adduct radical **2** is formed. This can fragment in a fast equilibrium reaction either to **1** or **3**. The leaving group R reacts with monomer species, thus generating another active polymer chain $P^{\bullet}_m$. In the following step, the main-equilibrium, $P^{\bullet}_m$ reacts with the macro-RAFT agent **3**, yielding the RAFT adduct radical **4**. This can fragment in a process of rapid interchange either into the left-hand or right-hand product, thus offering the possibility of polymer chain growth. In this way the activity of the radicals is shared among all polymer species ensuring equal growth and thus a narrow polydispersity. The termination reaction is possible, but very unlikely as most of the polymer chains are in a dormant state as depicted with **3**.

The design of the RAFT agent has to be adjusted for every monomer. The stabilizing group Z [195] as well as the radical leaving group R[196] are crucial for the control over the polymerization. For example, the Z group has to be chosen carefully in order to have a macro-RAFT agent (**2** or **4**) more stable than the propagating chains, but not too stable as it would prevent the fragmentation to **3**.
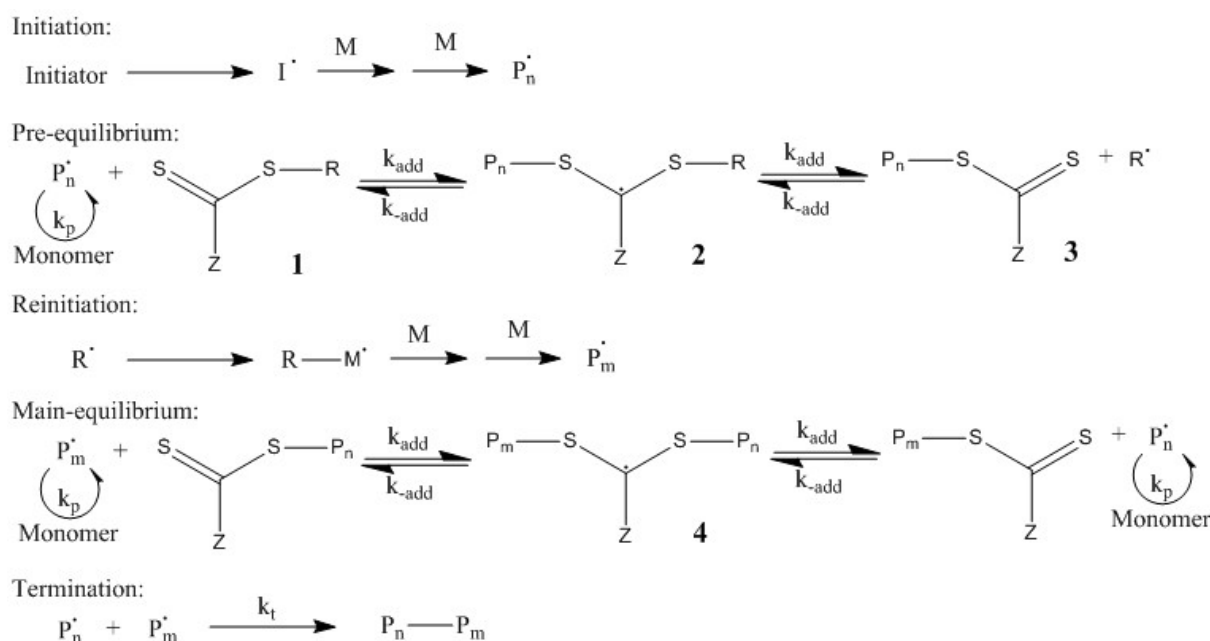
Figure 1.9.: Mechanism of the RAFT polymerization (with the monomer M and the rate of addition $k_{add}$ for the reaction of the propagating chain with the RAFT agens). Adapted with permission from [193].

The RAFT agent leads also to a disadvantage of the RAFT polymerization, as the agents hold a high potential for discoloration or pungent odor due to the decomposition of the dithioester moiety[193].

**Biocompatibility of poly(2-hydroxyethyl methacrylate) (pHEMA)**    2-hydroxyethyl methacry-late (HEMA) is a reasonable choice for its utilization in a polymer brush for cell studies. The synthesis of pHEMA is possible in many configurations enabling the fabrication in a variety of shapes[197].

pHEMA is regarded as biocompatible due to its inertness to biological processes, stability, permeability to metabolites and resistance to adsorption by the body as well as heat sterilization[198]. Furthermore, the abundance of hydroxyl groups gives the possibility of an easy post-functionalization with biomolecules. Thus, it has been used in biomedical devices for many years[199, 200], e.g. as contact lenses, for drug delivery systems or tissue engineering scaffolds and it has received safety approval by the US Food and Drug Administration for use in industrial, biomedical and pharmaceutical applications[201].

The high hydrophilicity of pHEMA is a feature of pHEMA. On the one hand, it establishes its non-fouling properties with low protein adsorption and thus the prevention of uncontrolled material-cell interactions[202, 203, 204]. On the other hand due to its high water content, it is frequently used as a hydrogel with a reasonable strength and elasticity[205].
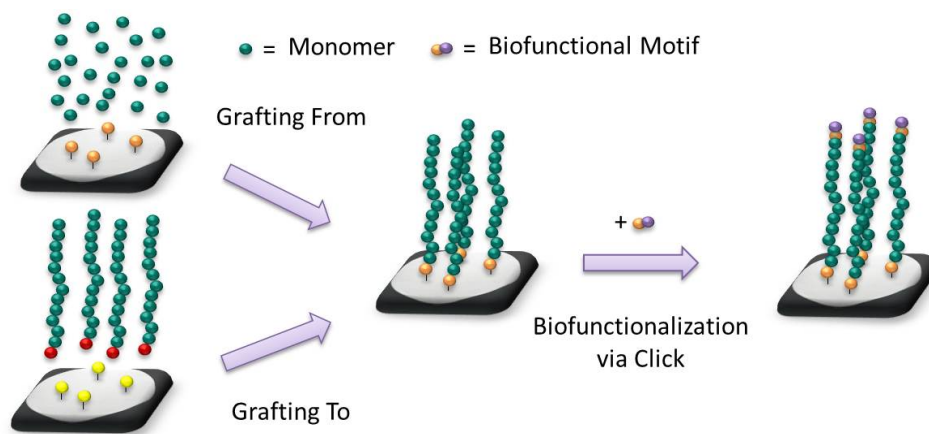
Figure 1.10.: Schematic presentation of the two routes for the preparation of polymer brushes and their biofunctionalization.

## 1.2.2. Surface Modification

Thin films of polymer chains that are fixed covalently to a substrate at one end are so-called polymer brushes. Due to their interesting properties, they are of great interest in different fields, especially for biological applications[206, 207, 208].

The presented techniques of RDRP are well suited for polymer brushes with finely tuned properties and this section discusses the strategies for their preparation and functionalization in order to use them in biological experiments.

**'Grafting From' and 'Grafting To'**   Figure 1.10 presents the two different routes for the synthesis of polymer brushes: The 'grafting to' compared to the 'grafting from' approach[209, 210, 211].

The 'grafting to' strategy comprises the attachment of prefabricated polymer via physisorption or chemisorption. With the synthesis of polymers before the attachment, this method is very flexible as any method for the usual polymerization in solution could be used and an in-depth analysis of the polymer prior to immobilization is possible. However, steric repulsions during the 'grafting to' process and a decreasing efficiency with increasing molecular polymer weight for the reaction between polymer end-group and corresponding substrate group are limitations during the 'grafting to' process. These make the production of thick and dense polymer brushes via 'grafting to' difficult.

A 'grafting from' method directly initiates the polymerization from functionalized surfaces. In a first step, an initiator molecule is immobilized on the surface followed by the addition of monomers to each initiation site. The film density depends on the density of initiation sites or grafting density while the film thickness is controlled by the degree of polymerization. Thus, the different RDRP techniques are distinctly suited for the fabrication of polymer brushes. However, it is unclear whether the known kinetics from polymerization in solution can be transferred to surface initiated reactions[212].
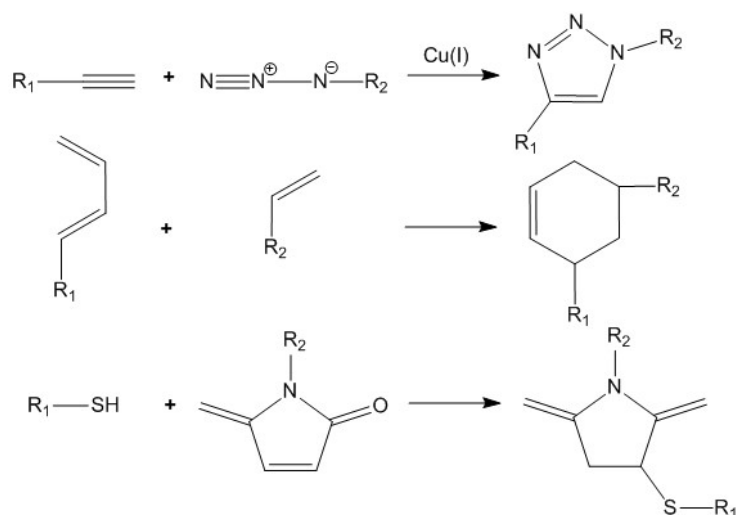
Figure 1.11.: Schemes of three typical click-reactions used in biological applications. Copper-catalyzed alkyne-azide cycloaddition (top), Diels-Alder reaction (middle), thiol-Michael type addition as one example of different thiol-ene reactions (bottom). Adapted with permission from [215]. Copyright 2011 American Chemical Society (ACS).

**Biofunctionalization**   The functionalization of polymer brushes with biologically active amino acid sequences is necessary to promote interaction of the brushes with cells, as many examples display strong antifouling properties[206].

A powerful tool for biofunctionalization is so-called 'click chemistry'[213], fast and specific reactions for the linkage of molecules. Adapted to polymer chemistry, the criteria for click reactions were defined as: modularity, applicability in a wide scope, chemoselectivity, a single reaction trajectory, fast timescale, high yields, stable compounds, equimolarity and easy purification[214].

Figure 1.11 displays schematic presentations of three click reactions that are typically used for the fabrication of biomaterials[215].

In the copper catalyzed azide alkyne cycloaddition, an organic azide reacts with an alkyne to form a triazole ring[216]. This reaction is highly popular in biochemistry due to its orthogonality, i.e. the azide group does neither exist among amino acids nor reacts with them. However, the employment of cytotoxic copper in these fields is problematic and truly high efficiency of the copper catalyst is necessary for working with low concentrations.

The Diels-Alder reaction is a highly selective cycloaddition between an electron-rich diene and an electron-poor dienophile[217]. It is the oldest known click reaction and offers high yields, minimal side reactions and low energy requirements. Furthermore, water accelerates Diels-Alder reactions what can be of interest in biomedical applications. However, longer reaction times are an disadvantage of this system.

The thiol-Michael type addition in Figure 1.11 with maleimides (bottom) is often ex-

ploited for protein conjugation and one example of different thiol click chemistries[218]. In this reaction, which is often base catalyzed, an electron-deficient ene-species is added to a thiol component in a one-pot process. This method shines with its simplicity. Though some cross-reactivity and the susceptibility of free thiols to disulfide bond formation via oxidation limits its efficiency.

## 1.2.3. Calculation of Chemical Parameters from the Characterization of Single Polymer Chains

The later introduced AFM based single molecule force spectroscopy (SMFS) enables the determination of chain lengths from surface-initiated (SI) polymerizations. With this parameter, that is usually hard to obtain, interesting characterizations of polymer brushes are possible, such as polymer weight distributions and grafting densities.

**Molecular Weight and Polydispersity**   The molar mass of a polymer chain $M_i$ is calculated from the contour length $l_c$ as

$$M_i = M_{mono} \frac{l_c}{l_{mono}} \tag{1.1}$$

with $l_{mono}$ as monomer length and $M_{mono}$ as molar mass of monomer.

The number averaged molar mass $M_n$ and the mass averaged molar mass $M_w$ is defined[219] as:

$$M_n = \frac{\sum_{i=1}^{f} N_i M_i}{\sum_{i=1}^{f} N_i} = \frac{1}{n} \sum M_i \tag{1.2}$$

$$M_w = \frac{\sum_{i=1}^{f} N_i M_i^2}{\sum_{i=1}^{f} N_i M_i} = \frac{\sum M_i^2}{\sum M_i} \tag{1.3}$$

with $n$ as the total number of measured polymer chains, the total number of fractions $f$ and $N_i = 1$ in the case of SMFS measurements (see 1.3.3) – which means fractions of single polymer chains.

The polydispersity Đ is an index for the width of the molecular weight distribution and can be calculated as

$$Đ = M_w / M_n \tag{1.4}$$

**Grafting Density**   Combining the contour length $l_c$ with measured film thickness $d$ of the dry polymer brush, the grafting density $\Gamma$ can be derived as

$$\Gamma = \frac{molecules}{area} = \frac{area \cdot d \cdot \rho}{area \cdot \frac{l_c}{l_{mono}} \cdot \frac{M_{mono}}{N_A}} = \frac{d\rho l_{mono} N_A}{l_c M_{mono}} \tag{1.5}$$

with polymer bulk density $\rho$ and Avogadro constant $N_A$ (see also [220]).

### 1.2.4. Overview of Systems to Study Cell Response to Stiffness

This overview follows some good reviews that cover material systems to study cell mechanobiology[94, 221, 222, 223].

**Hydrogels from Extracellular Matrix Components** Hydrogels are polymeric porous networks with a high hydrophilicity. Due to their high flexibility and water content similar to natural tissues, they are often used as scaffolds in tissue engineering. They can be used as flat substrates (2D hydrogels) or as 3D microenvironments for cells and their porosity can be utilized for the supply with nutrients or growth factors.

Purified extracellular matrix components are one source for the fabrication of hydrogels. Glycoproteins such as collagen and fibrin[224], gelatin[225] or Matrigel[48] could be physically or chemically cross-linked to form porous hydrophilic networks. Also sugars from the extracellular matrix such as hyaluronic acid[67] were utilized for hydrogels.

These components offer a physiological environment for *in vitro* studies and were the first used materials to suggest an impact of stiffness on cell functionality. However, they have a poorly defined composition due to their high polydispersity (when starting from purified extracellular matrix components, e.g. collagen, and not the basic structural unit tropocollagen). Moreover, they present many different biological and physical cues which are often coupled together: Raising the component concentration enables a limited increase in stiffness but also a higher concentration of adhesion ligands while increased cross-linking reduces adhesion ligand availability.

Another drawback is their limited tunability of stiffness from less than 100 Pa up to very few kPa[221]. One exception are hydrogels based on hyaluronic acid. Many functional groups along the polymer backbone allowed a fine adjustment of cross-linking to achieve a stiffness from 4 kPa to 95 kPa. Though some hyaluronic acid hydrogels owned high degradation rates[67].

**Hydrogels from Other Natural Resources** The two polysaccharides alginate and agarose can be extracted from algae. Similar to hyaluronic acid, an abundance of functional moieties enables cross-linking or modification with bioactive molecules. Thus, their stiffness could be tuned in a wide range[66] comparable to hyaluronic acid. As they jellify under mild conditions, an easy retrieval of encapsulated cells from such 3D matrices is possible[226].

Biofunctionalization is necessary due to their poor cell adhesion properties. Furthermore, they lack stability and degradation rates are hard to control.

**Hydrogels from Polymers** Polymeric substrates are highly tunable in terms of molecular weight and offer modification of stiffness from the density of cross-links while density of adhesion ligands is altered independently.

Two typical and widely used synthetic materials for hydrogels are PAAm[55, 62, 227] and polyethylenglycol (PEG) hydrogels[73, 46]. However, these materials do not support cell adhesion and are often coated with extracellular matrix proteins that can introduce new mechanical cues. In combination with changing porosity caused from cross-linking, stiffness tuning in these hydrogels was accompanied with changes in topography as well as differences in protein tethering[61].

In contrast to PAAm, unpolymerized parts of PEG hydrogels are non-cytotoxic. Thus, they were used for the encapsulation of cells in three dimensions[65]. However, these systems have different disadvantages, such as osmotic gradients.

**Hydrogels from Polymeric Biomaterials** The development of polymeric biomaterials with defined structure and properties were enabled with the progress of recombinant protein expression and advanced synthetic polymer chemistry[228]. Some are also exploited for tissue engineering and mechanosensitivity studies.

Hydrogels from recombinant polypeptides, such as elastin-like or resilin-like polypeptides as well as self-assembling peptides, are an attractive choice for biological applications due to their monodispersity and biocompatibility.

An independent control of matrix stiffness and adhesiveness was achieved with a 3D self-assembling peptide hydrogel[229]. However, it has to be considered that those systems displayed changing fiber structures[230].

While elastin-like polypeptides allowed the independent tuning of stiffness and ligand density[231], such systems suffered from changing pore sizes when stiffness is altered via cross-linking[232]. Furthermore, they offered a limited stiffness range of very few kPa[231].

All in all, these are highly elaborate systems for mechanosensitivity studies with stiffness decoupled from adhesiveness, but they still present slightly changing structural cues from changing topographies.

**Beyond Hydrogels** Although hydrogels offer good properties for mechanosensitivity studies, other systems were developed or have to be considered for future uses.

**Elastomeric PDMS Substrates** Substrates based on PDMS with different base to curing agent ratio were also often utilized to study the influence of stiffness on cell functions [62, 61, 69]. They appear smooth to cells as they do not possess the problem of changing porosity. The fouling of PDMS[233] and adsorbtion of small molecules[234] is pro and con alike: Cell culture could sometimes be performed without coating or biofunctionalization, but medium composition could change in an uncontrolled way[235].

**PDMS Microposts** Micromolded elastic micropost arrays from PDMS are an interesting system for the modulation of substrate stiffness[236, 72], e.g. to decouple stiffness from spread area[237]. As displayed in Figure 1.12, right, the effective Young's modulus

can be tuned spanning over a 1000 fold range with a change of pillar height alone, keeping adhesive contact geometry (from surface area and micropost density) and material properties constant. Nevertheless, it has to be kept in mind that the microposts display a different topographical signal than flat surfaces.

**Fibrous Meshes**   Fibrous networks with high porosity, a structure similar to the extracellular matrix, can be fabricated via electrospinning and their application in tissue engineering is increasing[238]. Although it can be performed with synthetic as well as natural fibers and used for many different cell systems, their utilization in mechanosensitivity studies is limited.

An influence of substrate stiffness on the differentiation of MSCs[239, 240] or the proliferation and migration of fibroblasts[241] was reported. However, the tunability in stiffness was restricted and accompanied with changes in porosity or composition.

**Thin Films**   Dry coating[128, 152] or multiple adsorptions and consecutive cross-linking of polyelectrolytes[242] are simple methods for the fabrication of thin layers, though they are rarely used for mechanosensitivity studies.

The elasticity of a coating with tropoelastin compared to cross-linked or truncated tropoelastin was characterized in terms of contour length of unfolded proteins adsorbed to the substrate[128]. However, this setup displayed limited tunability for substrate elasticity and it was accompanied with changes in biological cues. Films from silk-elastin blends could be tuned in their stiffness by variation of composition[152]. Beside biological cues, also topography was altered in this system.

Polyelectrolyte multilayer films are an alternative to produce films of controlled stiffness[243]. One example is the covalent cross-linking after layer-by-layer deposition of polyelectrolytes. This allowed the variation of Young's modulus from a few to hundreds of kPa dependent on the degree of cross-linking[242]. Drawbacks are toxic cross-linking agents, difficult control of the distribution of cross-links via diffusion and a time-consuming process.

**Polymer Brushes**   Although polymer brushes have found many applications in the biomedical field[208, 206], only few publications reported their utilization in mechanosensitivity studies.

The group of Schönherr et al. developed a nice system of tunable polymer brushes that they used for cell studies. They fabricated PAAm brushes by SI ATRP and tuned the Young's modulus of the brush via cross-linking[244] (at this point, the borders between polymer brushes and hydrogels are arguable). For the decoupling of stiffness from signaling, block-copolymers were produced with a thin block of RGD-functionalized PAAm on top with constant RGD concentration[245]. Young's modulus varied from 0.6 kPa to 3.6 kPa

and resulted in a lower number and smaller projected cell area of fibroblasts adherent on soft substrates than on stiff ones.

Other groups could make only qualitative statements on the stiffness as they characterized the polymer brushes only in terms of thickness[246] or polymer weight from ungrafted chains in solution[247] and often lacked control of grafting independent from the size of the polymer[248]. Results were in general less cell adhesion on thicker brushes[249] and once cells that were more elongated on substrates without cross-linking[247].

Another group determined the lateral deformation of polymer brushes, which correlated with brush thickness[64]. MSCs displayed a decrease in cell area and a small tendency for fewer cells with increasing lateral strain of the brush. Furthermore, focal adhesion decreased in size and become more rounded.

Up to date, only one group characterized single polymer chains of brushes and correlated it with cellular behaviour[250]. Attwood et al. grafted PEG chains of three different lengths onto substrates and covalently modified them with RGD. "Tether" or contour length was determined as 10 nm, 40 nm and 320 nm. The cell spread area and surface density decreased with longer tether lengths and focal adhesion were smaller and shorter. With the aim of building a bridge between their experiments and mechanosensitivity studies on hydrogels, they developed a model for tether lengths being perceived similar to substrate stiffnesses.

## 1.3. Mechanical Characterization of Cell Culture Substrates

Speaking of mechanosensation, *stiffness* is the mechanical parameter whose influence on cells has been investigated the most. However, this term has often been used imprecisely in the biomechanical community. This was the case when stiffness is treated as equivalent with Young's modulus what holds only true under certain circumstances[251].

Stiffness (sometimes also termed rigidity) is the resistance to deformation of a structure under load, or expressed in a formula:

$$stiffness = \frac{deformation}{load} \tag{1.6}$$

With this general definition, several stiffnesses can be named depending on the shape and boundary conditions of a measurement. One can define stiffness for an elastic spring, for the elongation of a rod, bending of a beam, torsion of a rod or shearing of a body.

However, only in the case of uniaxial normal stress $\sigma = \frac{F}{A}$ (see Figure 1.12, left) for a body with constant cross-sectional area $A$ under the force $F$ with a change in length $l$ defined as strain $\epsilon = \frac{\delta l}{l}$, the Young's modulus $E$ can be used as an exact equivalent for stiffness with

$$E = \frac{\sigma}{\epsilon} \tag{1.7}$$
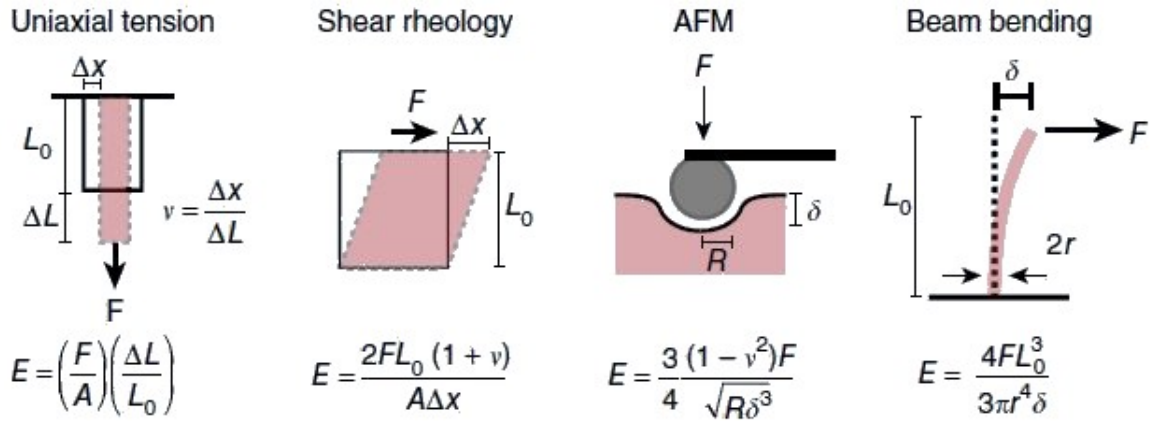
Figure 1.12.: Common methods for the determination of Young's modulus. With permission from [253].

what is also known as Hooke's law. The difference between these two terms can also be made clear by saying that the Young's modulus is an intensive property of a material while stiffness is an extensive parameter also dependent on the measurement mode. For some materials, the situation is even more complicated due to time-dependent behavior when viscose flow occurs[252].

Under this point of view, it becomes clear that the definition of stiffness has to be precisely checked for any mechanosensitivity study. Moreover, it can be questioned whether a macroscopically determined parameter is always the best choice to define a material's property. The load that a cell applies to a structure is often very different from the load used to characterize a material. In addition, tissues consisting of a fibrous network of proteins such as the extracellular matrix introduced a length-scale dependency to their mechanical properties as individual fibers are much stiffer than an overall hydrogel[253].

Thus, measurement techniques for the determination of very local material properties have to be considered[62]. With the idea of one cell receptor pulling at one molecule and probing its specific mechanical properties, techniques to measure the forces of single molecules come into play.

This section gives a short overview of the stiffness measurement of a bulk structure and a more detailed introduction into the mechanics of single molecules.

### 1.3.1. Techniques for the Measurement of Mechanical Bulk Properties

Uniaxial tensile testing as depicted in Figure 1.12, left, is a standardized method for the measurement of the Youngs's modulus $E$[254]. Bone-shaped samples with a defined cross-sectional Area $A$ are placed into a testing machine that slowly extends them until fracture while measuring elongation against the applied force. This method delivers elastic
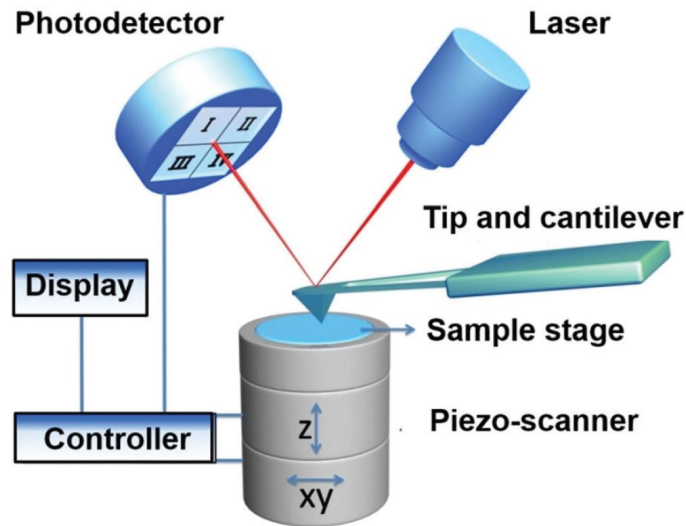
Figure 1.13.: Schematic view for the setup of an AFM. With permission from [257].

parameters as well as information about plastic deformation. However, it is rarely used for the very soft materials of cell culture substrates due to difficulties in gripping compliant and hydrated samples.

Shear rheology and indentation in Figure 1.12, middle, are more commonly used for tissue culture materials. For rheology measurements, samples are placed between two plates that apply an oscillating shear. Frequency dependent measurements allow the characterization of elastic as well as viscoelastic properties. Assuming an isotropic material, the resulting shear modulus can be easily transformed to Young's modulus[253].

Indentation experiments are carried out with a probe of known geometry that is brought into contact with a sample. Recording the load-depth profile, the Young's modulus can be calculated with the use of contact theories such as Hertz[255] or Johnson-Kendall-Roberts model[256]. Thereby, the measurements require minimal sample preparation and only small restrictions on sample geometry. The length scale of this technique can be easily adapted. In this way, hydrogels have been studied from the $nm$ up to the $mm$ scale[254].

Beam bending as shown in Figure 1.12, right, is not utilized for the characterization of hydrogels. However, its theory is used for a different system to study mechanosensitivity: The Young's modulus $E$ of microposts is easily tuned by their length without the change of displayed contact area and form[236].

## 1.3.2. Atomic Force Microscopy (AFM)

The AFM[258] is a powerful and versatile tool for different scientific fields. It can provide images from surfaces in a vacuum with atomic resolution but also robust measurements on a lab bench in the $nm$ up to $\mu m$ range. The AFM is applicable to all material classes and can be used on living cells[259] or even to manipulate single atoms[260].

The setup and working principle is displayed in Figure 1.13. The interaction of a very sharp tip with the sample surface forces a deflection of the cantilever[258]. This small movement is recorded by a photodetector that captures the reflection of a laser from the back of a cantilever. Calibration of its spring constant allows calculation of the respective force[261, 262].

Keeping the cantilever displacement at a constant value, scanning of the sample surface gives an image of its topography. Sample movement in $z$ direction allows force measurement for the compression of a material or its stretching. Thus, very local measurements of the Young's modulus via indentation are possible that can register inhomogeneities or gradients in material properties[263, 264]. The unfolding of single molecules can be measured, too, as will be introduced in the following section.

### 1.3.3. Measuring the Mechanics of Single Molecules

Forces play a fundamental role in many chemical and biological processes, often depending on the interaction of a single molecule with another one, being it chemical bonds or the interplay between cell receptors and ligands. Thus, a measurement of these processes at a single molecule scale can deliver valuable insights and lead to an understanding of mechanical mechanisms in a bottom-up approach.

Examples for single molecule studies on inter- and intramolecular interactions are the folding of proteins and investigation of conformational entropy, force-induced chemical and enzymatic reactions, macromolecular assembly, molecule adsorption and transport as well as ligand and inhibitor binding [265, 266, 267, 268, 269, 270].

Different techniques have been developed for the investigation of single molecule mechanics. What follows is an overview with a special emphasize on AFM based SMFS.

**Optical Tweezers** The radiation pressure of a focused laser beam exerts force on a bead or particle[271]. The force applied to the bead is proportional to its displacement from the center of the trap. Bead position can be detected from interferometry of the light scattered from the bead and unscattered light.

By tethering a protein to a particle, this can be moved in three dimensions and force dependent changes in protein activity or bond lifetime can be measured. Drawbacks are the limitation to highly purified samples to avoid optical perturbations, lack of sensitivity to the trapped particle, local heating, optical damage as well as limited force and displacement ranges[272].

**Magnetic Tweezers** This technique resembles optical tweezers in a point that a magnetic particle is controlled with a magnetic field[271]. In the case of a superparamagnetic particle, the applied force is proportional to the gradient of the magnetic field. Particle position is measured with video based detection.

A drawback of this technique is either the lack of manipulation ability when permanent magnets are used or the significant heat from electromagnets[272]. Furthermore, the sensitivity is limited due to the video based detection.

**Molecular Force Probes**   These are based on the fluorescence resonance energy transfer (FRET)[271]. The relative transfer of energy between an acceptor and donor fluorophore corresponds to their distance. Connecting the two fluorophores with an elastic linker defines the mechanical properties of this construct. An *in vitro* calibration of the fluorescence intensity dependent on the applied tension allows the later measurement of forces *in vivo*, when the probe is incorporated into a protein of interest[273]. However, the sensor has to be designed in a way that does not disturb the protein function. Furthermore, the measurable force is limited to a very narrow window depending on the elastic linker[271].

**AFM based single molecule force spectroscopy**   Force measurement is achieved by the attachment of a surface bound molecule to an AFM tip. Thus, the corresponding cantilever is deflected upon retraction[272]. While extension of the molecule is determined from the movement of piezo-electric actuators, force is proportional to the bending of the cantilever with known spring stiffness.

Two main modes of operation are possible for AFM based SMFS: Force-extension measurements determine the force during retraction of the AFM tip with a constant speed to measure the unfolding of bound molecules or molecular bonds[266]. In force-clamp experiments, the applied force is fixed and the extension over time is measured what proves useful for mechanochemistry, e.g. when the effect of force on enzyme activity is investigated[274, 268, 275].

The attachment of the molecule to the tip is possible via physisorption or chemisorption[276, 272]. While being the simplest way for attachment, unspecific adsorption delivers no control over the attachment point. Antibodies or functionalizations with streptavidin/biotin can be utilized for the specifical binding of a molecule at its both ends. However, their contribution to the elastic response of the construct has to be taken into account. Hexahistidine/Ni-nitrilotriacetic acid or gold/SH-group[277] interactions are mechanically very strong, but also sensitive to reducing agents. To ensure the binding of only one molecule, its surface concentration is very diluted and statistical analysis is performed with hundreds or thousands of measurements and the rejection of any unspecific measuring events[272].

The simple and rapid sample preparation is a great advantage of AFM based SMFS[272]. Furthermore, biological samples can be measured under near physiological conditions. The large size and relatively high stiffness of cantilevers are a drawback of the AFM as this defines a lower bound to the detectable force range. In addition, the specificity is a problem in AFM pulling experiments as the discrimination of interactions with the molecule of interest from interactions with non-specific ones or inappropriate contacts, i.g. binding at
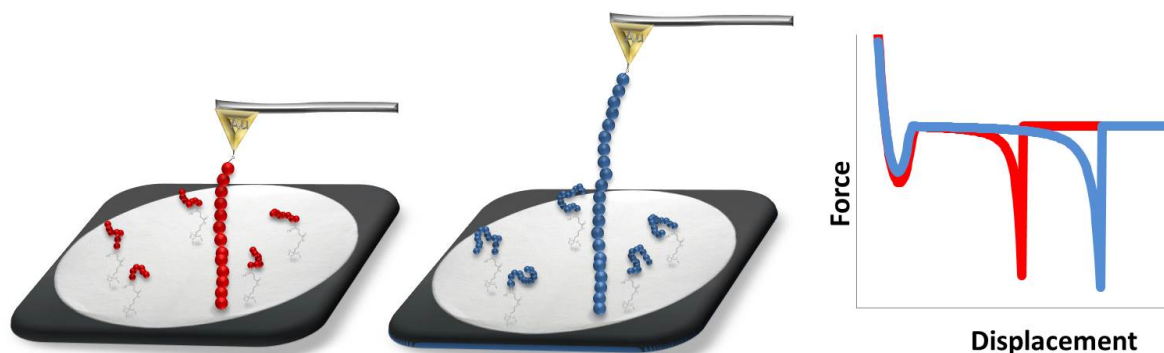
Figure 1.14.: Scheme of SMFS of two molecules with different contour lengths and the corresponding force-extension curves. Reprinted with permission from [278]. Copyright 2016 ACS.

intermediate positions, can be difficult[272].

Stretching of a molecule can be measured in a very straightforward manner. The AFM tip and sample surface are approached with piezo-electric actuators followed by pressing the tip into the sample surface with a predetermined force. Subsequently, the tip is retracted and the cantilever bends resulting from being tethered via the molecule to the surface. A cantilever calibration is necessary for the calculation of force, e.g. using thermal vibrations[261, 262].

Figure 1.14 depicts the typical unfolding curves of two molecules with different lengths. The force-extension curve displays a peak of unspecific adhesion when starting the retraction. This is followed by a linear increase of force with a minimal slope which follows the Equation A.9 for rubber elasticity as derived in Appendix A.1. A non-linear rise of force occurs when the extension draws closer to the complete length of the molecule. This part can be fitted to various mechanical models for polymer chains as explained in the following section for the purpose of characterizing the molecule length and its stiffness. Measurement is closed with a rupture event that gives the bond strength of the employed system[263, 268].

A variant of SMFS is *Single Cell Force Spectroscopy*. In this case, a cell is bound to a tipless cantilever with a biocompatible glue. This allows to measure the adhesion force of single cells with different substrates[279].

## 1.3.4. Models for the Description of Polymers and Proteins

The equilibrium state of a polymer chain is the random coil with maximum entropy. A huge number of configurations are taken over a period of time due to thermal fluctuations. These configurations are formulated with statistical mechanical models to specify the average properties of the polymer chain. Some of these models for the elasticity of single polymer chains to describe their force-extension behavior are outlined in the following section.
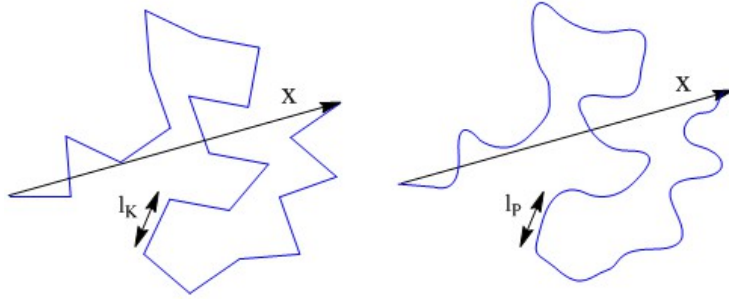
Figure 1.15.: Schematic representation of the freely jointed chain (FJC) and worm-like chain (WLC) models. The FJC consists of rigid links with free joints between them (left). The WLC is a continuous, but curved filament with resistance to bending. The persistence length $l_p$ is the average length over which the direction becomes random (right). $x$ is the end-to-end distance of the polymer chain. With permission from [282].

**Freely Jointed Chain (FJC) Model** The FJC model[280, 281] considers a polymer as a series of $n$ segments with a length of $l_K$ (*Kuhn length*), often also denoted as $a$), which are joined at freely revolving pivots as depicted in Figure 1.15, left. This leads to a fully extended chain length or contour length $l_c = nl_K$.

Several assumptions are made in the FJC model for polymer chain in the absence of external constraints:

- chain follows a *random walk*, i.e. all bond angles are equally probable and uncorrelated to all other bond directions

- free rotation at the bond junctions

- interactions of the chain with itself are excluded, e.g. volume effects

The elastic restoring force $F$ during extension of a single polymer chain can be derived from the configurational entropy and the use of non-Gaussian chain statistics as described in Appendix A.1. Result is the formula[282]:

$$x(F) = l_c \left[ \coth(\frac{Fl_K}{k_BT}) - \frac{k_BT}{Fl_K} \right] \tag{1.8}$$

with the Boltzmann constant $k_B$ and the absolute temperature $T$.

This formula reduces to the solution from Gaussian statistics in Equation A.9 for small displacements ($F_{elastic}l_K << k_BT$). Approaching the contour length $l_c$, the force converges and a finite extensibility is reached, meaning that the chain becomes harder and harder to stretch when it straightens out[283].

**Extensible Freely Jointed Chain (E-FJC) Model**  The E-FJC model takes also enthalpic deformation of the chain segments into account by modeling them as elastic springs[284]. The stretch modulus $\kappa$ is introduced as an additional fit parameter that is the spring constant of single chain elements. This gives the possibility of end-to-end distances $x$ being larger than the contour length. The formula of the FJC model is modified to[284]:

$$x(F) = l_c \left[\coth(\frac{Fl_K}{k_B T}) - \frac{k_B T}{Fl_K}\right] \left(1 + \frac{F}{\kappa L}\right) \tag{1.9}$$

This model eliminates the finite extensibility of the FJC. Instead, the fitting curve approaches a constant slope value and a reduced force at high deformations[283].

**Worm Like Chain (WLC) Model**  In the WLC model[285, 282], the polymer chain is a continuous and curved filament (*worm*) as depicted in Figure 1.15, right, and it describes an intermediate state between a rigid rod and a flexible coil that is used for stiff polymers. The direction of curvature is assumed to be random and the bonds to be freely rotating.

The WLC possesses a resistance to bending expressed in the parameter of persistence length $l_p$. This is the average length over which the direction becomes random. Mathematically, it describes the decay in correlations of the tangent vectors of subsequent chain segments. Appendix A.2 demonstrates that persistence length $l_p$ correlates to half the Kuhn length $l_K$ for contour lengths $l_c$ much greater than the persistence length.

For polymers, a change of monomer tunes the persistence length $l_p$ only to a slight degree[286]. Introduction of rigid secondary structures such as alpha-Helices or beta-sheets[149] or double strands as for deoxyribonucleic acid (DNA) ($l_p = 50\,\mathrm{nm}$[287]) are necessary to significantly increase this value.

There is no analytical solution for the extension of the WLC formula, it can only be calculated numerically (as shown here[287, 288] and roughly sketched in Appendix A.2). However, a good interpolation formula was developed[287] that covers the analytical asymptotic solutions for small and large forces:

$$F(x) = \frac{k_B T}{l_p} \left(\frac{1}{4(1 - \frac{x}{l_c})^2} - \frac{1}{4} + \frac{x}{l_c}\right) \tag{1.10}$$

where $x$ is the distance of the AFM tip from the surface or the polymer end-to-end length, $k_B$ is the Boltzmann constant, $T$ the absolute temperature, $l_p$ the persistence length and $l_c$ the contour length.

The interpolation formula can differ up to $10\,\%$ at extensions roughly half the contour length $l_c$[289]. However, the force rises sooner for the stiffer WLC than for the FJC and the divergence is smaller as the polymer is enabled to bend continuously rather than only at specific joints. For small displacements, the formula converges to the form of classical rubber elasticity as shown in Equation A.9. At large displacements, the accessible conformations are reduced to quadratic fluctuations of the straightened chain leading to an asymptotic increase of the force at extensions close to the contour length[283].

**Correlation of Microscopic and Macroscopic Stiffness**   Applying beam mechanics to polymer chains, the persistence length $l_p$ can be correlated to the flexural rigidity of a beam[290]. The Young's modulus $E$ can be then calculated as

$$E = \frac{l_p k_B T}{I} = \frac{4 l_p k_B T}{\pi r^4} \tag{1.11}$$

with the moment of inertia $I$ and the radius of the polymer molecule $r$.

## 1.4. Aim of the Thesis

### Development of a New Polymer Model System

In the course of this theses, a new model system for mechanosensitivity studies with cells shall be developed. It should be a defined synthetic system with a complete control over the mechanical properties which are decoupled from biological and topographical cues.

The model system aims to overcome certain flaws from previous systems utilized in mechanosensitivity studies. Elasticity should be established as the only variable parameter and not accompanied with changes in roughness and other topographical cues, chemical reactivity, hydrophobicity or biological activity. For this purpose, its structure should display a small complexity. Furthermore, although biocompatibility is a prerequisite, ideal culture conditions are of secondary interest, i.e. it does not have to be a 3D culture system to mimic *in vivo* conditions.

The idea of this thesis is the development of a biofunctionalized polymer brush with the contour length of the polymer chains as the only variable. This inherits an asymmetry in the behavior under compression or tension but with the extensibility in the event of cells pulling at the substrate being tuned.

The contour length is a parameter that can be easily compared to other relevant parameters. On the one hand, a model is available that corresponds short and long contour lengths to the reaction of stiff and soft substrates, respectively. On the other hand, relations to length scales of cell receptors can be drawn.

In order to guarantee a cell relevant range of the utilized contour lengths, the polymer chains are build after the example of tropoelastin - an exceptional elastic biomolecule - and mimics the contour lengths of this protein with and without cross-linking. Furthermore, literature is available to compare cell behavior on tropoelastin with the polymer model system.

Finally, a good reproducibility under 'Good Manufacturing Practice' (GMP) conditions is ensured with a fully synthetic - thus xenogenfree - system with low protein absorbance and serum free culture conditions.

## Characterization of Chemical and Mechanical Parameters

The SI-RAFT polymerization of pHEMA and its subsequent biofunctionalization via click reaction is proofed with chemical analysis via x-ray photoelectron spectroscopy (XPS) and time of flight – secondary ion mass spectrometry (ToF-SIMS) measurements (Section 3.2).

Subsequently, the mechanics in terms of contour length of surface bound polymer molecules is characterized via SMFS (Section 3.3) and compared to own experiments (Section 3.1) and literature on tropoelastin. Furthermore, surface roughness and grafting density is analyzed to validate the substrate extensibility as the only changing parameter.

## Validation in Mechanosensitivity Studies

The functionality of the pHEMA model system is demonstrated in mechanosensitivity studies with fibroblasts from which an strong dependence of cell morphology on mechanical parameters of a substrate is known (Section 3.4.1).

Furthermore, experiments with HSPCs should clarify whether the proposed effect of substrate extensibility in terms of contour length on the proliferation of undifferentiated cells can be confirmed (Section 3.4.2).

# 2. Materials and Methods

## 2.1. Materials

**Chemicals**   The chemical synthesis and analysis was achieved with the chemicals listed in Table 2.1. HEMA was purified by passing through basic alumina to remove hydroquinone and monomethylether inhibitors. The free radical initiator AIBN was recrystallized twice from methanol. Lyophilized tropoelastin was diluted within its serum vial with a sterile $0.25\,\%$ glacial acetic acid solution for a stock solution with $1\,\mathrm{mg\,mL^{-1}}$ tropoelastin. Further dilution for experiments were done with phosphate-buffered saline (PBS). All other chemicals were used as received.

Where MilliQ water was used, deionised water was purified with an Arium Pro UF/VF purification system (Sartorius, Göttingen, Germany).

The pHEMA samples were synthesized on different substrates depending on the later use of the surfaces. Silicon wafers ([100], p-doped with B, International Wafer Service, Inc., Colfax, USA) were functionalized for AFM experiments, while glass cover slips (Karl Hecht GmbH, Sondheim/Rhön) with a diameter of $15\,\mathrm{mm}$ were used in the case of mechanosensitivity and cell adhesion tests.

Dr. Hubert Kalbacher (Interfaculty Institute of Biochemistry, University Tuebingen) kindly synthesized and provided the C-terminus of tropoelastin functionalyzed with a maleimide group connected via $\beta$-alanin (Figure 2.1) as well as N-maleoyl-$\beta$-alanine-SGS-GRKRK (SGS inserted for better handling during synthesis), the peptides VGVAPG, GRKRK, and the C-terminus of tropoelastin without functionalization. He used the Fmoc/$t$Bu-strategy with a multiple Synthesizer Syro (MultiSynTech, Witten). The peptides were delivered freeze dried. For cell test, aliquots with stock solutions of $2\,\mathrm{mM}$ were produced and stored at $-20\,^{\circ}\mathrm{C}$.

**Cell Laboratory Equipment**   Table 2.2 lists the equipment used in cell laboratory experiments.

**Media, Buffer and Solutions**   The buffers in Table 2.3 were used in the isolation of HSPCs and were produced beforehand. Table 2.4 lists all chemicals, media and solutions used for cell experiments. The fetal bovine serum (FBS) heat inactivated for $30\,\mathrm{min}$ in a water bath at $56\,^{\circ}\mathrm{C}$ prior to use.

Table 2.1.: All chemicals that were used for the chemical synthesis and analysis

| Chemicals | Supplier |
| --- | --- |
| (3-aminopropyl)triethoxysilane (99%) | Sigma-Aldrich, Darmstadt |
| 4-cyano-4-(phenylcarbonothioylthio)-pentanoic acid (97%) | Sigma-Aldrich, Darmstadt |
| 1-(3-dimethylaminopropyl)-3-ethyl-carbo-diimide hydrochloride (98+%) | Sigma-Aldrich, Darmstadt |
| dichloromethane (99.5%, stabilized) | Sigma-Aldrich, Darmstadt |
| Ethanol (AnalaR NORMAPUR, absolute) | VWR, Darmstadt |
| 1,4-dioxane (ReagentPlus 99+%) | Sigma-Aldrich, Darmstadt |
| Ethyl acetate (ACS reagent, 99.5%) | Sigma-Aldrich, Darmstadt |
| Acetone (ACS reagent, 99.5%) | Sigma-Aldrich, Darmstadt |
| Toluene (ACS reagent, 99.9+%) | Merck, Darmstadt |
| 2-hydroxyethyl methacrylate (97%) | Sigma-Aldrich, Darmstadt |
| 2,2-bis-azobis-isobutyronitrile (98%) | Sigma-Aldrich, Darmstadt |
| $MgSO_4$ | Sigma-Aldrich, Darmstadt |
| dimethylformamid (ACS reagent) | Merck, Darmstadt |
| tetrahydrofuran (ACS reagent, 99+%) | VWR, Darmstadt |
| Hexylamine (99+%) | Sigma-Aldrich, Darmstadt |
| Triethylamine (99.5+%) | Sigma-Aldrich, Darmstadt |
| dimethyl Sulfoxide (ReagentPlus 99+%) | Sigma-Aldrich, Darmstadt |
| N,N-dimethylacetamide (99.6%, extra pure) | Acros Organics, Geel, Belgium |
| Human tropoelastin, lyophilized | Advanced BioMatrix, San Diego, USA |
| phosphate-buffered saline | Sigma-Aldrich, Darmstadt |

**Cells**   Different cells were used in the course of the thesis:

**KG-1a cell line**   The human KG-1a cell line is derived from leukaemia cells [291]. They have a similar receptor repertoire as HSPCs, e.g. they express CD34 [292, 293]. They can be kept in cell culture and are always available, hence they can be utilized as a model cell line for HSPCs and are used for preliminary experiments. KG-1a cells were purchased from the Leibniz Institute DSMZ (German Collection of Microorganisms and Cell Cultures, Braunschweig).

**REF52 Cell Line**   REF52 is an established fibroblast cell line from rat embryos and it is used as a fibroblast model system. Due to their high adhesion and branching, they are used for demonstrating cell-material interactions[294]. REF52 cells were obtained from Dr. Dr. Ada Cavalcanti-Adam (Max Planck Institute for Medical Research, Heidelberg).
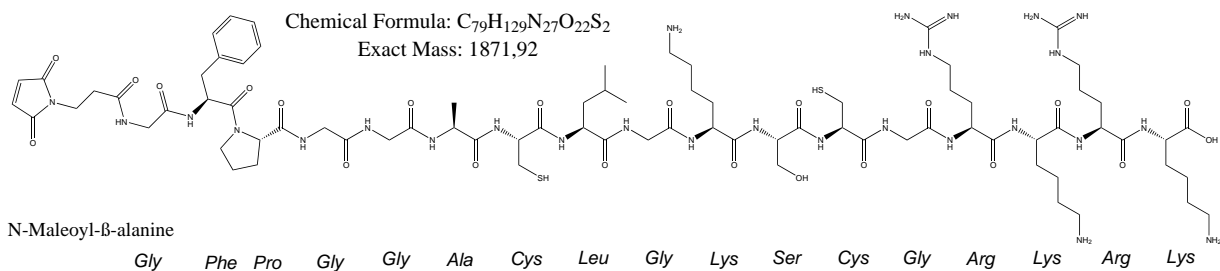
Figure 2.1.: C-terminus of tropoelastin functionalized with maleimide (N-maleoyl-$\beta$-alanine-GFPGGACLGKSCGRKRK).

Table 2.2.: Equipment that was used for cell experiments

| laboratory equipment | Supplier |
| --- | --- |
| 50 mL and 15 mL centrifuge tubes | Greiner Bio One, Frickenhausen |
| MS columns | Myltenyi Biotec, Bergisch-Gladbach |
| Neubauer chamber | Paul Marienfeld GmbH, Lauda-Königshofen |
| MACSMix™ tube rotator | Myltenyi Biotec, Bergisch-Gladbach |
| MiniMACS™ separator | Myltenyi Biotec, Bergisch-Gladbach |
| CELLSTAR® TC 250 mL Cell Culture Flask | Greiner Bio One, Frickenhausen |
| CELLSTAR® TC 250 mL Suspension Culture Flask | Greiner Bio One, Frickenhausen |
| CELLSTAR® 35 mm petri dish | Greiner Bio One, Frickenhausen |
| CELLSTAR® 96 well and 24 well culture plates | Greiner Bio One, Frickenhausen |
| 8-chamber slides with glass bottoms | Sarstedt, Nümbrecht |

Table 2.3.: Buffers mixed for the isolation of HSPCs from UCB

| Buffer | Components |
| --- | --- |
| rinsing buffer | 2 mM ethylenediaminetetraacetic acid (EDTA) without $Ca_{2+}$/$Mg_{2+}$ in PBS |
| running buffer | MACS BSA Stock Solution (Miltenyi Biotec, Bergisch Gladbach) in rinsing solution, 1 : 20 ($V : V$) |
| erythrocyte lysis buffer | 1.5 M $NH_4Cl$ (Merck), 100 mM mM $NaHCO_3$ (VWR), 1 mM EDTA disodium salt (Sigma-Aldrich) in MilliQ water, pH set as 7.4 with 1 M NaOH |

Table 2.4.: All chemicals, media and solutions that were used for cell experiments.

| Material | Supplier |
| --- | --- |
| EDTA (1 %) without $Ca_{2+}/Mg_{2+}$ in PBS | Biochrom, Berlin |
| Trypanblau | Amresco LLC, Solon, USA |
| Lymphocyte separation medium | PromoCell, Heidelberg |
| FcR Blocking Reagent | Miltenyi Biotec, Bergisch-Gladbach |
| CD34 Micro Beads | Miltenyi Biotec, Bergisch-Gladbach |
| RPMI 1640 medium | Sigma-Aldrich, Darmstadt |
| DMEM 4500 g glucose | Sigma-Aldrich, Darmstadt |
| fetal bovine serum low in Endotoxin | Sigma-Aldrich, Darmstadt |
| bovine serum albumin | Sigma-Aldrich, Darmstadt |
| Penicillium Streptomycin | Sigma-Aldrich, Darmstadt |
| $MnCl_2$ | Sigma-Aldrich, Darmstadt |
| CyQUANT® Cell Proliferation Assay Kit | Thermo Fisher Scientific, Waltham, USA |
| Fibronectin from bovine plasma | Sigma-Aldrich, Darmstadt |
| Glutaraldehyde solution, 25 % in water | Sigma-Aldrich, Darmstadt |
| 1 M Tris buffer (pH 7.0) | Thermo Fisher Scientific, Waltham, USA |
| Paraformaldehyde | Sigma-Aldrich, Darmstadt |
| Triton™X-100 | Thermo Fisher Scientific, Waltham, USA |
| Alexa FluorÂő 488 Phalloidin | Thermo Fisher Scientific, Waltham, USA |
| DAPI | Thermo Fisher Scientific, Waltham, USA |
| Mowiol® | Sigma-Aldrich, Darmstadt |
| Hematopoietic Progenitor Expansion Medium DXF + Cytokine Mix E | PromoCell, Heidelberg |
| anti human CD34-PC5 (clone 581) | Beckman Coulter, Brea, USA |
| IgG1-PC5 (clone 679.1Mc7) | Beckman Coulter, Brea, USA |
| anti human CD38-FITC (clone HIT2) | Thermo Fisher Scientific, Waltham, USA |
| IgG1-FITC (clone P3.6.2.8.1) | Thermo Fisher Scientific, Waltham, USA |
| AbC™ Anti-Mouse Bead Kit | Thermo Fisher Scientific, Waltham, USA |
| IMDM with 2 % FBS | Stemcell Technologies, Grenoble, France |
| Methocult™ H4344 Classic medium | Stemcell Technologies, Grenoble, France |

**Primary HSPCs**  HSPCs are the stem cells that give rise to all the other blood cells. Primary HSPCs were isolated from umbilical cord blood (UCB) 24 h to 48 h after blood collection by positive selection for CD34 via magnetic activated cell sorting (MACS; Miltenyi Biotec, Bergisch Gladbach). The UCB was obtained from the Mannheim Cord Blood Bank (Mannheim) or the DKMS Cord Blood Bank (German Bone Marrow Donor Centre, Dresden). The informed agreement by the parents and the approval by the local ethics committee (Ethik-Kommission bei der Landesärztekammer Baden-Württemberg; B-F-2013-111) were obtained.

**AFM accessories**  Falcon$^{®}$ 50 mm x 9 mm (not TC-treated, tight-fit lid, Corning Inc., Corning, USA) petri dishes were used as sample holders. pHEMA samples were fixed with double sided tape and immersed in MilliQ water, while tropoelastin measurements were performed in PBS.

AFM imaging was conducted with TR400PSA cantilevers (Au reflex coated, nominal spring constant of $0.08\,\mathrm{N\,m^{-1}}$, tip radius of 20 nm, Olympus, Tokyo, Japan). TR400PB cantilevers (Au reflex/tip coated, nominal spring constant of $0.02\,\mathrm{N\,m^{-1}}$, Olympus, Tokyo, Japan) were utilized for SMFS measurements.

AFM indentation experiments were performed with HQ:NSC36/tipless/No Al cantilevers (nominal spring constant of $0.6\,\mathrm{N\,m^{-1}}$, Mikromasch$^{®}$, Sofia, Bulgaria). Silica spheres with a diameter of 7.6 μm were fixed to the cantilever with two component glue (UHU Plus Endfest 300, UHU, Bühl).

**Software**  AFM measurements and analysis was performed within IgorPro (WaveMetrics, Portland, USA) with an AFM plugin developed by Asylum Research (Santa Barbara, USA) and with the JPK Data Processing Software (JPK Instruments AG, Berlin).

Microscopic images of cells were aquired and processed with ZEN blue edition (Carl Zeiss AG, Oberkochen). Cell counting and analysis of cell morphology were done with ImageJ (now called Fiji)[295]. The Fiji plugins Skeletonize3D and AnalyzeSkeleton [296] were also used for this purpose. The cell morphology was visualized with Matlab (Mathworks, Natick, USA) and the Plugin PhenoPlot [297].

Flow cytometry data was analyzed with FlowJo (FlowJo,LLC, Ashland, USA). The significance of experimental data was calculated with Prism (GraphPad Software Inc. La Jolla, USA).

Table 2.5.: $^1$H-NMR analysis of the chain transfer agent

| $\sigma$ [ppm] | 0.64 | 1.23 | 1.65 | 1.94 | 2.40-2.65 | 3.3 | 3.83 | 5.91 | 7.36-7.95 |
|---|---|---|---|---|---|---|---|---|---|
| | t, 2H | t, 9H | m, 2H | s, 3H | m, 4H | m, 2H | q, 6H | s, 1H | m, 5H |

## 2.2. Chemical Synthesis

The development of the polymer model system was realized with Dr. Thomas Tischer (Institute for Functional Interfaces (IFG) in Karlsruhe). The biofunctionalization of pHEMA surface were achieved with Dr. Domenic Kratzer (IFG). The synthesis of the polymer surfaces was performed together with Dr. Thomas Tischer and Dr. Domenic Kratzer.

In the following course of the text, the nomenclature pHEMA x h will be used for substrates with HEMA that was polymerized for x hours, e.g. pHEMA 1 h for 1 h. The functional group can differ depending on the context the nomenclature pHEMA x h is used, with a thiol in the case of SMFS experiments, the C-terminus of tropoelastin where HSPCs are cultured or the amino acid sequence GRKRK where REF52 cells are used.

### 2.2.1. Synthesis of poly(2-hydroxyethyl methacrylate) (pHEMA) Functional Surfaces

**Synthesis of Chain Transfer Agent**  The chain transfer agent 4-(3-(triethoxysilyl)propyl-carbamoyl)-2-cyanobutan-2-yl benzodithioate was synthesized according to a literature procedure[298]. 4-Cyano-4-(phenylcarbonothioylthio)pentanoic acid (500 mg, 1.79 mmol, 1.2 eq ) and 1-(3-dimethylaminopropyl)-3-ethyl-carbodiimide hydrochloride (EDC) (343 mg, 1.79 mmol, 1 eq ) were dissolved in 100 mL of anhydrous dichloromethane (DCM). Subsequently, (3-aminopropyl)triethoxysilane (APTES) (419 mL, 1.79 mmol, 1 eq ) was added using a degassed syringe.

After 1 h reaction at ambient temperature, the reaction mixture was washed twice with 1 M HCl, thrice with saturated sodium hydrogen carbonate solution and finally thrice with brine. The organic phase was dried over MgSO$_4$. The solvent was evaporated to gain a viscous pink oil which was used without further purification. The purity was determined via $^1$H-NMR spectroscopy (400 MHz, CDCl$_3$, 25 °C) as listed in Table 2.5.

**Synthesis of RAFT Functional Surfaces**  Different substrates were used for the miscellaneous experiments. For AFM experiments, silicon wafers were cut into chips of roughly 1 cm$^2$. Fragile glass cover slips were only used where necessary. For cell culture experiments, glass cover slips with a diameter of 15 mm were utilized. The silanization of all substrates was achieved with the same reactions as described below. When the samples were aimed for SMFS analysis, a dilution of the chain transfer agent of $1 : 1,000$ ($V : V$) was selected.

The substrates were rinsed with ethanol, acetone and copious amounts of MilliQ water. After being dried in a stream of nitrogen, the substrates were activated by plasma cleaning ($O_2$-Plasma, 0.5 mbar, 200 W, 100 %, 10 min, Pico, Diener, Ebhausen). Subsequently, the surfaces were immersed in a solution of the chain transfer agent 4-(3-(triethoxysilyl)propyl-carbamoyl)-2-cyanobutan-2-yl benzodithioate (10 mg, 20 µmol) in 10 mL toluene. The reaction mixture was heated to 50 °C for 4 h and overnight at ambient temperature. The substrates were thoroughly rinsed with toluene, DCM and acetone and dried in a stream of nitrogen.

**Polymerization**    The RAFT agent functional surfaces were placed in sample vials with a rubber septum and freed from oxygen for 30 min by repeated vacuum/nitrogen cycles. A solution of HEMA (4 mL, 32.9 mmol, 1735 eq.), AIBN (3.1 mg, 0.019 mmol, 1eq.) with 4-cyano-4-(phenylcarbonothioylthio)pentanoic acid (5.4 mg, 0.019 mmol, 1 eq.) added as as sacrificial RAFT agent in a mixture of 15 mL dioxane and 15 mL MilliQ water was freed from oxygen by three freeze-pump-thaw cycles. Subsequently, 2 mL aliquots of the polymerization mixture were transferred to each vial using a degassed air-tight syringe.

The polymerization was carried out in a thermo-stabilized bath at 80 °C. After pre-determined time intervals, the polymerization was quenched by opening the corresponding vials and rapidly cooling in an ice-bath. The surfaces were rinsed with dimethyl-formamid (DMF), MilliQ water, acetone and ultimately dried under a flow of nitrogen. An aliquot of the polymerization mixture was extracted for determining the monomer conversion by $^1$H-NMR and the rest of the free polymer was precipitated in ice-cold tetrahydrofuran (THF) for size exclusion chromatography (SEC) analysis.

**Aminolysis of the pHEMA Functional Surfaces**    pHEMA functional surfaces were transferred into new sample vials with a rubber septum and purged with nitrogen. The reaction mixture was mixed by adding hexylamine (20 µL, 0.153 mmol) and triethylamine (20 µL, 0.143 mmol) to another sample vial with 5 mL of ethanol. It was freed from oxygen by blowing with nitrogen for 10 min. 1.5 mL of the reaction mixture was added to every surface. After shaking the vials for 3 h, rinsing with ethanol and acetone and subsequently drying in a stream of nitrogen, the samples were analyzed via AFM and ellipsometry.

## 2.2.2. Biofunctionalization of pHEMA

pHEMA samples for cell experiments were functionalyzed with the C-terminus of tropo-elastin. This synthesis step was conducted *in situ* with the aminolysis reaction.

pHEMA functional surfaces were transferred into new sample vials with a rubber septum and purged with nitrogen. 1 mg of the peptide maleimide construct (1 eq ) were dissolved in 10 mg dimethyl Sulfoxide (DMSO) and degassed. 1 mL aliquots of the polymerization mixture were transferred to each vial using a degassed air-tight syringe.

A stock solution of 9.5 µL hexylamine and 10 µL triethylamine in 4.5 mL of DMSO was mixed and degassed. 10 µL of this stock solution were added to the peptides in each vial, thus adding 3 eq of each amine. The reaction was allowed to take place for 3 h at ambient temperature. After rinsing with ethanol and acetone and subsequently drying in a stream of nitrogen, the samples were used for chemical analysis or cell experiments.

## 2.3. Chemical Analysis

The x-ray photoelectron spectroscopy (XPS) and time of flight – secondary ion mass spectrometry (ToF-SIMS) analysis was performed by Vanessa Trouillet at the Institute for Applied Materials (IAM) in Karlsruhe. size exclusion chromatography (SEC) and nuclear magnetic resonance (NMR) spectroscopy were conducted by Dr. Thomas Tischer (Institute for Functional Interfaces (IFG) in Karlsruhe). Dr. Domenic Kratzer (IFG) helped with the interpretation of chemical analysis data.

### 2.3.1. X-ray Photoelectron Spectroscopy (XPS)

XPS investigations were performed on a K-Alpha+ spectrometer (ThermoFisher Scientific, East Grinstead, UK) using a microfocused, monochromated $Al-K_\alpha$ X-ray source (400 µm spot size). The kinetic energy of the electrons was measured by a 180 deg hemispherical energy analyzer operated in the constant analyzer energy mode at 50 eV pass energy for elemental spectra. The K-Alpha+ charge compensation system was employed during analysis, using electrons of 8 eV energy, and low-energy argon ions to prevent any localized charge build-up.

Data acquisition and processing using the Thermo Avantage software is described elsewhere[299]. The spectra were fitted with one or more Voigt profiles (binding energy uncertainty: ± 0.2 eV). The analyzer transmission function[300], Scofield sensitivity factors and effective attenuation lengths for photoelectrons were applied for quantification. Effective attenuation lengths were calculated using the standard TPP-2M formalism [301]. All spectra were referenced to the $C1s$ peak (C-C, C-H) at 285.0 eV binding energy controlled by means of the well known photoelectron peaks of metallic Cu, Ag and Au, respectively.

### 2.3.2. Time of Flight - Secondary Ion Mass Spectroscopy (ToF-SIMS)

ToF-SIMS was performed on a TOF.SIMS[5] instrument (ION-TOF GmbH, Münster). This spectrometer is equipped with a bismuth cluster liquid metal primary ion source and a reflectron type time-of-flight analyzer. Main chamber pressure was below $2 \times 10^{-8}$ mbar. For high mass resolution the Bi source was operated in the "high current bunched" mode

providing short $Bi^{3+}$ primary ion pulses at $25\,keV$ energy and a lateral resolution of approximately $4\,\mu m$. Primary ion doses were kept below $1 \times 10^{11}\,ions/cm^2$ (static SIMS limit) for all measurements. Negative and positive polarity spectra were respectively calibrated on the omnipresent $C^-$, $CH^-$, $CH_2^-$, $OH^-$; and on the $C^+$, $CH^+$, $CH_2^+$, and $CH_3^+$ peaks.

### 2.3.3. Size Exclusion Chromatography (SEC)

SEC measurements were performed on a PL-GPC 50 Plus Integrated System (Agilent, Santa Clara, USA), comprising an autosampler, a PLgel $5\,\mu m$ beadsize guard column ($50\,mm \times 7.5\,mm$) followed by three PLgel $5\,\mu m$ Mixed-C columns ($300\,mm \times 7.5\,mm$, both Agilent) and a differential refractive index detector using N,N-dimethylacetamide (DMAc) as the eluent at $50\,°C$ with a flow rate of $1\,mL\,min^{-1}$. The SEC system was calibrated using linear poly(methyl methacrylate) standards ranging from $160\,g\,mol^{-1}$ to $6 \times 10^6\,g\,mol^{-1}$. Molecular weights are reported relative to poly(methyl methacrylate). Calculation of the molecular weight of poly(methyl methacrylate) proceeded via the Mark-Houwink parameters for poly(methyl methacrylate) ($K =12.8 \times 10^{-5}\,dL\,g^{-1}$ and $\lambda =0.69$)[302].

### 2.3.4. Nuclear Magnetic Resonance (NMR)

$^1$H-NMR spectra were recorded in suitable solvents on an Avance $400\,MHz$ spectrometer (Bruker, Karlsruhe) equipped with ultrashield magnets. The $\delta$ scale is referenced to the internal standard trimethylsilane (TMS, $\delta =0.00\,ppm$). The conversion during polymerization was calculated from the ratio of the signals from monomers ($\delta =0.95\,ppm$ and $1.1\,ppm$) to polymers ($\delta =5.7\,ppm$ and $6.18\,ppm$) and recorded in $CD_3OD$[303].

## 2.4. Physical Characterization

The AFM measurements in Section 3.3.2 were carried out with Prof. Dr. Ruby Sullan (University of Toronto, Canada) on a Force Robot 300 (FR-300, JPK, Germany) during a visit of Dr. Kerstin Blank's group Mechano(bio)chemistry at the Max Planck Institute of Colloids and Interfaces in Potsdam. All other AFM measurements were performed on a Molecular Force Probe 3D BIO system (MFP-3D-BIO, Asylum Research, Santa Barbara, USA).

### 2.4.1. AFM Imaging

Tropoelastin was absorbed to a petri dish by pouring $100\,\mu L$ of a $0.1\,mg\,mL^{-1}$ solution of tropoelastin in PBS into the petri dish. The droplet was allowed to dry for $30\,min$, carefully washed away with PBS and surplus PBS was aspirated. The surface topography of

dried tropoelastin and pHEMA surfaces were measured in contact mode with TR400PSA cantilevers (cleaned with UV light prior to the measurement) and a setpoint that corresponds to roughly 2 nN. The standard deviation of the height signal in a 5 µm x 5 µm image with 512 x 512 pixels was used for the calculation of roughness.

## 2.4.2. Single Molecule Force Spectroscopy (SMFS)

SMFS measurements were executed using TR400PB cantilevers (Au reflex/tip coated, cleaned with UV light prior to the measurement). The spring constant of each cantilever and the inverse optical lever sensitivity were calibrated without touching the tip by combining the Sader method[262] with the thermal noise method[261]. The spring constant was determined as $(0.029 \pm 0.002)\,\mathrm{N\,m^{-1}}$.

The sample preparation for SMFS with pHEMA was done as described in Section 2.2. The pHEMA samples were glued with double sided tape into petri dishes and immersed in MilliQ water. In the case of SMFS with tropoelastin, 100 µL of a $10\,\mathrm{\mu g\,mL^{-1}}$ solution of tropoelastin in PBS was put in a petri dish and dried for 15 min. Subsequently, the droplet was carefully washed away with PBS and taken up and the petri dish was filled with PBS. In the case of cross-linked tropoelastin, the dried droplet was covered for 1 h with 0.1 % glutaraldehyde, which was subsequently washed away with PBS.

The unfolding of single molecules was measured with a statistical approach: thousands of force curves were recorded in a Force Map distributed over the surface. Only force curves showing unfolding of a single molecule chain followed by a clear detachment of the tip were selected for analysis (refer to Figure 3.4). Approximately 3% of the total number of recorded force curves showed unfolding and subsequent rupture and were selected for analysis. Approach and retraction velocity were $500\,\mathrm{nm\,s^{-1}}$ with a trigger force of 1 nN. A dwell time of 1 s was selected to achieve covalent bonding between the thiol functionalized pHEMA and the gold coating or adhesive bonding between tip and tropoelastin. The obtained force-distance curves were fitted with the Asylum Research AFM software plug-in for Igor Pro to the worm-like chain (WLC) model[288].

## 2.4.3. Layer Thickness Measurements

**AFM Indentation**  AFM indentation was performed with colloidal probes on pHEMA samples fixed to a petri dish. The spring constant and the inverse optical lever sensitivity were determined with a force curve on a silicon wafer and the thermal noise method[261]. Force curves were conducted with a loading rate of $500\,\mathrm{nm\,s^{-1}}$ and a trigger force of 3 nN.

**Ellipsometry**  The thickness of dry polymer layers was determined by spectroscopic ellipsometry on a M44 (J.A. Woollam Co., Inc., Lincoln, USA) in the wavelength range of 280 nm to 800 nm[304].

## 2.5. Biological methods

The isolation of HSPCs and the adhesion experiments of REF52 cells on pHEMA in Section 3.4.1 were performed by Saskia Kraus (IFG). Mai Nguyen (IFG) carried out the experiments about the adhesion of HSPCs on tropoelastin in Section 3.1.2.

When materials were used for cell culture, work was performed under a laminar flow hood (Thermo Scientific, Waltham, USA) and exclusively sterile equipment was utilized.

### 2.5.1. Isolation of HSPCs

HSPCs were isolated from UCB by positive selection for CD34 via MACS. The procedure was carried out following the manufacturer's instructions.

Two MS columns, running buffer, erythrocyte lysis buffer and sterile MilliQ water were stored in the fridge before use. Rinsing buffer and lymphocyte separation medium were used at ambient temperature. All steps were accomplished in $50\,\mathrm{mL}$ centrifuge tubes, unless stated otherwise.

The UCB was diluted $1:3$ $(V:V)$ with rinsing buffer. $35\,\mathrm{mL}$ of the diluted UCB was carefully layered on top of $15\,\mathrm{mL}$ lymphocyte separation medium. Mononuclear cells were isolated from UCB by density gradient centrifugation at $1500\,\mathrm{g}$ for $20\,\mathrm{min}$ with slow acceleration and without brake, carried out at ambient temperature. The yellow top layer containing diluted plasma was carefully pipetted off and the white interphase of several centrifuge tubes, consisting of mononuclear cells, was harvested, combined in a new centrifuge tube and filled up to $50\,\mathrm{mL}$ with rinsing buffer. This cell suspension was mixed in order to dilute possible remainings of the lymphocyte separation medium. It was washed by two steps of centrifugation ($300\,\mathrm{g}$ for $15\,\mathrm{min}$) and discarding the supernatant, with transferring the resuspended cells into a $15\,\mathrm{mL}$ centrifuge tube in between those to steps. The cells were resuspended in $10\,\mathrm{mL}$ erythrocyte lysis buffer. After an incubation of $5\,\mathrm{min}$, the erythrocyte lysis buffer was removed by centrifugation at $300\,\mathrm{g}$ for $5\,\mathrm{min}$ at ambient temperature. The supernatant was removed completely and the cell pellet was resuspended in $10\,\mathrm{mL}$ rinsing buffer.

Cells were counted in a Neubauer chamber at a dilution of $1:20$ $(V:V)$ in rinsing buffer and with the use of trypan blue $0.4\,\%$ to distinguish live and dead cells. The cells were diluted with running buffer to a concentration of $10^8$ cells per $300\,\mathrm{\mu L}$. Per $10^8$ cells, $100\,\mathrm{\mu L}$ FcR blocking reagent and CD34 micro beads were added to the suspension. The cells were incubated for $30\,\mathrm{min}$ at $5\,\mathrm{°C}$ while being constantly mingled on a MACSMix™ tube rotator. Following that, $10\,\mathrm{mL}$ of cold running buffer was added and the cell suspension was concentrated in $500\,\mathrm{\mu L}$ per $10^8$ cells by two centrifugation steps at $300\,\mathrm{g}$ for $5\,\mathrm{min}$ and a following resuspension in $1\,\mathrm{mL}$ and then $500\,\mathrm{\mu L}$ per $10^8$ cells, respectively.

The cold MS columns were equilibrated with $750\,\mathrm{\mu L}$ running buffer and placed into the magnetic field of a MiniMACS™ separator. The MS column was loaded with the cell

suspension and rinsed thrice with $500\,\mu\text{L}$ running buffer to wash out the CD34$^-$ cells. The CD34$^+$ cells were eluted by removing the MS coloumn from the magnetic field and pressing $1\,\text{mL}$ runnning buffer through the column with a provided syringe stamp. This procedure was repeated in the second MS column and elution with only $500\,\mu\text{L}$ running buffer. The overall cell yield was determined by counting the cells in a Neubauer chamber.

The purity of isolated HSPCs was tested via flow cytometry as described in Section 2.5.6. HSPCs were not used if the amount of CD34$^+$ cells was below $95\,\%$.

## 2.5.2. Cell Culture

**KG-1a Cell Line** KG-1a cells were maintained by adding fresh RPMI medium supplemented with $20\,\%$ FBS ($V : V$) to suspension culture flasks. They were incubated at $37\,°\text{C}$ and $5\,\%$ CO$_2$ and splitted thrice a week to keep the cell density between $2 \times 10^5$ to $1 \times 10^6\,\text{cells/mL}$.

**REF52 Cell Line** REF52 cells were maintained at $37\,°\text{C}$ and $5\,\%$ CO$_2$ in DMEM $1000\,\text{g}$ glucose supplemented with $10\,\%$ FBS ($V : V$). These adherent cells were splitted twice a week. The supernatant was removed, the cells were detached from the cell culture flask by enzymatic digestion using trypsin/EDTA and they were passaged by a dilution of $1 : 5$ ($V : V$) with fresh medium.

## 2.5.3. Adhesion Tests

**Spot Assay** The adhesion of KG-1a cells to tropoelastin was tested with a concentration series of tropoelastin in PBS in a spot assay in order to get the ideal tropoelastin concentration for following experiments. $1\,\mu\text{L}$ droplets were placed in a petri dish ($35\,\text{mm}$) and dried for $1\,\text{h}$ under the laminar flow hood. Subsequently, the petri dish was blocked for $2\,\text{h}$ with a solution of $10\,\text{mg}\,\text{mL}^{-1}$ bovine serum albumin (BSA) in PBS and washed twice with PBS. $3 \times 10^6$ KG-1a cells were resuspended in $2\,\text{mL}$ adhesion medium consisting of $1\,\%$ Penicillium Streptomycin, $1\,\%$ FBS and $25\,\mu\text{M}$ MnCl$_2$ in RPMI 1640. The cell suspension was filled into the petri dish and incubated for $1\,\text{h}$ at $37\,°\text{C}$ and $5\,\%$ CO$_2$. Thereafter, the petri dish was washed with adhesion medium and with PBS. The cell density analyzed with an Axio Vert.A1 light microscope (Carl Zeiss, Oberkochen) and Fiji.

In a comparison of the adhesion of KG-1a cells to tropoelastin and the C-terminus of tropoelastin, droplets from solution of $0.1\,\text{mg}\,\text{mL}^{-1}$ tropoelasstin, $0.5\,\text{mg}\,\text{mL}^{-1}$ fibronectin and $1\,\text{mg}\,\text{mL}^{-1}$ maleimide functionalyed C-terminus of tropoelastin were used for the coating of a petri dish.

**CyQuant Cell Proliferation Assay**  Due to the lower number of available HSPCs compared to KG-1a, the adhesion of HSPCs to tropoelastin was tested in a CyQUANT® cell proliferation assay. A dye is binding to the DNA of the cell, thus measured fluorescence intensities are proportional to the cell number. To determine the bioactive sequences of tropoelastin to which HSPCs are able to adhere, different peptides were used as inhibitors, working as competitors for the cell-tropoelastin binding (see Section 2.1; for the peptide mix, all the three peptides were added to the suspension).

The assay was conducted according to the manufacturer's instructions. On the day before the CyQUANT® analysis, 96 well plates were coated overnight at $4\,°C$ with $70\,µL$ of $0.1\,mg\,mL^{-1}$ tropoelastin in PBS or $50\,mg\,mL^{-1}$ BSA in PBS as a negative control, preparing triplicates for every condition. Subsequently, the solutions were beaten out of the well plate and the wells were blocked with $200\,µL$ of $10\,mg\,mL^{-1}$ BSA in PBS. After $2\,h$, the wells were washed with PBS.

In the meantime, cell suspensions were prepared with $3 \times 10^5\,cells/mL$ in adhesion medium. For inhibition experiments, the peptides were added to the suspension for a $0.02\,mM$ peptide concentration and the cells were incubated for $20\,min$ at $37\,°C$ and $5\,\%$ $CO_2$. $100\,µL$ cell suspension was added to every well and the cells were incubated for $1\,h$ at $37\,°C$ and $5\,\%$ $CO_2$. Subsequently, the cell suspension was removed with a pipette and the wells were washed with adhesion medium. $100\,µL$ of dye binding solution from the CyQUANT kit were added to the adherent cells and they were incubated for $40\,min$ at $37\,°C$ and $5\,\%$ $CO_2$. Finally, the fluorescence intensities were analyzed with EnSpire™ multilabel plate reader (Perkin Elmer, Massachusetts, USA). Used parameters were $30\,s$ shaking with $60\,rpm$, $100$ flashes, an excitation wave length of $485\,nm$ and an emission wave length of $530\,nm$.

## 2.5.4. Cell Morphology Analysis of REF52 Cells on Proteins and pHEMA

rat embryonic fibroblast cell line (REF52) cells were seeded on pHEMA surfaces functionalized with the C-terminus of tropoelastin to investigate their spreading behavior on the polymers compared to other proteins. Cell adhesion and cell morphology were assessed using fluorescence microscopy and analysis via Fiji.

**Seeding and Fixation of REF52 Cells on Substrates**  pHEMA substrates were prepared on glass cover slips with a diameter of $15\,mm$ as described in Section 2.2. After synthesis and biofunctionalization, the pHEMA surfaces were sterilized for $5\,min$ in $70\,\%$ ethanol and completely dried in air under laminar flow. Following that, the surfaces were washed three times with PBS to remove residues of ethanol and put into 12 well culture plates. One day prior the experiment, 8-chamber slides with glass bottoms were coated with a solution of $10\,µg\,mL^{-1}$ fibronectin and $0.1\,mg\,mL^{-1}$ tropoelastin in PBS overnight at $4\,°C$,

respectively. BSA at a concentration of $50\,\mathrm{mg\,mL^{-1}}$ served as a negative control. A part of the tropoelastin coated chambers was cross-linked with $0.1\,\%$ glutaraldehyde for $1\,\mathrm{h}$ at ambient temperature and then quenched twice with $1\,\mathrm{M}$ Tris buffer for $5\,\mathrm{min}$. All coated chambers were washed twice with PBS to remove remaining proteins or glutaraldehyde.

REF52 cells were resuspended in adhesion medium consisting of DMEM $4500\,\mathrm{g}$ glucose supplemented with $7.5\,\%$ FBS $(V:V)$ for a concentration of $1\times10^4\,\mathrm{cells/mL}$. $400\,\mathrm{\mu L}$ of cell suspension was added to every chamber and $2\,\mathrm{mL}$ to every well and cells were allowed to adhere for $4\,\mathrm{h}$ at $37\,°\mathrm{C}$ and $5\,\%$ $CO_2$. Following that, unbound cells were removed by washing once with PBS and the remaining adherent cells were fixed with $4\,\%$ paraformaldehyde in PBS for $15\,\mathrm{min}$ at ambient temperature.

**Staining and Fluorescence Microscopy**  Cell membranes were permeabilized with $0.1\,\%$ Triton™X-100 in PBS $(V:V)$ for $5\,\mathrm{min}$ at ambient temperature followed by blocking of non-specific binding sites for $30\,\mathrm{min}$ with $1\,\%$ BSA in PBS $(w:w)$. The actin filaments of the cytoskeleton were stained with Alexa Fluor™ 488 Phalloidin diluted $1:40$ $(V:V)$ in PBS and cell nuclei were counterstained with DAPI diluted $1:1,000$ $(V:V)$ in PBS. Finally, the dyes were removed by washing the substrates six times with PBS and embedded in Mowiol®.

Images were taken with the Axio Observer.Z1 Fluorescent Microscope (Carl Zeiss AG, Oberkochen) equipped with an EC Plan-Neofluar 10x/0.3 objective (Carl Zeiss AG) using the ZEN Microscope Software.

**Cell Morphology Analysis**  Cell morphology was quantified using Fiji. The analyzed parameters were cell area, major and minor axis of a ellipse fitted to the cell boundaries, the mean gray value of the cell area, circularity, solidity and number of branches of a cell. The solidity is defined as the cell area divided by the area of the convex hull of the a cell and can be used to describe the area of protrusions of a cell as it is inversely correlated with deformability of a cell[305]. The circularity is defined as $4\pi$ multiplied with the cell area divided by the perimeter to the square. Due to the perimeter, it emphasizes the length of protrusions [306]. For the number of protrusions, the cells' outlines were converted to binary images. With the Fiji plugins Skeletonize and Analyze Skeleton, the number of end point voxels of the cells' skeletons were assessed.

The assessed values are the corresponding mean values of at least 40 cells per surfaces, randomly selected from several images in 2 experiments for proteins and 3 experiments for pHEMA substrates.

In addition to the presentation of the data as bar plots, PhenoPlot was used to visualize the cell morphology data[297]. Instead of describing the cellular phenotype as high-dimensional vectors of features, the data is presented as easily interpretable glyphs. Table 2.6 lists the Fiji parameters used for the visualization with PhenoPlot. It also explains the normalization of every parameter to a 0 to 1 interval.

Table 2.6.: Overview of used Fiji parameters for PhenoPlot visualization. VSC means the value of any measured single cell for this parameter.

| PhenoPlot | Fiji | Minimum = 0 | Maximum = 1 |
|---|---|---|---|
| cell length | major axis | 0 | max. mean major axis |
| cell width | minor axis | 0 | max. mean major axis |
| spikes fraction | no. end point voxels | 0 | max. VSC |
| spikes height | circularity$^{-1}$ | min. VSC | max. VSC |
| relative protrusion area | solidity$^{-1}$ | min. VSC | max. VSC |
| ellipse color | mean gray value | 0 | max. VSC |

## 2.5.5. Culture of HSPCs on pHEMA

Mechanosensitivity tests were performed by culturing HSPCs for 1 week on different substrates. pHEMA 1 h and pHEMA 6 h samples were used as short and long polymer substrates. Two different reference systems were used for comparison: TCP and TCP coated with tropoelastin as most experiments with tropoelastin in the literature were performed on TCP. The other reference system is glass cover slips with a diameter of 15 mm and the same glass cover slips coated with tropoelastin. This was chosen as the pHEMA samples were also synthesized on these glass cover slips.

The experiments were conducted as triplicates for every substrate and with the HSPCs of three different blood donors.

One day prior the experiment, glass cover slips were cleaned with ethanol, washed twice with sterilized MilliQ water and put into 24 well plates. A part of the glass cover slips and the empty TCP wells were coated overnight at 4 °C with 330 µL of 0.1 mg mL$^{-1}$ tropoelasstin in PBS, respectively. Directly before an experiment, the tropoelastin solution was removed and the surfaces were washed once with PBS. pHEMA samples were also cleaned with ethanol, washed twice with sterilized MilliQ water and put into some empty wells.

The cell culture medium for the expansion of HSPCs was serumfree PromoCell medium with 10 µg mL$^{-1}$ Citokinmix E and Penicillium Streptomycin. 1500 of the CD34$^{+}$ cells were removed for colony-forming unit (CFU) assay on day zero, while the concentration of the remaining CD34$^{+}$ cells was adjusted to 20 000 cells/mL cell culture medium. 1 mL of the cell suspension was seeded per well and incubated at 37 °C and 5 % CO$_2$. After 3 d, 1 mL of medium was added to each well to supply the cells with fresh nutrients.

On day 7, cells were harvested and each well was washed with PBS which was added to the according cell suspension. The cells were counted in a Neubauer chamber and prepared for further analysis via flow cytometry and CFU assay.

## 2.5.6. Flow Cytometry

Flow cytometry measurements were carried out with an Attune$^{®}$ Cytometer (Applied Biosystems, Foster City, USA). 50 000 cells per sample were washed with PBS, centrifuged at (300 g for 5 min at ambient temperature and resuspended in 50 mL PBS with 0.1 percent FBS ($V : V$). 5 µL of the antibodies conjugated with fluorescent dyes or the corresponding isotype controls were added to the sample vials and the cells were incubated for 1 h at 4 °C in the dark. The cells were washed with 50 mL PBS with 0.1 percent FBS and fixated with 3.7 % paraformaldehyd in 50 mL PBS with 0.1 percent FBS ($V : V$). Prior to the measurement, sample vials were filled with 2 mL of PBS.

Data Analysis was performed with FlowJo. A compensation matrix was determined with a bead kit correcting for slightly overlapping emmision spectra of the fluorescent dyes. Cell debris was excluded in the graph of the side scattered versus the forward scattered signal. The gates for the cell antigens were chosen as 1 % false positive in the isotype control measurement. Therewith, the CD34 and the CD38 expression of the analyzed HSPCs were displayed.

## 2.5.7. Colony Forming Assay

The differentiation capacity of freshly isolated HSPCs and cells after culture on different substrates can be assessed via CFU assay. The result of this analysis stands for the frequency of myeloid progenitor cells.

1500 cells per sample were diluted in 300 µL IMDM / 2 % FBS. This cell suspension was added to a 3 mL aliquot of MethoCult and vortexed. The cell suspension rested for at least 5 min for allowing the bubbles to vanish. Subsequently, it was distributed in three 35 mm petri dishes and transferred to a humid chamber. The cells were incubated at 37 °C and 5 % $CO_2$.

After 14 d, the formed colonies were counted with a Axio Vert.A1 light microscope (Carl Zeiss, Oberkochen) and classified according to the progenitor cell types displayed in Table 2.7 and in Figure 3.41.

## 2.5.8. Statistical Analysis

Data are depicted as mean and standard deviation, unless stated otherwise.

Statistical analysis was carried out with the software Prism. For a group of samples, the significance was calculated via one-way ANOVA with a Tukey's multiple comparison test. In the case of two groups of data, a two-tailed t-test was used. Significances were depicted with asterisks: one for significant $p \leq 0.05$, two for very significant $p \leq 0.01$, three for extremely significant $p \leq 0.001$ and four for highly significant $p \leq 0.0001$. Not significant is indicated as $ns$.

Table 2.7.: Constituents and appearances of the colonies formed in CFU assays.

| Colony | Constituents |
| --- | --- |
| CFU-GEMM | Colony Forming Unit - Granulocytes, Erythrocytes, Monocytes and Megakaryocytes |
| | Mixed colonies consisting of white and red cells. They derive from progenitor cells with the capacity to differentiate into all blood cell types. |
| CFU-GM | Colony Forming Unit - Granulocytes and Monocytes |
| | Exclusively white cells. They derive from progenitor cells that were already committed to differentiate into granulocytes or monocytes. |
| BFU-E | Burst Forming Unit - Erythroid |
| | Mainly red cells in compact colonies. They are derived from progenitor cells that were already committed to differentiate into erythrocytes. |

# 3. Results and Discussion

Elastin is the most elastic biological material known[150]. Its soluble monomeric subunit tropoelastin shows interesting biological properties: enhanced cell adhesion [162] and increased expansion of HSPCs[128] compared to TCP. The latter publication correlated its beneficial effect on HSPCs with its elasticity. This unique combination of properties highlight tropoelastin as a promising candidate for being an archetype for the design of biomimetic substrates.

## 3.1. Characterization of Tropoelastin

As a first step, the characterization of biological and mechanical properties of tropoelastin were described in this section for defining the boundaries for the later development of a polymeric model system for mechanosensitivity studies, starting from section 3.2.

### 3.1.1. Adhesion of Blood Cells on Tropoelastin

The adhesion of cells to tropoelastin was investigated in many publications[177, 161, 173, 307, 308, 128] with a used concentration range from $0.002\,\mathrm{mg\,mL^{-1}}$ to $1.5\,\mathrm{mg\,mL^{-1}}$. In the case of HSPCs, substrates were coated with a solution of tropoelastin in PBS at a concentration of $1.5\,\mathrm{mg\,mL^{-1}}$, but this solution was reused over several experiments. For cost reasons and a better reproducibility, a minimum concentration of tropoelastin was seeked, that still offered a good adhesion of blood cells.

Therefore, cell adhesion tests with a concentration series of tropoelastin were conducted with KG-1a cells. Figure 3.1 shows KG-1a cells adhered to a dried droplet of tropoelastin solution with a concentration of $0.1\,\mathrm{mg\,mL^{-1}}$ on TCP. The KG-1a cells favored dried tropoelastin over the BSA blocked TCP in terms of adhesion. The concentration series showed an increased cell density with increasing amount of tropoelastin until it reached a saturation level at $0.1\,\mathrm{mg\,mL^{-1}}$. Thus, this concentration was used for all coatings with tropoelastin in subsequent cell experiments. It was above the saturation level of $0.002\,\mathrm{mg\,mL^{-1}}$ that was measured for the adhesion of dermal fibroblasts on tropoelastin[161]. However, KG-1a cells are less adhesive than fibroblasts and could therefore need a higher tropoelastin concentration on a substrate for efficient adhesion.
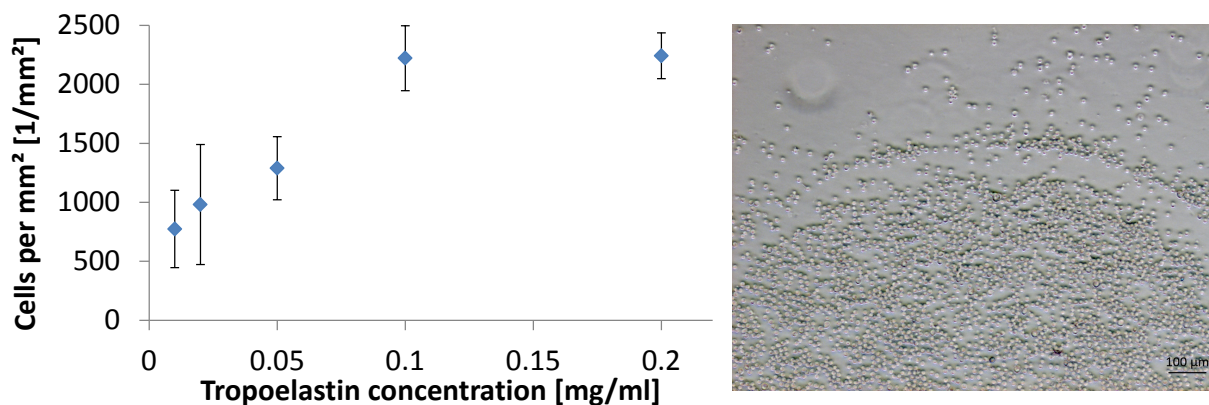
Figure 3.1.: Concentration series for the adhesion of KG-1a cells on TCP coated with tropoelastin (Left). Microscopic image of adherent KG-1a cells on a dried droplet of $0.1\,\mathrm{mg\,mL^{-1}}$ tropoelastin solution surrounded by TCP blocked with BSA (Right).

### 3.1.2. Bioactive Sequence of Tropoelastin

For an adequate model system mimicking tropoelastin, it was important to know the receptors via which blood cells are binding to tropoelastin and the bioactive sequences of tropoelastin to which they are binding. This allowed adding the right functional group to the model system.

**Adhesion Experiments of HSPCs on Tropoelastin**  Mai Nguyen studied the adhesion of hematopoietic cells on tropoelastin[309]. She discovered, that KG-1a cells and HSPCs adhere via integrins, the EBP and GAG to tropoelastin but to different degrees. The adhesion of HSPCs was inhibited most strongly by heparin and lactose, blocking the interaction via GAG and EBP, respectively (For reference, see Figure 1.7).

Following that work, cell adhesion experiments were conducted with HSPCs on tropoelastin, as shown in Figure 3.2. Different amino sequences were added to the adhesion medium. They worked as inhibitors that competed with tropoelastin for the corresponding receptors. The only significant decrease in cell adhesion was observed for the peptide representing the C-terminus of tropoelastin. Inhibition with the amino sequences was not additive as the adhesion was even higher when inhibiting with a mix of all three sequences compared to the C-terminus alone.

The results implied that the binding of HSPC happened through cell surface proteoglycans[173, 175]. The small, but insignificant effect of GRKRK on the adhesion could be explained from GRKRK being a part of the C-terminus with a length of 13 amino acids thus already contributing a small effect on inhibition. Because of these results, the C-terminus was used for functionalizing pHEMA samples for mechanosensitivity studies with HSPCs.
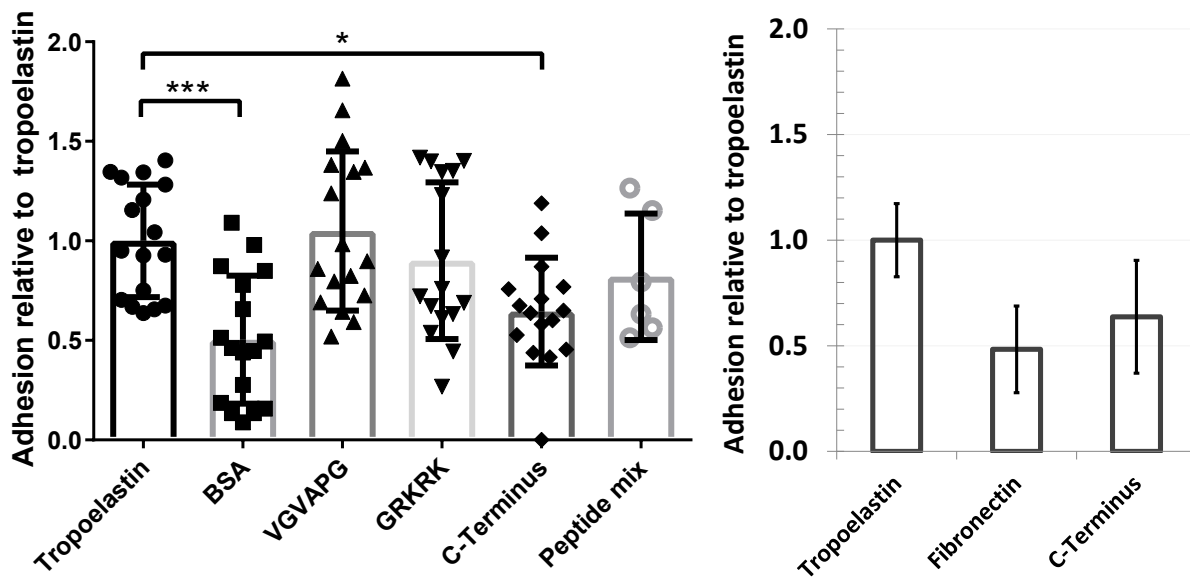
Figure 3.2.: Inhibition of the adhesion of HSPCs to tropoelastin $(0.1\,\mathrm{mg\,mL^{-1}})$ coated TCP with the use of different amino sequences. Coating of tropoelastin with and without blocking via BSA served as positive and negative control (Left). Adhesion of KG-1a cells to the C-Terminus of tropoelastin was compared to tropoelastin and fibronectin. C-terminus of tropoelastin functionalized with an maleimide moiety could provided a valuable adhesion of hematopoietic cells (Right).

**Adhesion of KG-1a to the C-Terminus of Tropoelastin** Figure 3.2 (right) shows a proof that a coating with the C-terminus of tropoelastin functionalized with N-maleoyl-$\beta$-alanine, was capable of providing adhesion to hematopoietic cells. However, although the coating with the C-terminus could have provided a much higher number of adhesion motifs compared to tropoelastin as is was used with an even higher weight concentration, the adhesion is smaller than on the tropoelastin coating. That could mean that further adhesion mechanisms, that are unknown up to this point, could have contributed to the adhesion of hematopoietic cells to tropoelastin or that adhesion of the small C-terminus was smaller than that of the large protein tropoelastin.
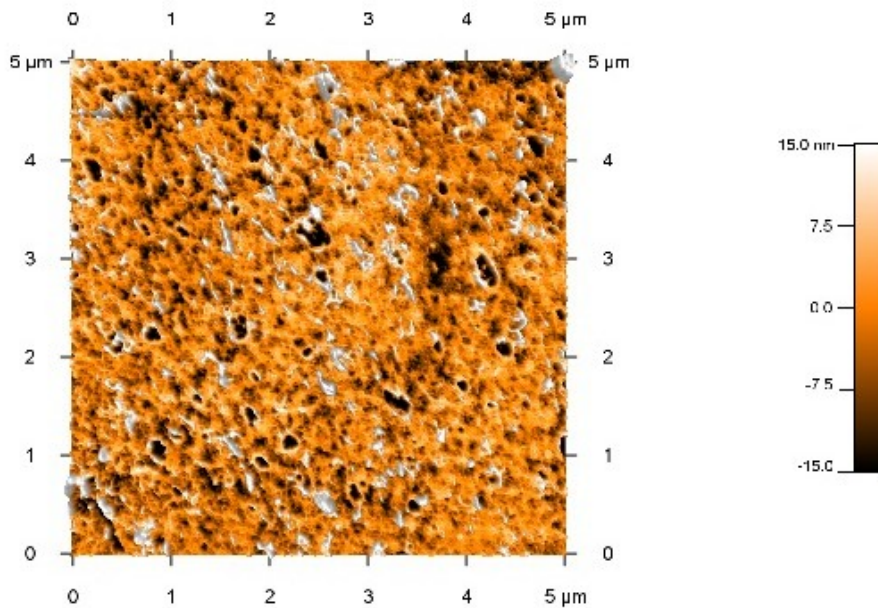
Figure 3.3.: Representative topographical AFM image of tropoelastin with a concentration of $100\,\mu g\,mL^{-1}$ in PBS adsorbed to a glass slide. Roughness $R_{RMS}$ was $7.5\,nm$. The black holes and white islands each corresponded to a depth and height of roughly $12\,nm$ and a size of $20\,nm$ to $300\,nm$.

### 3.1.3. Topographical Properties

The topography of a tropoelastin coating on a glass slide is depicted in figure 3.3. Tropoelastin formed a layer with a roughness of $7.5\,nm$. Topographical features such as holes and islands with a size of $20\,nm$ to $300\,nm$ were visible. From the depth of the holes, the thickness of the tropoelastin layer could be estimated to roughly $12\,nm$. That was more than reported elsewhere[128], but that could be contributed to the different substrates (glass to polystyrene).

For the combination of HSPCs on tropoelastin, the effect of roughness on the culture of HSPCs was not discussed[128] although a difference between coated and uncoated TCP was conceivable. Therefore, the roughness of tropoelastin was discussed later in section 3.3.5.

### 3.1.4. Elasticity of Tropoelastin Single Molecules

Single tropoelastin molecules were mechanically characterized via AFM based SMFS as depicted in Figure 3.4. Tropoelastin molecules were deposited to a petri dish from a solution in PBS with a low concentration of $0.1\,mg\,mL^{-1}$ to receive mostly single molecules on the substrate. Attachment of tropoelastin to the surface and picking up with the AFM tip was achieved solely via adsorption.

Figure 3.4 (bottom) shows an exemplary force-extension curve. It depicts:

a) an unspecific adhesion peak that can be attributed to tip-substrate interactions

b) the unfolding of tropoelastin beginning with high extension at small forces devolving into high increase in the pulling force at a nearly fully extended molecule

c) the rupture of the tropoelastin molecule from the AFM tip

The force-distance curve during unfolding could be fitted to the WLC model in Equation 1.10 with a contour length $l_c$ of 227 nm and a persistence length $l_p$ of 0.26 nm. Rupture force $F_r$ depended from the adhesion of tropoelastin to the substrate. However, due to the
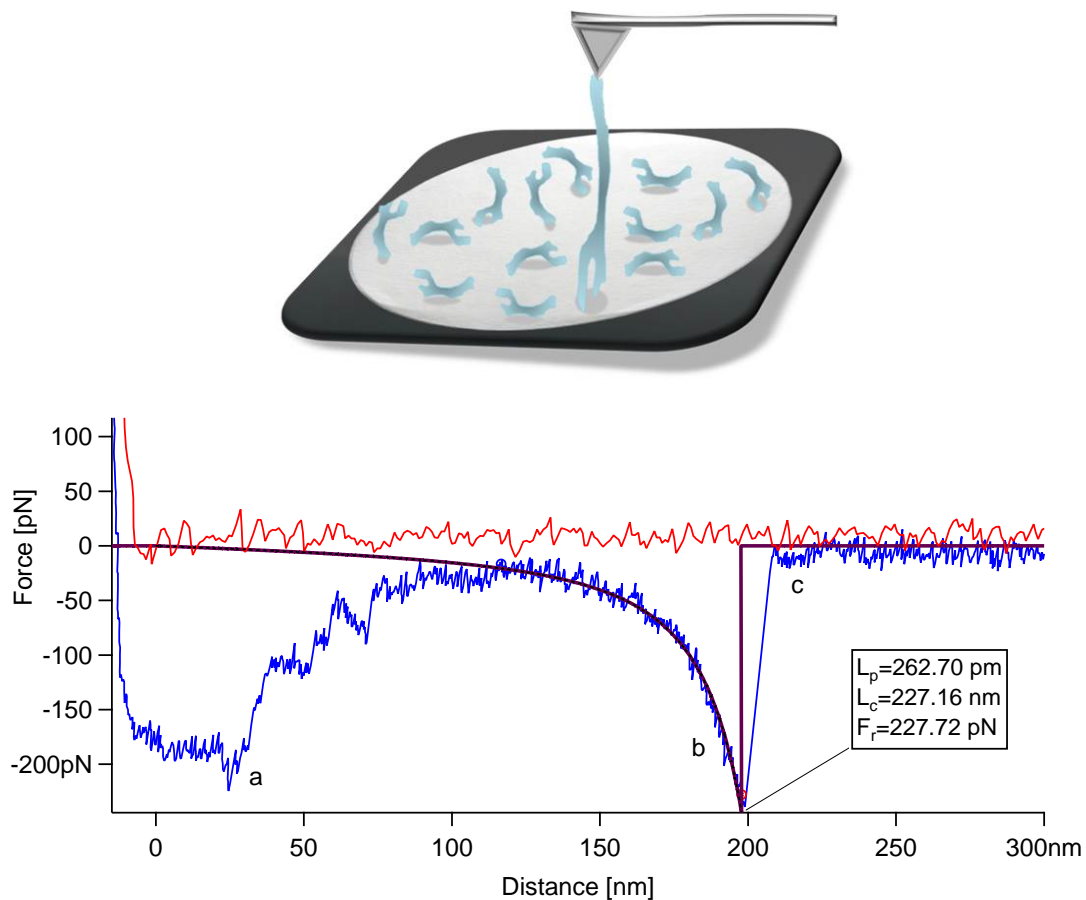


Figure 3.4.: Characterization of the mechanical properties of tropoelastin via SMFS. (Top) Schematic view of the measurement of single tropoelastin molecules with an AFM. (Bottom) Example of a force-extension curve. The red and blue line show the force during approach and retraction of the AFM tip. The dark red line shows a fit to the WLC model with a contour length $l_c$ of 227 nm and a persistence length $l_p$ of 0.26 nm.
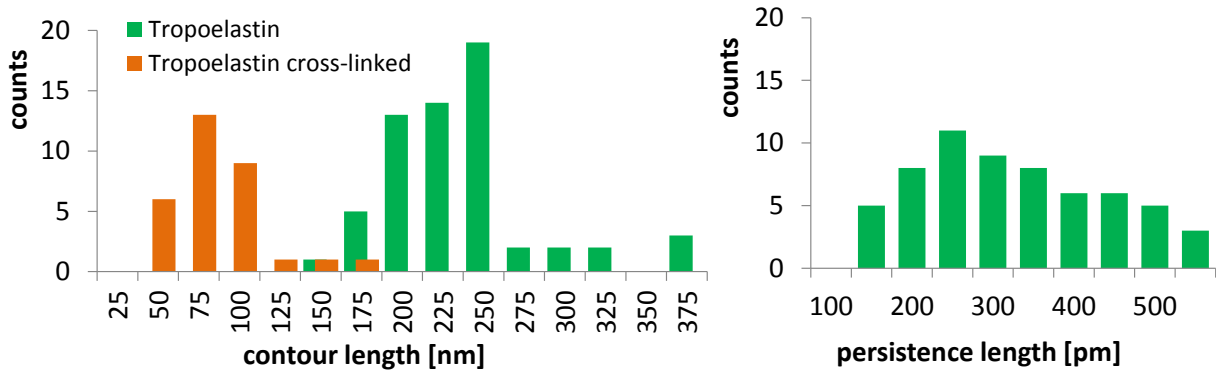
Figure 3.5.: Frequency histograms for contour length $l_c$ and persistence length $l_p$ in SMFS measurements of tropoelastin. $n = 67$ fits for tropoelastin and 30 fits for cross-linked tropoelastin.

random nature for finding and attaching a molecule to the tip, only 3.5% of the recorded force measurements showed a clear unfolding event.

The mean values were estimated from 67 measurements as $l_c = (223 \pm 48)$ nm for the contour lengh and $l_p = (0.30 \pm 0.12)$ nm for the persistence length as summarized in Figure 3.5. The contour length was smaller than predicted for a polypeptide chain with a length of 698 amino acids (254 nm) as the AFM picked tropoelastin at random positions within the molecule, but it was in accordance with other SMFS measurements[149, 128]. An additional source of error could be neglected: Deviation from the fix point of the molecules to the substrate not being under the AFM tip lead to a maximum error of 1 %[310].

Tropoelastin possesses two types of alternating domains which build its structure: On the one hand hydrophilic cross-linking domains that form $\alpha$ helices and on the other hand hydrophobic domains that tend to form $\beta$ turns which are present in the relaxed state as compact amorphous structures and which give tropoelastin its elasticity[146]. The smooth unfolding curve however, as depicted in Figure 3.4, suggested that its tertiary structure is only of transient nature[149].

The determined persistence length for tropoelastin of $l_p = 0.3$ nm was much smaller than the one of other biomolecules such as DNA (50 nm), actin filaments (10 µm) and microtubules (up to several mm)[311]. A high molecular elasticity near ideal polymer chains could be concluded[312], thus it should be possible to mimic the elasticity of tropoelastin with polymers as was demonstrated in section 3.3.5.

Tropoelastin could be cross-linked with a glutaraldehyde treatment as it induced inter- and intramolecular covalent bonds[313]. In doing so, free ends of the tropoelastin molecule were shortened as was measured with SMFS. The mean contour length decreased to $l_c = (71 \pm 28)$ nm due to the cross-linking. This value was likewise comparable to the literature[128], thus a valid execution of the SMFS experiments was assumed and the procedure was transfered to the application on polymers described in section 3.3.2.
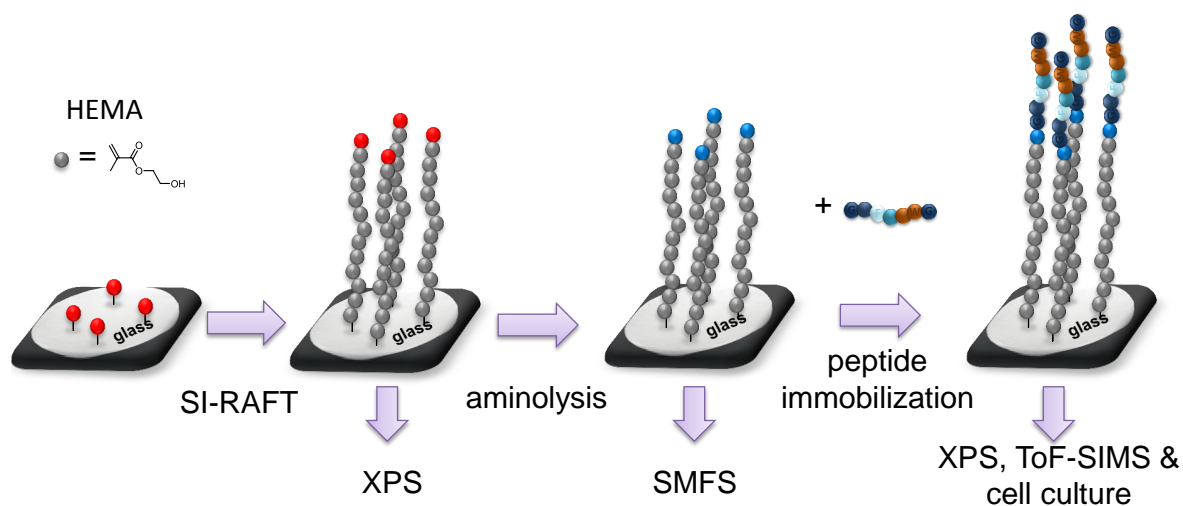
Figure 3.6.: Strategy for the development of a polymer model system for mechanosensitivity studies. The polymer monolayer was fabricated via SI-RAFT polymerization from HEMA. The RAFT agent was cleaved off in an aminolysis and replaced in a click reaction with a biofunctional group for cell adhesion. The product was analyzed at different steps of the synthesis process via XPS, ToF-SIMS and SMFS and subsequently tested in mechanosensitivity studies with HSPCs and REF52 cells.

## 3.2. Development of a Polymer Model System for Mechanosensitivity Studies

A polymer model system for mechanosensitivity studies was developed inspired by the exceptional mechanical properties of tropoelastin. An elasticity equal to tropoelastin was desired in terms of chain flexibility and molecule length. However, the molecule length was used as a tunable parameter that offered cells different pulling distances when adhering to the polymer substrate. Thus, the extensibility of the substrate was tested as a parameter for mechanosensitivity.

Strategy for synthesis and analysis is depicted in Figure 3.6. The polymer monolayer was fabricated via SI polymerization which has been established as an important tool for functional surface design and was frequently used for the functionalization of biosurfaces[208]. An excellent variant for this purpose was RAFT polymerization that offered good control of chain length over polymerization time with a narrow distribution and a high end-group fidelity[179]. Furthermore, without the need of toxic ingredients such as metallic catalysts, it was biologically compatible and was used for many biomedical applications[189].

The monomer of choice was HEMA. pHEMA demonstrated a high biocompatibility and was frequently used in biomedical devices[199, 200]. Furthermore, its non-fouling properties reduced the adsorption of proteins onto the substrate[314], thus prevented uncontrolled
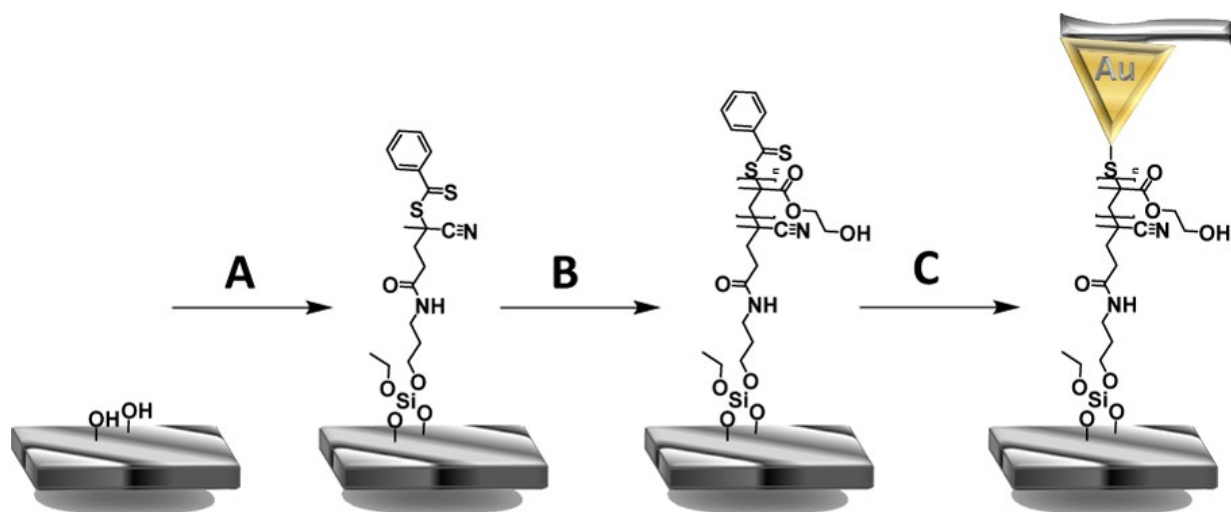
Figure 3.7.: Reaction sequence for surface anchored pHEMA. (A) Immobilization of RAFT-silane on a plasma activated glass; (B) SI-RAFT polymerization with HEMA and control of the chain length over polymerization time; (C) Aminolysis of RAFT end group. The generated thiol terminus allowed for an analysis via SMFS. Reprinted with permission from [278]. Copyright 2016 ACS.

protein-cell interactions at the surface of the polymer model system.

Further steps were required to add functionality to the polymer. The RAFT agens was cleaved off in an aminolysis enabling SMFS measurements with the polymer (Section 3.3). Cell adhesive functionality was added in a click reaction with high efficiency and under environmentally friendly conditions[315]. The chemical composition was determined after polymerization and biofunctionalization via XPS. The final product was investigated via ToF-SIMS and in mechanosensitivity studies with HSPCs and REF52 cells (Section 3.4).

## 3.2.1. Synthesis of pHEMA brushes

The pHEMA monolayer was synthesized by SI-RAFT polymerization using the *R*-group approach as depicted in Figure 3.7. For this purpose, an established procedure[298] was adopted to generate pHEMA strands on a glass substrate.

**Reaction Sequence** Prior to the polymerization, glass substrates or silicon wafers were plasma activated. The substrates were functionalized with a tailor-made RAFT-silane anchor 4-(3-(triethoxysilyl) propylcarbamoyl)-2-cyanobutan-2-yl benzo dithioate by immersing them over night in a solution of the chain transfer agent in toluol as seen in Figure 3.7 (A) at a temperature of 50 °C. For SMFS samples, a dilution of the chain transfer agent to a thousandth compared to the concentration used for XPS measurements and cell experiments was utilized to promote isolated polymer chains on the surface.

Subsequently, HEMA was polymerized in the presence of sacrificial RAFT agent 4-cyano-4-(phenylcarbonothioylthio)-pentanoic acid via SI-RAFT polymerization (B) with AIBN in dioxane/water at 80 °C. Polymer chain length was influenced by varying polymerization time from 1 h to 6 h. The resulting surfaces were analyzed employing AFM imaging, XPS and ellipsometry.

Finally, an aminolysis was carried out with triethylamine and hexylamine in ethanol at ambient temperature for 5 h to transform the terminal RAFT moieties into thiol groups (C), which tethered to the *Au* surface of an AFM cantilever and therefore could be exploited for the characterization via SMFS.
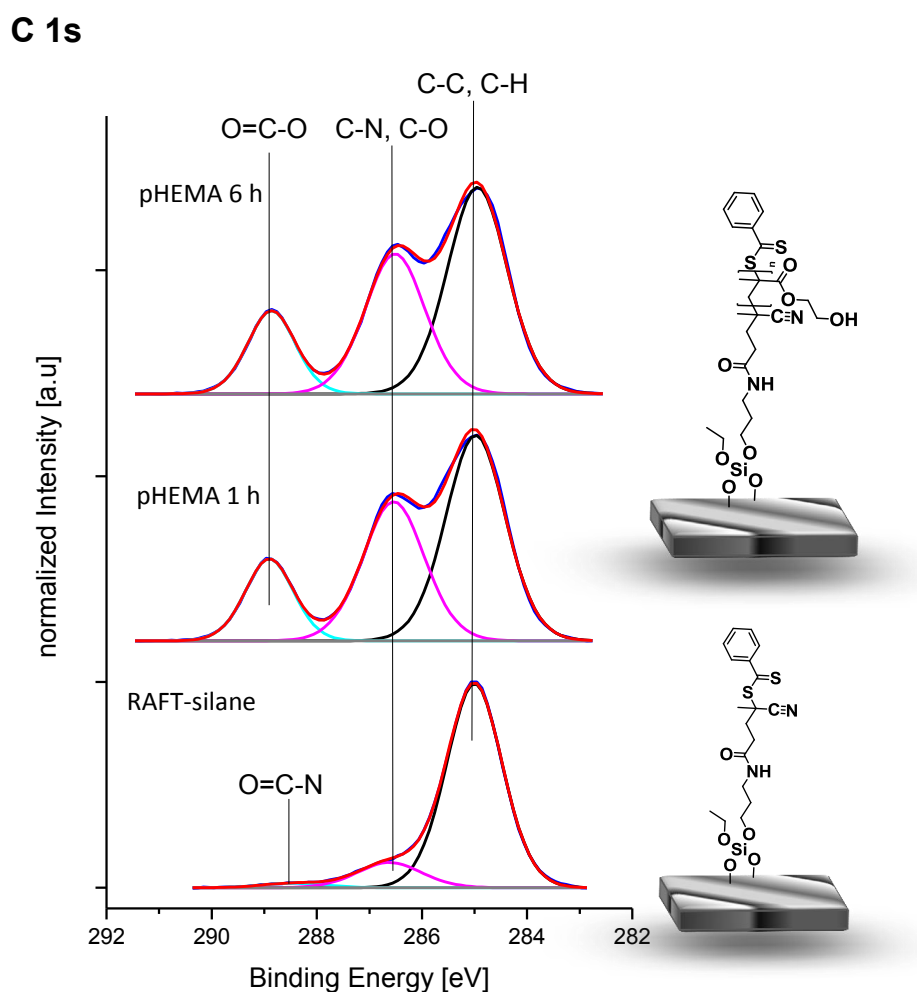


Figure 3.8.: XPS analysis of pHEMA before and after polymerization. (from Bottom to Top) RAFT-silane functional substrate; substrate after 1 h RAFT polymerization of HEMA; 6 h RAFT polymerization of HEMA. All spectra were normalized to the highest intensity. Adapted with permission from [278]. Copyright 2016 ACS.

**Analysis via XPS**  This paragraph is reproduced in part with permission from [278]. Copyright 2016 ACS.

The chemical composition of the polymer layers was characterized by XPS. It is a valuable tool to determine the changes in thin layer coatings due to its high surface sensitivity[316].

The XP spectrum of the substrate with the RAFT functional silane in Figure 3.8 (bottom) showed the distinctive signal at the $C1s$ peak at 285.0 eV binding energy corresponding to C-C/C-H groups. In addition, the expected $C1s$ peaks at 286.7 eV and 288.5 eV could be attributed to the C-N/C-O and the O=C-N structural motifs of the RAFT-silane anchor, respectively[317, 318].

In the subsequent polymerization step, the XP spectrum changed in favor of the C-O and O=C-O ($C1s$ peak at 288.9 eV) groups, which corresponded to the attached HEMA monomer units (Figure 3.8 pHEMA 1 h in the middle)[298] and resembled the one after a 6 h polymerization time (Figure 3.8, top). Since XPS has a sampling depth of approximately 10 nm for organic materials[319], after 1 h of polymerization, only bulk polymer could be detected as the thickness of the grafted surface exceeded 10 nm (see Figure 3.15). Therefore, the presence of the RAFT end group could only be proven with the O=C-N motif on the silane functional substrate before polymerization and not within the signal of the bulk polymer. Nevertheless, it could be assumed that the RAFT moiety was still intact after the polymerization, as was also demonstrated via SMFS in section 3.3.2.

## 3.2.2. Synthesis and Analysis of Biofunctionalized pHEMA

The biofunctionalization of pHEMA was achieved with a base-catalyzed Michael-type addition, a so-called "click reaction"[315], as depicted in Figure 3.9.

**Reaction Sequence**  The biofunctionalization of pHEMA was started after the polymerization (B) in Figure 3.7. The base-catalyzed thiol-ene reaction (D) in Figure 3.9 could be carried out *in situ* with the aminolysis (C). The peptide functionalyzed with N-maleoyl-$\beta$-alanine was added to the solution of triethylamine and hexyl amine in ethanol and was kept at ambient temperature for 5 h. The terminal RAFT moieties were transformed into thiol groups (C) and subsequently, the functionalyzed peptide was added to the thiol group(D).

**Analysis via XPS**  The biofunctionalization was verified by XPS. Due to its high sensitivity, it is a appropriate tool to demonstrate the modification of the polymer substrate[316]. Only the sample surface is analyzed due to the small penetration depth of 10 nm for XPS[319], thus it is perfectly suitable for the evaluation of the biofunctionalization of pHEMA.
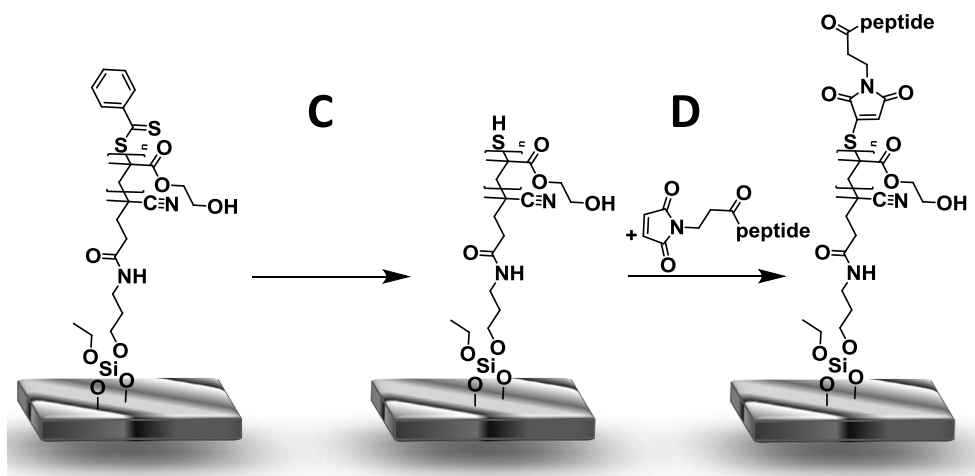
Figure 3.9.: Reaction sequence for the base catalyzed thiol-ene reaction used for the functionalization of pHEMA with an *in-situ* cleavage of the thiocarbonylthio endgroups of the pHEMA layer under basic conditions (aminolysis, C) and a direct reaction of the resulting thiol groups with the maleimide end-groups of the peptides (D).

The addition of the peptide to pHEMA was demonstrated with Figure 3.10. For that purpose, different samples were analyzed and compared:

- the polymer layer after the base catalyzed Michael-type thiol-ene reaction (positive, green line)

- a sample consisting of pHEMA which was exposed to the maleimide-functionalized peptide but without the necessary amine bases (negative, blue line)

- the unmodified polymer layer consisting solely of pHEMA (reference, black line)

For the positive sample, an *in-situ* cleavage of the thiocarbonylthio end-groups of the pHEMA layer under basic conditions (aminolysis) resulted in thiol groups that could react directly with the maleimide end-groups of the peptides. For the negative sample in contrast, the amine bases were absent in order to prevent a reaction between the peptide and the pHEMA layer at otherwise identical reaction conditions. This experiment was expected to prove the covalent immobilization of the peptide, rather than non-specific adsorption. The reference sample was used to exclude the possibility of signals being caused by impurities from the production process or transport. Thus, this sample was at no time in contact with the peptide or other components of the thiol-ene reaction solution and consisted solely of the pHEMA layer.

The $N1s$ spectrum was selected to prove the existence of a peptide on the pHEMA samples. The peak could be deconvoluted in two components: a main peak at $400.1\,\text{eV}$ which corresponded to the amide groups in the peptide backbone as well as amine groups
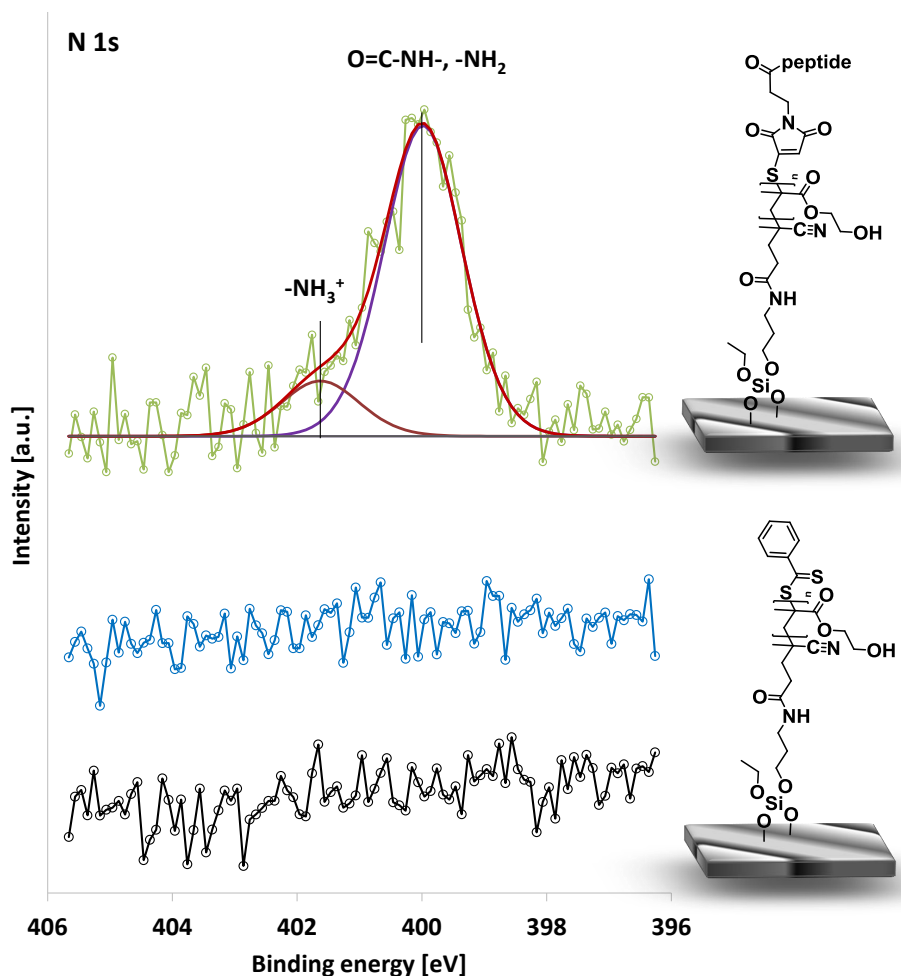
Figure 3.10.: XPS analysis of biofunctionalized pHEMA. (from Bottom to Top) reference sample was pHEMA prior to biofunctionalization; negative sample was treated equally as the functionalized pHEMA except for the missing base catalyst; pHEMA functionalized with the C-terminus of tropoelastin. All spectra were normalized to the highest intensity.

on the side chains and a weak peak at ca. $402\,\text{eV}$ indicating the presence of protonated amine groups[320, 321]. With this analysis in mind, the thiol-ene click-reaction was carried out in DMSO instead of the often used DMF to avoid a possible contamination with a O=C-N motif.

As expected, no $N1s$ peak was detected in the measurement of the reference sample as it was never in contact with any peptide. The distinct $N1s$ peak for the positive sample verified the presence of the peptide on the pHEMA sample and indicated a N concentration of $0.2\,\text{at}\%$ to $0.3\,\text{at}\%$. The missing peak for the negative sample showed that no physisorbed protein molecules were present on the surface.
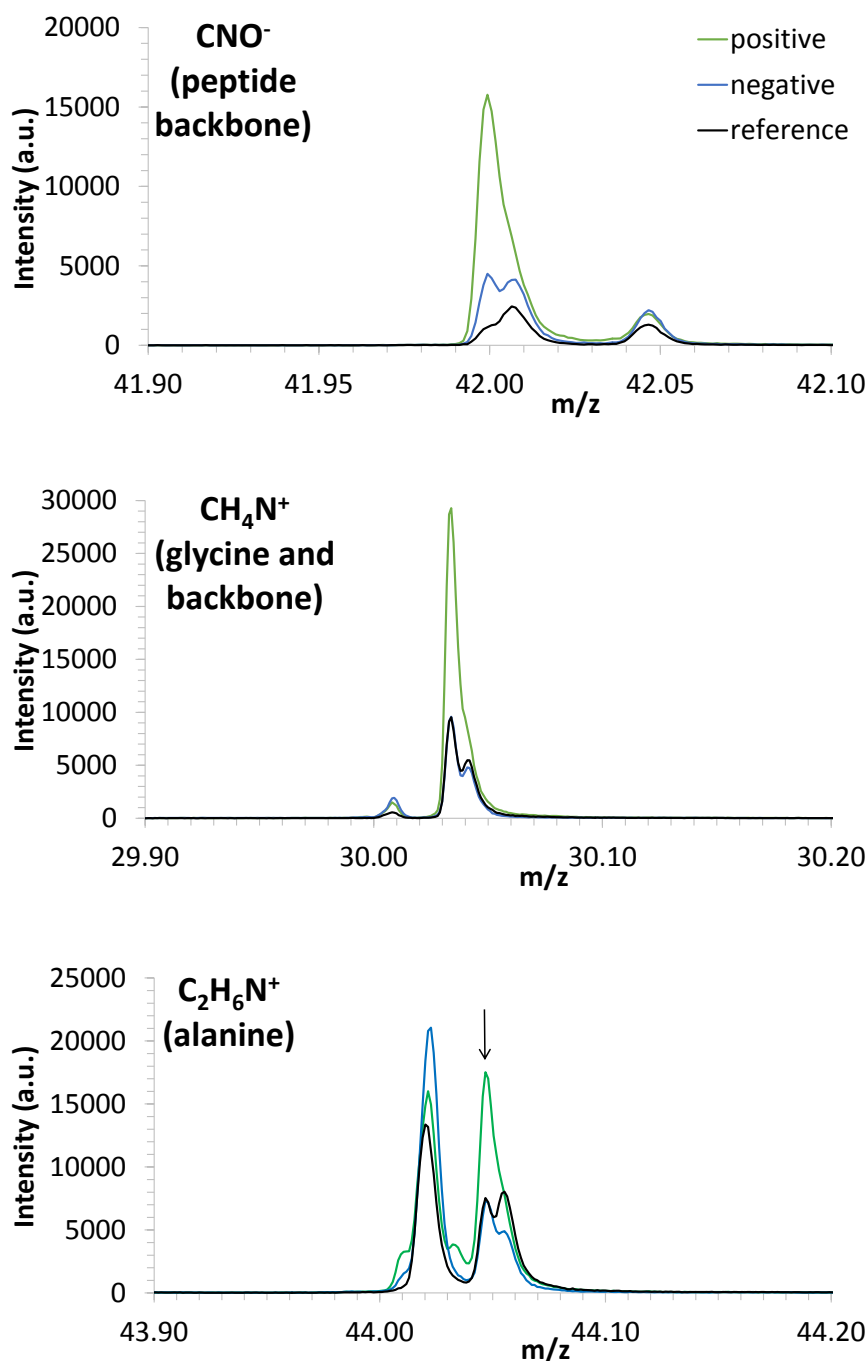
Figure 3.11.: ToF-SIMS results proving the successful covalent attachment of the peptide on the pHEMA polymer layer. The depicted diagrams show the signals assigned to CNO$^-$ (top) and CH4N$^+$ (middle) arising from the fragmentation of the peptide backbone (CH4N$^+$ peak can be indicative of both the peptide backbone and the amino acid glycine[322, 323, 324]) as well as the signal assigned to C2H6N$^+$ (bottom) originating from the fragmentation of the amino acid alanine. Each diagram compares an untreated reference, a negative sample exposed to peptides but without amine bases and a sample after thiol-ene reaction (positive).

**Analysis via ToF-SIMS**  ToF-SIMS was conducted as an additional characterization method to prove the covalent immobilization of the peptide on the surface-bound pHEMA polymer layer (Figure 3.11)[322]. Identical samples to the ones for the XPS analysis were used and they were displayed in Figure 3.11 with the same color code.

CNO$^-$ signal in Figure 3.11 (top) was indicative of the amide backbone of peptides and proteins[323]. As expected, it was strongest for the positive sample (green) and significantly lower (almost by one order of magnitude) for the blank sample (blue) and indistinct for the reference sample (black). However, a low intensity peak slightly shifted towards higher $m/z$ was observed from the negative and reference sample which could be considered as an unidentified fragment presumably originating from the pHEMA layer or from unspecific impurities as ToF-SIMS is a highly sensitive surface characterization method[322, 324] with a sampling depth of 1 nm to 2 nm[322] and is therefore able to detect even traces of impurities adsorbed on surfaces. These aspects clearly suggested that the peptide was indeed covalently linked to the pHEMA on the positive sample and that only a small amount of peptide was non-specifically adsorbed on the surface of the negative sample.

This conclusion was verified with a measurement of the immonium ion CH4N$^+$ signal displayed in Figure 3.11 (middle)[321]. The CH4N$^+$ fragment peak was the most intense signal observed in pure poly(glycine) ToF-SIMS spectra[324], though many other amino acids exhibited a fragment signal at the same $m/z$ with a significant intensity[322, 323, 324], too. Since the C-terminus of tropoelastin contained glycine among other amino acids (see Figure 2.1), it was considered to be indicative of the peptide backbone signal and glycine as well. Again, the peak with the highest intensity was obtained from the positive sample (green) while signals obtained from the negative (blue) and the reference sample (black) appeared identical, but both with a significantly lower intensity. While the distinct signal from the positive sample confirmed the covalent immobilization of the peptide to the pHEMA layer, the low intensity peaks for the negative and positive sample implied that these peaks originated from fragments of the pHEMA layer having the same $m/z$ as the immonium ion and not from unspecific adsorption of the peptide.

The signal of the C2H6N$^+$ fragment was characteristic for the amino acid alanine[323, 324] which was represent in the applied peptide (Figure 2.1). When analyzing the C2H6N$^+$ fragment, only the spectrum of the positive sample showed increased levels (Figure 3.11, bottom, green) at the corresponding $m/z$ confirming the results discussed above.

In conclusion, the results from the ToF-SIMS analysis clearly confirmed the successful covalent immobilization of the peptide on the pHEMA layer of the positive samples. A non-specific adsorption of small amounts of the peptide was lightly indicated by the CNO$^-$ signals, but not confirmed by the signals of CH4N$^+$ and C2H6N$^+$. This effect can be explained by the extreme high sensitivity of the ToF-SIMS analysis[322, 324].

After the biofunctionalization, an additional determination of its surface density would be helpful, but the use of excess peptide constructs should guarantee a nearly complete conversion.
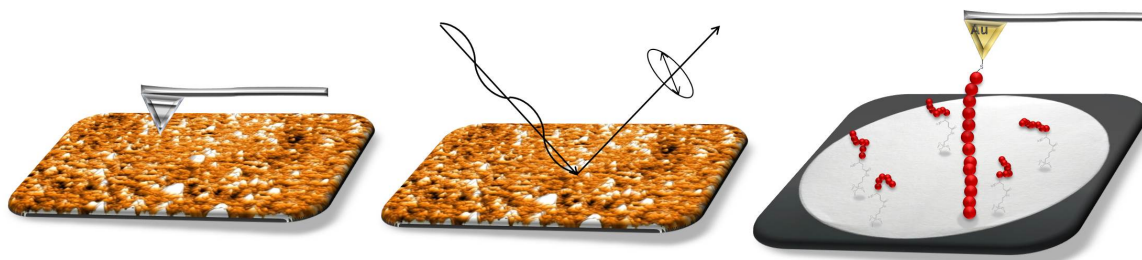
Figure 3.12.: Mechanical characterization applied to pHEMA samples. Topography via AFM imaging (left), Ellipsometry for thickness measurements (middle) and AFM based SMFS on surface tethered pHEMA molecules (right).

## 3.3. Mechanical Characterization of pHEMA

Synthesized pHEMA monolayers were characterized regarding their roughness and thickness as depicted in Figure 3.12. Furthermore, surface grafted polymer chains were analyzed via SMFS to determine their chain flexibility and elasticity in terms of polymer chain length. A comparison to the mechanical properties of tropoelastin, described in section 3.3.5, enabled the selection of an expandable polymer monolayer and one with limited expandability for mechanosensitivity studies (see section 3.4). In addition, the macromolecular growth on surfaces was monitored and compared to the growth of polymers in solution as shown in section 3.3.4.

### 3.3.1. Topographical Properties

AFM imaging was applied to study the roughness and nanotopography of the generated pHEMA films.

**Demonstration of Substrate Coverage** Two distinctive types of pHEMA samples were prepared by varying the concentration of chain transfer agent: an established protocol was used for the production of dense films[298], while a dilution of the chain transfer agent to a thousandth aimed for isolated polymer chains for SMFS.

Figure 3.13 demonstrates the different substrate coverages with RAFT anchors of SMFS samples (top) and cell studies samples (bottom). Very few isolated islands were observable on the surface prepared for SMFS. Compared with that, samples for cell studies showed much more islands and some clusters on their surface.

It has to be made clear that this is only a qualitative comparison as no information about the actual grafting density could be extracted from those images. A height of roughly 2 nm can be expected for the RAFT molecules attached to the surface. While the vertical resolution is good enough for the recognition of single molecules, the lateral resolution prevents the detection of all surface molecules.
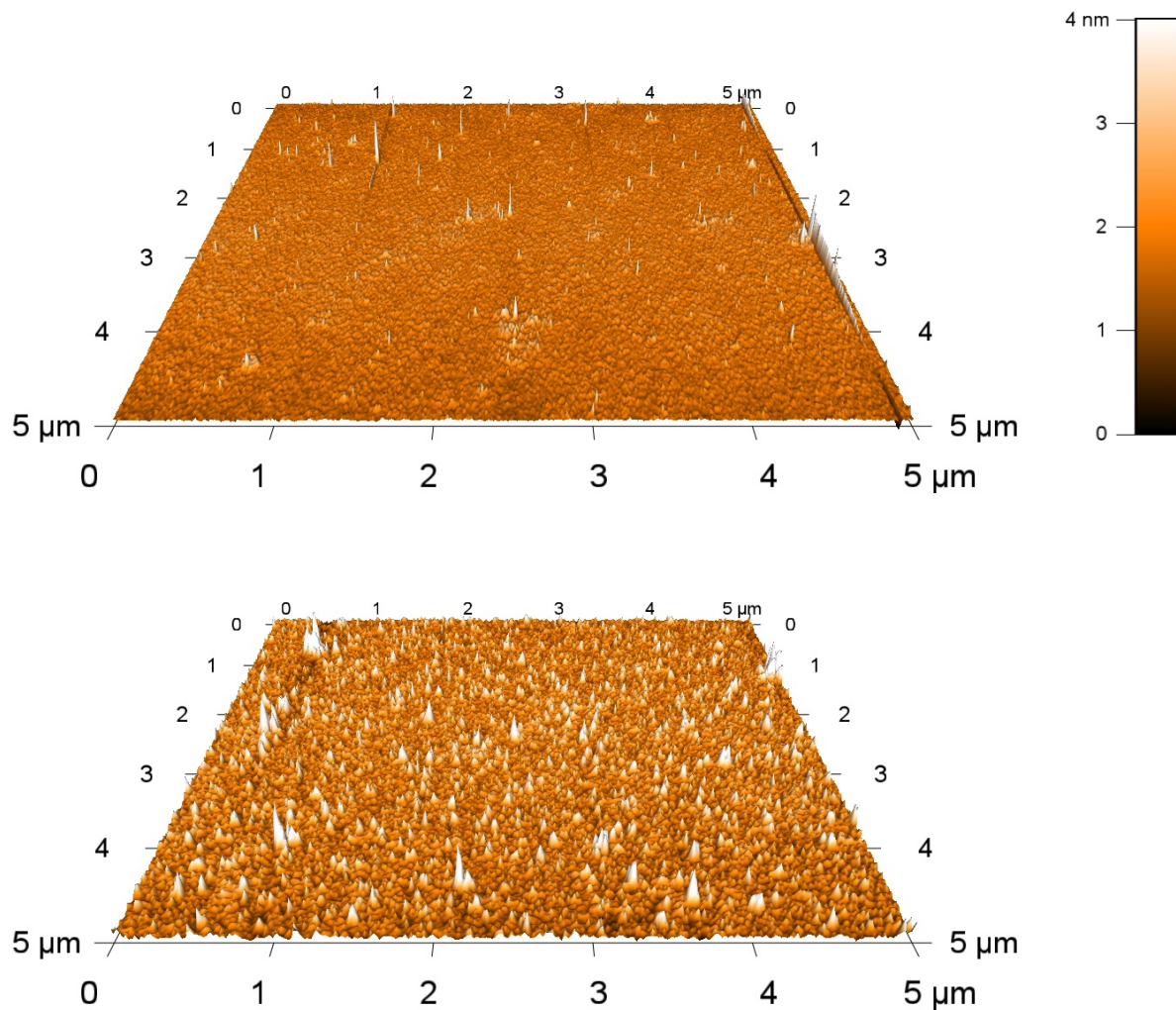
Figure 3.13.: AFM imaging of RAFT-functionalized glass substrates produced with different concentrations of chain transfer agent. Samples for SMFS measurements (top) were prepared using a thousandth of the concentration for samples in cell studies (bottom). The size of 5 µm x 5 µm was chosen for this and following images as it depicts the surface topography on the length scale of a HSPC[325].
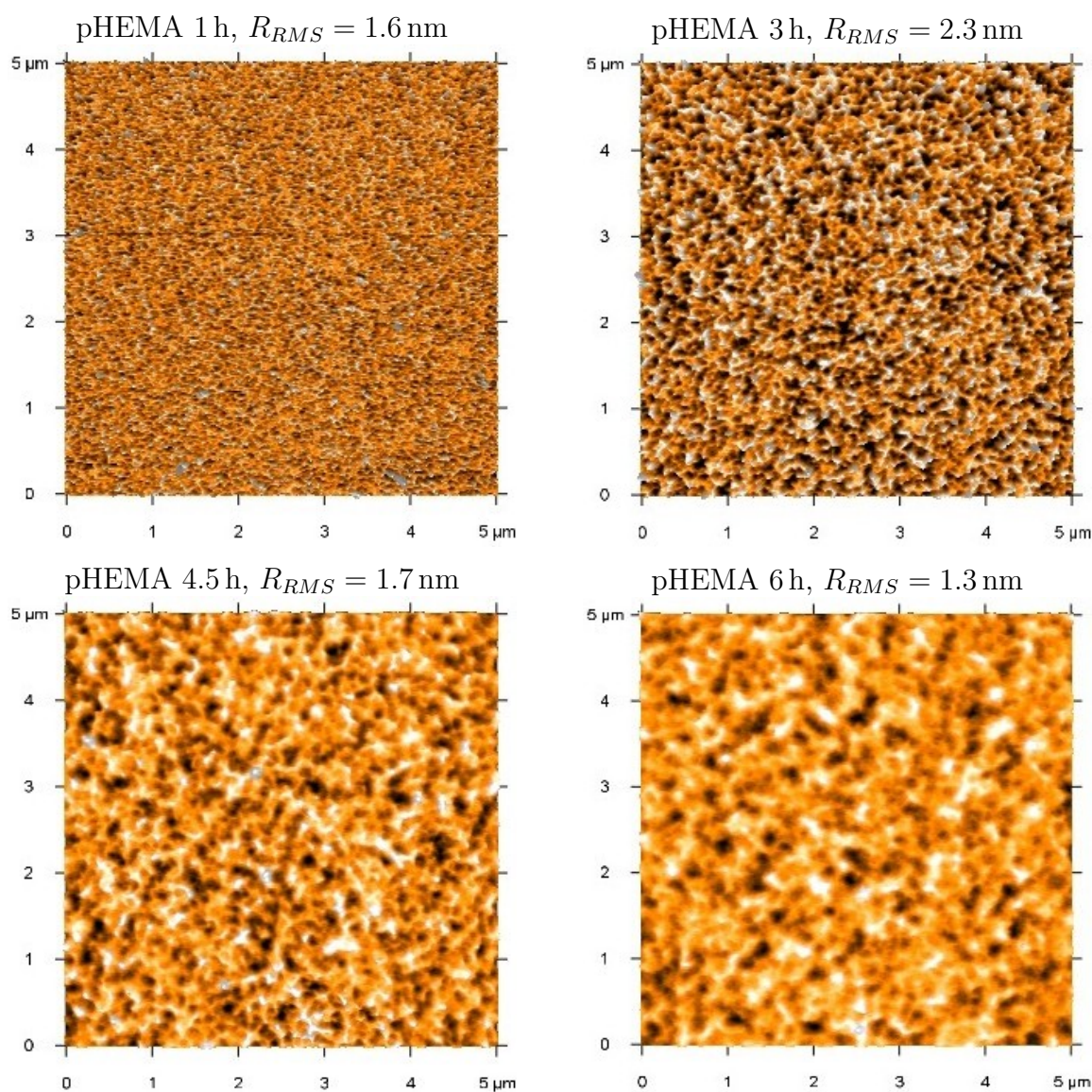
Figure 3.14.: AFM imaging of pHEMA samples at different polymerization times and their respective roughness (root-mean squared). Reprinted with permission from [278]. Copyright 2016 ACS.

**Surface Topography of pHEMA Monolayers**  To study the nanotopography of generated pHEMA surfaces, AFM imaging was applied. For this purpose, pHEMA samples fabricated with a high concentration of the RAFT agent were used (after the same protocol as those for cell studies).

Figure 3.14 depicts the respective AFM scans of representative, dried surfaces with the corresponding roughness (root-mean squared). The pHEMA surfaces showed a very low roughness in the range of 1 nm to 2 nm, which was comparable to other pHEMA substrates[298]. The smooth morphology suggested a homogeneous distribution of polymer chains on the surface and that the polymers grew in a controlled way, what is necessary for a dense packed brush[326]. In the case of lower grafting densities, a more globular mor-
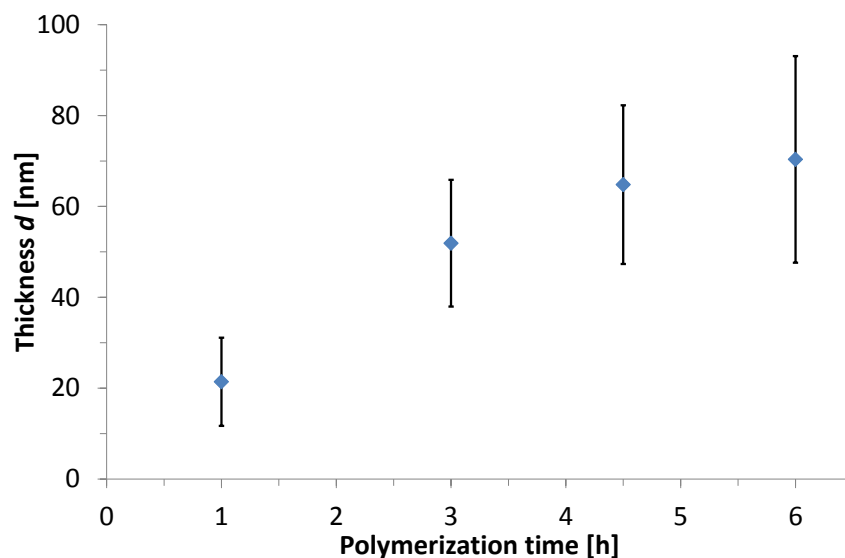
Figure 3.15.: Polymer film thickness $d$ of dry pHEMA samples measured via Ellipsometry.
$n = 3$

phology would be expected distinctive for the mushroom regime of polymer brushes[326].

A remarking difference between the topographies was that the size of observed features on the substrates increased with longer polymerization times. This could be interpreted as a measurement artifact from an interplay between AFM tip and the free polymer chain ends. Short chains could be more parallel in a densely packed stated, while longer chains could have a larger freedom of movement due to a larger deviation in chain length. Thus they would have moved around with the tip causing apparent larger features on the surface.

It can be summarized that the polymerization generated a dense, fully covering polymer film allowing for a characterization via ellipsometry and a later use in cell studies.

**Thickness Measurements** Polymer layer thickness depicted in Figure 3.15 was determined from three batches of dry pHEMA samples via ellipsometry. Measurements revealed that the film thickness ranges from 20 nm to 70 nm and seemed to increase linearly with polymerization time at the beginning. Furthermore, they were in the range reported earlier[298].

However, at higher polymerization times, the increase in layer thickness decelerated. Termination reaction could not be excluded from radical polymerizations and could cause this decrease in the surface polymerization rate. Even a small number of termination processes could cause a drastically reduction of the amount of surface radicals, and thus the rate of growth, too, as the estimated number of radicals among the tethered polymer chains was rather small[327]. Nevertheless, polymerization proceeded as the high number of dormant chains on the surface did not change significantly and allowed a re-initiation of the polymerization[327].

Table 3.1.: Grafting density $\Gamma$ calculated from film thickness $d$ and contour length $l_c$

| polymerization time [h] | 1 | 3 | 4.5 | 6 |
|---|---|---|---|---|
| grafting density $\Gamma$ $[\frac{1}{100nm^2}]$ | 28.5 | 42.6 | 40.7 | 35.7 |
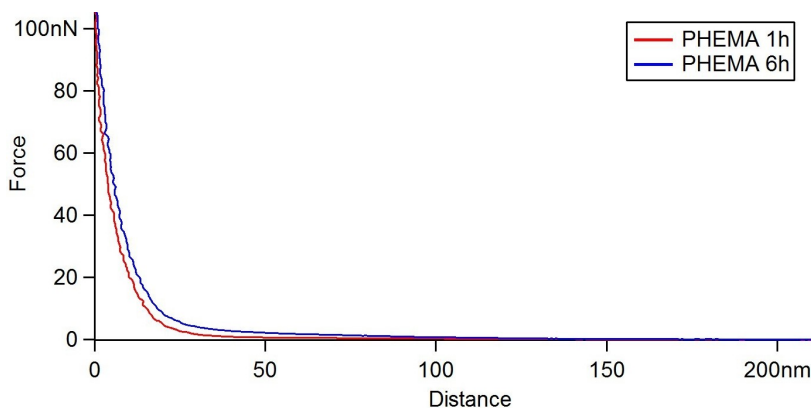


Figure 3.16.: Force measurements on wet pHEMA 1 h and pHEMA 6 h samples performed with an colloidal AFM probe. The first onsets of force give a rough estimation on the thickness of wet pHEMA films.

**Calculation of Grafting Density** The grafting density $\Gamma$ was calculated with equation 1.5 from the thickness $d$ of the dry brush using number averaged molecular mass $M_n$ and the bulk density $\rho$ of the polymer[328]. While ellipsometry measurements delivered the dry thickness $d$, the molecular mass was obtained from the average contour length $l_c$ from section 3.3.3.

The results are listed in Table 3.1. With a large error of roughly $25\,\text{chains}/100\text{nm}^2$ from propagation of error, the grafting density was constant for different polymerization times at a value of roughly $35\,\text{chains}/100\text{nm}^2$. That confirmed the expectations as all samples were polymerized from identical RAFT-functionalized substrates.

**Conformation Under Wet Conditions** In figure 3.16, the polymer layers were compressed with a colloidal AFM probe. These measurements gave a rough estimate of the polymer chain conformation under wet conditions[329].

First onsets of force, and thus the swollen thickness in water, were observed at roughly $70\,\text{nm}$ and $120\,\text{nm}$ for pHEMA 1 h and pHEMA 6 h, respectively. That corresponded to swelling ratios $l_{wet}/l_{dry}$ of 3.3 and 1.7 and a chain extensions $l_{wet}/l_c$ of 0.7 and 0.5, in good correspondence to values found elsewhere[330, 331].

Unfortunately, force curves could not be fitted to a known model such as the one from Alexander-de Gennes[331, 332, 333]. The estimated grafting densities $\Gamma$ were in the "high-density" regime above $5\,\text{chains}/100\text{nm}^2$ where higher-order interactions among grafted chains played an important role[334] which could be only modeled with computer simulations[335, 336, 337].
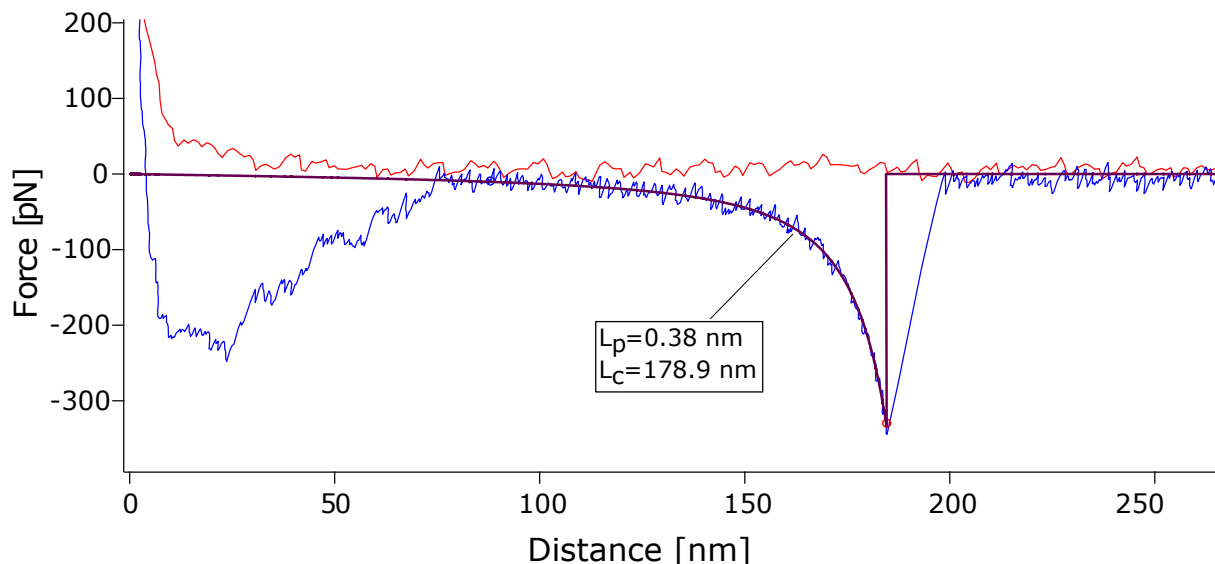
Figure 3.17.: Example of a SMFS measurement on pHEMA 5.5 h with the approach in red, the retraction in blue and the WLC fit in black. Adapted with permission from [278]. Copyright 2016 ACS.

### 3.3.2. SMFS of pHEMA

The mechanical properties of single pHEMA molecules with different polymerization times were analyzed via AFM based SMFS as schematized in Figure 3.12. In contrast to the tropoelastin measurements in section 3.1.4, surface tethered pHEMA strands were elongated with the use of an *Au* coated AFM tip picking up the thiol moieties at the free polymer ends.

Figure 3.17 displays a typical force curve of a pHEMA sample after 5.5 h of polymerization. Similarly to tropoelastin, the blue retraction curve shows an unspecific adhesion peak before the polymers chain is unfolded followed by the detachment from the tip. The unfolding part of the force curve was again fitted to the WLC model with the two parameters contour length $l_c$ and persistence length $l_p$[288]. By variation of polymerization time, polymer samples with different lengths were generated. The contour length $l_c$ of a multitude of polymer chains was recorded by SMFS and the distribution of contour length $l_c$ after different polymerization times was compared.

For SMFS, only force curves showing unfolding of a single polymer chain followed by a clear rupture event of the tip from the polymer were selected for analysis in the following section. Approximately 3.1% of the total number of recorded force curves showed unfolding and subsequent rupture. This value was similar to the yield from SMFS measurements on tropoelastin, however, in both cases, there was no data about the surface density of molecules which heavily influences the number of measured unfolding events.

Table 3.2.: Fit results for different polymer models from a batch of 85 measurements on a pHEMA 4.5 h sample. For comparison, the persistence length for the FJC and the E-FJC is given as half the Kuhn length as demonstrated in Appendix A.2.

| | contour length $l_c$ [nm] | persistence length $l_p$ [pm] | root-mean-square error [pN] |
|---|---|---|---|
| FJC | $(160 \pm 40)$ nm | $(160 \pm 50)$ pm | $(14.2 \pm 7.4)$ pN |
| WLC | $(180 \pm 50)$ nm | $(290 \pm 90)$ pm | $(10.7 \pm 2.8)$ pN |
| E-FJC | $(160 \pm 40)$ nm | $(220 \pm 70)$ pm | $(9.2 \pm 1.3)$ pN |

**Comparison of Different Elasticity Models for Single Polymer Chains**   The WLC model is often used for natural molecules such as the protein tropoelastin[128, 149] or DNA[287, 289] as this models suitably fits for stiff polymers[287, 282]. Measurements in this section enabled the investigation whether this models is also adequate for pHEMA strands.

Force-extension measurements on a single pHEMA 4.5 h sample were fitted to the models of a FJC, WLC and E-FJC. Figure 3.18 shows examples of the fits to a single measurement curve.

The FJC model deviated at lower displacements as well as at high displacements (Figure 3.18, top). The nonlinear upturn in force at high displacements was too steep to fit to the measured curve.

The force-extension of pHEMA could be reproduced more precisely with the WLC models in Figure 3.18, middle. Although there was a small overestimation at low displacements and a small underestimation at high displacements, the fit always lied within the scatter of measurement. The force rised sooner for the stiff WLC compared to the FJC and the divergence was smaller due to the continuous bending of a WLC.

The fit quality could be even increased with the E-FJC models as displayed in Figure 3.18, bottom, and demonstrated with the root-mean-square error of the fit in Table 3.2. The introduction of a stretch modulus for the chain segments led to a "softening" of the polymer chain that fitted the force-extension data over the full measurement.

As both models for FJC describe a softer chain than the WLC model, a fit to the same data gave a lower contour length $l_c$ as listed in Table 3.2. However, due to the restriction of discontinuous bending in the FJC model, a lower persistence length $l_p$ (calculated from Kuhn length as demonstrated in Appendix A.2) was necessary to reflect the more moderate force increase from the data. For the E-FJC with elastic chain segments, this was less the case resulting in a persistence length between the other two models.

In conclusion, the FJC model was not suited to describe the extension of pHEMA strands under force. Although the WLC fitted the pHEMA behavior slightly worse than the E-FJC, this model gave a good result and was used for the following work. A comparison between the elastic behavior of tropoelastin and pHEMA was intended and this should be based on the same model.
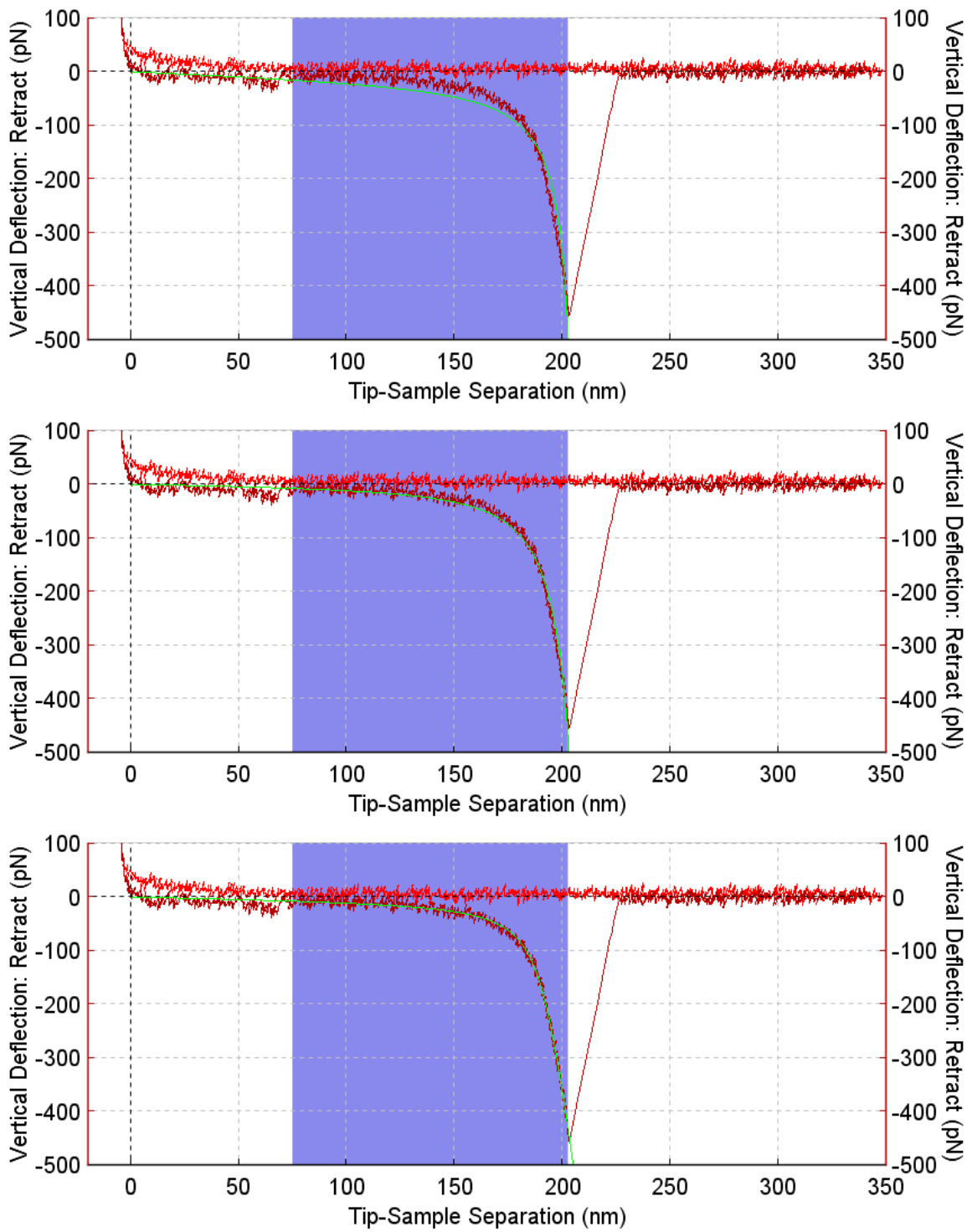
Figure 3.18.: Comparison of various elasticity models for polymer chains: FJC (top), WLC (middle) and E-FJC (bottom).

72

**Specific Binding of the Cantilever** As described before, the AFM cantilever tip specifically attached to thiol moieties at the surface-distant polymer ends of the prepared pHEMA surfaces. The binding specificity was shown by the strong increase in the number of observed unfolding events when comparing the data in Figure 3.19 of polymer chains before (bulky RAFT agent exposed at the free chain end) and after aminolysis, which transformed the thiocarbonylthio terminus of the pHEMA chains into a thiol moiety.

For the protected termini (top), a rather high unspecific adhesion peak between the sample and the cantilever and very few events of polymer unfolding could be observed. In the case of the freshly deprotected thiol group (middle), a clear unfolding of polymers with different chain lengths could be observed in many force curves. After 3 h (bottom), unspecific adhesion increased and the number of unfolding events decreased. In this specific batch, the deprotection through aminolysis led to a 10 fold higher number of unfolding events compared to the RAFT-terminal polymers. This was comparable with other systems in which a change from unspecific binding to binding between thiol and $Au$ raised the number of successful unfolding events from $0.8\,\%$ to $4\,\%$[338].

Thus, the specific binding of the polymer to the AFM tip implied that the polymer chains were bound at their both ends when stretched between substrate and AFM tip. This ensured that the full polymer chain length contributed to the measured contour length $l_c$[276]. Furthermore, this experiment demonstrated indirectly that the RAFT moiety was present and still intact after the polymerization.

**Influence of Grafting Density on Polymer Surface Growth** The use of isolated polymer strands was necessary for SMFS measurements to determine the mechanical properties of single molecules as intended in this work and for a good comparison to studies on single tropoelastin molecules[128, 149]. In the middle and high density regime of polymer brushes, mechanical interaction between adjacent polymer chains is possible[331].

Thus, the grafting density $\Gamma$ was varied for pHEMA surfaces that were intended for SMFS or cell studies. However, grafting density can influence reactions at the surface as it does for the cleavage of polymers[339]. It was also reported that the grafting density affects the growth rate of polymer chains[340] and that very high grafting densities can lead to additional termination mechanisms[327]. Therefore, the influence of grafting density on chain growth was studied in our system as summarized in Figure 3.20.

No significant difference in the contour length $l_c$ could be observed between pHEMA samples with low and high grafting density. However, the number of successful unfolding events increased from $1.6\,\%$ to $3.6\,\%$ for small grafting densities in this experiment giving another reason for the use of isolated molecules in SMFS studies.

In the above mentioned paper, measurements on one monomer were left aside in their calculations as its density dependent growth did not fit other analyzed monomers[340]. Thus, this aspect could have varied from system to system for which reason the influence of grafting density on polymer growth must not be generalized.
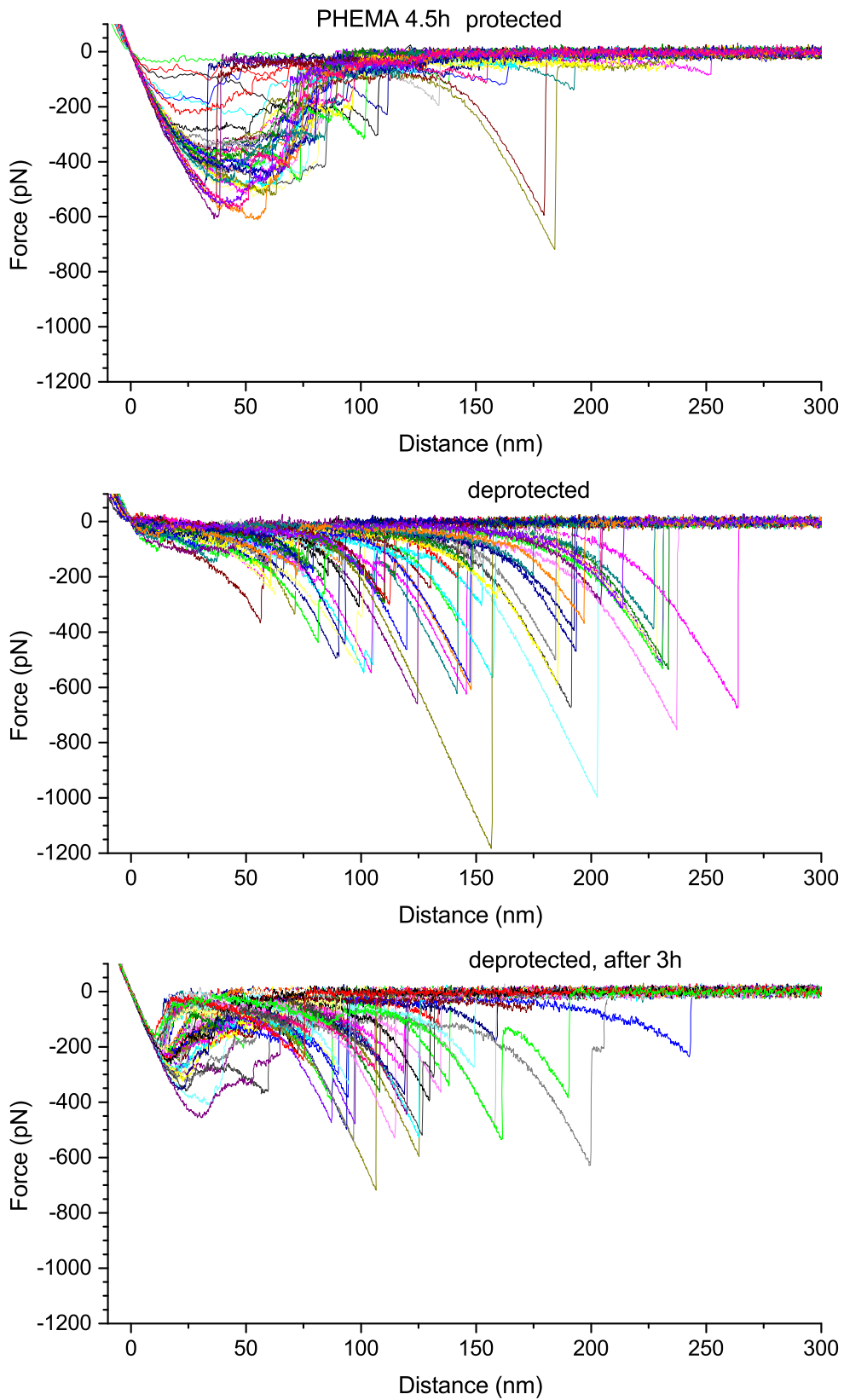
Figure 3.19.: Comparison of 40 random force measurements of the same sample surface before aminolysis (top), freshly after aminolysis (starting from 10 min, middle) and 3 h after aminolysis (bottom).
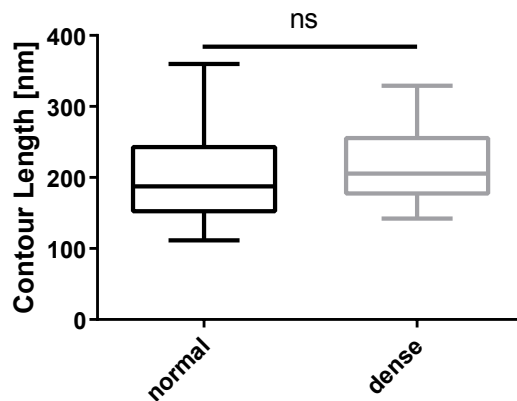
Figure 3.20.: Comparison of contour length $l_c$ for pHEMA utilized for SMFS (normal) and cell studies (dense) that vary in grafting density $\Gamma$.

**Chain Stiffness from Persistence Length**  The chain flexibility can be determined as the Kuhn length or persistence length $l_p$ which is half the Kuhn length[341]. The persistence length $l_p$ was determined as $(0.2 \pm 0.1)\,\mathrm{nm}$ for all pHEMA samples which was close to its reported value[342]. It is only dependent on the chemical structure and not on the molecular weight[343] as could be confirmed with the present measurements. As the persistence length of pHEMA was in the range of the value determined for tropoelastin $(0.3\,\mathrm{nm})$ and due to its good biocompatibility[200], work with pHEMA was continued in further mechanical characterization and cell studies.

### 3.3.3. Mapping of Surface Initiated Polymer Growth

The polymer growth of SI-RAFT polymerization was mapped using SMFS. Figure 3.21 shows representative force–distance curves for the unfolding of single surface-anchored pHEMA chains synthesized with different polymerization times and which differed in their chain length. The force measurements displayed a distinct change in measured contour length $l_c$ over polymerization time while maintaining the persistence length $l_p$ constant at roughly $(0.2 \pm 0.1)\,\mathrm{nm}$.

The contour length and its distribution is displayed in Figure 3.22 for four pHEMA samples with varying polymerization times. As expected, contour length $l_c$ increased with longer polymerization time. The average contour length changed from nearly $110\,\mathrm{nm}$ for a polymerization of $1\,\mathrm{h}$ over $180\,\mathrm{nm}$ $(3\,\mathrm{h})$ to approximately $280\,\mathrm{nm}$ and $390\,\mathrm{nm}$ for $6\,\mathrm{h}$ and $10\,\mathrm{h}$, respectively. In addition, the deviation for each sample increased slightly, too. However, as the polydispersity Đ is related to the average molar mass, its value was constant for all polymerization times.

When plotting the contour length $l_c$ against the polymerization time as executed in Figure 3.23, the linear increase of contour length came to light. Thus, this result suggested
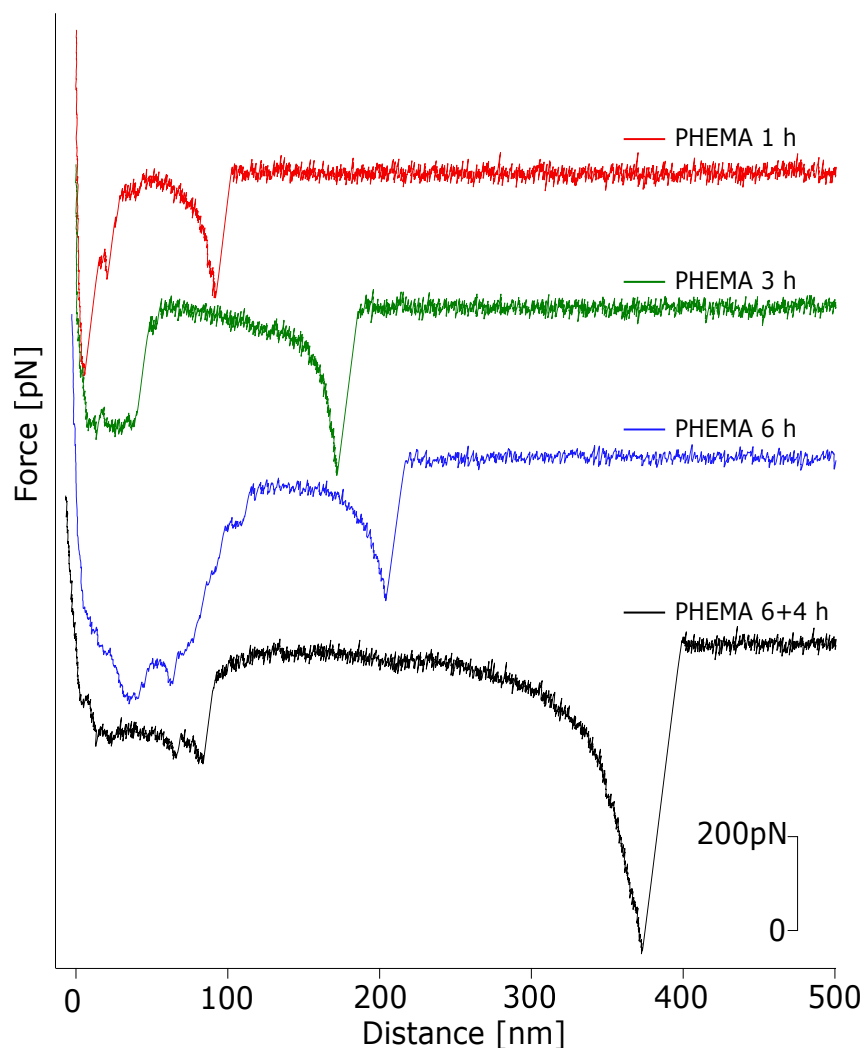
Figure 3.21.: Representative force–distance curves of pHEMA strands with four different polymerization times. Reprinted with permission from [278]. Copyright 2016 ACS.

a process with controlled characteristic for the SI-RAFT polymerization.

Figure 3.23 displays an initial increase in contour length before 1 h of polymerization. For very early reaction times, the system could exhibit a combination of a controlled free-radical and the conventional RAFT polymerization, a so-called "hybrid" behavior as discussed in section 3.3.4.

With the sample pHEMA $6 + 4$ h (black data in Figures 3.21 and 3.22), the livingness of the RAFT polymerization was proven. The pHEMA substrate was removed after 6 h from the reaction mixture and transferred the following day to a fresh polymerization solution. The chain could be extended without any performance loss as this sample fitted into the linear growth of contour length $l_c$ in Figure 3.23.
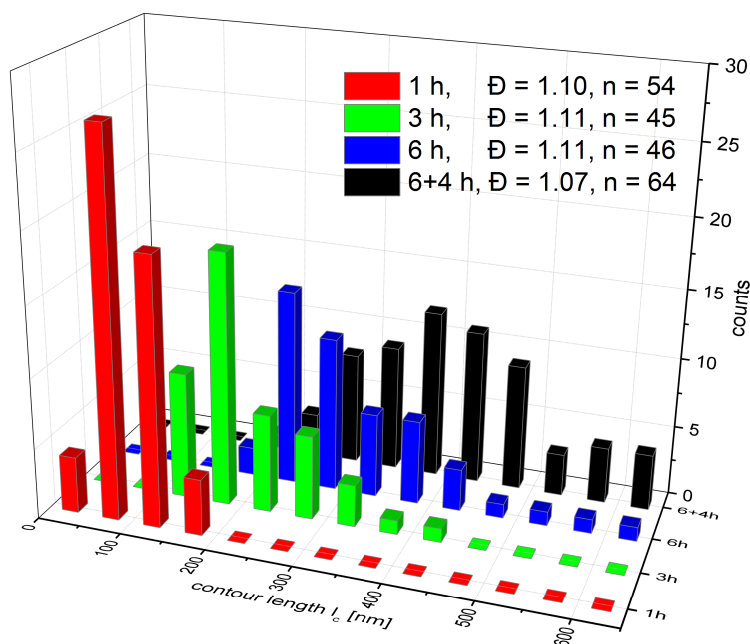
Figure 3.22.: Contour length $l_c$ distribution for different polymerization times. The corresponding polydispersity Đ can be calculated by converting the contour length into molar masses. n = number of analyzed force curves. Reprinted with permission from [278]. Copyright 2016 ACS.
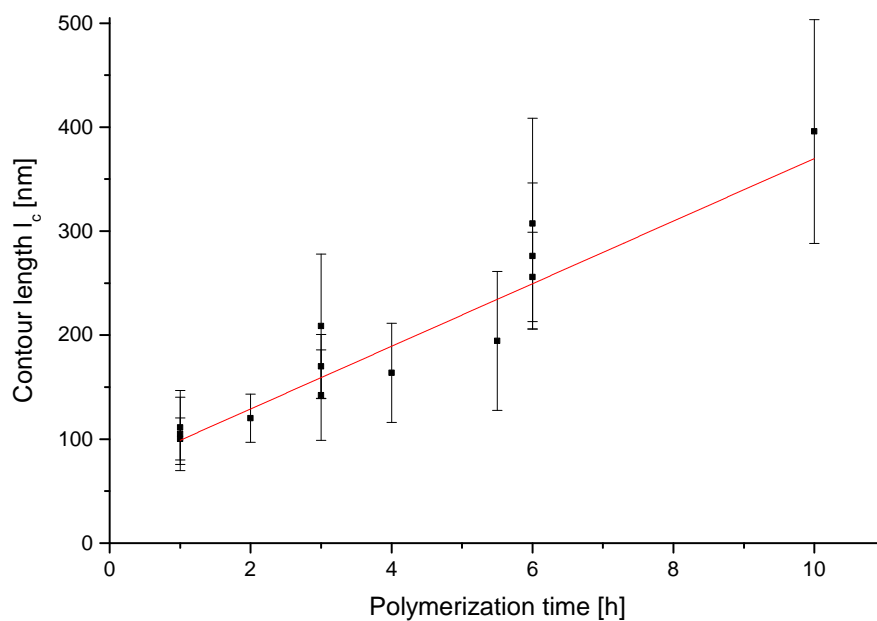


Figure 3.23.: Contour length $l_c$ dependent on the polymerization time for all analyzed pHEMA samples. A linear increase of contour length is observed with an initial increase at very early polymerization times. Reprinted with permission from [278]. Copyright 2016 ACS.
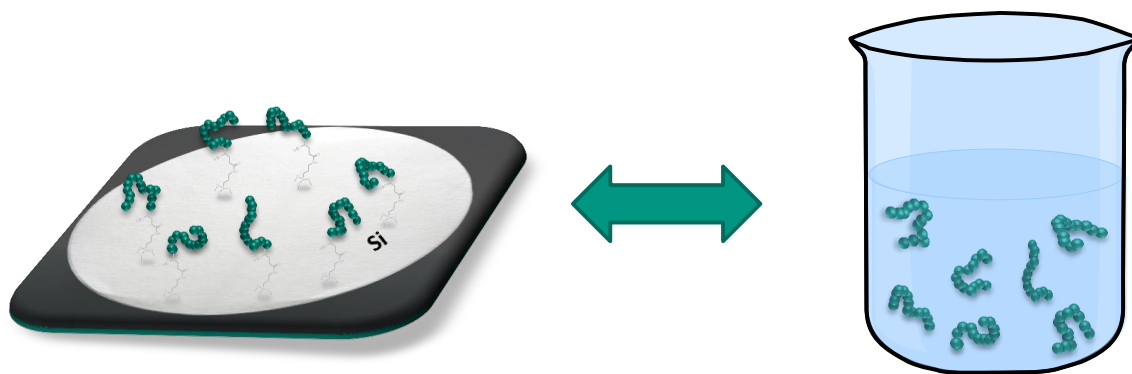
Figure 3.24.: Scheme for polymerization in solution and 'grafting from' polymerization.

## 3.3.4. SI Polymerization Compared to Polymerization in Solution

SI polymerization is a technique of increasing importance for the design of functional interfaces, especially for biosurfaces[208]. Thus, an in-depth understanding of the processes directly at the surface is necessary. SI has been investigated with many different methods: Time-resolved electron spin resonance spectroscopy shed light on surface termination kinetics[344], surface plasmon resonance[345] as well as quartz crystal microbalance[346] were employed to follow the addition of monomer units to the surface tethered polymers, SEC was used for the analysis of SI polymers that were cleaved of from cellulose surfaces[347], nanoparticles[348] or silicon substrates[340]. However, the characterization is rather challenging due to the low amount of detachable polymer or the requirement of a gentle detachment from substrate.

Recently, surface anchored pHEMA grafts generated via SI-RAFT polymerization were analyzed with XPS, AFM imaging, ellipsometry and contact angle measurements aiming for the chemical composition or morphology of films[298]. These studies delivered only information about the bulk polymer film and missed the characterization of the polymer chains. Investigations on polymer chains in turn were mainly possible in solution. Thus, SMFS was introduced as a powerful technique for nondestructive mapping of the growth of single polymer strands on surfaces[278]. In addition, it allowed the characterization of surface tethered polymer chains in a solvated environment thereby enabling a direct comparison of chain length or rather molecular weight of polymers in solution with those on the surface as displayed in Figure 3.24.

In this section, the investigation of RAFT polymerization of pHEMA in solution was described by SEC and NMR and opposed to the preceding results from SMFS studies.
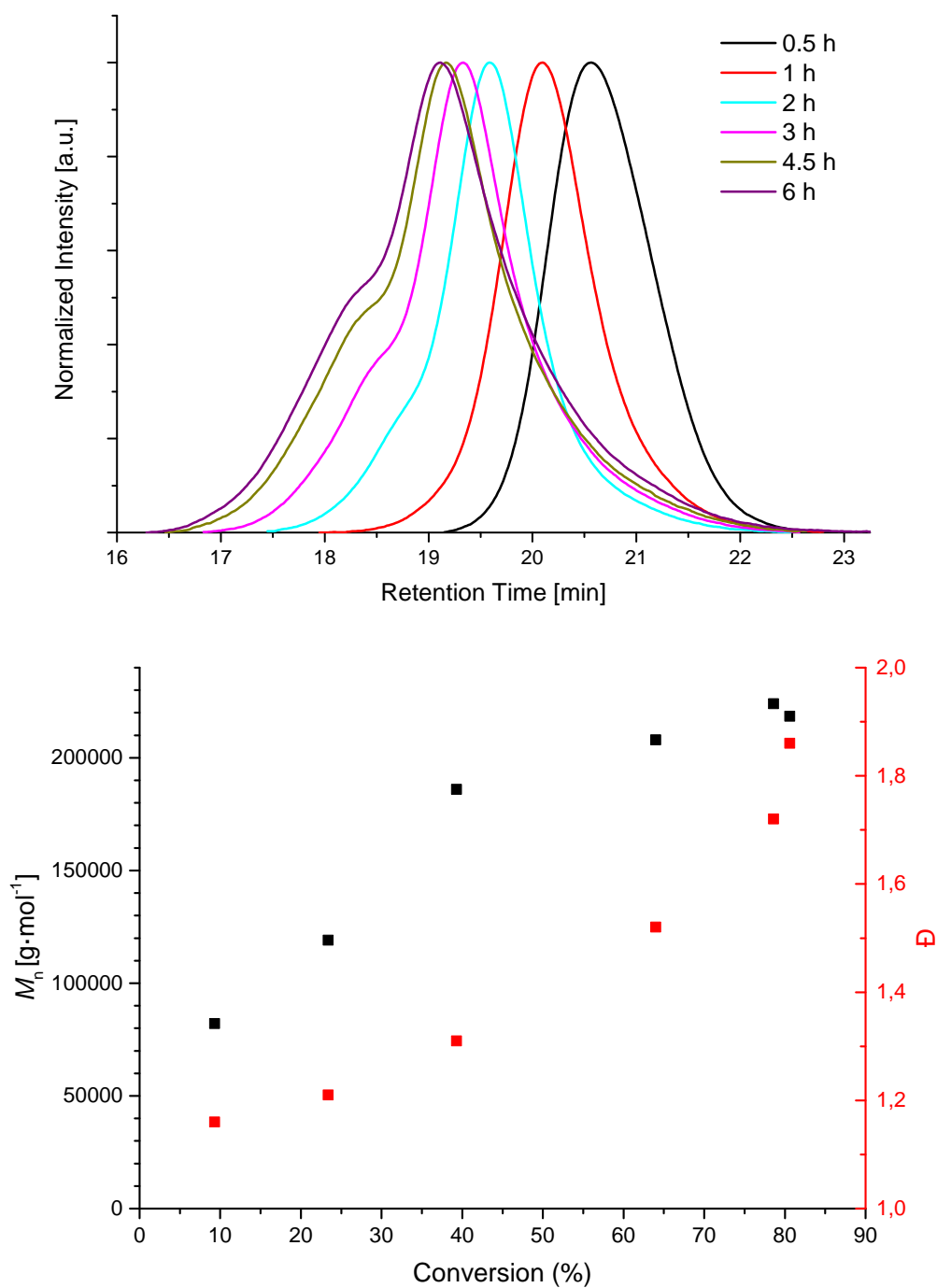
Figure 3.25.: pHEMA precipitated after different polymerization times analyzed via SEC. DMAc was employed as SEC solvent. Molecular weight was determined using a poly(methyl methacrylate) (PMMA) calibration. NMR measurements delivered the conversion data. Reprinted with permission from [278]. Copyright 2016 ACS.

**Characterization of pHEMA in Solution**  Figure 3.25 compares the growth of polymers measured in solution with SEC at different time points. The polymer growth could be divided into three phases: An initial rapid increase in molecular weight at very early polymerization times passing over to a steady increase between 0.5 h to 2 h of reaction time until reaching a plateau after 3 h. Also the conversion in solution from NMR measurements, which hardly increased between 4.5 h to 6 h, indicated cease of polymer growth. Plateauing at a conversion of roughly 70% was congruent with previous observations[298, 331]. Meanwhile, the polydispersity Đ increased steadily with a steep rise after 4.5 h.

The course at early reaction times could be attributed to a combination of controlled free-radical and chain transfer polymerization, a so-called hybrid behavior[349]. Furthermore, it also explained the significant tailing to low molecular weights as a considerable amount of non-extendable chains could have been generated by disproportional processes events at early polymerization times. While the steady increase of molecular weight corresponded to the RAFT polymerization, formation of additional high molecular weight material – and thus the steep rise in polydispersity – was caused by bimolecular termination.

**Comparison of Polymerization in Solution and on the Surface**  When comparing the polymer growth through RAFT polymerization on surfaces and in solution, the so-called hybrid behavior at very early polymerization times could be observed for both cases, via SMFS in Figure 3.23 and via SEC in Figure 3.25. For the ellipsometry data in Figure 3.15, this interpretation was likewise possible but not compelling due to the high standard deviation between different batches.

For the further progress of the polymerization, a linear increase in polymer chain length over time was observed. While the SI-RAFT polymerization showed this dynamic behavior up to 6 h of polymerization – even beyond in the chain extension experiment with an exchange of the polymerization solution after 6 h – the polymers in solution already ceased macromolecular growth at this time point since the molecular weight distribution and the conversion indicated limited growth. The correlation between contour length $l_c$ and the conversion in Figure 3.26 showed that the SI-RAFT polymerization proceeded even up to high conversions of roughly 85 %.

The molar mass of a surface bound polymer $M_i$ was calculated with equation 1.1 from the contour length $l_c$ with the molar mass of the monomer HEMA $M_{mono} = 130.13\,\text{g mol}^{-1}$ and the length of a monomer $l_{mono} = 0.25\,\text{nm}$ (the projected C-C-C distance in the polymer backbone). With the use of the number averaged molar mass $M_n$ and the mass averaged molar mass $M_w$ the polydispersity Đ could be computed (equations 1.2 to 1.4) as was already done by other groups[350, 351]. The development of the molecular weight of pHEMA molecules in solution and of surface-anchored polymer strands is opposed in Figure 3.27. The comparison of the different molecular weights confirmed that the RAFT polymerization continued when the molecular weight in solution already reached a plateau, although it seemed to reach an overall higher value than the molecular weight on the surface. At
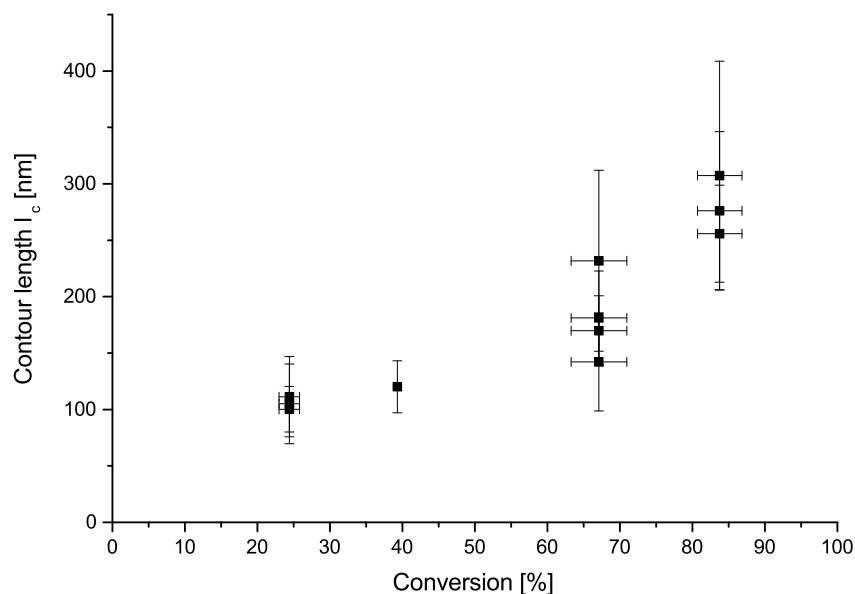
Figure 3.26.: Contour length $l_c$ determined via SMFS against conversion calculated from NMR. Reprinted with permission from [278]. Copyright 2016 ACS.

this point, it should be noted that molecular weight values from SEC measurements were values relative to PMMA and thus not absolute values in contrast to the ones from SMFS. Therefore, the comparison of that data only allowed for conclusion on relative polymer growth, yet not for the absolute correlation of molecular weight data from SMFS and SEC.

The SMFS analysis of surface tethered pHEMA terminated by a thiol moiety delivered a very narrow distribution with a polydispersity Đ of roughly 1.1 constant over the whole polymerization process (see Figure 3.22). In contrast to that, the polydispersity of polymers in solution increased with longer polymerization time reaching Đ = 1.8 after 6 h as displayed in Figure 3.25. As discussed before, this increase could be contributed to the significant tailing to low molecular weights and the formation of additional high molecular weight material.

The disparate result from SMFS and SEC data in our measurements could be easily understood: SMFS with a gold coated tip favored the unfolding of thiol terminated polymer chains as discussed in section 3.3.2 over polymer strands that were terminated by radical processes. This explained on the one hand that the polydispersity obtained from SMFS was lower than in solution and on the other hand the missing plateauing of contour length after long polymerization times. In contrast to that, the ellipsometry data did show a similar leveling off in thickness measurements as it captured the entire distribution with the inclusion of nonfunctional chains generated by disproportionation events.

Nevertheless, no proposition was possible from the SMFS measurements whether there were fewer termination events on the surface or that the corresponding polymer chains
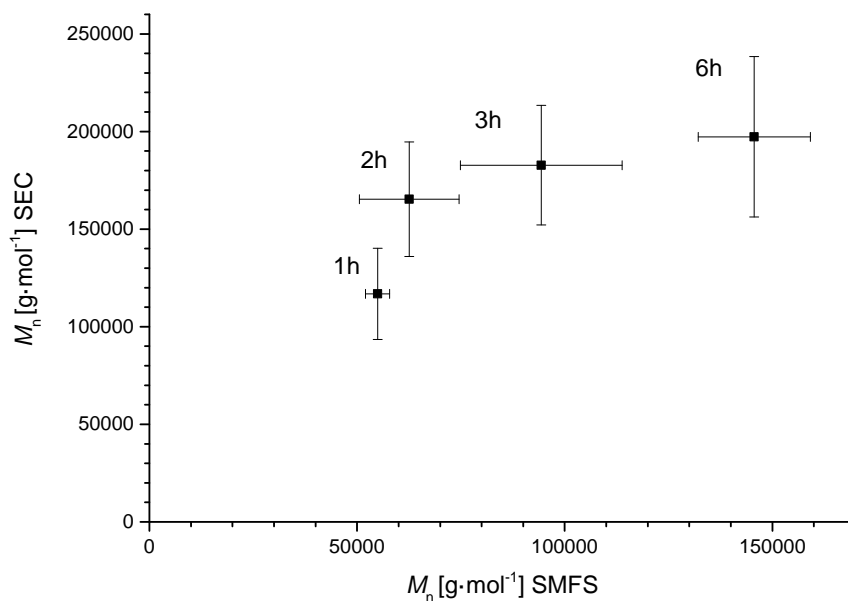
Figure 3.27.: Number averaged molar mass $M_n$ derived from SEC compared to the one from SMFS obtained after different polymerization times. For SMFS, the molar mass was calculated from contour length $l_c$ with the use of the mass of a HEMA monomer. Horizontal and vertical error bars represent the standard deviation of averaging several SMFS experiments and the standard error of an SEC experiment, respectively. Reprinted with permission from [278]. Copyright 2016 ACS.

were less often unfolded. In a kinetic analysis of RAFT polymerization on flat surfaces, a model was developed that predicted additional termination processes on surfaces[327]. However, those processes should come more into account with high grafting densities and not in the case of isolated pHEMA strands.

The observation on the polydispersity was in contrast to results reported by other authors performing SMFS on polymer brushes of poly(N-isopropylacrylamide) polymerized via SI ATRP on latex particles[351]. A higher polydispersity was determined for surface bound polymer than measured in solution. However, apart from the differences in the polymerization process and the monomer, unfolding over the full length of polymer chains was not ensured due to a missing specific binding to the polymer chain end moiety and thus allowing separations smaller than the contour length.

In conclusion, SMFS was introduced as a versatile and direct characterization technique for the analysis of SI-RAFT polymerization that could be carried out under a wide range of conditions and monomers and the use of thiocarbonylthio aminolysis is applicable to all SI-RAFT systems. With its accurate determination of polymer chain length it could thereby shed new light on polymerization processes on surfaces. A small preference for polymers with a functional RAFT end group over terminated chains could be observed

which set the focus on the characterization of single molecules instead of the whole polymer film. However, this fact could be used in combination with other techniques to deduct polymerization from termination processes. For the purpose of this work, a selective characterization of polymer strands with functional RAFT moieties was advantageous as only those polymers could be transferred into biofunctional end groups that acted as adhesion anchors for cells as employed in section 3.4. Thus only cell relevant polymer chains were tested for their mechanical properties. Furthermore, SMFS was necessary for the determination of contour length on surfaces as this was not possible from solution due to the differences in measured molecular masses on surfaces and in solution.

### 3.3.5. Comparison of pHEMA to Tropoelastin

pHEMA substrates were compared to tropoelastin in terms of mechanical properties to decide whether it could function as a biomimetic and xenogen-free model system for mechanosensitivity studies with extensibility of the substrate being the only varying parameter.

**Surface Topography**    Figure 3.28 demonstrates the smoothness of pHEMA samples compared to tropoelastin coated samples. Viewed at the same scale, pHEMA with a roughness in the range of 1 nm to 2 nm was flat compared to tropoelastin with a roughness of 7.5 nm and islands with a height of roughly 12 nm.
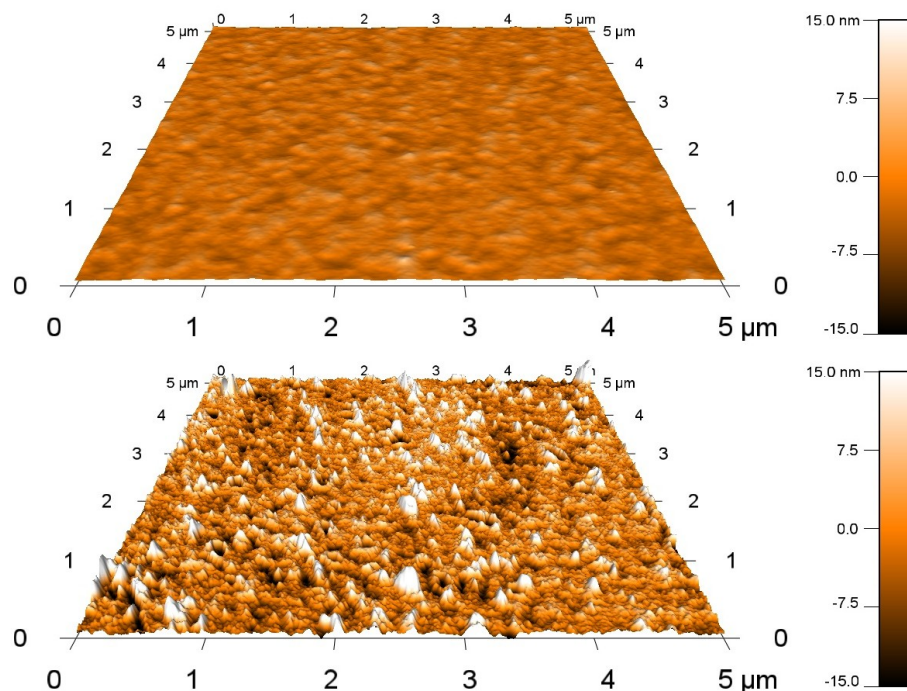


Figure 3.28.: AFM imaging of a pHEMA 6 h sample (top) compared to a substrate coated with tropoelastin (bottom) displayed with the same scale.
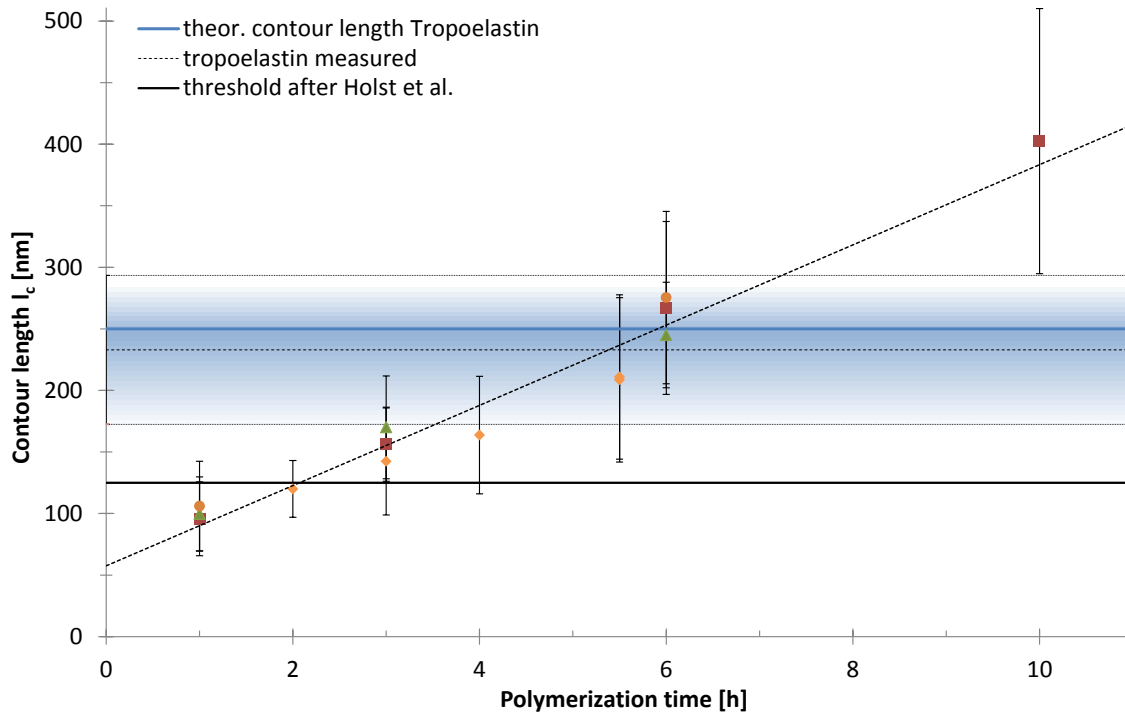
Figure 3.29.: Summary of pHEMA contour length $l_c$ in comparison with values obtained from a tropoelastin study[128]. The blue shaded target range is derived from the mean contour length and standard deviation of SMFS measurements on tropoelastin. Below 125 nm, no beneficial effect of tropoelastin on HSPC proliferation was observed.

Most studies investigated the effect of roughness on cell adhesion on a larger scale of hundreds of nanometers or even micrometer. However, it was also reported that an increase of roughness from roughly 5 nm to 10 nm of $Ti$ samples already increased the viability and number of adherent osteoblast cells[352]. In addition, topographies with an island height of 12 nm could already have an influence on the mechanosensitivity of MSCs[88]. Thus, the roughness of tropoelastin could not be neglected and was a possible parameter influencing cell adhesion. For the roughness range of pHEMA samples, no effect on cell adhesion was reported. Therefore, roughness could be ruled out as an influencing parameter in mechanosensitivity studies for a pHEMA model system.

**pHEMA Replicates the Mechanical Properties of Tropoelastin** Figure 3.29 summarizes contour length $l_c$ obtained from pHEMA studies and opposes it to tropoelastin. The blue shaded target range was aimed for to reproduce the beneficial effect of tropoelastin on HSPC proliferation[128]. This range was defined by SMFS studies on tropoelastin using the mean contour length and its standard deviation. A threshold value of 125 nm was drawn for tropoelastin elasticity affecting HSPCs[128].
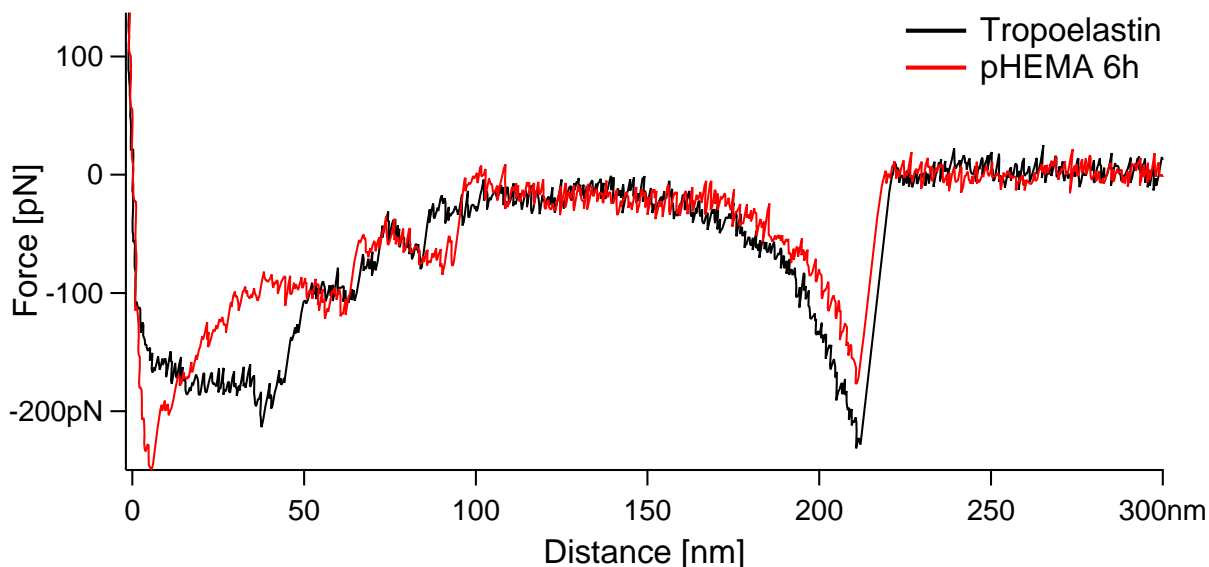
Figure 3.30.: Direct comparison of two exemplary unfolding curves from SMFS measurements on tropoelastin and pHEMA 6 h.

Using the mapping of pHEMA growth on substrates, samples with a polymerization time of 6 h could be recognized as similar to tropoelastin. The shorter contour length of cross-linked tropoelastin could be mimicked by pHEMA 1 h samples.

Figure 3.30 shows a nearly matching overlay of two force-distance curves from SMFS on tropoelastin and a pHEMA 6 h molecule. Both force curves showed unspecific adhesion at the beginning of the retraction curve in the same range followed by a very similar behaviour during unfolding. The values for the WLC fit agreed in the contour length $l_c$ and the persistence length $l_p$. This concluded matching mechanical properties in terms of pulling at single molecules.

When comparing a whole bunch of SMFS measurements as in Figure 3.31, different distributions could be noticed. Although pHEMA from SI-RAFT polymerization bore a very small polydispersity Đ in the range of 1.1, the distribution of contour lengths appeared rather broad in Figure 3.31 whilst having a comparable mean contour length to tropoelastin. Tropoelastin in contrast is a biomolecule with a defined molar mass. Thus, the occurring differences in measured contour length was only caused when tropoelastin molecules were not picked up at a terminal end by the AFM tip. An seeming polydispersity Đ of 1.05 could be calculated for the SMFS measurements of tropoelastin which was even smaller than that of pHEMA. This small disparity had to be kept in mind when performing cell studies with pHEMA and tropoelastin. However, the differences in cell reaction should have been small because of HSPCs seeming to be tolerant to a range of contour lengths: also truncated tropoelastin molecules increased their proliferation[128].

Two additional differences between pHEMA and tropoelastin had to be discussed. Figure
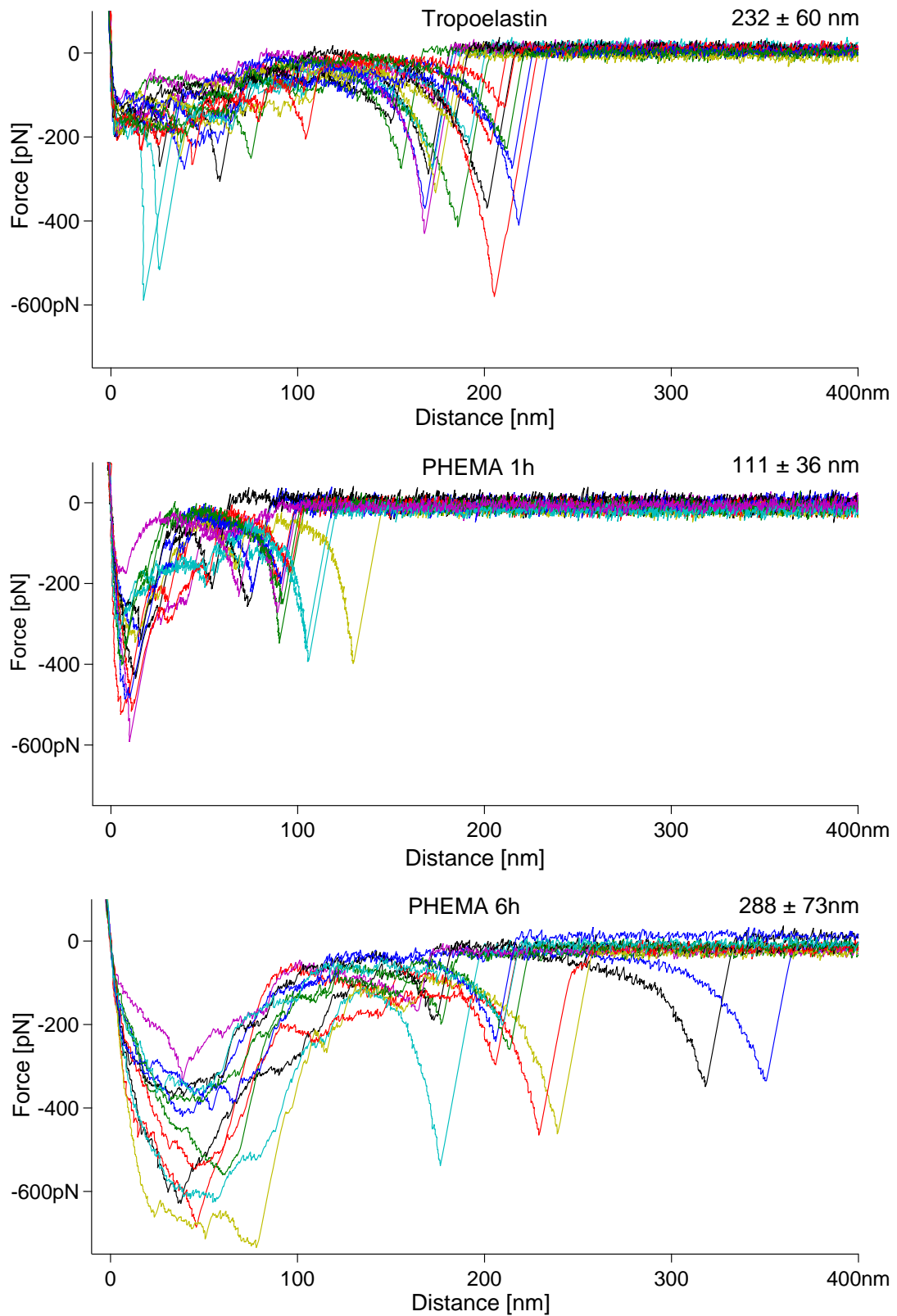
Figure 3.31.: Comparison of 15 exemplary unfolding curves of tropoelastin, pHEMA 1 h and pHEMA 6 h. Mean contour length $l_c$ and standard deviation are inserted into the plots.
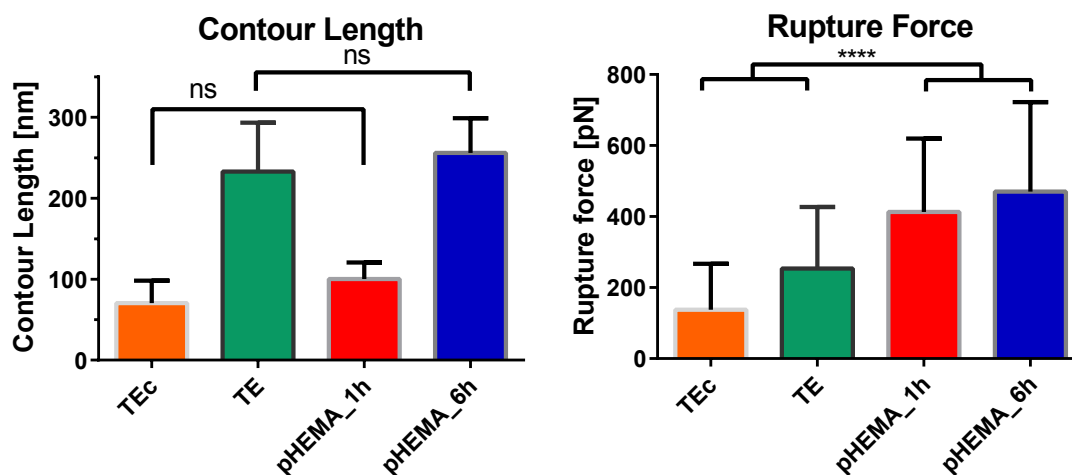
Figure 3.32.: Summary of SMFS on tropoelastin (TE), cross-linked tropoelastin (TEc) and pHEMA. pHEMA 6 h samples were selected for mimicking tropoelastin in mechanosensitivity studies while pHEMA 1 h emulated the reduced extensibility of cross-linked tropoelastin. The increased rupture force for pHEMA reflected the better characterization with a covalent tip-molecule bond in SMFS experiments as compared to binding via adsorption between tropoelastin and the AFM tip.

3.31 displays that unspecific adhesion in SMFS of pHEMA increased with longer polymer chains. A possible cause were interactions of the AFM tip with additional polymers attached to the tip or not end-fixed polymers and the interaction of polymer chain segments with the substrate[268]. These could be measured before unfolding of only one end-fixed polymer chain were recorded. The rupture force increased as well for pHEMA compared to tropoelastin as summarized in Figure 3.32 (right). This higher rupture force reflected the covalent attachment of pHEMA to the tip as well as to the substrate compared to the adhesion of tropoelastin. Therewith, a better molecule characterization in SMFS could be achieved with truly end-fixed molecules or at least fixed to the tip[276]. However, this tip-sample binding was only relevant for SMFS measurements as pHEMA was functionalized with a cell adhesive motif for cell experiments. Thus, the mechanism of cells adhering to a molecule was different from tip-sample binding for tropoelastin as well as pHEMA.

In conclusion, the mechanical properties of tropoelastin when extending single molecules could be mimicked by pHEMA. Figure 3.32 (left) shows that pHEMA 6 h bore a matching contour length to tropoelastin and pHEMA 1 h reflected the properties of cross-linked tropoelastin with a reduced extensibility. Thus, pHEMA with varying polymerization times was utilized for mechanosensitivity studies with the contour length – a measure for the extensibility of a substrate – being the only changed parameter.
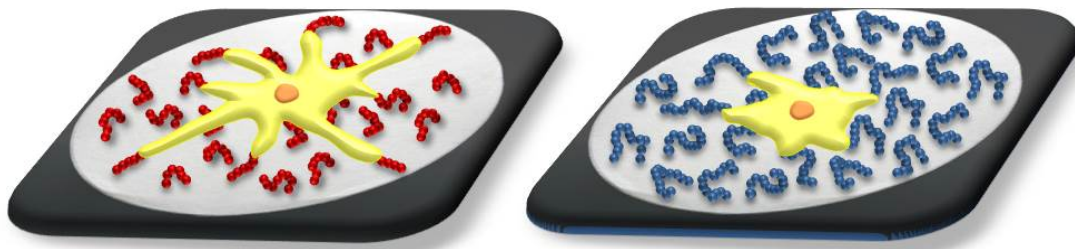
Figure 3.33.: Scheme of Mechanosensitivity studies

## 3.4. Cellular Interactions with pHEMA

This section described the demonstration of the functionality of the pHEMA model system as a substrate for mechanosensitivity studies as schematized in Figure 3.33. For this purpose, an established cell line was used which shows high adhesion and therefore is known for its strong cell-material interactions. Furthermore, the influence of substrate elasticity on HSPCs was studied to answer the question whether very extensible substrates promote the expansion of undifferentiated cells. Finally, the relevance of contour length as a mechanical parameter of pHEMA for cell-material interactions was discussed.

### 3.4.1. Proof of Principle – REF52 Adhesion to pHEMA

To investigate whether or not the extensibility of a substrate, as provided by the developed pHEMA model system, is a parameter that impacts cellular functionality, cell morphology of REF52 on pHEMA with long and short contour length were observed. REF52 is an established cell line from rat embryos and it was used as a fibroblast model system. Due to their high adhesion and branching, they were used for demonstrating cell-material interactions[353].

Figure 3.34 shows light microscopy images of REF52 cells on deposited proteins and pHEMA substrates. The adhesive protein fibronectin[354] was used as positive control for cell adhesion, while BSA with its anti-fouling properties[355] served as a non-adhesive negative control. Mechanical control samples were represented by coatings with tropoelastin. It offered unique elastic properties as described in section 1.1.3 and promoted cell adhesion[162]. Cross-linking with glutaraldehyde reduced elasticity by reducing the unfoldable contour length from the remaining free ends ot tropoelastin[128]. pHEMA samples with a polymerization time of 1 h and 6 h offered short and long polymer chains, respectively. The length was selected to constitute similar extensibility to cross-linked tropoelastin in the case of pHEMA 1 h and untreated tropoelastin for pHEMA 6 h. Cell adhesion was achieved by functionalization of pHEMA with the amino acid sequence $GRKRK$ as this C-terminal motif of tropoelastin was identified as the amino acid sequence binding to the integrin $\alpha_V\beta_3$ of human dermal fibroblasts[161].

**Fibronectin**



**BSA**



**Tropoelastin**



**Tropoelastin, crosslinked**



**pHEMA 1h**



**pHEMA 6h**



50 µm
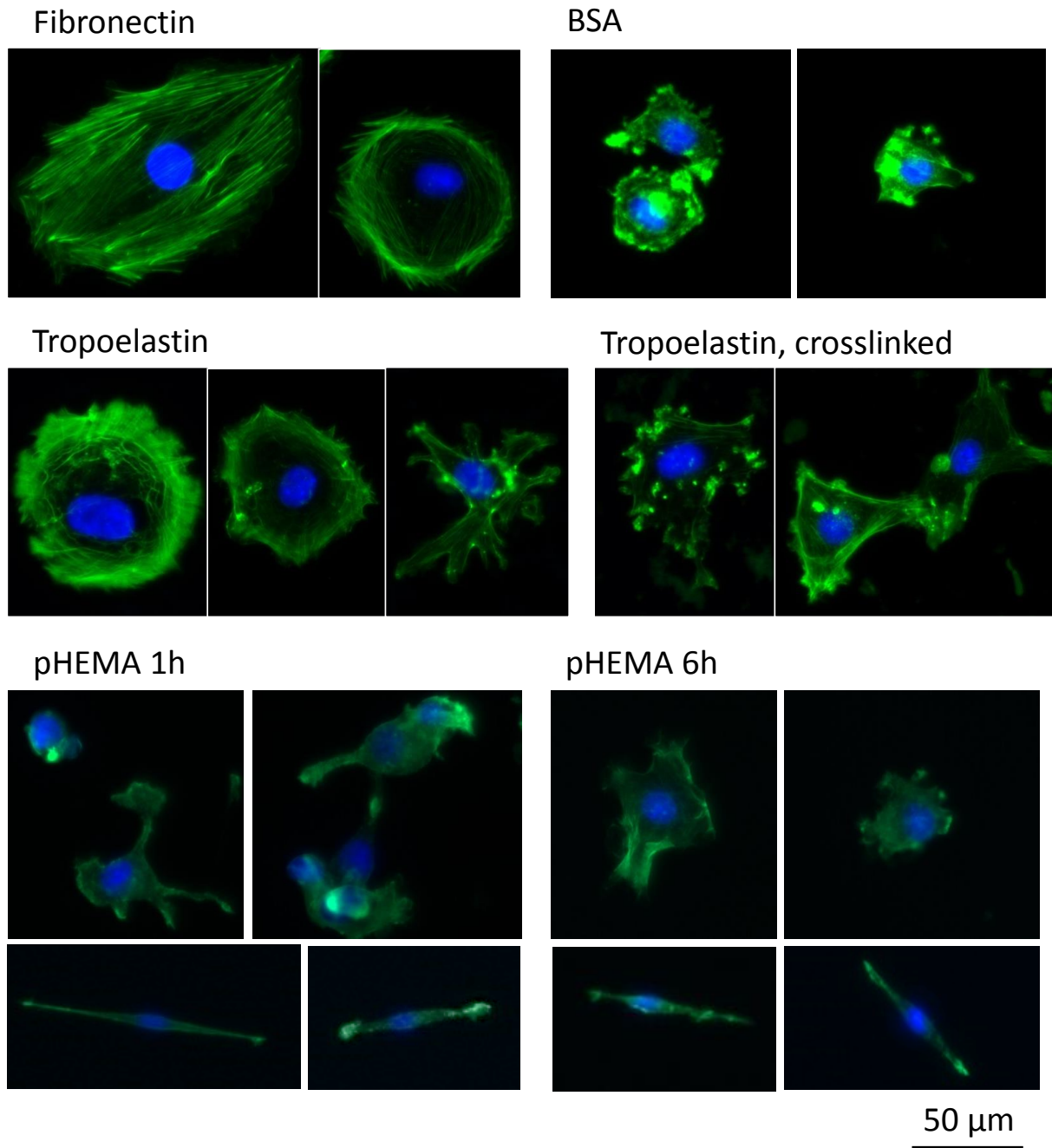
Figure 3.34.: Light microscopy images of REF52 cells after adhesion to proteins adsorbed to substrates and to pHEMA surfaces depicting the cell morphologies varying with substrate extensibility. The actin filaments of the cytoskeleton were stained with Alexa Fluor™ 488 Phalloidin while the cell nuclei were counterstained with DAPI. Two kind of morphologies occurred on pHEMA: unpolarized (upper panels) and bipolar cells (lower panels). They were separated for analysis into two clusters depending on the aspect ratio.

At a first glance, cell area was larger on adhesive samples such as fibronectin and tropoelastin compared to BSA and it decreased on cross-linked tropoelastin compared to intact tropoelastin. Fewer protrusions were formed on the extensible substrate tropoelastin compared to the cross-linked molecules. For pHEMA, cell area was small in both cases and it was hard to make a statement on the protrusions. Few cells displayed a spindle shape and their data was separated into a second cluster for morphological analysis. A quantitative analysis shed light on the details of morphological changes.

**Quantitative Analysis of Cell Morphology on pHEMA** The cell morphologies from images such as the representative ones in Figure 3.34 were quantified through the analysis of several dozens of imaged cells via the image processing package Fiji. Cell morphological features were summarized in Figure 3.35. The criterion for separation of spindle shaped cells from polygonal cells was set to an aspect ratio of 5 as the values of this parameter showed a gap between 4 and 8. Due to low number of bipolar cells (less than 10 % of analyzed cells), but their distinctively different morphology, they were left aside in the morphological analysis for a better consistency.

The impressions from the light microscopy images were confirmed and extended. However, the graphical presentation as bars can sometimes be hardly overlooked. Thus, data from Figure 3.35 was transformed with the visualization tool PhenoPlot[297] into a glyph-based presentation in Figure 3.36 that was easily interpretable.

The analysis of cell protrusions was performed by presenting the cell area in a black and white image and skeletonizing this area. The number of end point voxels of a skeleton was interpreted as the number of protrusions and converted to the parameter spikes fraction in the presentation with PhenoPlot. For the spikes' length and relative protrusion area, the reciprocals of circularity[306] and solidity[305] were utilized, respectively. The fluorescence intensity of the staining was not interpreted as this value was not calibrated and could slightly change between experiments.

On the basis of morphological analysis, several observations could be made:

- Protein comparison: Fibroblasts behaved similar on fibronectin and tropoelastin. The largest difference was found in the mean length of protrusions, which was larger upon adhesion to fibronectin.

- Adhesiveness: Cells on the adhesive protein fibronectin were larger in terms of area and major axis compared to the non-adhesive BSA. Furthermore, the relative protrusion area was higher on the non-adhesive protein.
  Cell length and area was small for BSA and both pHEMA samples but aspect ratio was high compared to the other samples. Also length of protrusions and protrusion area was similar for these samples and higher than for the more adhesive substrates.

- Cross-linking: Cross-linked tropoelastin had a decreased cell size (area and major
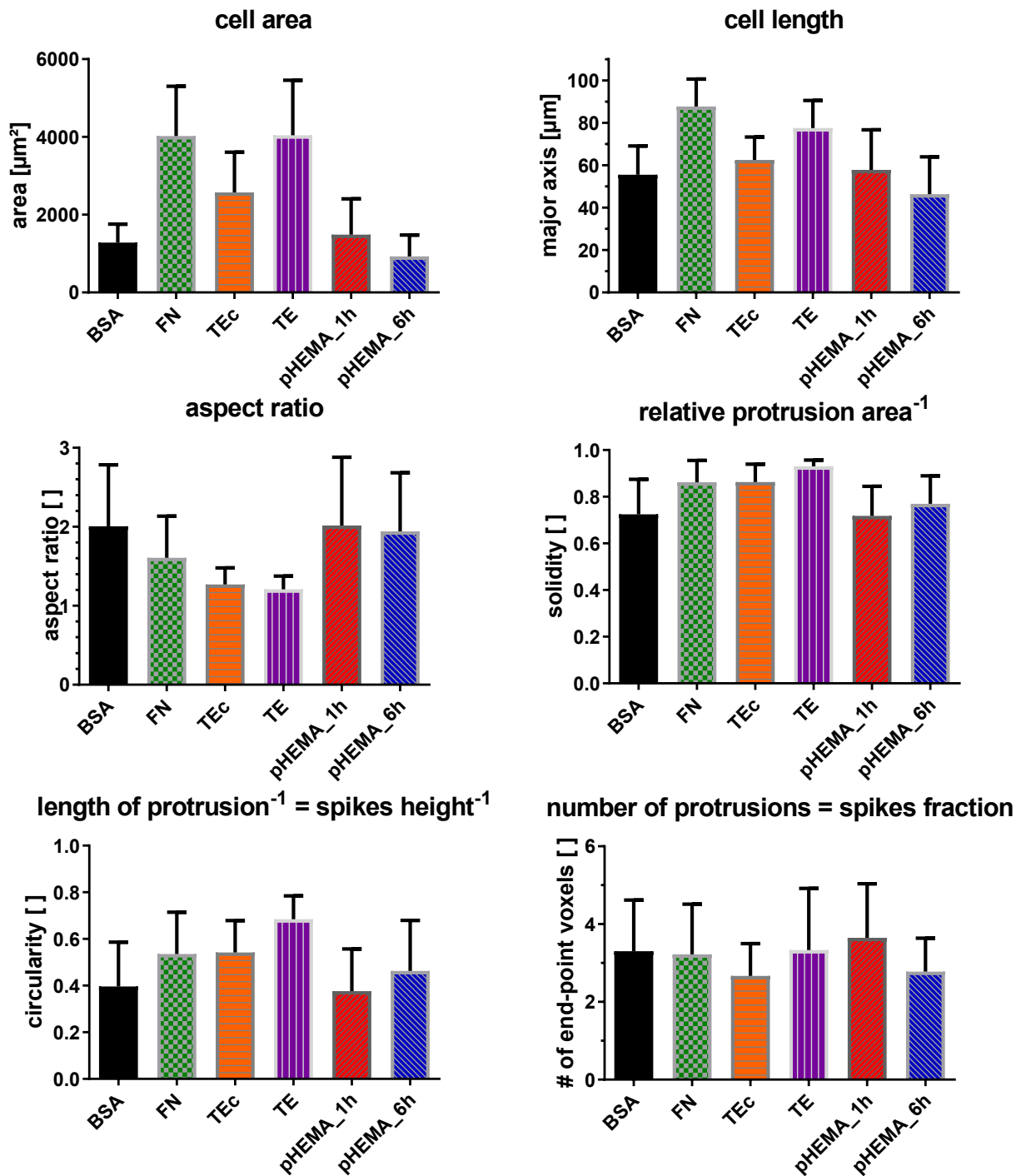
Figure 3.35.: Analysis of morphological features for REF52 on proteins and pHEMA substrates (bovine serum albumin (BSA), fibronectin (FN), cross-linked tropoelastin (TEc), tropoelastin (TE)). Important significances were summarized in Figure 3.36.

| | | cell area | cell length | aspect ratio | rel. protrusion area | spikes height = length of protrusions | spikes fraction = number of protrusion |
|---|---|---|---|---|---|---|---|
| FN vs. BSA | | **** | **** | ns | **** | * | ns |
| FN vs. TE | | ns | * | * | * | *** | ns |
| TEc vs. TE | | **** | **** | ns | * | *** | **** |
| pHEMA 1 h vs. pHEMA 6 h | | *** | *** | ns | * | * | **** |
| TEc vs. pHEMA 1 h | | **** | ns | **** | **** | **** | ns |
| TE vs. pHEMA 6 h | | **** | **** | **** | **** | **** | ns |
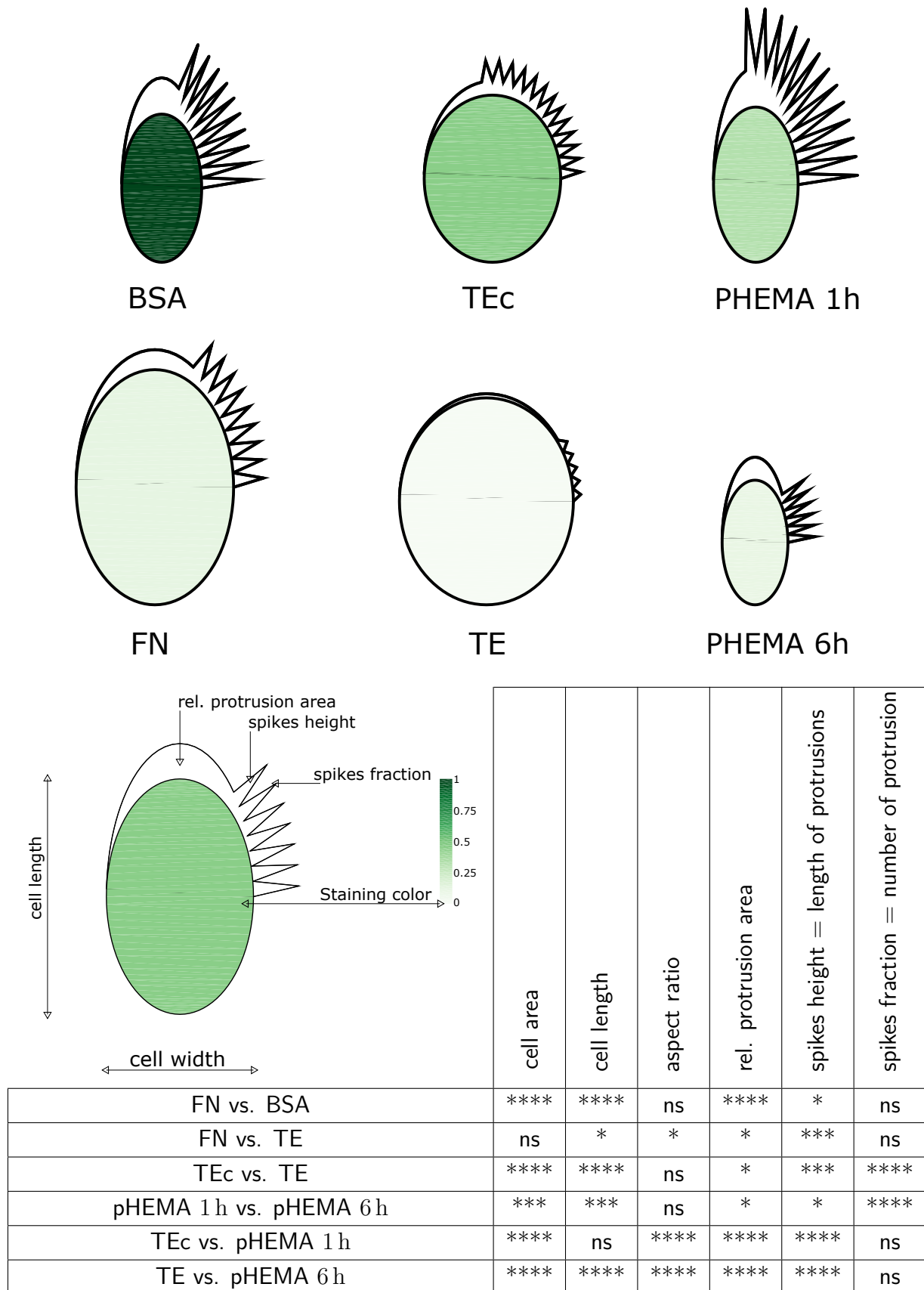
Figure 3.36.: Visualization of REF52 morphology with PhenoPlot and the corresponding significances (bovine serum albumin (BSA), fibronectin (FN), cross-linked tropoelastin (TEc), tropoelastin (TE)).

axis) and increased length and number of protrusions compared to untreated tropoelastin.

- pHEMA extensibility: On pHEMA, cell size decreased and the number of protrusions became larger with increasing extensibility.

- Tropoelastin extensibility: While cell size (area and major axis) on pHEMA decreased with increasing extensibility, this was contrary to the trend on cross-linked tropoelatin and tropoelastin.

- Difference between model system and tropoelastin: When comparing substrates with similar mechanical properties (cross-linked tropoelatin vs. pHEMA 1 h and tropoelastin vs. pHEMA 6 h), the number of protrusions stood out as the only morphological parameter that was equal on the respective pair of substrates. All other parameters differed significantly, thus these differences could not be contributed to mechanical properties of the substrates.

- Spindle shaped cells: These cells showed a much higher aspect ratio (per definition), larger cell length and increased length as well as area of protrusion than other cells on the same substrate, but no change in the number of protrusions. The only difference between spindle shaped cells on both pHEMA samples was the even higher aspect ratio for pHEMA 1 h.

Summarizing the results of the morphological analysis, two properties of the proteins and protein mimicking polymers had to be considered: On the one hand extensibility as discussed in the comparison of tropoelastin and pHEMA in section 3.3.5, and on the other hand, cell adhesiveness which meant the number and character of cell adhesive motifs that a molecule offers.

The tested substrates could be divided into two groups based on adhesiveness: adhesive proteins such as fibronectin and tropoelastin and non-adhesive molecules such as BSA and pHEMA polymers. pHEMA molecules possessed a terminal cell adhesive amino acid sequence, but tropoelastin offered over its full length much more cell adhesive motifs, known and unknown ones[177]. The number of adhesive motifs changed cell size and length as well as area of protrusions.

In terms of extensibility, substrates could be divided in low (TEc & pHEMA 1 h) and high extensibility (TE & pHEMA 6 h). Comparing these substrates revealed that the number of protrusions was the first parameter that depended on the extensibility of the substrate. Decreasing number of protrusions could be observed with increasing extensibility. It was also the only parameter that was similar on the respective protein and pHEMA samples. Cell size, in terms of cell area and length, was the second parameter that decreases with higher extensibility on pHEMA samples. However, an opposing trend could be observed on tropoelastin which meant that the effect of adhesiveness was much higher. Thus, the

number of protrusions was the only parameter that changed on the different tropoelastin and pHEMA samples due to the altered extensibility.

It could be concluded that pHEMA was not a copy of tropoelastin: it only replicated the mechanical properties and the C-terminal motif which fibroblasts attach to[161]. The results implicated that cell adhesion depended on other domains of tropoelastin, too. Furthermore, cross-linking of tropoelastin or use of some truncations[128] was not a good model for testing the effect of extensibility. Cross-linking destroyed some domains which lost their function and truncations, too, offered fewer (intact) adhesive groups to cells. Thus, the biological functionality changed in both cases. Varying the polymer length of pHEMA samples was a better model system for explicitly investigating the effect of extensibility on cells, because the extensibility and the biochemical properties (e.g. availability of cell adhesive motifs) were decoupled and could be change independent from each other.

**Fibroblasts on Substrates with Varying Stiffness**   Cell-substrate interaction occured in a push-pull force mechanism[356, 357]: While tensions in the cytoskeleton induced pulling of the substrate at cell's edge, the substrate was pushed vertically under the cell's nucleus to achieve force equilibrium. This influenced the stress a nucleus is subjected to. However, the pHEMA model system is asymmetrical in case of the forces cells can exert on the substrate: The potential for substrate extension could be tuned, however, cells always "felt" stiff glass when pushing the substrate. Thus, this system enabled a decoupling of the effect of tensile force in the cytoskeleton and stress in the nucleus.

Despite the asymmetry of applicable force, cell morphology of fibroblasts on pHEMA substrates changed similar to hydrogels with varying stiffness. Treating pHEMA 1 h as a stiff and pHEMA 6 h as a soft substrate, the trend was much the same displaying increasing cell area with higher substrate stiffness[358]. Furthermore, circularity decreased, too, and polarized cells appeared when the stiffness was changed from 9 kPa to 20 kPa to 27 kPa, but increased again for very high stiffnesses higher than the corresponding connective tissue from which the cells originate[358]. Another finding for REF52 was higher motility on stiff substrates[359].

The observation were also very similar with human lung fibroblasts: cell area and perimeter increased with higher substrate stiffness and circularity decreased down to a minimum value at 25 kPa substrate stiffness[227]. Furthermore, an increased number of migrated cells, indicating a higher motility, was found on stiff substrates.

The increased cell spreading area with increasing substrate stiffness was in general agreement with other studies[360, 361, 362]. In addition, an increased perimeter was also observed [44] and interestingly more protrusions on stiff substrates, too[363]. One study reported a contradictory effect on the number of protrusions, however, the experiments were carried out in soft 3D hydrogels and thus can not be adequately compared[364].

Protrusions were a key requirement for fibroblast movement[365] and motile fibroblasts were known for frayed cell contours causing low circularity[358]. Thus, the increased

number of protrusion on short pHEMA could be regarded as a sign of higher motility that should be confirmed in studies of cell movement.

In conclusion, pHEMA substrates actually offered tunable mechanical stimuli that resembled the ones from hydrogels. However, asymmetry of the model system gave a hint that tensional forces from fibroblasts were a key mechanism for their mechanosensitivity.

## 3.4.2. Mechanosensitivity Studies with HSPCs

A reported increase of human HSPCs on tropoelastin[128] was the original inspiration for the pHEMA model system with tunable extensibility. An effect of tropoelastin on HSPCs *in vivo* was conceivable as they emerge from aortic endothelium during development[366] suggesting a possible contact of elastin with HSPCs. The exceptional elasticity of tropoelastin was pointed out as the key factor for the increased percentage of $CD34^+CD38^+$ on tropoelastin compared to uncoated TCP.

Thus, mechanosensitivity studies with HSPCs were carried out on pHEMA to study the effect on substrate extensibility on HSPCs. At the same time, the effect of tropoelastin on HSPCs was tried to be reproduced. The experiments were not exactly executed as in the mentioned study[128] but comparable to established protocols for HSPCs alone[367]. Isolated $CD34^+$ cells alone were seeded on pHEMA and comparison substrates instead of all UCB mononuclear cells and cell culture lasted 7 d instead of 3 d. These changes were chosen to gain a high number of HSPCs. UCB cells comprised only 1 % to 2 % of HSPCs[128]. Thus, and in combination with the short cell culture duration, the retrieved number of HSPCs was very low and far from any potential therapeutic use. Furthermore, for reproducibility reasons, TCP was coated with a solution of $0.1\,\mathrm{mg\,mL^{-1}}$ tropoelastin in PBS as determined with the experiments in section 3.1.1 instead of a solution with $1.5\,\mathrm{mg\,mL^{-1}}$ which was reused for several experiments[128]. Due to the low adhesion of HSPCs, a phenotype analysis as in section 3.4.1 was not useful. Instead cell number, expression of surface markers and differentiation capacity were analyzed.

**Expansion of HSPCs on pHEMA** The proliferation and expansion of HSPCs was assessed by determining the number of cells retrieved from pHEMA and comparison substrates after culturing over a period of 7 d as summarized in Figure 3.37.

In order to study the effect of extensibility, pHEMA 1 h and pHEMA 6 h samples were used as substrates. These were opposed to uncoated TCP and TCP coated with tropoelastin for comparison with another study[128]. As solvents from the RAFT polymerization process were not compatible with TCP, the polymers were grafted to glass substrates. Thus, glass substrates with and without tropoelastin coating were utilized to investigate a possible influence of glass compared to TCP.

The number of cells found upon a culture of 7 d on the different surfaces ranged from 535 k to 958 k cells with the lowest sum on glass and the highest number on TCP plated
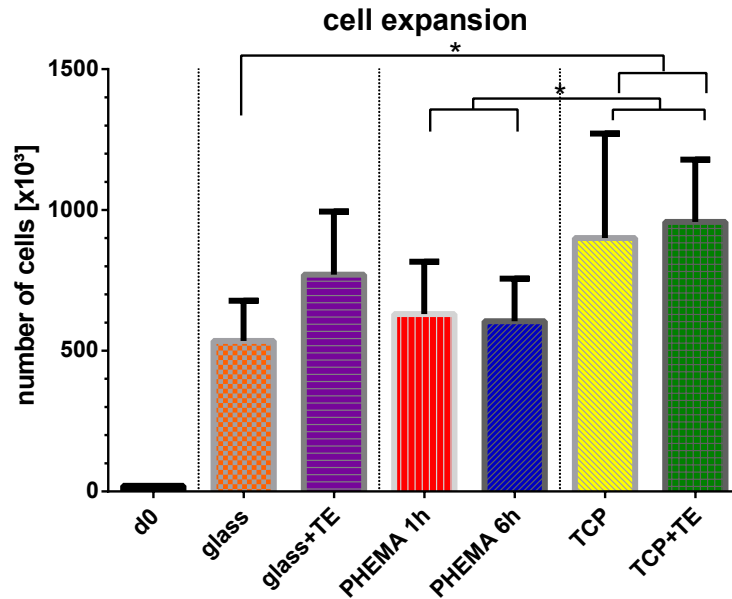
Figure 3.37.: Expansion of HSPCs on substrates with varying extensibility. The number of retrieved cells after a period of $7\,\mathrm{d}$, which grew from $20\,\mathrm{k}$ CD34$^+$ cells seeded on the different substrates, is shown. $N = 3$ independent experiments, performed in triplicate.

with tropoelastin. Thus, the number of cells was multiplied by a factor of 27 to 48. There was no significant difference in the number of cells on both pHEMA samples and it was comparable to glass. The number of cells that were cultured on TCP is significantly higher than on pHEMA substrates and glass, but neither on glass or TCP, no significant effect for coating with tropoelastin was observable. That was even the case for tropoelastin on glass due to the large deviation between experiments with blood from different donors.

**Expression of HSPCs Surface Markers on pHEMA** Expression of the HSPC surface markers CD34 and CD38 was assessed via flow cytometry (FACS) to identify the cells' development stage during hematopoiesis. Figure 3.38 shows representative plots for the different steps in the process of FACS analysis.

Figure 3.39 shows expression of the stem cell relevant surface markers for HSPCs on pHEMA and substrates coated with and without Tropoelastin. $20\,\mathrm{k}$ cells with on average $96.3\,\%$ of CD34$^+$ cells were seeded on top of each substrate. The proportion of CD34$^+$ cells dropped to a range from $25\,\%$ to $30.8\,\%$ after $7\,\mathrm{d}$ cell culture with no significant difference between the substrates.

The seeded cells mainly consisted of early progenitors (CD34$^+$CD38$^-$) with a percentage of 55 at the same time. $41.1\,\%$ of CD34$^+$CD38$^+$ cells were detected and only a very small portion of $2.2\,\%$ of late progenitors (CD34$^-$CD38$^+$). This composition shifted after $7\,\mathrm{d}$ of culture to values of $20.3\,\%$ to $26.6\,\%$, $4.4\,\%$ to $5.8\,\%$ and $5.5\,\%$ to $9.4\,\%$, respectively,
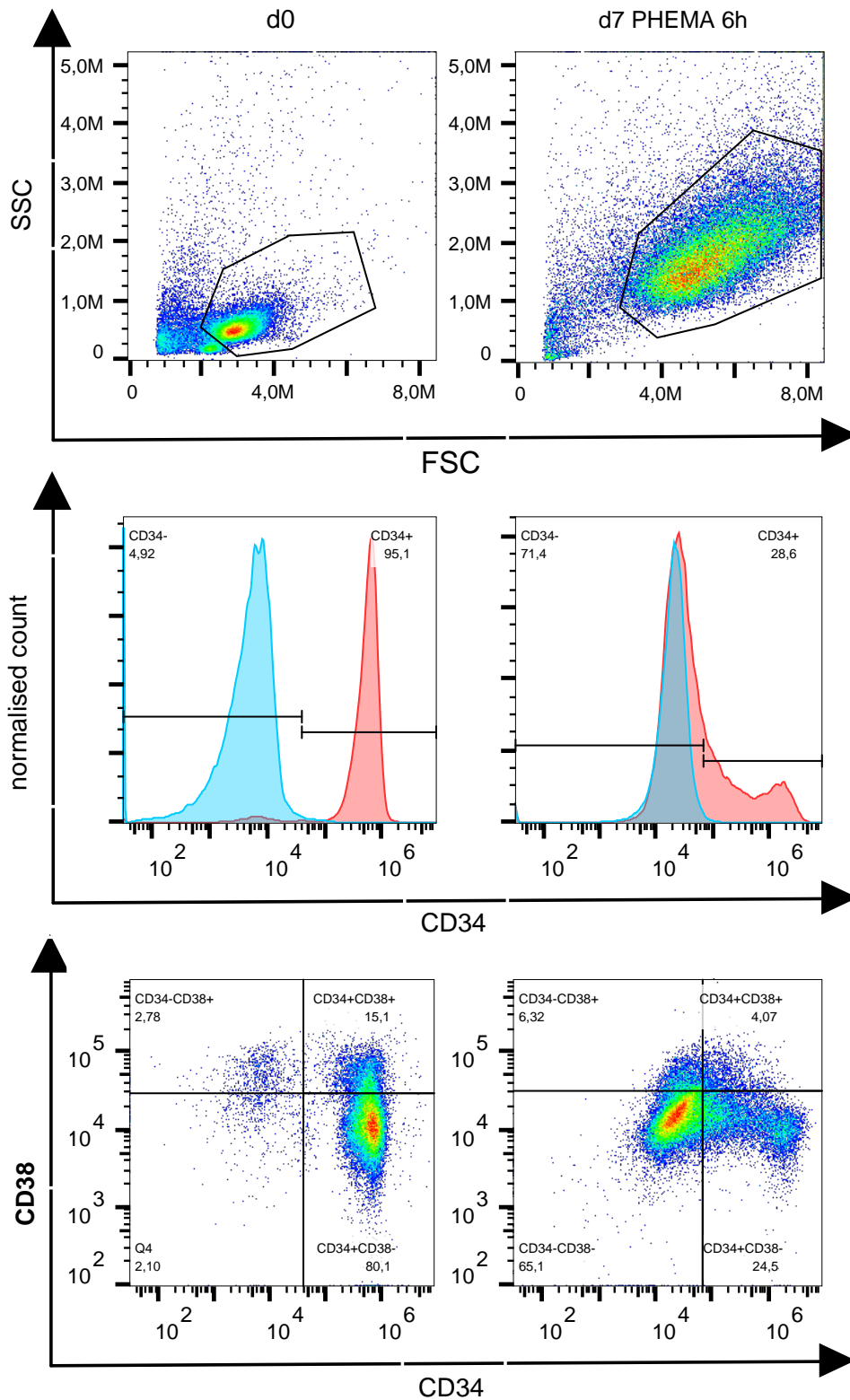
Figure 3.38.: Representative plots for FACS analysis. Cell populations were selected dependent on the forward scatter (FSC), a measure of cell size, and sidewards scatter (SSC), a measure for granularity (top). For every staining, gates were set with an isotype control (blue) that bound unspecifically (middle). Cells were divided into four sub-populations characterized by their expression of the surface markers CD34 and CD38 (bottom).
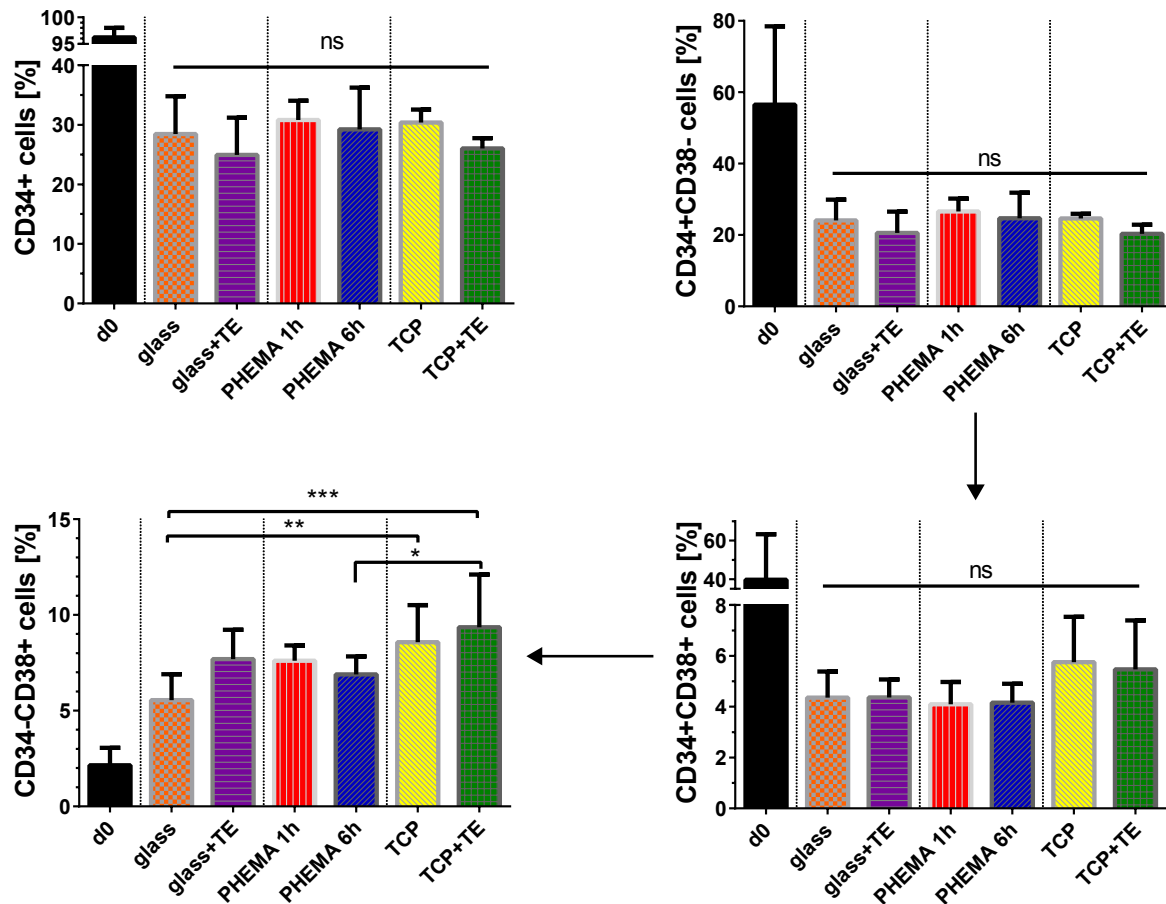
Figure 3.39.: Analysis of HSPC differentiation. The percentage of cells expressing the surface markers CD34 and CD38 on pHEMA and substrates coated with and without tropoelastin after cell culture of 7 d is given. Arrows indicate maturing of the subpopulations. $N = 3$ independent experiments, performed in triplicate.

with late progenitors being then the second largest of the HSPC populations. The only significant difference between the substrates was the value for late progenitors on glass which dropped off against culture on TCP with or without tropoelastin.

**Expansion of CD34$^+$ Cells** The total number of CD34$^+$ cells could be obtained from the cell number and percentage of CD34$^+$ cells for every substrate. Figure 3.40 showed the expansion of CD34$^+$ cells on different substrates after 7 d culture.

The number of CD34$^+$ cells ranged from 152 k to 274 k cells with the lowest sum on glass and the highest number on TCP without tropoelastin leading to a expansion factor of 8 to 14. There was no significant difference in the number of CD34$^+$ cells due to the large deviation between experiments with blood from different donors.
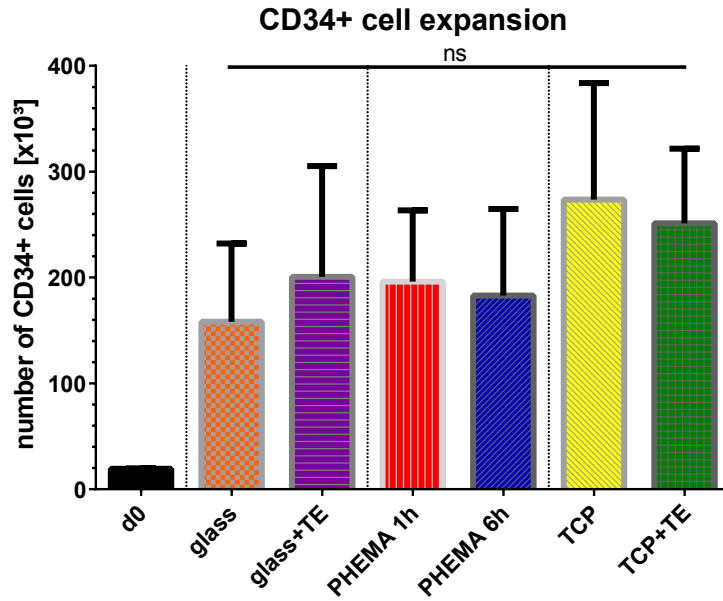
Figure 3.40.: Analysis of HSPC expansion. The number of CD34$^+$ cells on different substrates after 7 d cell culture is displayed. $N = 3$ independent experiments, performed in triplicate.

**Differentiation Capacity**  The differentiation capacity could be obtained by determining the number of early myeloid progenitor cells via CFU assays. 500 cells were seeded into a highly viscous medium and the number of colonies that arose within 14 d was counted. Not only the total number of colonies was assessed, colonies were also distinguished between red, white and mixed ones as depicted in Figure 3.41 what stood for burst-forming unit-erythroid (BFU-E), colony-forming unit-granulocyte and monocytes/macrophages (CFU-GM) and colony-forming unit-granulocytes, erythrocytes, monocytes/macrophages and megakaryocytes (CFU-GEMM), respectively.

Figure 3.41 summarizes the number of colonies for the distinct units and substrates. On average, 81 colonies arose from HSPC at $d0$ what was normalized to 100 % for each experiment. The number dropped to 25 to 39 colonies for the cells that were cultured for 7 d on the different substrates. However, no significant difference could be observed between the substrates. The fraction of red colonies within the total number of colonies increased for the cultured cells, but the fraction of white colonies was still the largest one. Again, there was no significant difference visible for the different types of colonies.

**Summary for the Culture of HSPCs on Substrates with Different Extensibilites**  In conclusion, no effect of substrate extensibility on HSPCs could be determined. The differences between pHEMA 1 h and pHEMA 6 h were not significant. For the total number of obtained cells, a slightly lower value for pHEMA compared to TCP was observed, but this difference diminished for the more relevant population of CD34$^+$ cells.
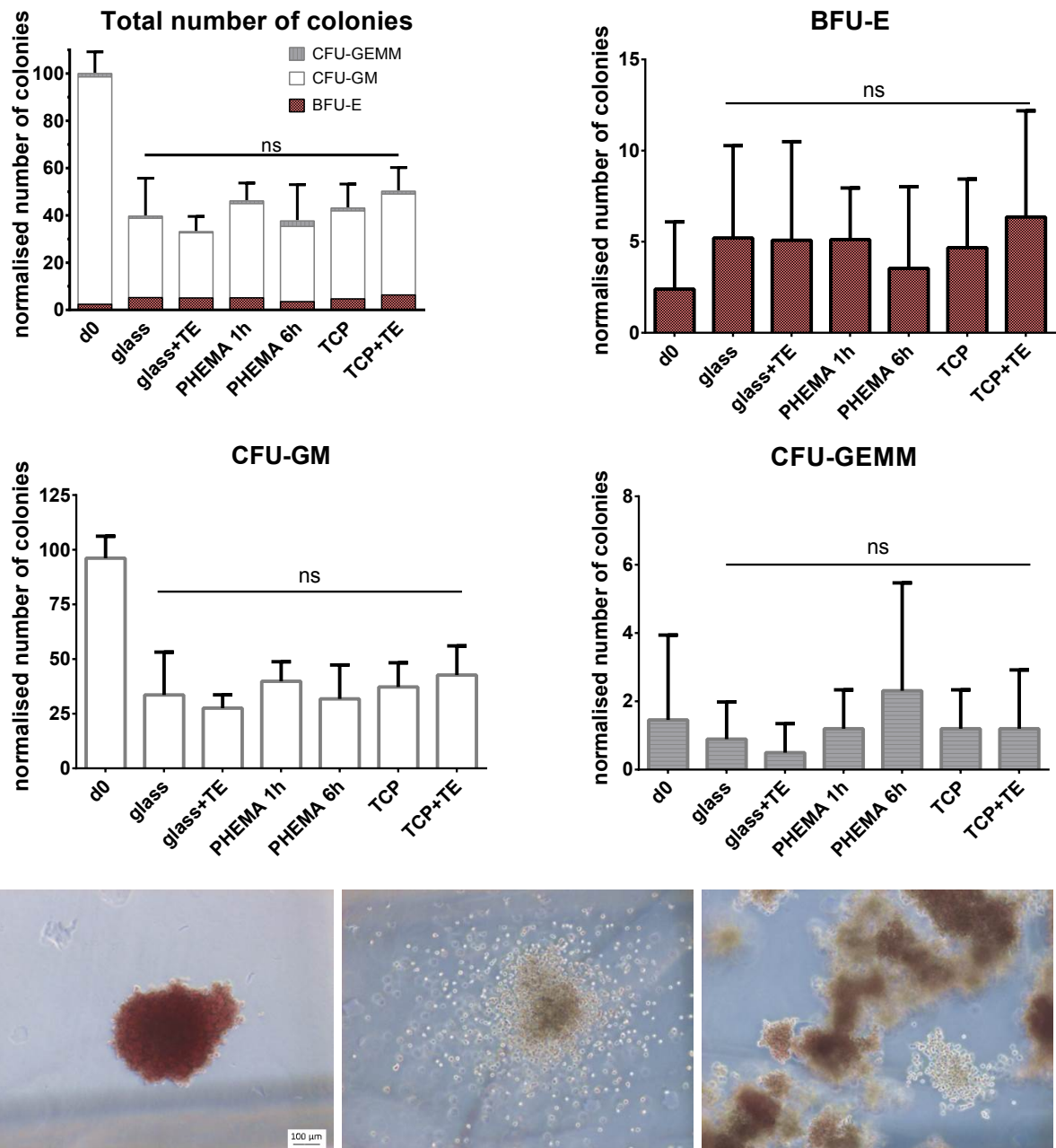
Figure 3.41.: CFU assay from the HSPCs cultured on different substrates. The number
of colonies was normalized to the number of colonies from the $d0$ samples
for each experiment. $N = 3$ independent experiments, performed in trip-
licate. Bottom row shows representative colonies for the three categorized
units (from left to right): BFU-E, CFU-GM and CFU-GEMM

A difference for glass and TCP was conceivable due to different substrate hydrophilicities[368]. An error due to lost cells under the glass should have been minimal as the cell suspension was carefully removed from the well. For pHEMA substrates, the chemical properties of the glass substrate should not have played any role as a densely covered surface was demonstrated in 3.3.1. However, roughness could have been a factor with the roughness of pHEMA samples being closer to glass than to surfaces of TCP[368].

The beneficial effect of tropoelastin on HSPCs described by Holst et al.[128] could not be reproduced. A difference between TCP with and without tropoelastin could not be observed and explicitly not in the fraction of CD34$^+$CD38$^+$ cells and the number of colonies as described in the mentioned paper[128].

Nevertheless, some difference in obtained results between the two studies were conceivable. The use of HSPC alone studied the direct effect on only this population. Using all mononuclear cells from the UCB could have led to some co-culturing effects as described i.e. for the culture of HSPCs with MSCs[367]. One study showed that the secretome of MSCs was modulated from the mechanical properties of the substrate[369]. Such an effect - in this case for other mononuclear cells from the UCB - could in turn drive HSPC differentiation in co-culture. The longer period of cell culture of 7 d compared to 3 d was chosen to test the long-term effect on HSPCs that would be needed for higher cell expansions for therapeutic use[112]. The effect of extensibility could diminish with time due to depositions from the cell secretome. However, substrate exchange every 3 d would be cost intensive and not practically applicable for long-term culture. Another difference was the higher concentration of tropoelastin that was used for coating TCP. However, that solution was re-used several times what led to questionable reproducibility. Moreover, it was demonstrated that the adhesion of KG-1a cells did not further increase with higher concentrations than 0.1 mg mL$^{-1}$ (Section 3.1.1) and that the subtrates were densely covered with pHEMA (Section 3.3.1). Thus, no effect of incomplete substrate coverage should have occurred. Furthermore, the described effect on human HSPCs was very small and most experiments were performed with mouse HSPCs[128]. Hence, it could be possible that not all results from the mouse model could be transferred to human HSPCs due to differences in these two systems[370].

pHEMA 6 h samples replicated the contour length of tropoelastin which was pointed out as the essential parameter in the previous study[128] and the pHEMA model system only changed this parameter as discussed in section 3.3.5. The developed system served better as a model for mechanosensitivity studies as it changed the substrate extensibility as the only variable parameter. Cross-linking or truncations of tropoelastin, as done in the Holst paper, potentially reduced biological functionality. All in all, the often cited (180 citations in June 2018) but never reproduced statement of this publication that tropoelastin increases the expansion of undifferentiated hematopoietic cells due to its elasticity[128] might be too general.

Looking into latest studies, the assumption that super elastic substrates could maintain HSPCs seems to be questionable. It was demonstrated that substrates with a stiffness comparable to the endosteum (inner layer of cavities in long bones) and not stiffnesses close to bone marrow could maintain HSPC population[137].

**Comparison to Established Systems for HSPC Culture**  Although no influence of substrate extensibility and especially no beneficial effect of super elastic substrates on HSPCs could be observed, it had to be pointed out, that the performance of the model system concerning cell expansion did not drop off compared to TCP or other established systems for studying the influence of stiffness in HSPC culture.

The combined influence of substrate elasticity and surface-grafted molecules was studied using hydrogels from polyvinylalcohol-co-itaconic acid with and without grafted proteins[132]. The expansion of $CD34^+CD38^-$ cells was lower on blank hydrogels compared to TCP, but coating with fibronectin improved HSPC expansion, especially at intermediate stiffnesses. 3 to 19 fold expansion could be achieved on hydrogels with different stiffness and fibronectin coating compared to 10 fold expansion on TCP. Thus the values relevant for HSPC expansion were comparable to the pHEMA model system with roughly 24 fold expansion of $CD34^+CD38^-$ cells on pHEMA and 31 fold expansion on TCP. A different study with collagen hydrogels described a 30 to 100 fold expansion for the total number of cells on gels with varying stiffness[133] which was comparable to the 31 fold expansion on pHEMA.

With regard to the high influence of grafted proteins on HSPC adhesion[132, 131], it had to be discussed whether functionalizing pHEMA with the C-terminus of tropoelastin was the best choice for cell culture with HSPCs. The amino sequence was chosen to achieve a similarity of the polymer model system to tropoelastin. If the enhanced proliferation of HSPCs due to tropoelastin[128] could have been reproduced, adhesion of HSPCs to pHEMA brushes would have been intended to use the same mechanism. As this is not the case, other sequences for biofunctionalization of pHEMA should be taken into account for future experiments. The before mentioned studies[132, 133], for example, based on the binding to RGD, a well studied minimal cell adhesive sequence[371, 372, 373] and this motif was also used in many other HSPC studies[374, 325, 367, 375, 137].

Interestingly, the pHEMA model system with the C-terminus – based on binding via GAG receptors[173, 175] – performed better with a nearly 10 fold expansion of $CD34^+$ than GAG-based hydrogels with a 2 to 4 fold expansion[134]. Although these studies were hardly comparable as GAG-based hydrogels were a $3D$ cell culture system and the control experiments on TCP differed remarkably (2 fold expansion[134] to 14 fold expansion), pHEMA brushes seemed to be not a promoting but at least adequate system for the culture of HSPCs.

### 3.4.3. Tunable Contour Length as a Cell Relevant Parameter

Even if there was no effect visible of substrate extensibility on HSPCs, experiments with REF52 cells demonstrated that extensibility in the form of contour length affected their morphology. Thus, cells could sense this mechanical parameter. This section discussed the importance of contour length as a cell relevant parameter and the advantages of the pHEMA model system for mechanosensitivity studies over other ones.

**What Do Cells Fell in the Case of Stiffness Sensing?**  Concerning stiffness sensing of cells, neither the cellular mechanism nor the relevant mechanical cue are completely understood. This can be seen at the debate whether cells sense force or deformation[376] and whether substrate elasticity or tethering of adhesive proteins to the substrate are the key mechanical cues for mechanosensitivity as described in section 1.1.1.

The discussions are further complicated as many different measurement methods were used and some mechanical parameters depend on measuring parameters. For instance, the effect of substrate elasticity influencing MSCs when using PAAm hydrogels[55] could not be replicated with PDMS substrates[61]. A later study could relate this to an inadequate mechanical characterization that did not account the viscoelastic properties of PDMS[62]. Measurements at cell mechanosensation scale were suggested as schemed in Figure 1.4, right. With AFM indentation at cell-relevant strains[377] and retraction speeds[378, 379], PDMS was much stiffer than for the utilized hydrogels and outside the range relevant for the examined cell differentiation[62].

The importance of the measuring setup is again illustrated with Figure 3.42. The characterization of a porous hydrogel with a large sphere according to the Hertz model[255] would result in a stiffness accounting the material and its porosity. However, indentation with a sharp AFM tip would define more the local properties of pore walls.

Although AFM indentation would often deliver more cell relevant results, the developed polymer model system and its analysis via SMFS could further improve the relevance of mechanical characterization. The measurement of single polymer molecules led to a better comparison to the values for single receptors, as *in situ*, one receptor would bind to an adhesion motif of one polymer strand. Furthermore, the utilized parameters for SMFS were in the range of cell receptor parameters with integrin-ligand rupture forces from $20\,\mathrm{pN}$ to $140\,\mathrm{pN}$[381], myosin motor velocities from $100\,\mathrm{nm\,s^{-1}}$ to $1000\,\mathrm{nm\,s^{-1}}$[382] and similar length scales (see below). This further justified the use of SMFS to characterize substrates for mechanosensitivity studies.

**Comparison to Other Systems for Mechanosensitivity Studies of Stiffness**  The most prominent system used for cell mechanosensation studies are hydrogels as their stiffness was easily tuned to match the values of human tissues[68]. Materials with large pores even enabled the culture of cells in a three dimensional microenvironment. However, the porosity
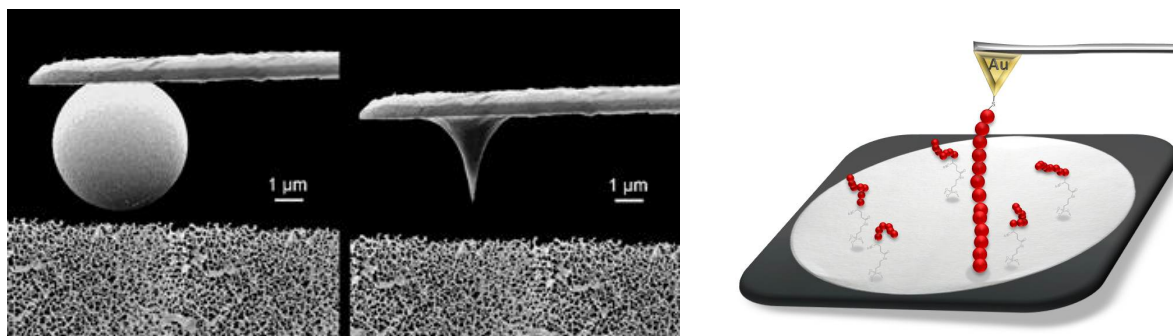
Figure 3.42.: Demonstration of different measurement methods for substrate stiffness. Indentation with a large sphere takes porosity into account and results in a much lower stiffness than a sample with the same material without porosity. Indentation with a sharp tip gives information about the pore walls. Retrieved from [380] on 01.06.2018. SMFS delivers mechanical parameters at a cell mechanosensing scale. Reprinted with permission from [278]. Copyright 2016 ACS.

represented also a problem of these systems. Stiffness was often varied with the change of monomer to cross-linker ratio which not only changed stiffness but also porosity[61]. Further altered material properties were surface chemistry, backbone flexibility and binding properties of immobilized adhesive ligands[236].

New hydrogels were developed that enabled a change of porosity without changing stiffness[62], but those two parameters were not completely decoupled as pore size for all soft hydrogels was larger than that for all stiff hydrogels. Thus, cross talk between substrate stiffness and nanotopography was always possible[383]. Furthermore, small differences in surface energies could alter the assembly of collagen ligands on PDMS surfaces, thus introducing a new parameter that changed topography and influenced cell differentiation[384].

Another problem for hydrogel systems was the required cell adhesiveness. This was often accomplished by coating with adhesive proteins leading to the before mentioned problem of protein tethering which could cause new mechanical cues[61]. The post-modification could be avoided with hydrogels from natural molecules derived from the extracellular matrix such as collagen[385] and hyaluronic acid[386]. Although in this case, the step of cross-linking to form a gel and tune the stiffness could also alter the biological activity of these hydrogels.

Microposts were a different system to control substrate rigidity[236]. The height of polymer pillars determined the bending in response to cellular traction forces. This system allowed the stiffness variation of PDMS to a cell relevant scale and the effect of viscoelasticity could be circumvented by using less viscoelastic PDMS mixtures. Albeit microposts of different height presented the same surface geometry, they nevertheless passed on a topographical signal with restricted areas for cell adhesion.

The pHEMA model system in contrast was a flat substrate densely covered with a polymer monolayer as could be seen in Figure 3.14. The biofunctionalization included an adhesion motif directly at the chain ends avoiding additional mechanical feedback as observed in other systems. Thus, the pHEMA model system allowed investigating one specific mechanical cue and this extensibility of polymer chains was completely decoupled from any other mechanical parameter, especially topography, and also biological ones.

**Estimated Young's Modulus of pHEMA Monolayers** Using the persistence length, the Young's Modulus of single pHEMA chains could be calculated from Equation 1.11. Assuming a radius of $r = 2\,\text{nm}$ from the size of the side group led to a Young's Modulus of $65\,\text{kPa}$. At a first glance, this was much higher than the values for hydrogels used in other mechanosensitivity studies[68, 383]. The difference arises from the fact that bulk measurement methods were used for hydrogel measurements accounting its porosity while the Young's modulus of polymer chains was only related to the molecules cross section.

For a better comparison, it had to be considered that many polymers in between cell receptors did not contribute to the modulus perceived by the cell. With an assumed integrin interspacing of $50\,\text{nm}$ for obligatory adhesive cells such as REF52[387, 353] or $50\,\text{nm}$ for HSPCs[325, 124], the area per integrin could be related to the area per molecule and an estimated Young's modulus of $0.3\,\text{kPa}$ which fitted the value of bone marrow with also $0.3\,\text{kPa}$[135]. Thus, the perceived Young's modulus of the pHEMA substrates was relevant for cell studies, especially with HSPCs.

**Contour Length Affects Cell Behaviour** This work used the term contour length to describe the mechanical parameter of polymer chains on a substrate in close reminiscence of the paper from Holst et al.[128]. Other publications described this parameter as tether length, as cell adhesion motifs such as RGD were tethered to the substrate via polymer spacers, often PEG[62, 388, 389].

Short and long spacers had to be distinguished. When short PEG spacers were varied between $1\,\text{nm}$ to $10\,\text{nm}$, cell count and spreading increased with longer PEG tether length as the binding probability increased due to the increased flexibility of the binding motif[390, 391, 392].

In contrast to that, this effect was reversed with long PEG spacers. Attwood et al. used PEG spacer with tether lengths of $10\,\text{nm}$, $40\,\text{nm}$ and $320\,\text{nm}$ in experiments with fibroblasts. In this case, cell spread area and cell surface density decreased with longer tether length[250]. In addition, focal adhesion area and length decreased. The fibroblasts seemed to sense the different mechanical cues from the varying contour length and their results coincide with the trend measured for REF52 in Figure 3.36.

However, one problem with this work was the grafting to approach for surface functionalization. It led to a 10 fold increased grafting density for short spacers compared to long ones. The authors wanted to tackle this difference with a dilution of the coupling solution

with short spacers and demonstrated no difference in the area and size of focal adhesions with a 1 : 10 dilution. However, the grafting density of the diluted short spacers was still 9 fold increased compared to long ones[250]. The pHEMA models system handled this problem better due to its grafting from approach. With the demonstrated low variation in grafting density in Table 3.1, an influence of grafting density could be ruled out.

Another interesting work investigated stress-stiffening of hydrogels and its influence on human MSC differentiation[63]. Very soft hydrogels were produced (0.2 kPa to 0.4 kPa) which varied in the polymer length between cross-linking points. Macroscopically, increased critical stress for the onset of stress stiffening was measured via rheology for large polymer lengths. Following that, a transition from adipogenic to osteogenic differentiation was observed for cells cultured in gels with low or high critical stress, respectively.

On a molecular perspective, parallels could be detected between this stiffening of hydrogels and the pHEMA model system. The hyberbolic force increase at large molecule unfoldings according to the WLC model as seen in Figure 3.17, could be regarded as a stiffening of the molecule. Looking at the molecular geometry, receptors attached in the middle between two cross-linking points could feel a – not same but similar – force profile corresponding to a pHEMA contour length which was half the polymer length in the hydrogels[63]. Thus, it would be of high interest to conduct differentiation experiments of human MSCs on pHEMA.

**Working Model for Sensing Contour Length**   Based on the recently proposed model from Attwood et al.[250], a hypothesis could be proposed for cells sensing contour/tether lengths. It built on the idea that intracellular sensors "reach into the void" when pulling molecules of very long contour lengths.

A mechanical link between the extracellular matrix or substrate and the cytoskeleton is necessary for mechanosensation. This is embodied by integrin receptors where the extracellular matrix, integrins, a force transducer and the actin cytoskeleton are chained together as seen in Figure 3.43. Probing of the substrate occures when actomyosin contraction applied a force with a constant rearward velocity[393] for a fixed time. For integrins attached to a short molecule, the force transducer experiences, within a short time, a certain trigger force $F_t$, permitting stretching of the force transducer and possible signaling. With long tethers, integrins are free to diffuse due to the increased flexibility. No signaling does occur as the force transducer is not stretched within a confined time interval. With this model, the analogous reception of tether length and substrate stiffness is explained as the relevant parameter – signaling depends on the time above a certain trigger force $F_t$ – corresponds for soft substrates/long linker and stiff substrates/short linker.

Looking at the structure of focal adhesions, talin stands out as candidate for the mentioned force transducer (Figure 1.1 D) It is known that mechanical forces are necessary for focal adhesions to mature[394] and during this process, vinculin is recruited[395]. This could be accomplished by stretching of talin which activates vinculin binding[396] and this

106
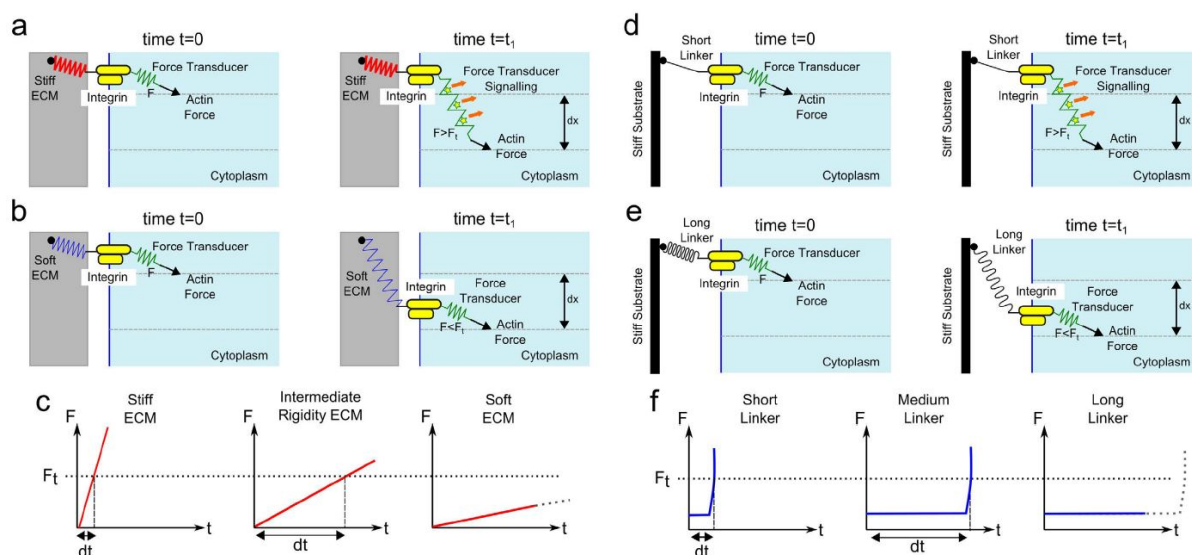
Figure 3.43.: Proposed working model from Attwood for explaining the reception of tether sensing (right) analogous to substrate stiffness (left). With permission from [250].

in turn locks talin in a unfolded state[397]. At this point, long polymer chains could be conceived as inhibitor for talin unfolding due to the increased flexibility of integrin. With a very small force as $5\,\mathrm{pN}$ for the unfolding of talin[397], pHEMA chains would already be extended to a large degree as shown in Figure 3.17. Thus, a critical tether length could be possible around the length of a talin molecule($60\,\mathrm{nm}$ in high salt buffers[398] and can be extended up to $160\,\mathrm{nm}$[396]).

Such a mechanism does not have to be restricted to talin and could be transfered to other cell receptors. The adhesion of cells to the C-terminus of tropoelastin was based on GAGs (see section 1.1.3). The chain lengths of this receptor range from $25\,\mathrm{nm}$ to $90\,\mathrm{nm}$[399] and its mechanosensing could be disturbed with lower shear forces experienced at the pHEMA-GAG-interface[400].

Future studies investigating critical tether lengths on mechanosensation should adjust the employed contour lengths of pHEMA. The lengths in this study were chosen to replicate the exceptional properties of tropoelastin and to use them in experiments with HSPCs. Following experiments could apply the length of talin molecules using pHEMA chains with similar as well as significantly shorter and longer contour lengths. Though, it has to be noted that for very short polymer chains of very few tens of nanometers, polymerization parameters would be required to be adjusted to slower polymerization velocities. At very short polymerization times, errors due to heating and cooling sample vials or not exactly simultaneously handling all vials of a batch could lead to unwanted deviations in contour lengths. Thus, a decreased concentration of the radical starter could lead to more control over short contour lengths, but a new mechanical characterization would be required.

In conclusion, the pHEMA model system offered a new tool for mechanosensitivity studies. It allowed to study the existence of critical lengths within the mechanisms of mechanosensation. At the same time, it provided mechanical feedback, which is analogous to soft and stiff substrates under tension. Due to its reduced structure, polymer contour length could be investigated as the only variable parameter thus allowing the decoupling of its effect from other mechanical or biological parameters changing in other systems for mechanosensitivity.

# 4. Summary and Outlook

With the growing evidence that cells are mechanosensitive, this thesis aimed at the development of a polymer model system for mechanosensitivity studies with substrate extensibility decoupled from other cues such as topography or biological activity. For this purpose, a biofunctionalized polymer brush was constructed with the contour length as the only variable parameter.

The contour length was selected after the example of tropoelastin with and without cross-linking as this protein has exceptional elasticity and was described to provide good cell adhesion and beneficial effects on HSPCs[128]. Thus, tropoelastin was characterized via SMFS with a contour length of roughly 230 nm what is in good agreement with literature. Furthermore, the C-terminal domain of tropoelastin was identified as the most promising amino acid sequence for biofunctionalization of the polymer brush to promote adhesion of hematopoietic cells in a similar way as to tropoelastin.

Subsequently, the polymer model system was developed based on the biocompatible and anti-fouling pHEMA. SI-RAFT polymerization was selected to achieve dense brushes and especially constant density independent from the polymer length. For cell experiments, biofunctionalization via click reaction with a construct of tropoelastin derived amino acid sequences functionalized with maleimide followed. Successful polymerization and biofunctionalization were confirmed with XPS and ToF-SIMS measurements.

Mechanical characterization via SMFS revealed for pHEMA samples a similar chain stiffness in terms of persistence length and a range with linear dependence of the contour length from polymerization time. With this information, pHEMA with polymerization times of 1 h and 6 h, hence contour lengths of 110 nm and 290 nm, respectively, were selected as similar to tropoelastin with and without cross-linking. Further measurements revealed a constant grafting density and very low roughness, thus unchanging biological and topographical cues.

The functionality of the polymer model systems was successfully demonstrated with mechanosensitivity studies using REF52 fibroblast cells. These cells displayed changes in morphology dependent on the substrate extensibility, i.e. decreasing cell size and lower number of protrusions on more extensible substrates. Hence, the contour length of substrate bound polymer chains is a cue that cells can sense and a recently developed model showed that the reception is comparable to substrates of different stiffness[250].

In the case of HSPCs, which do hardly spread on surfaces, proliferation and differen-

tiation was studied instead of morphology. These experiments displayed no influence of substrate extensibility on the proliferation of undifferentiated cells as stated elsewhere[128]. Furthermore, even the coating with tropoelastin had no influence on HSPCs. Because of that, the general and monocausal conclusion that high substrate extensibility promotes the proliferation of undifferentiated hematopoietic cells[128] could be proven wrong.

An interesting side result of the thesis was the mapping of RAFT controlled macromolecular growth on surfaces with the aid of SMFS as published in [278]. An extended linear polymerization rate was observed compared to polymerization in solution. The relevance for investigations of surface polymer kinetics is underpinned with very recent real time measurement of single polymer growth dynamics[401].

**Outlook**  It has to be mentioned that some additional experiments would have rounded up this thesis. In the mechanical characterization, the hysteresis of single pHEMA strands would be a nice measurement for comparison with tropoelastin. An additional control sample with non-functionalized pHEMA would display the anti-fouling properties of the polymer. Furthermore, using a broader range of contour length would enable to study the trend of the contour length dependence instead of a binary long/short discrimination.

The developed model system is an interesting tool that opens possibilities for future investigations. Divers new studies can be imagined using this system.

First of all, it would be of great interest to conduct differentiation experiments of human MSCs on the developed pHEMA system and compare it the existing literature on stiffness dependent behavior of these stem cells. Furthermore, the measurement of overall cell adhesion strength via shearing forces on rotating discs or via Single Cell Force Spectroscopy[279] would give hints whether the polymer model system can compete with its natural model. As mentioned before, length of the polymer chains could be varied. It could be tuned to adopt other interesting adhesive proteins than tropoelastin or adjusted to the length of cell receptor compartments such as talin.

The synthesis of the polymer layer could be also altered in other ways. Variation in grafting density could be studied or the use of different adhesive ligands. The RAFT polymerization can be applied to various monomers and could be carried out with known candidates such as PEG and PAAm. Also the hydrophobicity of tropoelastin could be tried to achieve, but anti-fouling properties should still be present. The idea of single chains attached to a substrate could be even realized with elastin-like polypeptides in a grafting-to process.

The relevance of such a model system becomes clear looking at the numerous studies recently published which aim at decoupling substrate stiffness from other cues[226, 229, 245, 402, 403, 404]. Few publications have even used a similar approach varying the length of attached polymer chains[250, 389].

In summary, polymer chains with different contour lengths attached to substrates are a good tool for future mechanosensitivity studies. This parameter offers a feedback similar to stiffness but it is easier to define and to compare with other cell compartments, thus it could possibly bring new insights into cellular mechanisms of mechanosensitivity.

# A. Appendix

## A.1. Derivation of the freely jointed chain Model

The FJC consists of $n$ segments of the length $l_K$, thus a contour length of $l_c = nl_K$. The model assumes that the direction of a segment is uncorrelated with adjacent segments which are represented by vectors $l_i$. The polymer chain can be characterized by its mean-square end-to-end distance $\langle x^2 \rangle$[405]:

$$\langle x^2 \rangle = \langle x \cdot x \rangle = \langle \sum_i^n l_i \cdot \sum_j^n l_j \rangle = \sum_i^n \sum_j^n \langle l_i \cdot l_j \rangle \tag{A.1}$$

$$= \sum_i^n \langle l_i \cdot l_i \rangle + \sum_i^n \sum_{j \neq 1}^n \langle l_i \cdot l_j \rangle = nl_K^2 = l_c l_K \tag{A.2}$$

### Statistical Formulation of the Microscopic Model

The mechanical formulation of the FJC model can be derived following the review of Ortiz[283].

The statistical properties can be calculated from the radial probability density function $P(x)$ with the vector $x$ as the end-to-end distance of a polymer chain. While chain end A is fixed at the origin, $P(x)$ gives the probability per unit volume for chain end B being situated within a spherical shell of radius $x$ and thickness $dx$ which is located at a distance $x$ from the chain end A at the origin. The probability density function is directly proportional to the number of possible chain configurations.

The configurational entropy, $S$, is

$$S(x) = k_B \ln P(x) \tag{A.3}$$

where $k_B$ is the Boltzmann's constant.

With the assumption, that each link is rigid and does not deform, the internal energy of the molecule is the same for all chain configurations. Thus, the entropy can be denoted from the Helmholtz free energy, $A$, as

$$A(x) = -TS(x) = k_B T \ln P(x) \tag{A.4}$$

utilizing the absolute temperature $T$.

Applying an external tensile force $F$ to the ends of the freely jointed chain in the direction of $x$, the chain extension leads to a reduction in the number of possible configurations and thus, a reduced configurational entropy. Since the polymer chain wants to be in its equilibrium state with maximum entropy, an elastic restoring force $F_{elastic}$ is induced. This force is related to the Helmholtz free energy with:

$$F_{elastic} = \frac{\partial A(x)}{\partial x} \tag{A.5}$$

The stiffness of the chain, $k_{chain}$ can be defined as follows:

$$k_{chain} = \frac{\partial F_{elastic}}{\partial x} \tag{A.6}$$

## Gaussian Chain Statistics

No simple mathematical expression is available for $P(x)$ in the FJC model, but it has been proven to be Gaussian for long chains at low extensions. Thus, the probability density function (in the third dimension) can be expressed as[406]

$$P(x) = \left(\frac{3}{2\pi l_c l_K}\right)^{3/2} \exp\left(-\frac{3x^2}{2\pi l_c l_K}\right) \tag{A.7}$$

with a variance $\sigma^2 = <x^2> = nl_K^2$ and $l_c = nl_K$. The Helmholtz free energy is expressed with the use of an arbitrary constant $c$:

$$A(x) = \left(\frac{3k_B T}{2l_c l_K}\right) x^2 + c \tag{A.8}$$

and the elastic restoring force can be calculated as:

$$F_{elastic} = \left(\frac{3k_B T}{l_c l_K}\right) x \tag{A.9}$$

$F_{elastic}$ is proportional to $x$, thus displays a linear elasticity obeying Hooke's law. The polymer chain can be modeled as a spring of zero unconstrained length. Equation A.9 is the basis of the classical theory of rubber elasticity.

## Non-Gaussian Chain Statistics

A problem with the Gaussian distribution are the nonvanishing probabilities for distance $x$ greater than the contour length $l_c$. Thus, a more accurate distribution function was developed with aid of the Langevin function $L(\beta)$ that describes the fractional chain extension $\frac{x}{nl_K}$ as

$$L(\beta) = \frac{x}{nl_K} = \coth(\beta) - (1/\beta) \tag{A.10}$$

while $\beta$ at this point is the inverse Langevin function

$$\beta = L^{-1}\left(\frac{x}{nl_K}\right) \tag{A.11}$$

The probability density function can be expressed now in its logarithmic form as

$$\ln P(x) = c - n\left(\frac{x}{nl_K}\beta + \ln\frac{\beta}{\sinh\beta}\right) \tag{A.12}$$

This gives for the Helmholtz free energy:

$$A(x) = -T(c - k_B n)\left(\frac{x}{nl_K}\beta + \ln\frac{\beta}{\sinh\beta}\right) \tag{A.13}$$

This leads to the exact inverse formula shown in Equation 1.8.

### The extensible freely jointed chain

The E-FJC model extends the FJC to cover elastic deformation of the backbone[284]. The contour length $l_c$ is replaced with the total length $l_{total}$, using the spring constant $\kappa$ of single chain elements:

$$l_{total} = l_c + n\frac{F}{\kappa} \tag{A.14}$$

With this, the relation between end-to-end distance and force in Equation 1.9 can be calculated.

## A.2. Mathematical Description of the worm-like chain

The WLC is represented by a continuous flexible rod with a resistance to bending that can be described with the persistence length $l_p$. This parameter details the decay in correlations of the tangent vectors as depicted in Figure A.1[407]:

$$\langle t(0) \cdot t(s)\rangle = \langle\cos\theta(s)\rangle = \exp\left(-\frac{s}{l_p}\right) \tag{A.15}$$

with arc length $s$, tangent vector $t(s)$ and $\cos\theta$ as the angle between tangent vector $t(s)$ and pulling axis $z$.
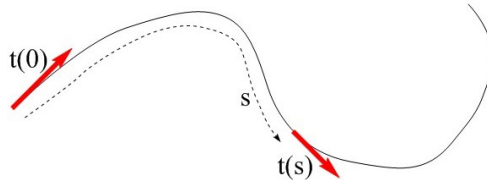


Figure A.1.: Bending WLC for the illustration of $l_p$. Adapted with permission from [407].

The polymer chain can be characterized by its mean-square end-to-end distance $\langle x^2 \rangle$:

$$\langle x^2 \rangle = \langle x \cdot x \rangle = \langle \int_0^{l_c} t(s)ds \cdot \int_0^{l_c} t(s')ds' \rangle \tag{A.16}$$

$$= \int_0^{l_c} ds \int_0^{l_c} \langle t(s)ds \cdot t(s') \rangle ds' = \int_0^{l_c} ds \int_0^{l_c} \exp\left(-\frac{|s-s'|}{l_p}\right) ds' \tag{A.17}$$

$$= 2l_p l_c \left(1 + \frac{l_p}{l_c}\left(\exp\left(-\frac{l_c}{l_p}\right) - 1\right)\right) \tag{A.18}$$

For $l_c \gg l_p$, this formula reduces to the results from the FJC in Equation A.1 where $l_K = 2l_p$. That allows the comparison of different polymer models.

## Exact Calculation of Force versus Extension for the WLC

An exact solution of the force-extension behavior of a polymer in the WLC model is possible[287, 288]. However, as only the interpolation formula in Equation 1.10 is mainly used in studies applying the WLC model to polymers or proteins, the derivation of the exact solution is only sketched.

The following term describes the resistance of a WLC to bending:

$$e_b(s) = \frac{A}{2}|\frac{dt(s)}{ds}|^2 \tag{A.19}$$

with $A = k_B T l_p$ and it is proportional to the inverse square of the radius of curvature.

The stretching energy $e_f(s)$ from the application of a force $F$ to the end of a molecular chain is given by:

$$e_f(s) = -F\cos\theta(s) \tag{A.20}$$

Integrating over the full length of the molecule $l_c$, the expression for the energy of a stretched molecule $E_{WLC}$ is:

$$E_{WLC} = \int_0^{l_c} ds \left(\frac{A}{2}|\frac{dt(s)}{ds}|^2 - F\cos\theta(s)\right) \tag{A.21}$$

The partition function $Z(l_c, F, t_0, t_1)$ is calculated from that with a path integral. This allows the formation of probability functions $\psi$, so-called eigenwavefunctions. The eigenvalue problem of this Schroedinger-like equation is solved numerically, with the free energy of a WLC being related to the smallest eigenvalue of the differential equation.

# Bibliography

[1]   A. Kamkin and I. Kiseleva. *Mechanosensitivity of Cells from Various Tissues*. Moscow: Academia, 2005, pp. 1–12.

[2]   K. R. Phillips, A. Biswas, and J. L. Cyr. "How hair cells hear: the molecular basis of hair-cell mechanotransduction". In: *Curr. Opin. Otolaryngol. Head Neck Surg.* 16.5 (Oct. 2008), pp. 445–451.

[3]   E. K. Paluch, C. M. Nelson, et al. "Mechanotransduction: use the force(s)". In: *BMC Biol.* 13.1 (2015), p. 47.

[4]   C. Seifert and F. Gräter. "Protein mechanics: How force regulates molecular function". In: *Biochim. Biophys. Acta - Gen. Subj.* 1830.10 (Oct. 2013), pp. 4762–4768.

[5]   D. Purves, G. Augustine, and D. Fitzpatrick. "Mechanoreceptors Specialized to Receive Tactile Information". In: *Neuroscience*. Sunderland (MA): Sinauer Associates, 2001.

[6]   D. Guo, Z. Kassiri, and G. Y. Oudit. "Role of Signaling Pathways in the Myocardial Response to Biomechanical Stress and in Mechanotransduction in the Heart". In: *Mechanosensitivity and Mechanotransduction*. Ed. by A. Kamkin and I. Kiseleva. Dordrecht: Springer Netherlands, 2010, pp. 141–166.

[7]   R. C. Lyon, F. Zanella, et al. "Mechanotransduction in cardiac hypertrophy and failure". In: *Circ. Res.* 116.8 (Apr. 2015), pp. 1462–1476.

[8]   C. Hahn and M. A. Schwartz. "Mechanotransduction in vascular physiology and atherogenesis". In: *Nat. Rev. Mol. Cell Biol.* 10.1 (2009), pp. 53–62.

[9]   J. C. Parker and M. I. Townsley. "Control of TRPV4 and Its Effect on the Lung". In: *Mechanosensitivity and Mechanotransduction*. Ed. by A. Kamkin and I. Kiseleva. Dordrecht: Springer Netherlands, 2011, pp. 239–254.

[10]  M. P. Yavropoulou and J. G. Yovos. "The molecular basis of bone mechanotransduction." In: *J. Musculoskelet. Neuronal Interact.* 16.3 (Sept. 2016), pp. 221–36.

[11]  S. R. L. Young and F. M. Pavalko. "Cellular Mechanisms of Mechanotransduction in Bone". In: *Mechanosensitivity and Mechanotransduction*. Ed. by A. Kamkin and I. Kiseleva. Dordrecht: Springer Netherlands, 2011, pp. 277–296.

[12]  A. E. Dubin and A. Patapoutian. "Nociceptors: the sensors of the pain pathway". In: *J. Clin. Invest.* 120.11 (Nov. 2010), pp. 3760–3772.

[13]  R. W. Banks. "The Muscle Spindle". In: *Peripher. Neuropathy*. Ed. by T. P. Dyck PJ. 4th edn. Vol. 4. Elsevier, 2005, pp. 131–150.

[14] W. Meng and M. Takeichi. "Adherens Junction: Molecular Architecture and Regulation". In: *Cold Spring Harb. Perspect. Biol.* 1.6 (Dec. 2009), a002899–a002899.

[15] S. Nag and A. Resnick. "Biophysics and Biofluiddynamics of Primary Cilia: evidence for and against the flow-sensing function". In: *Am. J. Physiol. - Ren. Physiol.* (June 2017).

[16] S. S. Ranade, R. Syeda, and A. Patapoutian. *Mechanically Activated Ion Channels.* 2015.

[17] C. Guilluy and K. Burridge. "Nuclear mechanotransduction: Forcing the nucleus to respond". In: *Nucleus* 6.1 (2015), pp. 19–22.

[18] P. W. Oakes and M. L. Gardel. "Stressing the limits of focal adhesion mechanosensitivity". In: *Curr. Opin. Cell Biol.* 30.1 (Oct. 2014), pp. 68–73.

[19] W. L. Murphy, T. C. McDevitt, and A. J. Engler. "Materials as stem cell regulators". In: *Nat. Mater.* 13.6 (May 2014), pp. 547–557.

[20] J. Eyckmans, T. Boudou, et al. "A Hitchhiker's Guide to Mechanobiology". In: *Dev. Cell* 21.1 (July 2011), pp. 35–47.

[21] A. Harris, P. Wild, and D. Stopak. "Silicone rubber substrata: a new wrinkle in the study of cell locomotion". In: *Science (80-. ).* 208.4440 (1980), pp. 177–179.

[22] N. Wang, J. Butler, and D. Ingber. "Mechanotransduction across the cell surface and through the cytoskeleton". In: *Science (80-. ).* 260.5111 (May 1993), pp. 1124–1127.

[23] J. R. Sims, S. Karp, and D. E. Ingber. "Altering the cellular mechanical force balance results in integrated changes in cell, cytoskeletal and nuclear shape." In: *J. Cell Sci.* 103 ( Pt 4 (Dec. 1992), pp. 1215–22.

[24] W. H. Goldmann. "Mechanosensation: A basic cellular process". In: *Prog. Mol. Biol. Transl. Sci.* 1st ed. Vol. 126. Elsevier Inc., 2014, pp. 75–102.

[25] D. A. Fletcher and R. D. Mullins. "Cell mechanics and the cytoskeleton". In: *Nature* 463.7280 (Jan. 2010), pp. 485–492.

[26] R. Paul, P. Heil, et al. "Propagation of Mechanical Stress through the Actin Cytoskeleton toward Focal Adhesions: Model and Experiment". In: *Biophys. J.* 94.4 (2008), pp. 1470–1482.

[27] M. Vicente-Manzanares, X. Ma, et al. "Non-muscle myosin II takes centre stage in cell adhesion and migration". In: *Nat. Rev. Mol. Cell Biol.* 10.11 (Nov. 2009), pp. 778–790.

[28] D. Choquet, D. P. Felsenfeld, and M. P. Sheetz. "Extracellular Matrix Rigidity Causes Strengthening of Integrin–Cytoskeleton Linkages". In: *Cell* 88.1 (1997), pp. 39–48.

[29] R. McBeath, D. M. Pirone, et al. "Cell shape, cytoskeletal tension, and RhoA regulate stemm cell lineage commitment". In: *Dev. Cell* 6 (2004), pp. 483–495.

[30] S. Miyamoto, H. Teramoto, et al. "Integrin function: Molecular hierarchies of cytoskeletal and signaling molecules". In: *J. Cell Biol.* 131.3 (1995), pp. 791–805.

[31] U. Blank, G. Karlsson, and S. Karlsson. "Signaling pathways governing stem-cell fate". In: *Blood* 111.2 (Jan. 2008), pp. 492–503.

[32] M. H. Kural and K. L. Billiar. "Regulating tension in three-dimensional culture environments". In: *Exp. Cell Res.* 319.16 (Oct. 2013), pp. 2447–2459.

[33] L. MacQueen, Y. Sun, and C. A. Simmons. "Mesenchymal stem cell mechanobiology and emerging experimental platforms". In: *J. R. Soc. Interface* 10.84 (2013), pp. 20130179–20130179.

[34] E. Bellas and C. S. Chen. "Forms, forces, and stem cell fate". In: *Curr. Opin. Cell Biol.* 31 (Dec. 2014), pp. 92–97.

[35] I. Ullah, R. B. Subbarao, and G.-J. Rho. "Human mesenchymal stem cells - current trends and future prospective". In: *Biosci. Rep.* 35.2 (Apr. 2015), pp. 1–18.

[36] P. Weiss and B. Garber. "Shape and Movement of Mesenchyme Cells as Functions of the Physical Structure of the Medium: Contributions to a Quantitative Morphology." In: *Proc. Natl. Acad. Sci. U. S. A.* 38.3 (1952), pp. 264–80.

[37] A. S. Curtis and M. Varde. "Control of Cell Behavior: Topological Factors". In: *J. Natl. Cancer Inst.* 33.1 (July 1964), pp. 15–26.

[38] M. F. Pittenger, A. M. Mackay, et al. "Multilineage Potential of Adult Human Mesenchymal Stem Cells". In: *Science (80-. ).* 284.April (1999), pp. 143–147.

[39] D. E. Discher. "Tissue Cells Feel and Respond to the Stiffness of Their Substrate". In: *Science (80-. ).* 310.5751 (2005), pp. 1139–1143.

[40] R. G. Wells. "The role of matrix stiffness in regulating cell behavior". In: *Hepatology* 47.4 (Jan. 2008), pp. 1394–1400.

[41] R. J. Pelham and Y.-l. Wang. "Cell locomotion and focal adhesions are regulated by substrate flexibility". In: *Proc. Natl. Acad. Sci.* 94.25 (Dec. 1997), pp. 13661–13665.

[42] C.-M. Lo, H.-B. Wang, et al. "Cell Movement Is Guided by the Rigidity of the Substrate". In: *Biophys. J.* 79.1 (July 2000), pp. 144–152.

[43] B. Ladoux, R.-M. Mège, and X. Trepat. "Front–Rear Polarization by Mechanical Cues: From Single Cells to Tissues". In: *Trends Cell Biol.* 26.6 (June 2016), pp. 420–433.

[44] T. Yeung, P. C. Georges, et al. "Effects of substrate stiffness on cell morphology, cytoskeletal structure, and adhesion". In: *Cell Motil. Cytoskeleton* 60.1 (2005), pp. 24–34.

[45] H. B. Wang, M. Dembo, and Y. L. Wang. "Substrate flexibility regulates growth and apoptosis of normal but not transformed cells." In: *Am. J. Physiol. Cell Physiol.* 279.5 (Nov. 2000), pp. C1345–50.

[46] F. P. Seib, M. Prewitz, et al. "Matrix elasticity regulates the secretory profile of human bone marrow-derived multipotent mesenchymal stromal cells (MSCs)". In: *Biochem. Biophys. Res. Commun.* 389.4 (Nov. 2009), pp. 663–667.

[47] A. A. Abdeen, J. B. Weiss, et al. "Matrix Composition and Mechanics Direct Proangiogenic Signaling from Mesenchymal Stem Cells". In: *Tissue Eng. Part A* 20.19-20 (Oct. 2014), pp. 2737–2745.

[48] A. Mammoto, K. M. Connor, et al. "A mechanosensitive transcriptional mechanism that controls angiogenesis". In: *Nature* 457.7233 (Feb. 2009), pp. 1103–1108.

[49] L. Chen, E. E. Tredget, et al. "Paracrine factors of mesenchymal stem cells recruit macrophages and endothelial lineage cells and enhance wound healing". In: *PLoS One* 3.4 (2008).

[50] A. J. Engler, C. Carag-Krieger, et al. "Embryonic cardiomyocytes beat best on a matrix with heart-like elasticity: scar-like rigidity inhibits beating". In: *J. Cell Sci.* 121.22 (2008), pp. 3794–3802.

[51] N. Hersch, B. Wolters, et al. "The constant beat: cardiomyocytes adapt their forces by equal contraction upon environmental stiffening". In: *Biol. Open* 2.3 (2013), pp. 351–361.

[52] D. E. Jaalouk and J. Lammerding. "Mechanotransduction gone awry". In: *Nat. Rev. Mol. Cell Biol.* 10.1 (2009), pp. 63–73.

[53] M. J. Paszek, N. Zahir, et al. "Tensional homeostasis and the malignant phenotype". In: *Cancer Cell* 8.3 (2005), pp. 241–254.

[54] K. R. Levental, H. Yu, et al. "Matrix Crosslinking Forces Tumor Progression by Enhancing Integrin Signaling". In: *Cell* 139.5 (2009), pp. 891–906.

[55] A. J. Engler, S. Sen, et al. "Matrix Elasticity Directs Stem Cell Lineage Specification". In: *Cell* 126.4 (Aug. 2006), pp. 677–689.

[56] J. P. Winer, P. A. Janmey, et al. "Bone Marrow-Derived Human Mesenchymal Stem Cells Become Quiescent on Soft Substrates but Remain Responsive to Chemical or Mechanical Stimuli". In: *Tissue Eng. Part A* 15.1 (Jan. 2009), pp. 147–154.

[57] J. S. Park, J. S. Chu, et al. "The effect of matrix stiffness on the differentiation of mesenchymal stem cells in response to TGF-$\beta$". In: *Biomaterials* 32.16 (June 2011), pp. 3921–3930.

[58] J. Swift, I. L. Ivanovska, et al. "Nuclear Lamin-A Scales with Tissue Stiffness and Enhances Matrix-Directed Differentiation". In: *Science (80-. ).* 341.6149 (Aug. 2013), pp. 1240104–1240104.

[59] C. Yang, M. W. Tibbitt, et al. "Mechanical memory and dosing influence stem cell fate". In: *Nat. Mater.* 13.6 (Mar. 2014), pp. 645–652.

[60] A. S. Rowlands, P. A. George, and J. J. Cooper-White. "Directing osteogenic and myogenic differentiation of MSCs: interplay of stiffness and adhesive ligand presentation". In: *AJP Cell Physiol.* 295.4 (2008), pp. C1037–C1044.

[61] B. Trappmann, J. E. Gautrot, et al. "Extracellular-matrix tethering regulates stem-cell fate". In: *Nat. Mater.* 11.8 (July 2012), pp. 742–742.

[62] J. H. Wen, L. G. Vincent, et al. "Interplay of matrix stiffness and protein tethering in stem cell differentiation". In: *Nat. Mater.* 13.10 (2014), pp. 979–987.

[63] R. K. Das, V. Gocheva, et al. "Stress-stiffening-mediated stem-cell commitment switch in soft responsive hydrogels". In: *Nat. Mater.* 15.3 (2015), pp. 318–325.

[64]  M. K. Gunnewiek, S. N. Ramakrishna, et al. "Stem-Cell Clinging by a Thread: AFM Measure of Polymer-Brush Lateral Deformation". In: *Adv. Mater. Interfaces* 3.3 (Feb. 2016), p. 1500456.

[65]  Y. S. Pek, A. C. Wan, and J. Y. Ying. "The effect of matrix stiffness on mesenchymal stem cell differentiation in a 3D thixotropic gel". In: *Biomaterials* 31.3 (Jan. 2010), pp. 385–391.

[66]  N. Huebsch, P. R. Arany, et al. "Harnessing traction-mediated manipulation of the cell/matrix interface to control stem-cell fate". In: *Nat. Mater.* 9.6 (June 2010), pp. 518–526.

[67]  S. Khetan, M. Guvendiren, et al. "Degradation-mediated cellular traction directs stem cell fate in covalently crosslinked three-dimensional hydrogels". In: *Nat. Mater.* 12.5 (Mar. 2013), pp. 458–465.

[68]  A. Higuchi, Q.-D. Ling, et al. "Physical Cues of Biomaterials Guide Stem Cell Differentiation Fate". In: *Chem. Rev.* 113.5 (May 2013), pp. 3297–3328.

[69]  N. D. Evans, C. Minelli, et al. "Substrate stiffness affects early differentiation events in embryonic stem cells". In: *Eur. Cells Mater.* 18 (Jan. 2009), pp. 1–13.

[70]  F. Chowdhury, Y. Li, et al. "Soft substrates promote homogeneous self-renewal of embryonic stem cells via downregulating cell-matrix tractions". In: *PLoS One* 5.12 (2010).

[71]  J. Zoldan, E. D. Karagiannis, et al. "The influence of scaffold elasticity on germ layer specification of human embryonic stem cells". In: *Biomaterials* 32.36 (Dec. 2011), pp. 9612–9621.

[72]  Y. Sun, L. G. Villa-Diaz, et al. "Mechanics regulates fate decisions of human embryonic stem cells". In: *PLoS One* 7.5 (2012).

[73]  P. M. Gilbert, K. L. Havenstrite, et al. "Substrate Elasticity Regulates Skeletal Muscle Stem Cell Self-Renewal in Culture". In: *Science (80-. ).* 329.5995 (Aug. 2010), pp. 1078–1081.

[74]  B. D. Cosgrove, P. M. Gilbert, et al. "Rejuvenation of the muscle stem cell population restores strength to injured aged muscles". In: *Nat. Med.* 20.3 (2014), pp. 255–264.

[75]  J. E. Dixon, D. A. Shah, et al. "Combined hydrogels that switch human pluripotent stem cells from self-renewal to differentiation". In: *Proc. Natl. Acad. Sci.* 111.15 (2014), pp. 5580–5585.

[76]  J. Fink, N. Carpi, et al. "External forces control mitotic spindle positioning". In: *Nat. Cell Biol.* 13.7 (2011), pp. 771–778.

[77]  K. M. Mabry, S. Z. Payne, and K. S. Anseth. "Microarray analyses to quantify advantages of 2D and 3D hydrogel culture systems in maintaining the native valvular interstitial cell phenotype". In: *Biomaterials* 74 (2016), pp. 31–41.

[78]  N. S. Hwang, S. Varghese, et al. "Regulation of osteogenic and chondrogenic differentiation of mesenchymal stem cells in PEG-ECM hydrogels". In: *Cell Tissue Res.* 344.3 (2011), pp. 499–509.

[79]  S. A. Ruiz and C. S. Chen. "Emergence of Patterned Stem Cell Differentiation Within Multicellular Structures". In: *Stem Cells* 26.11 (2008), pp. 2921–2927.

[80]  K. A. Kilian, B. Bugarija, et al. "Geometric cues for directing the differentiation of mesenchymal stem cells". In: *Proc. Natl. Acad. Sci.* 107.11 (Mar. 2010), pp. 4872–4877.

[81]  T. Gong, L. Lu, et al. "Dynamically tunable polymer microwells for directing mesenchymal stem cell differentiation into osteogenesis". In: *J. Mater. Chem. B* 3.46 (2015), pp. 9011–9022.

[82]  S.-Y. Tee, J. Fu, et al. "Cell Shape and Substrate Rigidity Both Regulate Cell Stiffness". In: *Biophys. J.* 100.5 (Mar. 2011), pp. L25–L27.

[83]  M. J. Dalby, N. Gadegaard, et al. "The control of human mesenchymal cell differentiation using nanoscale symmetry and disorder". In: *Nat. Mater.* 6.12 (Dec. 2007), pp. 997–1003.

[84]  R. J. McMurray, N. Gadegaard, et al. "Nanoscale surfaces for the long-term maintenance of mesenchymal stem cell phenotype and multipotency". In: *Nat. Mater.* 10.8 (2011), pp. 637–644.

[85]  P. Tsimbouri, N. Gadegaard, et al. "Nanotopographical effects on mesenchymal stem cell morphology and phenotype". In: *J. Cell. Biochem.* 115.2 (2014), pp. 380–390.

[86]  W. Chen, L. G. Villa-Diaz, et al. "Nanotopography influences adhesion, spreading, and self-renewal of Human embryonic stem cells". In: *ACS Nano* 6.5 (May 2012), pp. 4094–4103.

[87]  J. K. Biehl, S. Yamanaka, et al. "Proliferation of mouse embryonic stem cell progeny and the spontaneous contractile activity of cardiomyocytes are affected by microtopography". In: *Dev. Dyn.* 238.8 (Aug. 2009), pp. 1964–1973.

[88]  J. D. Salvi, J. Yul Lim, and H. J. Donahue. "Increased mechanosensitivity of cells cultured on nanotopographies". In: *J. Biomech.* 43.15 (2010), pp. 3058–3062.

[89]  Y. Li, J. S. Chu, et al. "Biophysical regulation of histone acetylation in mesenchymal stem cells". In: *Biophys. J.* 100.8 (2011), pp. 1902–1909.

[90]  T. L. Downing, J. Soto, et al. "Biophysical regulation of epigenetic state and cell reprogramming". In: *Nat. Mater.* 12.12 (2013), pp. 1154–1162.

[91]  J. M. Curran, R. Chen, and J. A. Hunt. "The guidance of human mesenchymal stem cell differentiation in vitro by controlled modifications to the cell substrate". In: *Biomaterials* 27.27 (Sept. 2006), pp. 4783–4793.

[92]  J. M. Curran, R. Stokes, et al. "Introducing dip pen nanolithography as a tool for controlling stem cell behaviour: unlocking the potential of the next generation of smart materials in regenerative medicine". In: *Lab Chip* 10.13 (2010), pp. 1662–1670.

[93]  M. Lanniel, E. Huq, et al. "Substrate induced differentiation of human mesenchymal stem cells on hydrogels with modified surface chemistry and controlled modulus". In: *Soft Matter* 7.14 (2011), p. 6501.

[94]  Y.-H. Tsou, J. Khoneisser, et al. "Hydrogel as a bioactive material to regulate stem cell fate". In: *Bioact. Mater.* 1.1 (Sept. 2016), pp. 39–55.

[95]  K. A. Kilian and M. Mrksich. "Directing stem cell fate by controlling the affinity and density of ligand-receptor interactions at the biomaterials interface". In: *Angew. Chemie - Int. Ed.* 51.20 (2012), pp. 4891–4895.

[96]  A. Conway, T. Vazin, et al. "Multivalent ligands control stem cell behaviour in vitro and in vivo". In: *Nat. Nanotechnol.* 8.11 (2013), pp. 831–838.

[97]  G. Yourek, S. M. McCormick, et al. "Shear stress induces osteogenic differentiation of human mesenchymal stem cells". In: *Regen. Med.* 5.5 (2010), pp. 713–24.

[98]  Y. K. Luu, E. Capilla, et al. "Mechanical stimulation of mesenchymal stem cell proliferation and differentiation promotes osteogenesis while preventing dietary-induced obesity." In: *J. bone Miner. Res. Off. J. Am. Soc. Bone Miner. Res.* 24.1 (2009), pp. 50–61.

[99]  H. Nikukar, S. Reid, et al. "Control of Mesenchymal Stem-Cell Fate by Engineering the Nanoenvironment". In: *Stem-Cell Nanoeng.* Hoboken, NJ: John Wiley & Sons, Inc, Jan. 2015, pp. 205–221.

[100]  A. S. Mao, J. W. Shin, and D. J. Mooney. "Effects of substrate stiffness and cell-cell contact on mesenchymal stem cell differentiation". In: *Biomaterials* 98 (2016), pp. 184–191.

[101]  M. Akhmanova, E. Osidak, et al. "Physical, Spatial, and Molecular Aspects of Extracellular Matrix of In Vivo Niches and Artificial Scaffolds Relevant to Stem Cells Research". In: *Stem Cells Int.* 2015 (2015), pp. 1–35.

[102]  M. A. Rieger and T. Schroeder. "Hematopoiesis". In: *Cold Spring Harb. Perspect. Biol.* 4.12 (Dec. 2012), a008250–a008250.

[103]  J. Oh, Y. D. Lee, and A. J. Wagers. "Stem cell aging: mechanisms, regulators and therapeutic opportunities". In: *Nat. Med.* 20.8 (Aug. 2014), pp. 870–880.

[104]  M. S. H. Ho, R. L. Medcalf, et al. "The dynamics of adult haematopoiesis in the bone and bone marrow environment". In: *Br. J. Haematol.* 170.4 (Aug. 2015), pp. 472–486.

[105]  J. Seita and I. L. Weissman. "Hematopoietic stem cell: self-renewal versus differentiation". In: *Wiley Interdiscip. Rev. Syst. Biol. Med.* 2.6 (Nov. 2010), pp. 640–653.

[106]  G. J. Cabrita, B. S. Ferreira, et al. "Hematopoietic stem cells: from the bone to the bioreactor". In: *Trends Biotechnol.* 21.5 (May 2003), pp. 233–240.

[107]  M. Tuthill and Hatzimichael. "Hematopoietic stem cell transplantation". In: *Stem Cells Cloning Adv. Appl.* 3.1 (Aug. 2010), p. 105.

[108]  E. A. Copelan. "Hematopoietic Stem-Cell Transplantation". In: *N. Engl. J. Med.* 354.17 (Apr. 2006), pp. 1813–1826.

[109]  M. G. Daniel, C.-F. Pereira, et al. "Making a Hematopoietic Stem Cell". In: *Trends Cell Biol.* 26.3 (2016), pp. 202–214.

[110] C. D. Porada, A. J. Atala, and G. Almeida-Porada. "The hematopoietic system in the context of regenerative medicine". In: *Methods* 99 (Apr. 2016), pp. 44–61.

[111] L. F. Newell, M. E. D. Flowers, et al. "Characteristics of chronic GVHD after cord blood transplantation". In: *Bone Marrow Transplant.* 48.10 (Oct. 2013), pp. 1285–1290.

[112] C. D. Hillyer. "Blood Banking and Transfusion Medicine – History, Industry, and Discipline". In: *Transfus. Med. Hemost.* Elsevier, 2013, pp. 3–9.

[113] A. Dahlberg, C. Delaney, and I. D. Bernstein. *Ex vivo expansion of human hematopoietic stem and progenitor cells.* 2011.

[114] C. C. Hofmeister, J. Zhang, et al. "Ex vivo expansion of umbilical cord blood stem cells for transplantation: growing knowledge from the hematopoietic niche". In: *Bone Marrow Transplant.* 39.1 (2007), pp. 11–23.

[115] F. Gattazzo, A. Urciuolo, and P. Bonaldo. "Extracellular matrix: A dynamic microenvironment for stem cell niche". In: *Biochim. Biophys. Acta - Gen. Subj.* 1840.8 (2014), pp. 2506–2519.

[116] R. Schofield. "The relationship between the spleen colony-forming cell and the haemopoietic stem cell." In: *Blood Cells* 4.1-2 (1978), pp. 7–25.

[117] S. J. Morrison and D. T. Scadden. "The bone marrow niche for haematopoietic stem cells". In: *Nature* 505.7483 (2014), pp. 327–334.

[118] S. Kumar and H. Geiger. "HSC Niche Biology and HSC Expansion Ex Vivo". In: *Trends Mol. Med.* 23.9 (Sept. 2017), pp. 799–819.

[119] M. A. Walasek, R. van Os, and G. de Haan. "Hematopoietic stem cell expansion: challenges and opportunities". In: *Ann. N. Y. Acad. Sci.* 1266.1 (Aug. 2012), pp. 138–150.

[120] I. G. Winkler, V. Barbier, et al. "Positioning of bone marrow hematopoietic and stromal cells relative to blood flow in vivo: Serially reconstituting hematopoietic stem cells reside in distinct nonperfused niches". In: *Blood* 116.3 (2010), pp. 375–385.

[121] A. Birbrair and P. S. Frenette. "Niche heterogeneity in the bone marrow". In: *Ann. N. Y. Acad. Sci.* 1370.1 (Apr. 2016), pp. 82–96.

[122] P. C. D. P. Dingal and D. E. Discher. "Combining insoluble and soluble factors to steer stem cell fate". In: *Nat. Mater.* 13.6 (2014), pp. 532–537.

[123] M. A. Schwartz and C. S. Chen. "Deconstructing Dimensionality". In: *Science (80-. ).* 339.6118 (Jan. 2013), pp. 402–404.

[124] E. Altrock, C. A. Muth, et al. "The significance of integrin ligand nanopatterning on lipid raft clustering in hematopoietic stem cells". In: *Biomaterials* 33.11 (2012), pp. 3107–3118.

[125] T. E. North, W. Goessling, et al. "Hematopoietic Stem Cell Development Is Dependent on Blood Flow". In: *Cell* 137.4 (May 2009), pp. 736–748.

[126] L. Adamo, O. Naveiras, et al. "Biomechanical forces promote embryonic haematopoiesis". In: *Nature* 459.7250 (June 2009), pp. 1131–1135.

[127]   J.-P. Lévesque, F. M. Helwani, and I. G. Winkler. "The endosteal 'osteoblastic' niche and its role in hematopoietic stem cell homing and mobilization". In: *Leukemia* 24.12 (2010), pp. 1979–1992.

[128]   J. Holst, S. Watson, et al. "Substrate elasticity provides mechanical signals for the expansion of hemopoietic stem and progenitor cells". In: *Nat. Biotechnol.* 28.10 (Oct. 2010), pp. 1123–8.

[129]   C. Lee-Thedieck, N. Rauch, et al. "Impact of substrate elasticity on human hematopoietic stem and progenitor cell adhesion and motility". In: *J. Cell Sci.* 125.16 (Aug. 2012), pp. 3765–3775.

[130]   Y. Katayama, M. Battista, et al. "Signals from the Sympathetic Nervous System Regulate Hematopoietic Stem Cell Egress from Bone Marrow". In: *Cell* 124.2 (Jan. 2006), pp. 407–421.

[131]   J. S. Choi and B. A. C. Harley. "The combined influence of substrate elasticity and ligand density on the viability and biophysical properties of hematopoietic stem and progenitor cells". In: *Biomaterials* 33.18 (2012), pp. 4460–4468.

[132]   S. S. Kumar, J.-H. Hsiao, et al. "The combined influence of substrate elasticity and surface-grafted molecules on the ex vivo expansion of hematopoietic stem and progenitor cells". In: *Biomaterials* 34.31 (Oct. 2013), pp. 7632–7644.

[133]   B. R. Chitteti, M. A. Kacena, et al. "Modulation of hematopoietic progenitor cell fate in vitro by varying collagen oligomer matrix stiffness in the presence or absence of osteoblasts". In: *J. Immunol. Methods* 425 (2015), pp. 108–113.

[134]   D. Gvaramia, E. Müller, et al. "Combined influence of biophysical and biochemical cues on maintenance and proliferation of hematopoietic stem cells". In: *Biomaterials* 138 (Sept. 2017), pp. 108–117.

[135]   J.-W. Shin, A. Buxboim, et al. "Contractile Forces Sustain and Polarize Hematopoiesis from Stem and Progenitor Cells". In: *Cell Stem Cell* 14.1 (Jan. 2014), pp. 81–93.

[136]   I. L. Ivanovska, J.-W. Shin, et al. "Stem cell mechanobiology: diverse lessons from bone marrow". In: *Trends Cell Biol.* 25.9 (Sept. 2015), pp. 523–532.

[137]   J. S. Choi and B. A. C. Harley. "Marrow-inspired matrix cues rapidly affect early fate decisions of hematopoietic stem and progenitor cells". In: *Sci. Adv.* 3.1 (Jan. 2017), e1600455.

[138]   M. Votteler, P. J. Kluger, et al. "Stem Cell Microenvironments - Unveiling the Secret of How Stem Cell Fate is Defined". In: *Macromol. Biosci.* 10.11 (Nov. 2010), pp. 1302–1315.

[139]   S. M. Mithieux, S. G. Wise, and A. S. Weiss. "Tropoelastin - A multifaceted naturally smart material". In: *Adv. Drug Deliv. Rev.* 65.4 (Apr. 2013), pp. 421–428.

[140]   D. M. Milewicz, Z. Urbán, and C. Boyd. "Genetic disorders of the elastic fiber system". In: *Matrix Biol.* 19.6 (Nov. 2000), pp. 471–480.

[141]   S. G. Wise and A. S. Weiss. "Tropoelastin". In: *Int. J. Biochem. Cell Biol.* 41.3 (Mar. 2009), pp. 494–497.

[142]    S. G. Wise, G. C. Yeo, et al. "Tropoelastin: A versatile, bioactive assembly module". In: *Acta Biomater.* 10.4 (Apr. 2014), pp. 1532–1541.

[143]    S. L. Martin, B. Vrhovski, and A. S. Weiss. "Total synthesis and expression in Escherichia coli of a gene encoding human tropoelastin". In: *Gene* 154.2 (Jan. 1995), pp. 159–166.

[144]    C. E. Ghezzi, J. Rnjak-Kovacina, et al. *Multifunctional silk-tropoelastin biomaterial systems.* 2013.

[145]    J. Ozsvar, S. M. Mithieux, et al. "Elastin-based biomaterials and mesenchymal stem cells". In: *Biomater Sci* 3.6 (2015), pp. 800–809.

[146]    B. Li and V. Daggett. "Molecular basis for the extensibility of elastin." In: *J. Muscle Res. Cell Motil.* 23.5-6 (May 2002), pp. 561–573.

[147]    L. Debelle and A. Tamburro. "Elastin: molecular description and function". In: *Int. J. Biochem. Cell Biol.* 31.2 (Feb. 1999), pp. 261–272.

[148]    S. Rauscher and R. Pomès. "Structural disorder and protein elasticity". In: *Adv. Exp. Med. Biol.* 725 (2012), pp. 159–183.

[149]    C. Baldock, A. F. Oberhauser, et al. "Shape of tropoelastin, the highly extensible protein that controls human tissue elasticity". In: *Proc. Natl. Acad. Sci.* 108.11 (Mar. 2011), pp. 4322–4327.

[150]    T. P. Knowles, A. W. Fitzpatrick, et al. "Role of Intermolecular Forces in Defining Material Properties of Protein Nanofibrils". In: *Science (80-. ).* 318.5858 (2007), pp. 1900–1903.

[151]    Y.-C. Fung. *Biomechanics.* Ed. by Y.-C. Fung. New York, NY: Springer New York, 1993, p. 568.

[152]    X. Hu, S.-H. Park, et al. "The influence of elasticity and surface roughness on myogenic and osteogenic-differentiation of cells on silk-elastin biomaterials". In: *Biomaterials* 32.34 (Dec. 2011), pp. 8979–8989.

[153]    G. C. Yeo, F. W. Keeley, and A. S. Weiss. "Coacervation of tropoelastin". In: *Adv. Colloid Interface Sci.* 167.1-2 (Sept. 2011), pp. 94–103.

[154]    B. Vrhovski, S. Jensen, and A. S. Weiss. "Coacervation Characteristics of Recombinant Human Tropoelastin". In: *Eur. J. Biochem.* 250.1 (Nov. 1997), pp. 92–98.

[155]    L. Dyksterhuis and A. Weiss. "Homology models for domains 21-23 of human tropoelastin shed light on lysine crosslinking". In: *Biochem. Biophys. Res. Commun.* 396.4 (June 2010), pp. 870–873.

[156]    J. Djajamuliadi, T. F. Kagawa, et al. "Insights into a putative hinge region in elastin using molecular dynamics simulations". In: *Matrix Biol.* 28.2 (Mar. 2009), pp. 92–100.

[157]    G. C. Yeo, C. Baldock, et al. "Tropoelastin bridge region positions the cell-interactive C-terminus and contributes to elastic fiber assembly". In: *Proc. Natl. Acad. Sci.* 109.8 (Feb. 2012), pp. 2878–2883.

[158] J. F. Almine, D. V. Bax, et al. "Elastin-based materials". In: *Chem. Soc. Rev.* 39.9 (2010), p. 3371.

[159] A. Kamoun, J.-M. Landeau, et al. "Growth Stimulation of Human Skin Fibroblasts by Elastin-Derived Peptides". In: *Cell Adhes. Commun.* 3.4 (Jan. 1995), pp. 273–281.

[160] L. E. Grosso and M. Scott. "Peptide sequences selected by BA4, a tropoelastin-specific monoclonal antibody, are ligands for the 67-kilodalton bovine elastin receptor". In: *Biochemistry* 32.48 (Dec. 1993), pp. 13369–13374.

[161] D. V. Bax, U. R. Rodgers, et al. "Cell Adhesion to Tropoelastin Is Mediated via the C-terminal GRKRK Motif and Integrin $\alpha$V $\beta$3". In: *J. Biol. Chem.* 284.42 (Oct. 2009), pp. 28616–28623.

[162] J. Rnjak, Z. Li, et al. "Primary human dermal fibroblast interactions with open weave three-dimensional scaffolds prepared from synthetic human elastin". In: *Biomaterials* 30.32 (Nov. 2009), pp. 6469–6477.

[163] N. Fujimoto, S. Tajima, and A. Ishibashi. "Elastin peptides induce migration and terminal differentiation of cultured keratinocytes via 67 kDa elastin receptor in vitro: 67 kDa elastin receptor is expressed in the keratinocytes eliminating elastic materials in elastosis perforans serpiginosa". In: *J. Invest. Dermatol.* 115.4 (2000), pp. 633–639.

[164] A. Robinet, A. Fahem, et al. "Elastin-derived peptides enhance angiogenesis by promoting endothelial cell migration and tubulogenesis through upregulation of MT1-MMP." In: *J. Cell Sci.* 118.Pt 2 (Jan. 2005), pp. 343–56.

[165] J. F. Almine, S. G. Wise, and A. S. Weiss. "Elastin signaling in wound repair". In: *Birth Defects Res. Part C Embryo Today Rev.* 96.3 (Sept. 2012), pp. 248–257.

[166] U. R. Rodgers and A. S. Weiss. "Cellular interactions with elastin". In: *Pathol. Biol.* 53.7 (Sept. 2005), pp. 390–398.

[167] A. Hinek and M. Rabinovitch. "67-kD elastin-binding protein is a protective "companion" of extracellular insoluble elastin and intracellular tropoelastin." In: *J. Cell Biol.* 126.2 (July 1994), pp. 563–74.

[168] C. Blanchevoye, N. Floquet, et al. "Interaction between the elastin peptide VGVAPG and human elastin binding protein". In: *J. Biol. Chem.* 288.2 (2013), pp. 1317–1328.

[169] R. M. Senior, G. L. Griffin, et al. "Val-Gly-Val-Ala-Pro-Gly, a repeating peptide in elastin, is chemotactic for fibroblasts and monocytes". In: *J. Cell Biol.* 99.3 (1984), pp. 870–874.

[170] J. M. Skeie, J. Hernandez, et al. "Molecular responses of choroidal endothelial cells to elastin derived peptides through the elastin-binding protein (GLB1)". In: *Matrix Biol.* 31.2 (Mar. 2012), pp. 113–119.

[171] S. K. Karnik, J. D. Wythe, et al. "Elastin induces myofibrillogenesis via a specific domain, VGVAPG". In: *Matrix Biol.* 22.5 (Sept. 2003), pp. 409–425.

[172] R. P. Mecham, A. Hinek, et al. "Elastin Binds to a Multifunctional 67-Kilodalton Peripheral Membrane Protein". In: *Biochemistry* 28.9 (1989), pp. 3716–3722.

[173]  T. J. Broekelmann, B. A. Kozel, et al. "Tropoelastin interacts with cell-surface gly-cosaminoglycans via its COOH-terminal domain". In: *J. Biol. Chem.* 280.49 (2005), pp. 40939–40947.

[174]  I. Mitsou, H. A. B. Multhaupt, and J. R. Couchman. "Proteoglycans, ion channels and cellfffdfffdfffdmatrix adhesion". In: *Biochem. J.* 474.12 (May 2017), 1965 LP –1979.

[175]  K. Akhtar, T. J. Broekelmann, et al. "Oxidative Modifications of the C-terminal Domain of Tropoelastin Prevent Cell Binding". In: *J. Biol. Chem.* 286.15 (Apr. 2011), pp. 13574–13582.

[176]  Y. Tu and A. S. Weiss. "Transient tropoelastin nanoparticles are early-stage intermediates in the coacervation of human tropoelastin whose aggregation is facilitated by heparan sulfate and heparin decasaccharides". In: *Matrix Biol.* 29.2 (Mar. 2010), pp. 152–159.

[177]  P. Lee, D. V. Bax, et al. "A Novel Cell Adhesion Region in Tropoelastin Mediates Attachment to Integrin $\alpha V \beta 5$". In: *J. Biol. Chem.* 289.3 (Jan. 2014), pp. 1467–1477.

[178]  Material Archiv. *Naturkautschuk.* http://www.materialarchiv.ch/app-tablet/#detail/7/naturkautschuk.

[179]  D. a. Shipp. "Reversible-Deactivation Radical Polymerizations". In: *Polym. Rev.* 51.2 (Apr. 2011), pp. 99–103.

[180]  A. D. Jenkins, R. G. Jones, and G. Moad. "Terminology for reversible-deactivation radical polymerization previously called "controlled" radical or "living" radical polymerization (IUPAC Recommendations 2010)". In: *Pure Appl. Chem.* 82.2 (2009).

[181]  K. Matyjaszewski and J. Spanswick. "Controlled/living radical polymerization". In: *Mater. Today* 8.3 (Mar. 2005), pp. 26–33.

[182]  M. K. Georges, R. P. Veregin, et al. "Narrow Molecular Weight Resins by a Free-Radical Polymerization Process". In: *Macromolecules* 26.11 (1993), pp. 2987–2988.

[183]  J. Nicolas, Y. Guillaneuf, et al. "Nitroxide-Mediated Polymerization". In: *Polym. Sci. A Compr. Ref.* Vol. 3. Elsevier, 2012, pp. 277–350.

[184]  M. Kato, M. Kamigaito, et al. "Polymerization of Methyl Methacrylate with the Carbon Tetrachloride/Dichlorotris-(triphenylphosphine)ruthenium(II)/ Methylaluminum Bis(2,6-di-tert-butylphenoxide) Initiating System: Possibility of Living Radical Polymerization". In: *Macromolecules* 28.5 (1995), pp. 1721–1723.

[185]  J. S. Wang and K. Matyjaszewski. "Controlled/'Living' Radical Polymerization. Atom Transfer Radical Polymerization in the Presence of Transition-Metal Complexes". In: *J. Am. Chem. Soc.* 117.20 (1995), pp. 5614–5615.

[186]  K. Matyjaszewski. "Atom Transfer Radical Polymerization (ATRP): Current status and future perspectives". In: *Macromolecules* 45.10 (2012), pp. 4015–4039.

[187]  E. Mastan, L. Xi, and S. Zhu. "What limits the chain growth from flat surfaces in surface-initiated ATRP: Propagation, termination or both?" In: *Macromol. Theory Simulations* 24.2 (2015), pp. 89–99.

[188]   K. Matyjaszewski, T. Pintauer, and S. Gaynor. "Removal of copper-based catalyst in atom transfer radical polymerization using ion exchange resins". In: *Macromolecules* 33.4 (2000), pp. 1476–1478.

[189]   B. D. Fairbanks, P. A. Gunatillake, and L. Meagher. "Biomedical applications of polymers derived by reversible addition - fragmentation chain-transfer (RAFT)". In: *Adv. Drug Deliv. Rev.* 91 (2015), pp. 141–152.

[190]   C. Guo and S. A. Morris. "Engineering cell identity: establishing new gene regulatory and chromatin landscapes". In: *Curr. Opin. Genet. Dev.* 46.16 (2017), pp. 50–57.

[191]   P. Corpart, D. Charmot, et al. *Method for block polymer synthesis by controlled radical polymerisation.* Nov. 2000.

[192]   G. Moad and C. Barner-Kowollik. "The Mechanism and Kinetics of the RAFT Process: Overview, Rates, Stabilities, Side Reactions, Product Spectrum and Outstanding Challenges". In: *Handb. RAFT Polym.* Weinheim, Germany: Wiley-VCH Verlag GmbH & Co. KGaA, 2008, pp. 51–104.

[193]   C. Barner-Kowollik. *Handbook of RAFT Polymerization.* Ed. by C. Barner-Kowollik. Weinheim, Germany: Wiley-VCH Verlag GmbH & Co. KGaA, Jan. 2008, pp. 1–543.

[194]   D.-C. T. Tischer. "Efficient Modular Surface Modification of Biopolymers via Thermal and Photochemical Ligation Techniques". PhD thesis. Karlsruhe Institute of Technology, 2014.

[195]   M. Destarac. "On the Critical Role of RAFT Agent Design in Reversible Addition-Fragmentation Chain Transfer (RAFT) Polymerization". In: *Polym. Rev.* 51.2 (2011), pp. 163–187.

[196]   B. Y. Chong, J. Krstina, et al. "Thiocarbonylthio compounds [S=C(Ph)S-R] in free radical polymerization with reversible addition-fragmentation chain transfer (RAFT polymerization). Role of the free-radical leaving group (R)". In: *Macromolecules* 36.7 (2003), pp. 2256–2272.

[197]   S. Atzet, S. Curtin, et al. "Degradable poly(2-hydroxyethyl methacrylate)-co-polycaprolactone hidrogels for tissue engineering scaffolds". In: *Biomacromolecules* 9.12 (2008), pp. 3370–3377.

[198]   D. Çetin, A. S. Kahraman, and M. Gümüsderelioglu. "Novel scaffolds based on poly(2-hydroxyethyl methacrylate) superporous hydrogels for bone tissue engineering". In: *J. Biomater. Sci. Polym. Ed.* 22.9 (2011), pp. 1157–1178.

[199]   J.-P. Montheard, M. Chatzopoulos, and D. Chappard. "2-Hydroxyethyl Methacrylate (HEMA): Chemical Properties and Applications in Biomedical Fields". In: *J. Macromol. Sci. Part C Polym. Rev.* 32.1 (1992), pp. 1–34.

[200]   E. De Giglio, D. Cafagna, et al. "PHEMA-based thin hydrogel films for biomedical applications". In: *J. Bioact. Compat. Polym.* 26.4 (July 2011), pp. 420–434.

[201]   S. Singh, Tiwari, et al. "A nonviral pHEMA+chitosan nanosphere-mediated high-efficiency gene delivery system". In: *Int. J. Nanomedicine* 8 (Apr. 2013), p. 1403.

[202] H. Fukazawa, S. Mizuno, and Y. Uehara. "A Microplate Assay for Quantitation of Anchorage-Independent Growth of Transformed Cells". In: *Anal. Biochem.* 228.1 (1995), pp. 83–90.

[203] C. Yoshikawa, S. Hattori, et al. "Non-biofouling property of well-defined concentrated poly(2-hydroxyethyl methacrylate) brush". In: *Mater. Lett.* 83 (2012), pp. 140–143.

[204] B. W. Hanak, C.-Y. Hsieh, et al. "Reduced cell attachment to poly(2-hydroxyethyl methacrylate)-coated ventricular catheters in vitro". In: *J. Biomed. Mater. Res. Part B Appl. Biomater.* 106.3 (Apr. 2018), pp. 1268–1279.

[205] A. Cretu, R. Gattin, et al. "Synthesis and degradation of poly (2-hydroxyethyl methacrylate)-graft-poly ($\epsilon$-caprolactone) copolymers". In: *Polym. Degrad. Stab.* 83.3 (Mar. 2004), pp. 399–404.

[206] O. Azzaroni and I. Szleifer. *Polymer and Biopolymer Brushes.* Hoboken, NJ, USA: John Wiley & Sons, Inc., Dec. 2017, pp. 3225–3258.

[207] W.-L. Chen, R. Cordero, et al. "Polymer Brushes: Novel Surfaces for Future Materials". In: *Macromolecules* 50.11 (June 2017), pp. 4089–4113.

[208] M. Krishnamoorthy, S. Hakobyan, et al. "Surface-Initiated Polymer Brushes in the Biomedical Field: Applications in Membrane Science, Biosensing, Cell Culture, Regenerative Medicine and Antibacterial Coatings". In: *Chem. Rev.* 114.21 (Nov. 2014), pp. 10976–11026.

[209] S. Hansson, V. Trouillet, et al. "Grafting Efficiency of Synthetic Polymers onto Biomaterials: A Comparative Study of Grafting- from versus Grafting- to". In: *Biomacromolecules* 14.1 (Jan. 2013), pp. 64–74.

[210] S. Minko. "Grafting on Solid Surfaces: 'Grafting to' and 'Grafting from' Methods". In: *Polym. Surfaces Interfaces.* Berlin, Heidelberg: Springer Berlin Heidelberg, 2008, pp. 215–234.

[211] T. Vladkova. *Surface Engineering of Polymeric Biomaterials.* Shawbury: Smithers Rapra Technology Ltd, 2013, p. 590.

[212] J. O. Zoppe, N. C. Ataman, et al. "Surface-Initiated Controlled Radical Polymerization: State-of-the-Art, Opportunities, and Challenges in Surface and Interface Engineering with Polymer Brushes". In: *Chem. Rev.* 117.3 (Feb. 2017), pp. 1105–1318.

[213] H. C. Kolb, M. G. Finn, and K. B. Sharpless. "Click Chemistry: Diverse Chemical Function from a Few Good Reactions". In: *Angew. Chemie Int. Ed.* 40.11 (June 2001), pp. 2004–2021.

[214] C. Barner-Kowollik, F. E. Du Prez, et al. "'Clicking' Polymers or Just Efficient Linking: What Is the Difference?" In: *Angew. Chemie Int. Ed.* 50.1 (Jan. 2011), pp. 60–62.

[215] C. M. Nimmo and M. S. Shoichet. "Regenerative Biomaterials that 'Click': Simple, Aqueous-Based Protocols for Hydrogel Synthesis, Surface Immobilization, and 3D Patterning". In: *Bioconjug. Chem.* 22.11 (Nov. 2011), pp. 2199–2209.

[216] L. Li and Z. Zhang. "Development and Applications of the Copper-Catalyzed Azide-Alkyne Cycloaddition (CuAAC) as a Bioorthogonal Reaction". In: *Molecules* 21.10 (Oct. 2016), p. 1393.

[217] R. J. Brea and N. K. Devaraj. "Diels-Alder and Inverse Diels-Alder Reactions". In: *Chemoselective Bioorthogonal Ligation React.* Weinheim, Germany: Wiley-VCH Verlag GmbH & Co. KGaA, Mar. 2017. Chap. 3, pp. 67–95.

[218] S. M. Brosnan and H. Schlaad. "Modification of polypeptide materials by Thiol-X chemistry". In: *Polym. (United Kingdom)* 55.22 (2014), pp. 5511–5516.

[219] B. Tieke. *Makromolekulare Chemie – Eine Einführung.* Vol. 78. Weinheim: Wiley-VCH, 2005, p. 391.

[220] S. V. Orski, R. J. Sheridan, et al. "Utilizing vapor swelling of surface-initiated polymer brushes to develop quantitative measurements of brush thermodynamics and grafting density". In: *Polymer (Guildf).* 72 (Aug. 2015), pp. 471–478.

[221] K. H. Vining and D. J. Mooney. "Mechanical forces direct stem cell behaviour in development and regeneration". In: *Nat. Rev. Mol. Cell Biol.* 18.12 (Nov. 2017), pp. 728–742.

[222] F. Han, C. Zhu, et al. "Cellular modulation by the elasticity of biomaterials". In: *J. Mater. Chem. B* 4.1 (2016), pp. 9–26.

[223] B. Trappmann and C. S. Chen. "How cells sense extracellular matrix stiffness: a material's perspective". In: *Curr. Opin. Biotechnol.* 24.5 (Oct. 2013), pp. 948–953.

[224] S. Nam, K. H. Hu, et al. "Strain-enhanced stress relaxation impacts nonlinear elasticity in collagen gels". In: *Proc. Natl. Acad. Sci.* 113.20 (May 2016), pp. 5492–5497.

[225] Y.-H. Kim, H. Furuya, and Y. Tabata. "Enhancement of bone regeneration by dual release of a macrophage recruitment agent and platelet-rich plasma from gelatin hydrogels". In: *Biomaterials* 35.1 (Jan. 2014), pp. 214–224.

[226] O. Chaudhuri, L. Gu, et al. "Hydrogels with tunable stress relaxation regulate stem cell fate and activity". In: *Nat. Mater.* 15.3 (Nov. 2015), pp. 326–334.

[227] S. Asano, S. Ito, et al. "Matrix stiffness regulates migration of human lung fibroblasts". In: *Physiol. Rep.* 5.9 (May 2017), e13281.

[228] Y. Liang, L. Li, et al. "Polymeric Biomaterials: Diverse Functions Enabled by Advances in Macromolecular Chemistry". In: *Macromolecules* 50.2 (Jan. 2017), pp. 483–502.

[229] N. J. Hogrebe, J. W. Reinhardt, et al. "Independent control of matrix adhesiveness and stiffness within a 3D self-assembling peptide hydrogel". In: *Acta Biomater.* 70 (Apr. 2018), pp. 110–119.

[230] M. D. Stevenson, H. Piristine, et al. "A self-assembling peptide matrix used to control stiffness and binding site density supports the formation of microvascular networks in three dimensions". In: *Acta Biomater.* 9.8 (2013), pp. 7651–7661.

[231] K. J. Lampe, A. L. Antaris, and S. C. Heilshorn. "Design of three-dimensional engineered protein hydrogels for tailored control of neurite growth". In: *Acta Biomater.* 9.3 (Mar. 2013), pp. 5590–5599.

[232] Y.-N. Zhang, R. K. Avery, et al. "A Highly Elastic and Rapidly Crosslinkable Elastin-Like Polypeptide-Based Hydrogel for Biomedical Applications". In: *Adv. Funct. Mater.* 25.30 (Aug. 2015), pp. 4814–4826.

[233] I. Wong and C.-M. Ho. "Surface molecular property modifications for poly(dimethylsiloxane) (PDMS) based microfluidic devices". In: *Microfluid. Nanofluidics* 7.3 (Sept. 2009), pp. 291–306.

[234] J. D. Wang, N. J. Douville, et al. "Quantitative Analysis of Molecular Absorption into PDMS Microfluidic Channels". In: *Ann. Biomed. Eng.* 40.9 (Sept. 2012), pp. 1862–1873.

[235] S. Halldorsson, E. Lucumi, et al. "Advantages and challenges of microfluidic cell culture in polydimethylsiloxane devices". In: *Biosens. Bioelectron.* 63 (Jan. 2015), pp. 218–231.

[236] J. Fu, Y.-K. Wang, et al. "Mechanical regulation of cell function with geometrically modulated elastomeric substrates". In: *Nat. Methods* 7.9 (Sept. 2010), pp. 733–736.

[237] S. J. Han, K. S. Bielawski, et al. "Decoupling Substrate Stiffness, Spread Area, and Micropost Density: A Close Spatial Relationship between Traction Forces and Focal Adhesions". In: *Biophys. J.* 103.4 (Aug. 2012), pp. 640–648.

[238] A. Haider, S. Haider, and I.-K. Kang. "A comprehensive review summarizing the effect of electrospinning parameters and potential applications of nanofibers in biomedical and biotechnology". In: *Arab. J. Chem.* (Dec. 2015).

[239] J. Nam, J. Johnson, et al. "Modulation of embryonic mesenchymal progenitor cell differentiation via control over pure mechanical modulus in electrospun nanofibers". In: *Acta Biomater.* 7.4 (Apr. 2011), pp. 1516–1524.

[240] K. Wingate, W. Bonani, et al. "Compressive elasticity of three-dimensional nanofiber matrix directs mesenchymal stem cell differentiation to vascular cells with endothelial or smooth muscle cell markers". In: *Acta Biomater.* 8.4 (Apr. 2012), pp. 1440–1449.

[241] J. Rnjak-Kovacina, S. G. Wise, et al. "Electrospun synthetic human elastin:collagen composite scaffolds for dermal tissue engineering". In: *Acta Biomater.* 8.10 (Oct. 2012), pp. 3714–3722.

[242] T. Boudou, T. Crouzier, et al. "Polyelectrolyte Multilayer Nanofilms Used as Thin Materials for Cell Mechano-Sensitivity Studies". In: *Macromol. Biosci.* 11.1 (Jan. 2011), pp. 77–89.

[243] N. Saha, C. Monge, et al. "Photocrosslinked Polyelectrolyte Films of Controlled Stiffness to Direct Cell Behavior". In: *Layer-by-Layer Film. Biomed. Appl.* Weinheim, Germany: Wiley-VCH Verlag GmbH & Co. KGaA, Jan. 2015, pp. 45–64.

[244] I. Lilge and H. Schönherr. "Covalently cross-linked poly(acrylamide) brushes on gold with tunable mechanical properties via surface-initiated atom transfer radical polymerization". In: *Eur. Polym. J.* Vol. 49. 8. 2013, pp. 1943–1951.

[245]  I. Lilge and H. Schönherr. "Block Copolymer Brushes for Completely Decoupled Control of Determinants of Cell–Surface Interactions". In: *Angew. Chemie - Int. Ed.* 55.42 (Oct. 2016), pp. 13114–13117.

[246]  Y. Mei, T. Wu, et al. "Tuning Cell Adhesion on Gradient Poly(2-hydroxyethyl methacrylate)-Grafted Surfaces". In: *Langmuir* 21.26 (Dec. 2005), pp. 12309–12314.

[247]  Y. Arisaka, Y. Nishijima, et al. "Photo-induced in situ crosslinking of polymer brushes with dimethyl maleimide moieties for dynamically stimulating stem cell differentiation". In: *J. Biomater. Sci. Polym. Ed.* 27.13 (Sept. 2016), pp. 1331–1340.

[248]  X. Sui, A. Di Luca, et al. "Stability and cell adhesion properties of poly(N-isopropylacrylamide) brushes with variable grafting densities". In: *Aust. J. Chem.* Vol. 64. 9. 2011, pp. 1259–1266.

[249]  J. Zhang. *Switchable and Responsive Surfaces and Materials for Biomedical Applications.* Elsevier, 2015, pp. 1–306.

[250]  S. J. Attwood, E. Cortes, et al. "Adhesive ligand tether length affects the size and length of focal adhesions and influences cell spreading and attachment". In: *Sci. Rep.* 6.1 (Dec. 2016), p. 34334.

[251]  S. Duncan and A. Weiland. "Minimally invasive reduction and osteosynthesis of articular fractures of the distal radius". In: *Injury* 31 (May 2000), pp. 14–24.

[252]  A. S. Wineman and K. R. Rajagopal. *Mechanical Response of Polymers: An Introduction.* Cambridge: Cambridge University Press, 2000, p. 317.

[253]  W. J. Polacheck and C. S. Chen. "Measuring cell-generated forces: a guide to the available tools". In: *Nat. Methods* 13.5 (May 2016), pp. 415–423.

[254]  M. L. Oyen. "Mechanical characterisation of hydrogel materials". In: *Int. Mater. Rev.* 59.1 (Jan. 2014), pp. 44–59.

[255]  H. Hertz. "Über die Berührung fester elastischer Körper." In: *J. für die reine und Angew. Math. (Crelle's Journal)* 1882.92 (1882), pp. 156–171.

[256]  K. L. Johnson, K. Kendall, and A. D. Roberts. "Surface Energy and the Contact of Elastic Solids". In: *Proc. R. Soc. A Math. Phys. Eng. Sci.* 324.1558 (Sept. 1971), pp. 301–313.

[257]  Y. Shan and H. Wang. "The structure and function of cell membranes examined by atomic force microscopy and single-molecule force spectroscopy". In: *Chem. Soc. Rev.* 44.11 (2015), pp. 3617–3638.

[258]  G. Binnig, C. F. Quate, and C. Gerber. "Atomic Force Microscope". In: *Phys. Rev. Lett.* 56.9 (Mar. 1986), pp. 930–933.

[259]  K. Haase and A. E. Pelling. "Investigating cell mechanics with atomic force microscopy". In: *J. R. Soc. Interface* 12.104 (Jan. 2015), pp. 20140970–20140970.

[260]  N. Pavliček and L. Gross. "Generation, manipulation and characterization of molecules by atomic force microscopy". In: *Nat. Rev. Chem.* 1.1 (Jan. 2017), p. 0005.

[261]  J. Hutter and J. Bechhoefer. "Calibration of atomic force microscope tips". In: *Rev. Sci. Instrum.* 64.7 (1993), p. 1868.

[262]  J. E. Sader, J. A. Sanelli, et al. "Spring constant calibration of atomic force microscope cantilevers of arbitrary shape". In: *Rev. Sci. Instrum.* 83.10 (2012), p. 103705.

[263]  D. Wang and T. P. Russell. "Advances in Atomic Force Microscopy for Probing Polymer Structure and Properties". In: *Macromolecules* 51.1 (Jan. 2018), pp. 3–24.

[264]  F. Variola. "Atomic force microscopy in biomaterials surface science". In: *Phys. Chem. Chem. Phys.* 17.5 (2015), pp. 2950–2959.

[265]  M. T. Woodside and S. M. Block. "Reconstructing Folding Energy Landscapes by Single-Molecule Force Spectroscopy". In: *Annu. Rev. Biophys.* 43.1 (May 2014), pp. 19–39.

[266]  W. Ott, M. A. Jobst, et al. "Single-molecule force spectroscopy on polyproteins and receptor-ligand complexes: The current toolbox". In: *J. Struct. Biol.* 197.1 (Jan. 2017), pp. 3–12.

[267]  P. Das and M. Reches. "Review insights into the interactions of amino acids and peptides with inorganic materials using single molecule force spectroscopy". In: *Biopolymers* 104.5 (Sept. 2015), pp. 480–494.

[268]  N. Liu and W. Zhang. "Feeling inter- or intramolecular interactions with the polymer chain as probe: Recent progress in SMFS studies on macromolecular interactions". In: *ChemPhysChem* 13.9 (2012), pp. 2238–2256.

[269]  Y. F. Dufrêne, E. Evans, et al. "Five challenges to bringing single-molecule force spectroscopy into living cells". In: *Nat. Methods* 8.2 (Feb. 2011), pp. 123–127.

[270]  M. J. Jacobs and K. Blank. "Joining forces: integrating the mechanical and optical single molecule toolkits". In: *Chem. Sci.* 5.5 (2014), pp. 1680–1697.

[271]  M. J. Siedlik, V. D. Varner, and C. M. Nelson. "Pushing, pulling, and squeezing our way to understanding mechanotransduction". In: *Methods* 94 (Feb. 2016), pp. 4–12.

[272]  K. C. Neuman and A. Nagy. "Single-molecule force spectroscopy: optical tweezers, magnetic tweezers and atomic force microscopy". In: *Nat. Methods* 5.6 (June 2008), pp. 491–505.

[273]  A.-L. Cost, P. Ringer, et al. "How to Measure Molecular Forces in Cells: A Guide to Evaluating Genetically-Encoded FRET-Based Tension Sensors". In: *Cell. Mol. Bioeng.* 8.1 (Mar. 2015), pp. 96–105.

[274]  B. Cheng and S. Cui. "Supramolecular Chemistry and Mechanochemistry of Macromolecules: Recent Advances by Single-Molecule Force Spectroscopy". In: *Top. Curr. Chem.* Ed. by R. Boulatov. Vol. 369. April. Cham: Springer International Publishing, 2015, pp. 97–134.

[275]  H. Li and Y. Cao. "Protein Mechanics: From Single Molecules to Functional Biomaterials". In: *Acc. Chem. Res.* 43.10 (Oct. 2010), pp. 1331–1341.

[276] B. Zhang, R. Shi, et al. "Direct comparison between chemisorption and physisorption: a study of poly(ethylene glycol) by means of single-molecule force spectroscopy". In: *RSC Adv.* 7.54 (2017), pp. 33883–33889.

[277] M. Rief, M. Gautel, et al. "The mechanical stability of immunoglobulin and fibronectin III domains in the muscle protein titin measured by atomic force microscopy". In: *Biophys. J.* 75.6 (1998), pp. 3008–3014.

[278] T. Tischer, R. Gralla-Koser, et al. "Direct Mapping of RAFT Controlled Macromolecular Growth on Surfaces via Single Molecule Force Spectroscopy". In: *ACS Macro Lett.* 5.4 (Apr. 2016), pp. 498–503.

[279] A. V. Taubenberger, D. W. Hutmacher, and D. J. Muller. "Single-Cell Force Spectroscopy, an Emerging Tool to Quantify Cell Adhesion to Biomaterials". In: *Tissue Eng. Part B Rev.* 20.1 (Feb. 2014), pp. 40–55.

[280] W. Kuhn and F. Grün. "Beziehungen zwischen elastischen Konstanten und Dehnungs-doppelbrechung hochelastischer Stoffe". In: *Kolloid-Zeitschrift* 101.3 (Dec. 1942), pp. 248–271.

[281] W. Kuhn and H. Kuhn. "Statistische und energieelastische Rückstellkraft bei stark auf Dehnung beanspruchten Fadenmolekülen". In: *Helv. Chim. Acta* 29.5 (1946), pp. 1095–1115.

[282] A. Janshoff, M. Neitzert, et al. "Force Spectroscopy of Molecular Systems – Single Molecule Spectroscopy of Polymers and Biomolecules". In: *Angew. Chemie* 39.18 (Sept. 2000), pp. 3212–3237.

[283] C. Ortiz. *A Review of Elasticity Models for Extension of Single Polymer Chains.* http://web.mit.edu/cortiz/www/3.052/3.052CourseReader/31_dcf_SMFSModels2.pdf. Boston, 2016.

[284] S. B. Smith, Y. Cui, and C. Bustamante. "Overstretching B-DNA: The Elastic Response of Individual Double-Stranded and Single-Stranded DNA Molecules". In: *Science (80-. ).* 271.5250 (Feb. 1996), pp. 795–799.

[285] O. Kratky and G. Porod. "Röntgenuntersuchung gelöster Fadenmoleküle". In: *Recl. des Trav. Chim. des Pays-Bas* 68.12 (Sept. 1949), pp. 1106–1122.

[286] J. Brandrup, E. Immergut, and E. Grulke. *Kuhn and Persistence Length of Polymers.* 2015.

[287] J. F. Marko and E. D. Siggia. "Stretching DNA". In: *Macromolecules* 28.26 (Dec. 1995), pp. 8759–8770.

[288] C. Bouchiat, M. M. D. Wang, et al. "Estimating the Persistence Length of a Worm-Like Chain Molecule from Force-Extension Measurements". In: *Biophys. J.* 76.1 Pt 1 (1999), pp. 409–413.

[289] M. D. Wang, H. Yin, et al. "Stretching DNA with optical tweezers". In: *Biophys. J.* 72.3 (1997), pp. 1335–1346.

[290] J. Howard. *Mechanics of motor proteins and the cytoskeleton.* Sunderland (MA): Sinauer Associates, 2001, p. 367.

[291] H. P. Koeffler, R. Billing, et al. "An undifferentiated variant derived from the human acute myelogenous leukemia cell line (KG-1)." In: *Blood* 56.2 (Aug. 1980), pp. 265–73.

[292] Z. Wu, B. Markovic, et al. "Characterization of IgG Fc receptors on CD34 antigen- expressing cell lines ( KG-1 and KG-la )". In: *Immunol. Cell Biol.* 141.1 (Feb. 1996), pp. 57–64.

[293] W. Holloway, A. R. Martinez, et al. "Key adhesion molecules are present on long podia extended by hematopoietic cells". In: *Cytometry* 37.3 (1999), pp. 171–177.

[294] J. M. Goffin, P. Pittet, et al. "Focal adhesion size controls tension-dependent recruitment of $\alpha$-smooth muscle actin to stress fibers". In: *J. Cell Biol.* 172.2 (Jan. 2006), pp. 259–268.

[295] J. Schindelin, C. T. Rueden, et al. "The ImageJ ecosystem: An open platform for biomedical image analysis". In: *Mol. Reprod. Dev.* 82.7-8 (July 2015), pp. 518–529.

[296] I. Arganda-Carreras, R. Fernández-González, et al. "3D reconstruction of histological sections: Application to mammary gland tissue". In: *Microsc. Res. Tech.* 73.11 (Oct. 2010), pp. 1019–1029.

[297] H. Z. Sailem, J. E. Sero, and C. Bakal. "Visualizing cellular imaging data using PhenoPlot". In: *Nat. Commun.* 6 (2015), p. 5825.

[298] M. Zamfir, C. Rodriguez-Emmenegger, et al. "Controlled growth of protein resistant PHEMA brushes via S-RAFT polymerization". In: *J. Mater. Chem. B* 1.44 (2013), pp. 6027–6034.

[299] K. L. Parry, A. G. Shard, et al. *ARXPS characterisation of plasma polymerised surface chemical gradients.* Nov. 2006.

[300] J. H. Scofield. "Hartree-Slater subshell photoionization cross-sections at 1254 and 1487 eV". In: *J. Electron Spectros. Relat. Phenomena* 8.2 (Jan. 1976), pp. 129–137.

[301] S. Tanuma, C. J. Powell, and D. R. Penn. "Calculations of electron inelastic mean free paths. VIII. Data for 15 elemental solids over the 50-2000 eV range". In: *Surf. Interface Anal.* 37.1 (2005), pp. 1–14.

[302] M. Stickler, D. Panke, and W. Wunderlich. "Solution properties of poly(methyl methacrylate) in methyl methacrylate, 1 Viscosities from the dilute to the concentrated solution regime". In: *Makromol. Chemie* 188.11 (Nov. 1987), pp. 2651–2664.

[303] G. F. Pauli, S.-N. Chen, et al. "Importance of Purity Evaluation and the Potential of Quantitative 1 H NMR as a Purity Assay". In: *J. Med. Chem.* 57.22 (Nov. 2014), pp. 9220–9231.

[304] C. M. Herzinger, B. Johs, et al. "Ellipsometric determination of optical constants for silicon and thermally grown silicon dioxide via a multi-sample, multi-wavelength, multi-angle investigation". In: *J. Appl. Phys.* 83.6 (1998), pp. 3323–3336.

[305] A. Pasqualato, V. Lei, et al. "Shape in migration: Quantitative image analysis of migrating chemoresistant HCT-8 colon cancer cells". In: *Cell Adhes. Migr.* 7.5 (2013), pp. 450–459.

[306] R. G. Thakar, M. G. Chown, et al. "Contractility-dependent modulation of cell proliferation and adhesion by microscale topographical cues". In: *Small* 4.9 (2008), pp. 1416–1424.

[307] W. Hornebeck, J. M. Tixier, and L. Robert. "Inducible adhesion of mesenchymal cells to elastic fibers: elastonectin." In: *Proc. Natl. Acad. Sci. U. S. A.* 83.15 (1986), pp. 5517–5520.

[308] Y. Yu, S. G. Wise, et al. "Characterization of endothelial progenitor cell interactions with human tropoelastin". In: *PLoS One* 10.6 (2015).

[309] M. B. Nguyen. "Adhäsion von hämatopoetischen Stammzellen an Tropoelastin". Bachelor thesis. Karlsruher Institut für Technologie, Karlsruhe, 2015, pp. 1–50.

[310] M. Carrion-Vazquez, P. E. Marszalek, et al. "Atomic force microscopy captures length phenotypes in single proteins." In: *Proc. Natl. Acad. Sci. U. S. A*. 96.September (1999), pp. 11288–11292.

[311] P. Gutjahr, R. Lipowsky, and J. Kierfeld. "Persistence length of semiflexible polymers and bending rigidity renormalization". In: *Europhys. Lett.* 76.6 (Dec. 2006), pp. 994–1000.

[312] R. Boulatov. *Polymer Mechanochemistry.* Ed. by R. Boulatov. Vol. 369. Topics in Current Chemistry. Cham: Springer International Publishing, 2015, p. 429.

[313] D. T. Cheung and M. E. Nimni. "Mechanism of crosslinking of proteins by glutaraldehyde II. Reaction with monomeric and polymeric collagen". In: *Connect. Tissue Res.* 10.2 (1982), pp. 201–216.

[314] C. Zhao, L. Li, et al. "Effect of Film Thickness on the Antifouling Performance of Poly(hydroxy-functional methacrylates) Grafted Surfaces". In: *Langmuir* 27.8 (Apr. 2011), pp. 4906–4913.

[315] D. P. Nair, M. Podgórski, et al. "The Thiol-Michael addition click reaction: A powerful and widely used tool in materials chemistry". In: *Chem. Mater.* 26.1 (2014), pp. 724–744.

[316] A. S. Goldmann, T. Tischer, et al. "Mild and Modular Surface Modification of Cellulose via Hetero Diels-Alder (HDA) Cycloaddition". In: *Biomacromolecules* 12.4 (Apr. 2011), pp. 1137–1145.

[317] J. S. Stevens and S. L. M. Schroeder. "Quantitative analysis of saccharides by X-ray photoelectron spectroscopy". In: *Surf. Interface Anal.* 41.6 (2009), pp. 453–462.

[318] E. Jagst. "Surface Functional Group Characterization Using Chemical Derivatization X-ray Photoelectron Spectroscopy (CD-XPS)". PhD thesis. Berlin: Freie Universität Berlin, 2010, p. 129.

[319] M. P. Seah and W. A. Dench. "Quantitative electron spectroscopy of surfaces: A standard data base for electron inelastic mean free paths in solids". In: *Surf. Interface Anal.* 1.1 (Feb. 1979), pp. 2–11.

[320] K. P. Fears, D. Y. Petrovykh, and T. D. Clark. "Evaluating protocols and analytical methods for peptide adsorption experiments". In: *Biointerphases* 8.1 (Dec. 2013), p. 20.

[321] A.-L. Winkler, M. Koenig, et al. "Bioinstructive Coatings for Hematopoietic Stem Cell Expansion Based on Chemical Vapor Deposition Copolymerization". In: *Biomacromolecules* 18.10 (Oct. 2017), pp. 3089–3098.

[322] R. Michel and D. G. Castner. "Advances in time-of-flight secondary ion mass spectrometry analysis of protein films". In: *Surf. Interface Anal.* 38.11 (Nov. 2006), pp. 1386–1392.

[323] M. S. Wagner and D. G. Castner. "Characterization of Adsorbed Protein Films by Time-of-Flight Secondary Ion Mass Spectrometry with Principal Component Analysis". In: *Langmuir* 17.15 (July 2001), pp. 4649–4660.

[324] J.-B. Lhoest, M. S. Wagner, et al. "Characterization of adsorbed protein films by time of flight secondary ion mass spectrometry". In: *J. Biomed. Mater. Res.* 57.3 (Dec. 2001), pp. 432–440.

[325] C. A. Muth, C. Steinl, et al. "Regulation of Hematopoietic Stem Cell Behavior by the Nanostructured Presentation of Extracellular Matrix Components". In: *PLoS One* 8.2 (Jan. 2013), e54778.

[326] J. Rühe. *Polymer Brushes: Synthesis, Characterization, Applications.* Ed. by R. C. Advincula, W. J. Brittain, et al. Weinheim, FRG: Wiley-VCH Verlag GmbH & Co. KGaA, July 2004, pp. 1–483.

[327] D. Zhou, E. Mastan, and S. Zhu. "Termination of Surface Radicals and Kinetic Analysis of Surface-Initiated RAFT Polymerization on Flat Surfaces". In: *Macromol. Theory Simulations* 21.9 (Nov. 2012), pp. 602–614.

[328] J. Brandrup, E. Immergut, and E. A. Grulke. "Polymer handbook". In: *John Wiley Sons, Inc* 12.3 (1990), p. 265.

[329] S. Gabriel, R. Je, et al. "First insights into electrografted polymers by AFM-based force spectroscopy". In: *Macromolecules* 39.24 (2006), pp. 8428–8433.

[330] S. Desseaux, J. P. Hinestrosa, et al. "Swelling Behavior and Nanomechanical Properties of (Peptide-Modified) Poly(2-hydroxyethyl methacrylate) and Poly(poly(ethylene glycol) methacrylate) Brushes". In: *Macromolecules* 49.12 (June 2016), pp. 4609–4618.

[331] Y. Tsujii, K. Ohno, et al. "Structure and Properties of High-Density Polymer Brushes Prepared by Surface-Initiated Living Radical Polymerization". In: *Surface-Initiated Polym. I.* Berlin, Heidelberg: Springer-Verlag, Jan. 2006, pp. 1–45.

[332] P. G. de Gennes. "Conformations of Polymers Attached to an Interface". In: *Macromolecules* 13.5 (1980), pp. 1069–1075.

[333] H.-J. Butt, M. Kappl, et al. "Steric Forces Measured with the Atomic Force Microscope at Various Temperatures". In: *Langmuir* 15.7 (Oct. 1999), pp. 2559–2565.

[334] S. Yamamoto, M. Ejaz, et al. "Surface interaction forces of well-defined, high-density polymer brushes studied by atomic force microscopy. 2. Effect of graft density". In: *Macromolecules* 33.15 (2000), pp. 5608–5612.

[335]  S. M. Balko, T. Kreer, et al. "Polymer Brushes under High Load". In: *PLoS One* 8.3 (2013).

[336]  D. Romeis and M. Lang. "Excluded volume effects in polymer brushes at moderate chain stretching". In: *J. Chem. Phys.* 141.10 (Sept. 2014), p. 104902.

[337]  C. Chen, P. Tang, et al. "Excluded volume effects in compressed polymer brushes: A density functional theory". In: *J. Chem. Phys.* 142.12 (Mar. 2015), p. 124904.

[338]  C. Liu, Z. Jiang, et al. "Intercalation interactions between dsDNA and acridine studied by single molecule force spectroscopy". In: *Langmuir* 23.18 (2007), pp. 9140–9142.

[339]  K. A. Melzak, K. Yu, et al. "Chain Length and Grafting Density Dependent Enhancement in the Hydrolysis of Ester-Linked Polymer Brushes". In: *Langmuir* 31.23 (2015), pp. 6463–6470.

[340]  C. Kang, R. Crockett, and N. D. Spencer. "The influence of surface grafting on the growth rate of polymer chains". In: *Polym. Chem.* 7.2 (2016), pp. 302–309.

[341]  H. B. Bohidar. *Fundamentals of Polymer Physics and Molecular Biophysics*. Cambridge: Cambridge University Press, 2014, pp. 1–321.

[342]  D. Zhang and C. Ortiz. "Synthesis and Single Molecule Force Spectroscopy of Graft Copolymers of Poly(2-hydroxyethyl methacrylate- g -ethylene glycol)". In: *Macromolecules* 37.11 (June 2004), pp. 4271–4282.

[343]  S. Koltzenburg, M. Maskos, and O. Nuyken. *Polymere: Synthese, Eigenschaften und Anwendungen*. Berlin, Heidelberg: Springer Berlin Heidelberg, 2014.

[344]  J. Moehrke and P. Vana. "Termination kinetics of surface-initiated radical polymerization measured by time-resolved ESR spectroscopy after laser-pulse initiation". In: *Macromolecules* 48.10 (2015), pp. 3190–3196.

[345]  Y.-R. Kim, H.-j. Paik, et al. "Real-Time Analysis of Enzymatic Surface-Initiated Polymerization Using Surface Plasmon Resonance (SPR)". In: *Macromol. Biosci.* 6.2 (Feb. 2006), pp. 145–152.

[346]  L. Carlsson, S. Utsel, et al. "Surface-initiated ring-opening polymerization from cellulose model surfaces monitored by a Quartz Crystal Microbalance". In: *Soft Matter* 8.2 (2012), pp. 512–517.

[347]  M. Barsbay, O. Güven, et al. "Verification of Controlled Grafting of Styrene from Cellulose via Radiation-Induced RAFT Polymerization". In: *Macromolecules* 40.20 (Oct. 2007), pp. 7140–7147.

[348]  J. Pyun, S. Jia, et al. "Synthesis and Characterization of Organic/Inorganic Hybrid Nanoparticles: Kinetics of Surface-Initiated Atom Transfer Radical Polymerization and Morphology of Hybrid Nanoparticle Ultrathin Films". In: *Macromolecules* 36.14 (July 2003), pp. 5094–5104.

[349]  C. Barner-Kowollik, J. F. Quinn, et al. "Kinetic investigations of reversible addition fragmentation chain transfer polymerizations: Cumyl phenyldithioacetate mediated homopolymerizations of styrene and methyl methacrylate". In: *Macromolecules* 34.22 (2001), pp. 7849–7857.

[350]  S. Al-Maawali, J. E. Bemis, et al. "Study of the Polydispersity of Grafted Poly(dimethylsiloxane) Surfaces Using Single-Molecule Atomic Force Microscopy fffdfffdfffd". In: *J. Phys. Chem. B* 105.18 (May 2001), pp. 3965–3971.

[351]  D. Goodman, J. N. Kizhakkedathu, and D. E. Brooks. "Molecular weight and polydispersity estimation of adsorbing polymer brushes by atomic force microscopy." In: *Langmuir* 20.8 (2004), pp. 3297–3303.

[352]  A. Zareidoost, M. Yousefpour, et al. "The relationship of surface roughness and cell response of chemical surface modification of titanium". In: *J. Mater. Sci. Mater. Med.* 23.6 (2012).

[353]  E. A. Cavalcanti-Adam, T. Volberg, et al. "Cell Spreading and Focal Adhesion Dynamics Are Regulated by Spacing of Integrin Ligands". In: *Biophys. J.* 92.8 (2007), pp. 2964–2974.

[354]  R. Pankov. "Fibronectin at a glance". In: *J. Cell Sci.* 115.20 (Oct. 2002), pp. 3861–3863.

[355]  J. Barisci, D. Hughes, et al. "Characterisation and analytical use of a polypyrrole electrode containing anti-human serum albumin". In: *Anal. Chim. Acta* 371.1 (Sept. 1998), pp. 39–48.

[356]  P. Hersen and B. Ladoux. "Biophysics: Push it, pull it." In: *Nature* 470.7334 (2011), pp. 340–341.

[357]  H. Delanoë-Ayari, J. P. Rieu, and M. Sano. "4D Traction Force Microscopy Reveals Asymmetric Cortical Forces in Migrating Dictyostelium Cells". In: *Phys. Rev. Lett.* 105.24 (Dec. 2010), p. 248103.

[358]  I. Platzman, K. M. Gadomska, et al. "Soft/Elastic Nanopatterned Biointerfaces in the Service of Cell Biology". In: *Methods Cell Biol.* 1st ed. Vol. 119. Heidelberg: Elsevier Inc., 2014. Chap. 13, pp. 237–260.

[359]  D. Aubry, M. Gupta, et al. "Mechanical link between durotaxis, cell polarity and anisotropy during cell migration". In: *Phys. Biol.* 12.2 (Apr. 2015), p. 026008.

[360]  H. El-Mohri, Y. Wu, et al. "Impact of matrix stiffness on fibroblast function". In: *Mater. Sci. Eng. C* 74 (May 2017), pp. 146–151.

[361]  J. Y. Park, S. J. Yoo, et al. "Increased poly(dimethylsiloxane) stiffness improves viability and morphology of mouse fibroblast cells". In: *BioChip J.* 4.3 (Sept. 2010), pp. 230–236.

[362]  J. Solon, I. Levental, et al. "Fibroblast Adaptation and Stiffness Matching to Soft Elastic Substrates". In: *Biophys. J.* 93.12 (Dec. 2007), pp. 4453–4461.

[363]  P. C. Georges. "Cell type-specific response to growth on soft materials". In: *J. Appl. Physiol.* 98.4 (Apr. 2005), pp. 1547–1553.

[364] K. A. Jansen, R. G. Bacabac, et al. "Cells Actively Stiffen Fibrin Networks by Generating Contractile Stress". In: *Biophys. J.* 105.10 (Nov. 2013), pp. 2240–2251.

[365] D. J. Tschumperlin. "Fibroblasts and the Ground They Walk On". In: *Physiology* 28.6 (Nov. 2013), pp. 380–390.

[366] J. Y. Bertrand, N. C. Chi, et al. "Haematopoietic stem cells derive directly from aortic endothelium during development". In: *Nature* 464.7285 (2010), pp. 108–111.

[367] A. Raic, L. Rödling, et al. "Biomimetic macroporous PEG hydrogels as 3D scaffolds for the multiplication of human hematopoietic stem and progenitor cells". In: *Biomaterials* 35.3 (Jan. 2014), pp. 929–940.

[368] S. Lavenus, P. Pilet, et al. "Behaviour of mesenchymal stem cells, fibroblasts and osteoblasts on smooth surfaces". In: *Acta Biomater.* 7.4 (Apr. 2011), pp. 1525–1534.

[369] F. D. Liu, N. Pishesha, et al. "Material Viscoelastic Properties Modulate the Mesenchymal Stem Cell Secretome for Applications in Hematopoietic Recovery". In: *ACS Biomater. Sci. Eng.* 3.12 (Dec. 2017), pp. 3292–3306.

[370] C. Parekh and G. M. Crooks. *Critical differences in hematopoiesis and lymphoid development between humans and mice.* 2013.

[371] M. D. Pierschbacher and E. Ruoslahti. "Variants of the cell recognition site of fibronectin that retain attachment-promoting activity." In: *Proc. Natl. Acad. Sci.* 81.19 (Oct. 1984), pp. 5985–5988.

[372] E. F. Plow, T. A. Haas, et al. "Ligand Binding to Integrins". In: *J. Biol. Chem.* 275.29 (July 2000), pp. 21785–21788.

[373] S. L. Bellis. "Advantages of RGD peptides for directing cell association with biomaterials". In: *Biomaterials* 32.18 (June 2011), pp. 4205–4210.

[374] C. Lee-thedieck and J. P. Spatz. "Supporting-Artificial Niches : Biomimetic Materials for Hematopoietic Stem Cell Culture". In: *Macromol. Rapid Commun.* 33 (2012), pp. 1–7.

[375] A.-L. Winkler, J. von Wulffen, et al. "Significance of Nanopatterned and Clustered DLL1 for Hematopoietic Stem Cell Proliferation". In: *Adv. Funct. Mater.* 27.21 (June 2017), p. 1606495.

[376] A. Saez, A. Buguin, et al. "Is the mechanical activity of epithelial cells controlled by deformations or forces?" In: *Biophys. J.* 89.6 (2005), pp. 52–54.

[377] M. Murrell, R. Kamm, and P. Matsudaira. "Substrate Viscosity Enhances Correlation in Epithelial Sheet Movement". In: *Biophys. J.* 101.2 (July 2011), pp. 297–306.

[378] S. V. Plotnikov, A. M. Pasapera, et al. "Force Fluctuations within Focal Adhesions Mediate ECM-Rigidity Sensing to Guide Directed Cell Migration". In: *Cell* 151.7 (Dec. 2012), pp. 1513–1527.

[379] B. L. Bangasser, S. S. Rosenfeld, and D. J. Odde. "Determinants of Maximal Force Transmission in a Motor-Clutch Model of Cell Traction in a Compliant Microenvironment". In: *Biophys. J.* 105.3 (Aug. 2013), pp. 581–592.

[380] T. Visart. *Hydrogels: Structure and Tribological properties.* http://cpmct.ulb.ac.be/cpmct_research.php?project=hydrogels#.Wn1wTSXOVhE.

[381] M. Goktas and K. G. Blank. "Molecular Force Sensors: From Fundamental Concepts toward Applications in Cell Biology". In: *Adv. Mater. Interfaces* 4.1 (Jan. 2017), p. 1600441.

[382] I. Schoen, B. L. Pruitt, and V. Vogel. "The Yin-Yang of Rigidity Sensing: How Forces and Mechanical Properties Regulate the Cellular Response to Materials". In: *Annu. Rev. Mater. Res.* 43.1 (July 2013), pp. 589–618.

[383] Y. Yang, K. Wang, et al. "Biophysical Regulation of Cell BehaviorfffdfffdfffdCross Talk between Substrate Stiffness and Nanotopography". In: *Engineering* 3.1 (Feb. 2017), pp. 36–54.

[384] T. Razafiarison, C. N. Holenstein, et al. "Biomaterial surface energy-driven ligand assembly strongly regulates stem cell mechanosensitivity and fate on very soft substrates". In: *Proc. Natl. Acad. Sci.* 115.18 (Apr. 2018), p. 201704543.

[385] E. Hadjipanayi, V. Mudera, and R. A. Brown. "Close dependence of fibroblast proliferation on collagen scaffold matrix stiffness". In: *J. Tissue Eng. Regen. Med.* 3.2 (Feb. 2009), pp. 77–84.

[386] A. K. Jha, X. Xu, et al. "Controlling the adhesion and differentiation of mesenchymal stem cells using hyaluronic acid-based, doubly crosslinked networks". In: *Biomaterials* 32.10 (2011), pp. 2466–2478.

[387] I. Patla, T. Volberg, et al. "Dissecting the molecular architecture of integrin adhesion sites by cryo-electron tomography". In: *Nat. Cell Biol.* 12.9 (2010), pp. 909–915.

[388] H. Kang, D. S. H. Wong, et al. "Remote Control of Multimodal Nanoscale Ligand Oscillations Regulates Stem Cell Adhesion and Differentiation". In: *ACS Nano* 11.10 (Oct. 2017), pp. 9636–9649.

[389] D. S. H. Wong, J. Li, et al. "Magnetically Tuning Tether Mobility of Integrin Ligand Regulates Adhesion, Spreading, and Differentiation of Stem Cells". In: *Nano Lett.* 17.3 (Mar. 2017), pp. 1685–1695.

[390] M. J. Wilson, S. J. Liliensiek, et al. "Hydrogels with well-defined peptide-hydrogel spacing and concentration: impact on epithelial cell behavior". In: *Soft Matter* 8.2 (2012), pp. 390–398.

[391] W. Kuhlman, I. Taniguchi, et al. "Interplay Between PEO Tether Length and Ligand Spacing Governs Cell Spreading on RGD-Modified PMMA- g- PEO Comb Copolymers". In: *Biomacromolecules* 8.10 (Oct. 2007), pp. 3206–3213.

[392] J. H. Beer, K. T. Springer, and B. S. Coller. "Immobilized Arg-Gly-Asp (RGD) peptides of varying lengths as structural probes of the platelet glycoprotein IIb/IIIa receptor." In: *Blood* 79.1 (Jan. 1992), pp. 117–28.

[393] G. Giannone, B. J. Dubin-Thaler, et al. "Periodic lamellipodial contractions correlate with rearward actin waves". In: *Cell* 116.3 (2004), pp. 431–443.

[394] J.-C. Kuo. "Mechanotransduction at focal adhesions: integrating cytoskeletal mechanics in migrating cells". In: *J. Cell. Mol. Med.* 17.6 (June 2013), pp. 704–712.

[395] C. G. Galbraith, K. M. Yamada, and M. P. Sheetz. "The relationship between force and focal complex development". In: *J. Cell Biol.* 159.4 (2002), pp. 695–705.

[396] A. del Rio, R. Perez-Jimenez, et al. "Stretching Single Talin Rod Molecules Activates Vinculin Binding". In: *Science (80-. ).* 323.5914 (Jan. 2009), pp. 638–641.

[397] M. Yao, B. T. Goult, et al. "Mechanical activation of vinculin binding to talin locks talin in an unfolded conformation". In: *Sci. Rep.* 4.1 (May 2015), p. 4610.

[398] G. C. K. Roberts and D. R. Critchley. "Structural and biophysical properties of the integrin-associated cytoskeletal protein talin". In: *Biophys. Rev.* 1.2 (July 2009), pp. 61–69.

[399] D. H. Rohrbach and R. Timpl. *Molecular and cellular aspects of basement membranes.* Academic Press, 1993, p. 448.

[400] B. M. Fu and J. M. Tarbell. "Mechano-sensing and transduction by endothelial surface glycocalyx: composition, structure, and function". In: *Wiley Interdiscip. Rev. Syst. Biol. Med.* 5.3 (May 2013), pp. 381–390.

[401] C. Liu, K. Kubo, et al. "Single polymer growth dynamics". In: *Science (80-. ).* 358.6361 (2017), pp. 352–355.

[402] C. D. Paul, A. Hruska, et al. "Decoupling cellular response to topography and stiffness in three dimensions". In: *bioRxiv* (2017), p. 232066.

[403] A. J. Berger, K. M. Linsmeier, et al. "Decoupling the effects of stiffness and fiber density on cellular behaviors via an interpenetrating network of gelatin-methacrylate and collagen". In: *Biomaterials* 141 (2017), pp. 125–135.

[404] R. S. Stowers, S. C. Allen, and L. J. Suggs. "Dynamic phototuning of 3D hydrogel stiffness". In: *Proc. Natl. Acad. Sci.* 112.7 (2015), pp. 1953–1958.

[405] J. Doye. *Applying polymer theory to biomolecules.* http://wallace.chem.ox.ac.uk/teaching/Biophyschem_2.pdf. Oxford, 2017.

[406] J. Bois. *Rudiments of Polymer Physics.* Tech. rep. Pasadena: California Institute of Technology, 2002, p. 29.

[407] J.-S. Chen, C.-H. Lee, et al. "Atomistic to Continuum Modeling of DNA Molecules". In: *Adv. Soft Matter Mech.* Vol. 9783642193. Berlin, Heidelberg: Springer Berlin Heidelberg, 2012, pp. 1–53.

# List of Figures

# List of Tables

145

# Acknowledgements - Danksagung